IOWA STATE UNIVERSITY
Digital Repository

Graduate Theses and Dissertations

Iowa State University Capstones, Theses and Dissertations

2014

Seismic behavior of hollow concrete columns

Ryan Beck
Iowa State University

Follow this and additional works at: https://lib.dr.iastate.edu/etd

 Part of the Civil Engineering Commons

Recommended Citation
Beck, Ryan, "Seismic behavior of hollow concrete columns" (2014). *Graduate Theses and Dissertations*. 14108.
https://lib.dr.iastate.edu/etd/14108

This Thesis is brought to you for free and open access by the Iowa State University Capstones, Theses and Dissertations at Iowa State University Digital Repository. It has been accepted for inclusion in Graduate Theses and Dissertations by an authorized administrator of Iowa State University Digital Repository. For more information, please contact digirep@iastate.edu.

Seismic behavior of hollow concrete columns

by

Ryan Beck

A thesis submitted to the graduate faculty

in partial fulfillment of the requirements for the degree of

MASTER OF SCIENCE

Major: Civil Engineering (Structural Engineering)

Program of Study Committee:
Sri Sritharan, Major Professor
Jay Shen
Song Zhang

Iowa State University

Ames, Iowa

2014

TABLE OF CONTENTS

LIST OF TABLES

LIST OF FIGURES

NOMENCLATURE

$A_g =$ gross area of concrete section

$A_h =$ area of transverse reinforcing bar

$A_{hx} =$ area of transverse reinforcing bar in X direction

$A_{hy} =$ area of transverse reinforcing bar in Y direction

$A_l =$ area of longitudinal reinforcing bar

$D =$ overall outside dimension of section

$d_i =$ diameter of inner void

$d_{ix} =$ diameter of inner void in X direction

$d_{iy} =$ diameter of inner void in Y direction

$d_s\ (= D') =$ diameter from center to center of transverse reinforcement

$d_{sx} =$ diameter from center to center of transverse reinforcement in X direction

$d_{sy} =$ diameter from center to center of transverse reinforcement in Y direction

$E_{cu} =$ label used in plots to represent ultimate compressive strain of confined concrete

$E_{cu} + 50\% =$ label used in plots to represent ultimate compressive strain of confined concrete increased by 50 percent

$f_c' =$ compressive strength of concrete

$f_{cc}' =$ compressive strength of confined concrete

$f_c =$ circumferential stress in circular concrete section

$f_h =$ stress in lateral reinforcement

$f_l' =$ effective lateral stress between transverse reinforcement and concrete

$f_l =$ lateral stress between transverse reinforcement and concrete

$f_{lx} =$ lateral stress between transverse reinforcement and concrete in X direction

$f_{ly} =$ lateral stress between transverse reinforcement and concrete in Y direction

$f_p =$ stress within concrete wall in direction parallel to transverse reinforcement

$f_r =$ radial stress in circular concrete section

f_u = ultimate stress in longitudinal reinforcement

f_y = yield stress in longitudinal reinforcement

f_{yh} = yield stress in transverse reinforcement

k_e = confinement effectiveness factor

k_h = hollow column confinement effectiveness factor

s = spacing of transverse reinforcement

t = thickness of wall in hollow section

t_s = thickness of wall within transverse reinforcement in hollow section

t_{sx} = thickness of wall in X direction in hollow section

t_{sy} = thickness of wall in Y direction in hollow section

P = axial load

V_{cg} = gross volume of concrete within transverse reinforcement

V_h = gross volume of transverse reinforcement

ε_c = strain in concrete

ε_{cc} = peak strain of confined concrete

ε_{cu} = ultimate strain of confined concrete

ε_{su} = ultimate strain of transverse reinforcement

ε_u = ultimate strain of longitudinal reinforcement

ACKNOWLEDGEMENTS

The research presented in this thesis was made possible by the support and education provided by the Department of Civil, Construction, and Environmental Engineering at Iowa State University, and through the sponsorship by the California Department of Transportation. I would especially like to thank Dr. Sri Sritharan for his continued support and guidance, as well as for providing me the opportunity to work on this project. I would also like to thank Xiao Liang for her contributions to this research topic and for her guidance throughout the project, as well as Dr. Sriram Aaleti and Dr. Aaron Shelman for their guidance and assistance during the research. Additionally, I would like to thank Dr. Jay Shen and Dr. Song Zhang for serving on my committee.

The experimental portion of this research was made possible through the valued support of the Senior Engineering Specialist and structures lab manager Doug Wood, as well as the Research Associate Owen Steffens. I would like to thank them for their continuous support and assistance, which made the testing possible. I would also like to thank the many undergraduate students and fellow graduate students who provided assistance in the structures lab. Their help substantially expedited the lab work, and it is greatly appreciated.

I would like to thank my parents, Robert and Kim Beck, for making my education possible and supporting me throughout it. I would also like to thank all of my family and friends, especially my wife Brianna Beck, for their support and encouragement.

ABSTRACT

Hollow reinforced concrete columns have been used in the past in place of their solid counterparts in the construction of bridges. These hollow columns have several benefits over solid columns, including the reduction of vertical load applied to the foundation as well as the reduction of seismic mass. Despite the benefits of hollow reinforced concrete columns, little is known about the effectiveness of transverse reinforcement to confine the concrete in these columns when only one layer of transverse reinforcement is provided.

The goal of this research is to develop design procedures and modeling techniques which can accurately describe the behavior of hollow columns with one layer of transverse reinforcement. To achieve this goal, a review of previous research was conducted and the findings were used to propose an adjustment to an existing confined concrete model. A modeling technique for hollow columns was then described, which utilizes the proposed confinement model adjustment. The model has been verified using test specimens presented in previous research, and it has been found to provide a conservative estimate of the response of these columns.

Experimental testing of hollow circular and square columns with one layer of transverse reinforcement was performed to gain more understanding of the hollow columns' behavior, as well as to provide further validation of the proposed model. The test results found that hollow specimens with low axial load, low flexural demand, and sufficient wall thickness can produce a limited ductile response. Additionally, it was found that shear effects can be more significant in hollow columns than in equivalent solid columns.

The literature review and experimental program demonstrate that hollow columns can achieve a response very similar to that of a solid column with the same outer dimensions and reinforcement details, as long as the hollow column is designed appropriately. A recommended design procedure is proposed, which provides a simple estimate of the required wall thickness to achieve a ductile response for hollow columns with one layer of transverse reinforcement. The modified analysis method is incorporated into this design procedure, producing guidelines for the design and analysis of these hollow columns.

CHAPTER 1. INTRODUCTION

1.1 Overview

Reinforced concrete bridge columns are widely used throughout the world in both seismic and non-seismic regions. In non-seismic regions, the main concern is often transferring the axial load to the foundation. In seismic regions, the axial load becomes less of a concern, and withstanding earthquake forces becomes more challenging. In fact, columns in seismic regions typically have a very low axial load ratio (i.e. $P/(f'_cA_g)$ where P is the axial load, f'_c is the compressive strength of concrete, and A_g is the gross area of the cross-section), usually around five percent. The main concern is the lateral loads induced in the column as a result of the bridge being subjected to earthquake motion. These loads generally produce large moments at the column fixed locations, as well as large shear demand in the column. Unlike in non-seismic regions, columns in seismic regions are designed to experience inelastic behavior. This behavior can be targeted to certain locations in the column by designing these locations with a limited capacity so that they develop plastic hinges. The formation of plastic hinges in targeted areas limits the seismic load that the rest of the structure would experience, enabling the designer to control where the seismic damage would occur, while avoiding damage in other regions.

Concrete is brittle in nature and can fail quickly after reaching peak strength in the inelastic range, typically under small strain near 0.002. For this reason, the plastic hinges of columns in high seismic areas must be provided with adequate amounts of transverse reinforcement to ensure sufficient ductility. This reinforcement typically occurs in the form of hoops and spirals. Concrete under axial compression will dilate, as described by the Poisson effect, until it ultimately fails by splitting in tension. The transverse reinforcement confines the concrete, resisting the dilation and providing improved strength to the concrete. The ductility is increased as well, due to the confinement effect and increased strain capacity. This is crucial to the safety of the structure, as ductile behavior is critical in avoiding sudden failure of the structure, and can ultimately help avoid structural collapse.

The mass of solid columns can become very significant, especially for taller columns. The large mass of these columns places larger demand on the foundation, as well as significantly contributing to the seismic mass of the structure. Using hollow columns instead of solid columns can greatly reduce the inertia demand of the bridges. Since columns in seismic regions are designed to experience low axial load ratios and larger moment demands, using hollow columns achieves a more efficient section. The central portion of a solid column provides little moment resistance and is not necessary to support the axial load. The longitudinal steel provides most of the moment resistance in concrete columns. By providing a hollow column, the moment capacity can be achieved through the longitudinal reinforcement, while the concrete ring is sufficient to support the axial compression.

The longitudinal steel in concrete columns is primarily responsible for the flexural resistance, while transverse reinforcement is responsible for the ductility of the concrete, as well as the shear resistance and anti-buckling resistance of the longitudinal reinforcement. To ensure the column behaves in a ductile manner, a sufficient amount of transverse reinforcement must be provided, which can increase the ultimate compressive strain of the concrete tenfold in well confined columns. Past researchers have proposed many different models in order to quantify the gain in strength and ductility of concrete due to transverse reinforcement. These models were mainly developed based on theory and experimentation involving solid specimens subjected to axial compression. The most commonly used of these is the model developed by Mander et al. (1988). This model is applicable for both circular and square hollow columns, and is used by both the Caltrans Seismic Design Criteria (2013) and the AASHTO LRFD Seismic Bridge Design Specifications (2011; 2012; 2014).

Mander's model was developed based on theoretical and experimental analysis of solid specimens confined with transverse reinforcement and subjected to pure axial compression. Although developed for pure axial compression, the model is used frequently for the design of confinement in seismic regions. The model is able to estimate the stress-strain response of confined concrete based on the section dimensions and material properties, and the amount of transverse reinforcement. The use of Mander's model has proven to provide satisfactory

designs for solid columns, but the extension of this model to hollow columns has only seen limited investigation. The model relies on equilibrium of forces between the concrete and confining steel to determine the increased ductility of the concrete. The presence of the inner void complicates the determination of pressure experienced by the transverse reinforcement due to concrete dilation, which leads to confusion in how to implement the model.

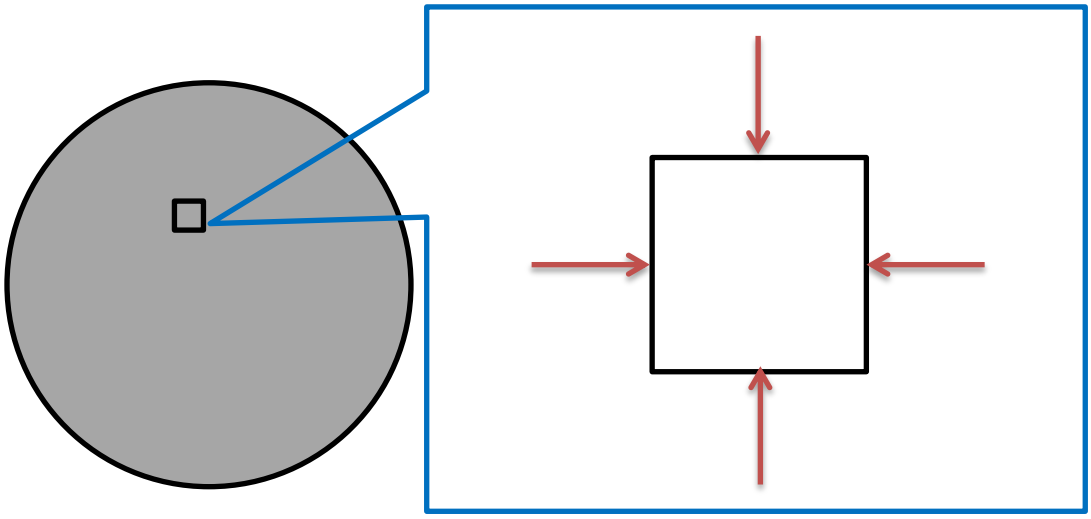

Figure 1-1: Stress-Block in Solid Section

Mander's model estimates the confined concrete properties by first estimating the stresses in orthogonal direction using equilibrium between the steel and concrete. Estimating the lateral stresses essentially yields a three dimensional stress-block, which is then used with previous models which were based on triaxial tests. This works well for the case of solid sections, where the in plane orthogonal stresses are approximately equal at any point throughout the section, as shown in Figure 1-1. Using a hollow column with one layer of transverse reinforcement complicates the issue for several reasons. The first issue is caused by the lack of an inner layer of confinement, instead leaving a free surface at which radial stress is zero. The second issue is that it is unclear how the concrete dilates, since instead of only being able to dilate outward as is the case in a solid column, the concrete can now possibly dilate inward as well.

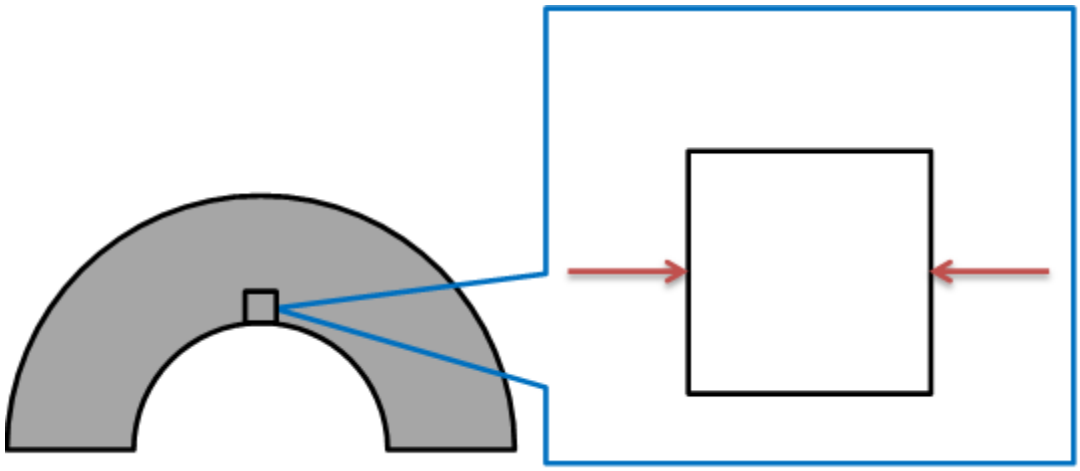

Figure 1-2: Stress-Block in Hollow Column with One Layer of Transverse Reinforcement

At the inside face of a hollow column with one layer of transverse reinforcement, no radial stress can develop, so the concrete is only biaxially confined. The biaxial confinement state at the inside face is illustrated in Figure 1-2. Mander's model is able to model confined concrete that is only biaxially confined, although it experiences much lower gains in strength and ductility. This can cause brittle failure due to crushing of the concrete at the inside face when subjected to high axial load or flexure. To combat the possibility of brittle failure at the inside face, an inner layer of transverse reinforcement is often provided. This inner layer is usually tied to the outer layer of transverse steel through cross-ties, in an effort to prevent the inside face from crushing. Although this inner layer of reinforcement is beneficial in confining the concrete, it is more time consuming and costly to construct.

1.2 Research Significance

Previous research has shown that hollow columns with one layer of transverse reinforcement can experience relatively ductile behavior when designed appropriately. Only a few previous studies have been performed which investigated hollow columns with one layer of

transverse reinforcement, and there are very few design guidelines or recommendations available.

Zahn et al. (1990) performed some of the earliest testing of hollow circular concrete columns with one layer of transverse reinforcement. Their experimental program consisted of testing columns with varying wall thickness and axial load ratios. It was found that the ductility of these columns greatly depends on the neutral axis location and that the neutral axis location must occur near the wall to limit axial compression strain at the inside face. They also proposed that the flexural capacity of hollow columns with a wall thickness ratio (wall thickness over column diameter, t/D) of 0.15 or greater was comparable to that of a solid column with the same reinforcement and outside diameter.

Further testing of hollow circular columns with one layer of transverse reinforcement was performed by Hoshikuma and Priestley (2000). The amount of longitudinal steel was the main variable in these tests. It was found that having a lower amount of longitudinal reinforcement allowed the specimen to achieve a limited displacement ductility of 3.3, while larger amounts of longitudinal steel caused a more brittle response, with a displacement ductility of 1.8. Crushing of concrete at the inside face controlled the response of the specimens, and it was found that there was a very small transverse reinforcement demand. The research again suggested that the neutral axis location is critical to the design and proposed an ultimate strain of inside face concrete of 0.005, with a safe design limit of 0.0035.

Testing of circular hollow columns similar to those tested by Hoshikuma and Priestley (2000) was performed by Ranzo and Priestley (2001). However, the goal of this testing was to determine the shear response and accuracy of shear models. Several specimens were tested, but only one specimen was tested which failed due to flexure, and it achieved a higher ductility due to it having a very low axial load ratio of 1.7 percent to the gross section (five percent to the net section) and low amounts of longitudinal reinforcement. This specimen ultimately failed by crushing of the inside face concrete.

There is a limited amount of research into hollow circular columns with one layer of transverse reinforcement, and there is even less research for hollow rectangular columns with

one layer of transverse reinforcement. One of the only experimental studies of these specimens was performed by Calvi et al. (2005), which tested hollow square columns with both one and two layers of reinforcement. The focus of this research was largely on shear behavior of these columns. Several hollow square columns with one layer of transverse reinforcement were tested as a part of this research, and all of them failed in shear, as they were intended, without crushing of the inside face concrete occurring.

The research described in this section has primarily focused on experimental behavior of hollow columns, with little attention given to the confinement effect of concrete in these columns. It has been verified that hollow concrete columns can experience limited ductility and similar capacity when compared to solid columns, but it is unclear how the design and analysis of these columns should be approached. The confinement behavior in these columns is not very well understood, and better understanding is needed in order to develop appropriate guidelines.

1.3 Scope of Research

The goal of this research is to analyze circular and square hollow columns with one layer of transverse reinforcement and to develop design recommendations and procedures. The desired objectives are as follows:

1.) Determine a method for predicting the flexural response of hollow columns
2.) Develop an experimental plan to obtain sufficient data using small scale models
3.) Establish a methodology to design hollow columns with one layer of transverse reinforcement

The above areas have been investigated using a combination of analysis and testing. The first objective has been achieved using OpenSees fiber-based analysis software (McKenna et al., 2000) to predict the response of the hollow concrete sections. This software was used to analyze whether the sections would behave in a ductile fashion and to estimate the maximum

force and displacement they would experience. The second objective was achieved by testing sixteen small scale test units. The test results were used to verify the analysis and to improve it wherever possible.

Findings of previous researchers as well as the results of the experimentation presented in this report were used to gain a better understanding of the hollow column confinement. Areas of improvement were identified, and an adjustment to Mander's model was provided. Analysis of measured strains in the test specimens were also used to determine agreement between tests and analyses. The findings were used to suggest improvements to the design process for hollow columns. Improvements were suggested which enable simple preliminary analysis of hollow columns with one layer of transverse reinforcement, including estimating wall thickness requirements and how to model the concrete using analysis methods readily available to practicing engineers.

1.4 Thesis Organization

The research findings and procedures are presented in six chapters. The first chapter provides an overview of the topic and identifies areas where there was limited information available on hollow column behavior. The available literature related to the topic is reviewed in the second chapter, further identifying key concepts as well as gaps in the current knowledge. These concepts are used in the third chapter to establish the methodology of the analytical methods used in this research, as well as to compare the current analysis method to the experimental results of previous researchers. To verify the analysis method and concepts of previous research a test program was developed, and the procedure of this program is discussed in the fourth chapter. The results of the experimental program are presented in chapter five, which also compares the analytical results to these experimental results. The conclusions and recommendations developed from the research are presented in chapter six, as well as areas which were identified where further research is recommended.

CHAPTER 2. LITERATURE REVIEW

2.1 Confinement of Solid Concrete Columns

Concrete experiences strong compression resistance, but it is fairly weak in tension. Additionally, concrete experiences brittle failure in compression due to tension splitting. For this reason, concrete is typically reinforced with steel, which enables a very ductile response for the concrete. Reinforcing steel is usually provided in tension regions in order to greatly increase the strength and ductility of the concrete member. In seismic regions, this reinforcing steel becomes especially important, since ductile behavior is often required. It is important that the concrete components which are designed to develop plastic hinges will experience ductile behavior and will not be subject to large strength degradation.

Even though concrete failure is considered in both compression and tension, technically concrete always fails in tension, even when subjected to axial compression. This is due to the dilation of concrete along the axes perpendicular to the loading axis, and this phenomenon is known as the Poisson's effect. Unreinforced concrete subjected to pure axial compression will experience dilation until the point where it fails due to tension splitting. It was determined that applying pressure in the plane perpendicular to loading would increase the strength and ductility of concrete subjected to axial compression. Early research applied this pressure using an active hydrostatic fluid pressure. This is not practical for field construction, so it was found by past researchers that using transverse reinforcement in the form of spirals or hoops could provide a passive pressure which increased the strength and the ductility of the concrete. As the concrete dilates laterally, it begins to push against the confining steel, which provides lateral pressure to the concrete and induces tension in the confinement.

Although transverse steel is provided, it does not become activated until the concrete has dilated. This is why confinement through the use of steel reinforcement is considered passive confinement. As the axial load in the concrete increases, the concrete dilates further, resulting in increased confining pressure until the transverse reinforcement yields. The continued dilation and axial compression also causes the cover concrete to spall off. Once the transverse steel has yielded, the confining pressure remains relatively constant until the transverse steel

fractures. The concrete is typically considered to be failed upon fracture of the transverse reinforcement, since more fractures and unwinding of the transverse reinforcement can happen fairly quickly.

Many models have been presented by past researchers which intend to describe the properties of concrete confined with transverse reinforcement. Many of these models were developed based on equilibrium between the force developed in the transverse reinforcement and the force developed in the concrete in solid sections. These models were also verified using confined solid sections subjected to pure axial compression. The confined concrete model presented by Mander et al. (1988) uses this method, and it is one of the most widely used models in current practice. It is recognized as such by the Caltrans Seismic Design Criteria (2013) as well as the AASHTO LRFD Seismic Bridge Design Specifications (2011; 2012; 2014). It has been commonly used for design and analysis purposes and has been shown to provide good accuracy. Due to the widespread use of this model, it has been deemed appropriate to focus solely on this model, to assess its applicability for hollow columns and to provide adjustments if necessary. An overview of companion papers by Mander et al. are provided in Sections 2.1.1 and 2.1.2 which describe the confined concrete model as well as the testing, which verified the model.

2.1.1 Confined column theory by Mander (1988)

Much of the strength and ductility of confined concrete depends on how effectively it is confined. The effectiveness of the confinement depends on a number of factors. Previous researchers have determined which factors have the largest effect on confinement effectiveness, which are summarized by Mander et al. (1988) as follows:

- Transverse reinforcement spacing
- Presence of additional supplementary overlapping hoops or cross-ties
- Distribution of longitudinal bars
- Volumetric ratio of transverse steel to concrete core (ρ_s)

- Yield strength of transverse reinforcement
- Type of transverse steel (spirals, circular hoops, or rectangular hoops with cross-ties)

The transverse reinforcement spacing is important because the more uniform the confining pressure is throughout the length of confined concrete, the more effective the confinement would be. If a large spacing for the transverse reinforcement is used, the reinforcement will not effectively resist the pressure resulting from the dilation of concrete. This concept is illustrated in Figure 2-1, which shows the arching action along the member length, assumed by Mander et al. (1988). Additionally, Figure 2-1 shows the effectively confined region for rectangular sections. As seen, the arching action was also assumed to occur between the longitudinal steel in these sections. The arching action between the longitudinal steel shows the importance of a good distribution of longitudinal steel. Uneven distribution can cause large areas of ineffectively confined concrete. The study used this arching action to determine the area of the effectively confined concrete core. Based on this arching action, a confinement effectiveness coefficient was then defined. This represents the ratio between the effectively confined core area and the area of the entire concrete reinforced by the transverse reinforcement. The confinement effectiveness coefficient is essentially used as a reduction factor to account for the longitudinal steel distribution and the spacing of the confinement.

As previously noted, Mander et al. used force equilibrium based on the tension stress in the transverse steel at yield and the lateral confining pressure on the concrete to determine the maximum confining pressure. It was found that the confining pressure depends entirely upon the ratio of the volume of the transverse confinement to the volume of the confined core, as well as the yield stress of the transverse steel. Supplemental cross-ties and overlapping hoops greatly impact the confinement effect, since providing this reinforcement will increase the volumetric ratio of transverse steel to the confined core and minimize the arching action.

The model uses the aforementioned factors to calculate the confining pressure as well as the confinement effectiveness factor. These values are then used to calculate an effective confinement pressure, which is essentially the confinement pressure multiplied by the confinement effectiveness factor. The model then calculates the confined compressive strength

of the concrete using the unconfined concrete compressive strength and the effective confining pressure. The calculation of the confined compressive strength is based upon a model which was originally used to predict triaxial test results. In this case, the effective confining pressure is used as the lateral pressure in the triaxial equation. The model is also capable of predicting behavior at various strain rates as well as predicting unloading and reloading at slow strain rates. Additionally, the model predicts the ultimate compressive strain of concrete. This strain is considered as the strain at which the first hoop fracture occurs, since the column can experience sudden failure or strength loss after the first hoop fracture.

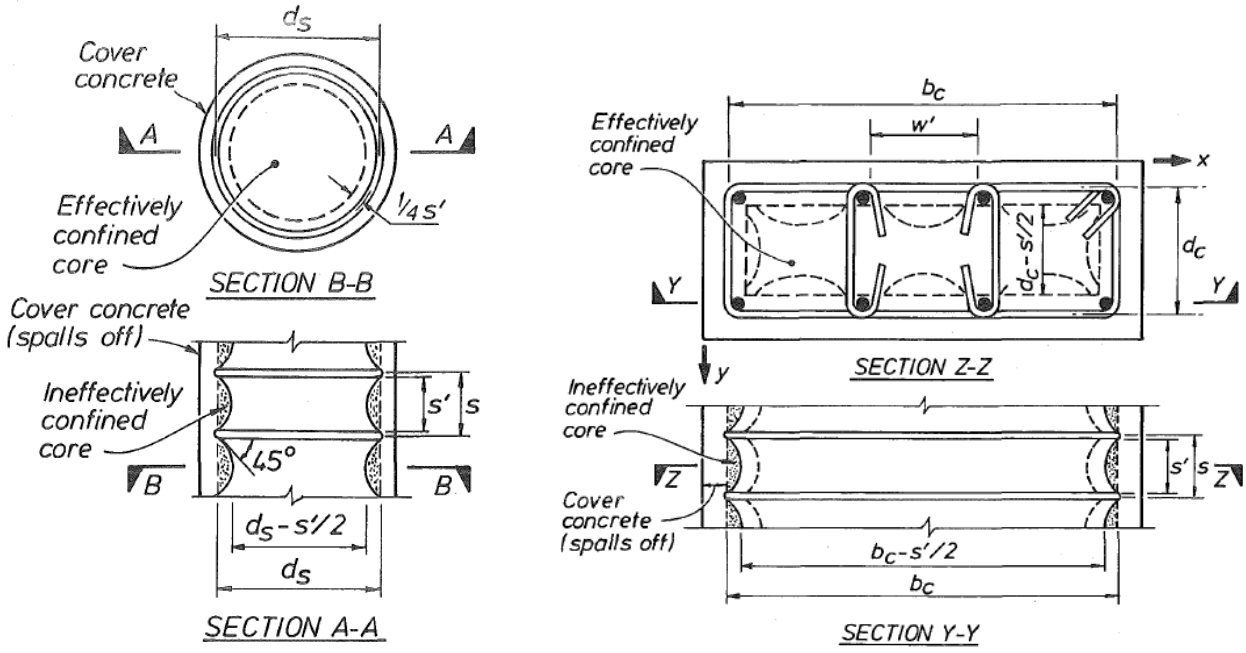

Figure 2-1: Effectively Confined Core for Circular and Rectangular Sections [Mander et al. (1988)]

2.1.2 Confined concrete testing by Mander (1988)

Mander also has performed testing of 31 nearly full-size concrete columns with varying cross-sections, including circular and square columns as well as rectangular walls (Mander et al. 1988). The circular columns had an aspect ratio of three, and the square columns had an aspect

ratio of 2.67. The columns had varying amounts of transverse and longitudinal reinforcement and were loaded concentrically in increasing axial compression with different strain rates. The circular sections tested used spiral reinforcement for the confining steel, and the square and rectangular sections used transverse hoops. The results of the tests were compared to the results predicted by the confined concrete model that they proposed in order to determine the accuracy of the model. All the columns were tested at a fast strain rate (0.0167/s) in order to simulate seismic effects. Each series of column sections had an unreinforced column cast as well, in order to compare the unconfined behavior to the confined behavior.

The columns had a variety of reinforcement arrangements in order to determine the accuracy of the model for an assortment of situations and to see the effects of changing some of these values. The first series reported is the circular column series. For these columns, there were two main sets tested with seven columns in each set. The first set contained six columns with the same amount of longitudinal steel but with different transverse reinforcement spacing. One of the seven columns was also unreinforced. The second series contained six columns with constant transverse reinforcement spacing but with varying amounts of longitudinal steel. This series also contained an unreinforced column. For both series, the confinement effectiveness coefficient was in the range of 0.89 to 1.002 (the confinement effectiveness coefficient may exceed 1.0 when the longitudinal reinforcement is high, as noted by Mander et al.). The concrete strength for each series was approximately between 4,000 and 5,000 psi. The square and circular specimens were all tested monotonically.

The results of the test were compared with the predicted tests using the model, and good agreement was generally found. It was found that for even the lightly confined columns, there was a significant increase in compressive strength and greatly improved ductility. The results showed that providing more confinement enhances this behavior, also providing increased compressive strength and an even more ductile response. Increasing the volume of confinement also resulted in an increase in the strain at which the hoop fracture occurred. The results showed that the predicted and actual stress-strain behaviors were very close. The peak stress and strain at peak stress were also very close to those predicted, with the experimental

peak strength exceeding the predicted strength by 1.7% on average. The experimental peak strain (i.e. the strain at peak strength) was about 1.3% on average less than predicted. The predicted strain at the hoop fracture also seemed to agree with the experimental results, although it seemed the prediction was somewhat conservative in most cases.

Mander et al. also found several important trends which furthered the understanding of confined concrete behavior. One important finding was that the amount of longitudinal bars had minimal effects on the concrete stress-strain behavior. The second series, which varied the amount of longitudinal steel but kept the confining steel volume constant, found very little variation in the stress-strain behavior. Additionally, the research found that the volumetric ratio of the confining steel was the most influential factor on the stress-strain behavior. Two cylinders which had a very similar volumetric ratio of confinement but had different arrangements were compared. One of these cylinders had a larger spiral spacing than the other, but had a larger confining steel diameter, resulting in approximately the same volumetric ratio. The results showed that the behavior was very similar. The cylinder with smaller spacing experienced a slightly more favorable descending branch. This suggests that the volumetric ratio was the more important factor, as long as the spacing of the confinement was reasonable and was close enough to effectively confine the concrete. These trends and results can be visualized in Figure 2-2, which also lists the volumetric ratios of the cylinders shown.

The grade of steel used for the confining reinforcement affects the confinement pressure as well. When using a higher grade of transverse steel, the yield stress is higher which causes a higher confinement pressure to be experienced. Although the yield stress is higher in higher steel grades, the ultimate strain of the steel is typically lower, which can cause premature fracture of the steel. Although Mander et al. did not test different confining steel strengths, this has been previously tested by Zahn et al. (1990). It was found that using a higher grade of transverse steel can allow the reduction of the volumetric ratio of transverse steel, while still achieving a similar confined concrete compressive strength. It was also found that due to the lower ultimate strain of the confinement, the ductility would slightly decrease, although the ductility was still high.

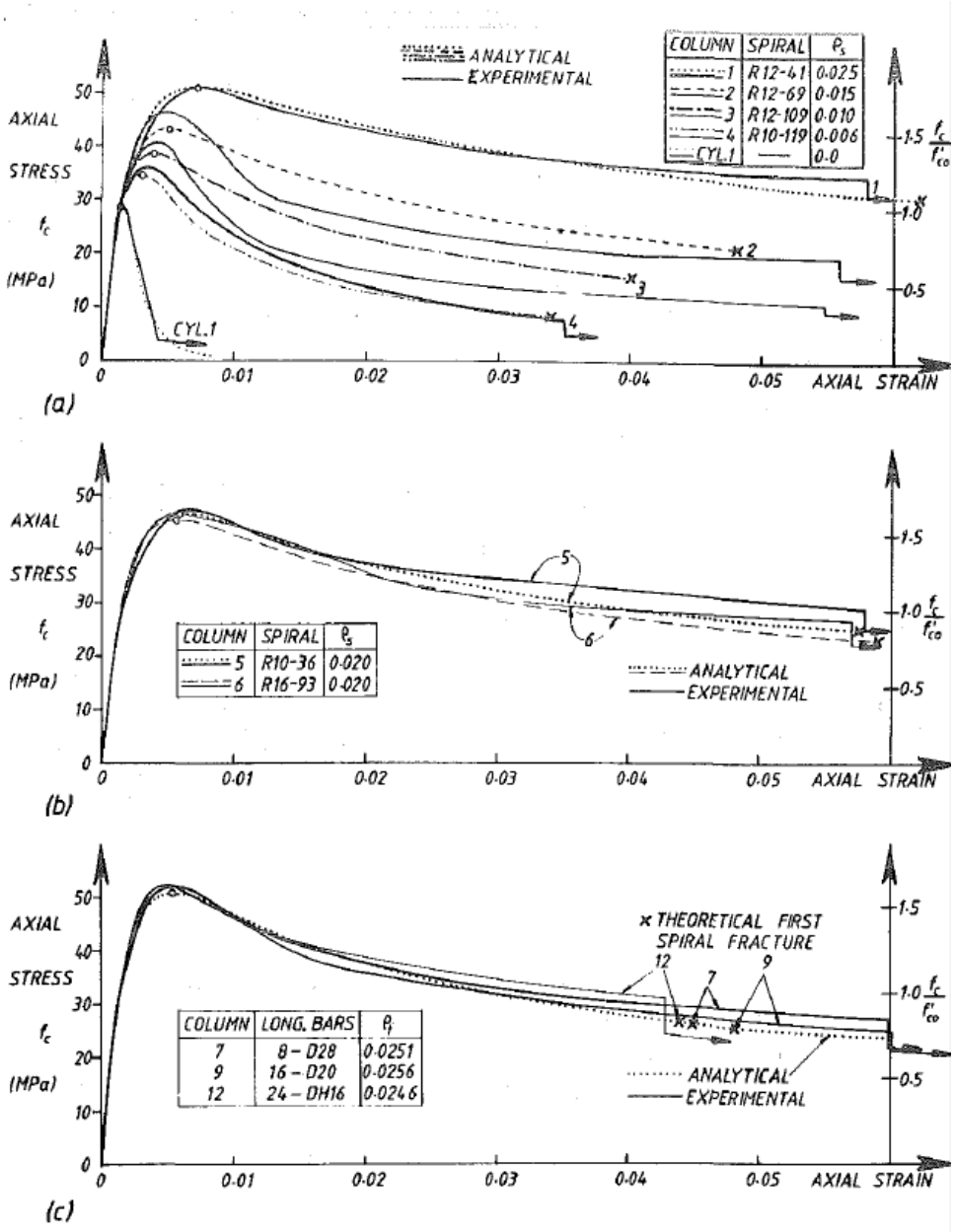

Figure 2-2: Comparison of Reinforcement Effects and Predicted to Actual [Mander et al (1988)]

Additional tests were performed on square columns and rectangular wall sections. The model was able to predict the response of these columns fairly accurately. The square columns also tested the influence of the age of concrete on the confinement behavior. Specimens with

ages between 60 and 80 days were compared to specimens with ages greater than 940 days. It was found that age of each specimen did not have much influence on the response of the specimens.

2.2 Confinement of Hollow Concrete Columns

Since the focus is on the flexural behavior of columns in seismic regions, it can be seen that the solid section is not always efficient, especially for tall columns with large diameters. Much of the central portion of these columns will experience low strain, and will contribute little to the moment resistance. This results in the columns having low strength to mass and stiffness to mass ratios, indicating that the efficiency of these sections is low. Additionally, these solid columns are often large, and contribute significantly to the seismic mass of the bridge, as well as contributing dead load to the foundation.

Hollow reinforced concrete columns have been used in an effort to increase the structural efficiency of the section. These sections provide enough axial loading area to resist the low axial loads applied to columns in seismic regions, as well as providing concrete and reinforcing steel where they will be more effectively utilized. These sections are able to greatly reduce the mass of the column, as well as the amount of materials used to construct the column. The reduction in mass can also help improve the seismic response, since the response will have a smaller mass contribution.

Although it is easy to see that providing hollow columns has many benefits, it is more difficult to determine the most effective design for these columns. The presence of the inner void changes the behavior of the concrete and the confinement when subjected to compression. The stresses due to flexure further complicate this. The concrete is not forced to expand outward only and can dilate into the inner void. The concrete near the void is no longer confined triaxially as it is in a solid column, and instead it has no pressure resisting its movement into the void. Due to this behavior, hollow columns can be subjected to premature failure due to the concrete failing at the inside face. The confinement near the outside face

would only have a minor effect on the concrete at the inside face, and the inside face failure would ensue in a brittle fashion.

To prevent crushing of the concrete at the inside face, a second layer of transverse reinforcement is often provided near the inside face of hollow columns. This second layer is typically tied back to the outer layer of reinforcement. This configuration allows for the concrete near the inside face to be triaxially confined instead of just biaxially confined. Although providing a second layer of transverse reinforcement helps prevent inside face failure, it is also more time consuming and costly to do so. Additionally, providing a second layer of transverse reinforcement in hollow columns with thin walls can cause congestion in these columns and create difficulties in achieving good concrete fill.

Hollow columns with two layers of transverse reinforcement have been studied by past researchers, and more information is available about these columns than for hollow columns with one layer of transverse reinforcement. Due to the issues in cost and time associated with these columns, and due to the higher quantity of available research about these columns, the focus of this research is solely on hollow columns with one layer of transverse reinforcement. If designed appropriately it has been shown that these columns can experience adequate ductility. The provision of only one layer of transverse reinforcement allows for a design which is more constructible and economical.

2.2.1 Confinement effectiveness

As discussed, the effectiveness of the transverse reinforcement has been taken into account in previous models in order to determine the confining pressure. Arching action between reinforcement is taken into account in Mander's model using a factor, which is known as the confinement effectiveness factor. For circular columns this value is typically used as 0.95, and for square or rectangular columns 0.75 is typically used. For hollow columns, it can be assumed that these values are still applicable, since the arching effect must still be taken into account. However, it is unclear if there is any additional reduction in confinement effectiveness due to

the presence of the inner void. There has been limited research on this topic, and it is difficult to determine through experimental testing due to the inability to directly measure the local stress-strain behavior of concrete in specimens, especially those tested under flexure.

Lignola et al. (2008) performed a study which provided a unified theory for the confinement of circular solid and hollow column sections. The study resulted in an adjusted confining pressure which was intended for use with columns confined with fiber reinforced polymer (FRP). However, the confinement model could be adjusted for application to other forms of confinement as well. The model is based on the Mander et al. model, and provides the adjusted confining pressure based on the concept of radial displacement compatibility between the concrete and confinement. Using displacement compatibility combined with stress relationships, the authors were able to provide an equation to calculate the pressure applied to the concrete by the confinement. The variables influencing this pressure are the concrete and confinement Poisson's ratios, concrete and confinement stiffness, and the external and internal radii of the column. For a solid column, the internal radius would be taken as zero. Using this confining pressure, an equivalent confining pressure can be calculated, which is equal to the confining pressure multiplied by a factor based on the internal and external concrete radius. For a solid column, the equivalent confining pressure is simply equal to the confining pressure. This equivalent confining pressure is then used with Mander's model.

An important concept discussed by this paper is that hollow columns have increased lateral deformability compared to solid columns. It suggested that the radial displacement at the outer edge of the concrete columns is the same, regardless of whether the columns are solid or hollow, but the hollow columns' radial displacement requires less external pressure to restrain. Therefore, for the same axial strain applied to a solid and a hollow column, the hollow column would require less pressure to be restrained radially. Since less pressure is required there would be less strain induced in the confinement. Their work suggested that the higher the internal radius of the specimen (the larger the void) the more deformable the specimen is and therefore, less pressure will be required to restrain radial displacement.

2.3 Testing of Hollow Columns with One Layer of Transverse Reinforcement

Limited testing of hollow columns with one layer of transverse reinforcement has been performed. Of these, some focused mainly on the shear response of these specimens. In general, previous testing has shown the importance of the neutral axis location and that hollow columns can experience limited ductility with low axial load and longitudinal reinforcement ratio. Additionally, previous researchers have typically reported the axial load ratio and the reinforcement ratios using the net area of present concrete instead of the gross concrete section. This can give the appearance of columns having larger axial load and larger amounts of reinforcement than they actually do.

Zahn et al. (1990) tested six hollow circular concrete columns with different axial load ratios and wall thicknesses to determine the behavior of circular hollow concrete columns with one layer of transverse reinforcement. Moment curvature analysis was used to model the flexural behavior. The confined concrete was assumed to be biaxially confined by the circumferential stress and the axial stress. Mander's model was used to calculate the confined concrete properties. The longitudinal reinforcement ratio was 2.56 percent to the gross section for all specimens (ranged from 3.67 to 5.4 percent when the net section was used). The tested columns had wall thickness ratios of 0.23, 0.19, and 0.14. Two columns were created for each wall thickness, with each being subjected to a different axial load, one high and one low. Axial load ratios were reported using the net section, and ranged from 8 percent to 40 percent (approximately 6 percent to 23 percent when using the gross section). The columns were tested quasi-statically under cyclic loading until failure.

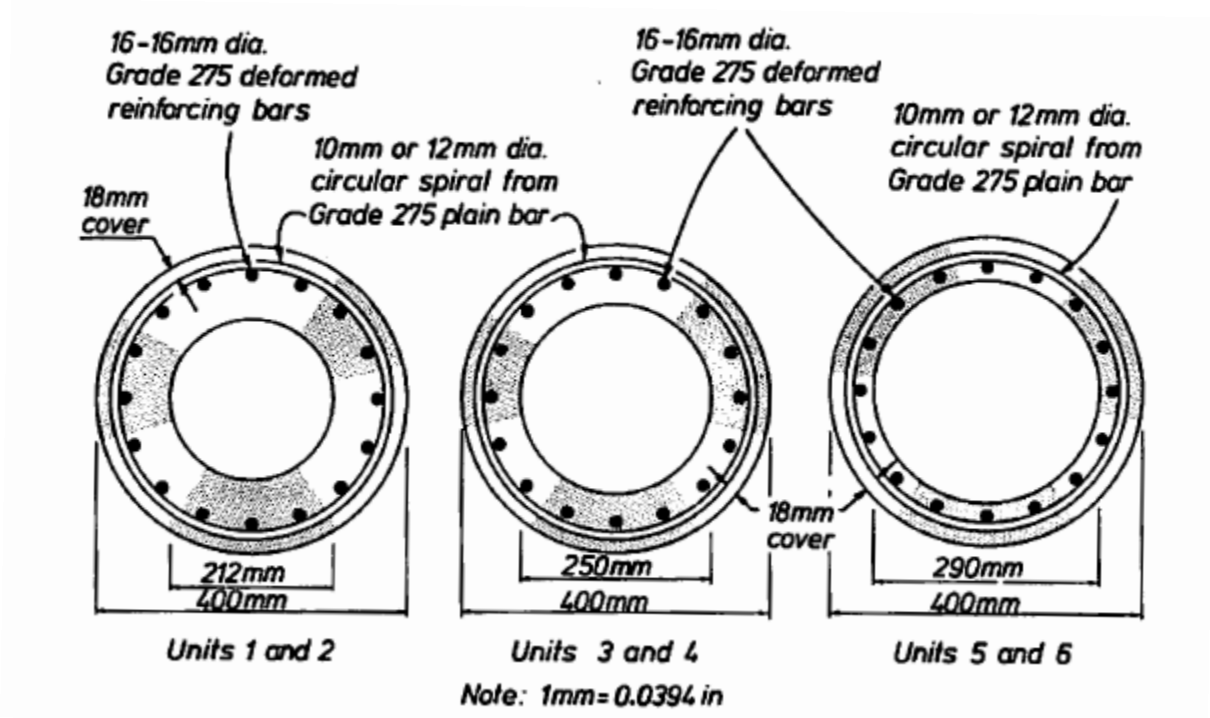

Figure 2-3: Zahn et al. (1990) Specimen Dimensions (1 mm = 0.0394 inch)

The columns with high axial load generally showed brittle behavior, with the neutral axis location further into the void. Columns with low axial load ratio generally had fairly good ductility for the thicker sections, with neutral axis locations closer to the inside face. Thin sections typically experienced more brittle behavior. All of the specimens eventually failed by collapse of the concrete compression wall due to failure of the concrete on the inner surface near the void.

The research concluded that the important factor is to limit the inside concrete face compression strain by ensuring that the neutral axis is within or near the concrete wall. The authors suggested that a strain at the inside concrete face of 0.008 could be used as a safe design limit to determine the ultimate curvature for design purposes. Additionally the authors suggested that for concrete columns with wall thickness ratios of 0.15 or higher, the flexural strength calculations can be based on an equivalent solid circular section with the same outside diameter and area of longitudinal reinforcing steel, as well as axial load ratio.

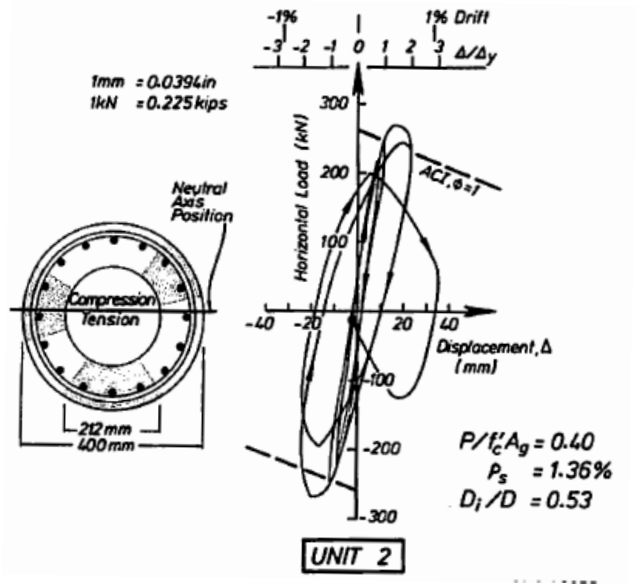

Figure 2-4: Zahn et al. (1990) Force-Displacement Response and Neutral Axis Location of Specimen Subjected to High Axial Load

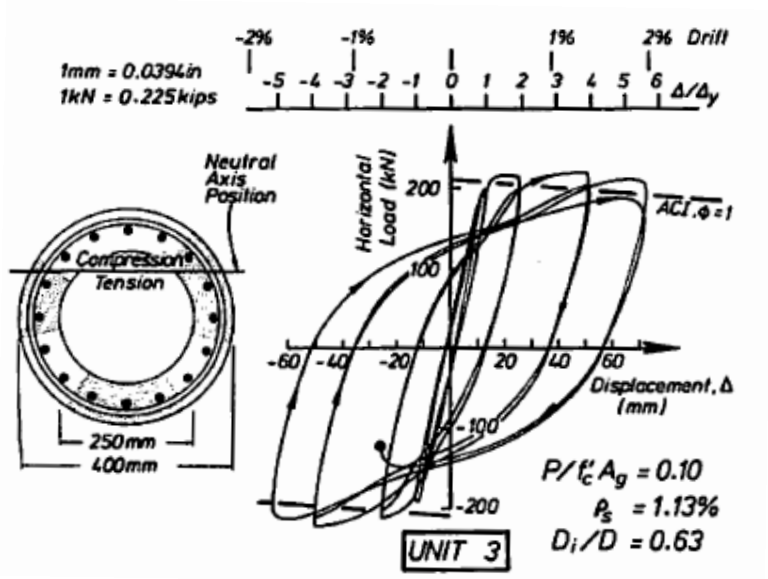

Figure 2-5: Zahn et al. (1990) Force-Displacement Response and Neutral Axis Location of Specimen Subjected to Lower Axial Load

Hoshikuma and Priestley (2000) investigated the behavior of hollow circular columns with one layer of transverse reinforcement in order to better understand the seismic performance of hollow columns. Two columns were tested which were designed to have dimensions similar to those typically found in California. The columns were 60 inches in diameter and had a wall thickness of 5.5 inches, corresponding to a wall thickness ratio of 0.092. Each column was identical except for different amounts of longitudinal reinforcement. The longitudinal reinforcement consisted of sets of two bundled bars, and the column with more longitudinal reinforcement used the same amount of bars but with larger bar sizes. The specimen with less longitudinal reinforcement was labeled HF1 and the specimen with more longitudinal reinforcement was labeled HF2. The longitudinal reinforcement ratios were 1.45 and 3.18 percent if taken to the net section, or 0.48 and 1.06 percent if taken to the gross section. Specimens were cast integrally with foundation blocks and were attached to a steel tube at the top which increased the length of the columns. The load was applied at the top of this tube. Axial load was held constant during the testing, and the axial load ratio was reported as 13 percent and was calculated using the net section, which corresponds to 4.3 percent when calculated using the gross section. The tube remained in the linear range during the testing.

The specimens were tested under cyclic pushover loading until failure. Both specimens failed due to crushing of the inside face concrete. The specimen with the lower amount of longitudinal reinforcement experienced a ductility of 3.3, and the specimen with more longitudinal reinforcement experienced a ductility of 1.8. It was found that the transverse reinforcement in the compression region only reached about 30 percent of the yield strain, indicating that there was not much demand on the confining reinforcement. The strain at which the inside face concrete crushed was 0.005. The authors suggest that this is the limiting strain for inside face concrete in hollow columns with one layer of transverse reinforcement and similar wall thickness ratios, and that a safe design limit should be a strain of 0.0035.

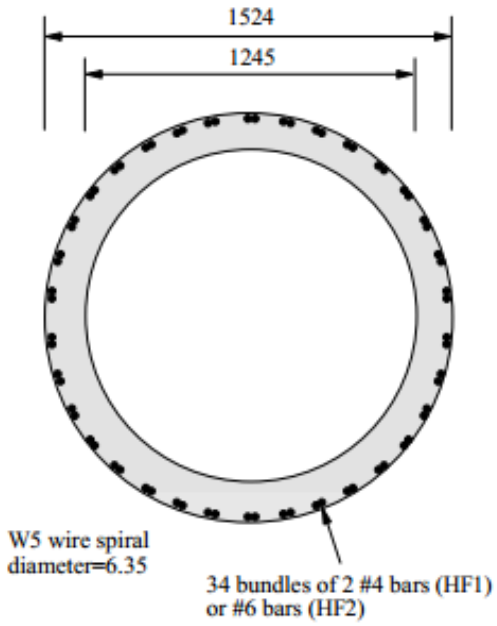

Figure 2-6: Hoshikuma and Priestley (2000) Specimen Dimensions (in mm, 1 mm = 0.0394 inch)

An analysis was also performed by the authors that attempted to model the results of the experimentation. The concrete was modeled using Mander's model and treating the concrete as biaxially confined. This method would ignore any radial stress contributed by the confinement, which they justified due to the radial stress being zero at the inside face. Only the circumferential stress was considered. The analysis showed good agreement to the experimental results, although the unit with less longitudinal reinforcement was predicted to fail due to crushing of confined concrete at the extreme fiber. The other specimen correctly predicted failure due to inside face concrete crushing. The measured transverse reinforcement strains during testing for both columns showed that the transverse reinforcement did not yield when the inside face failures had occurred. For the more ductile column, the transverse steel strain only reached 50 percent of yield, and for the less ductile column, the strain only reached 30 percent of yield. These reduced pressures were taken into account when the authors calculated the circumferential stress for the confined concrete properties in the analyses.

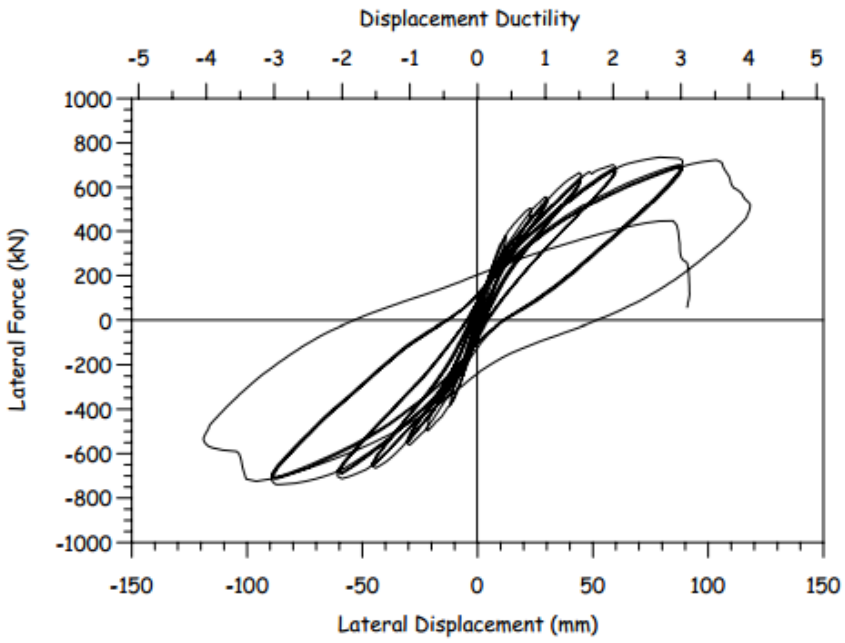

Figure 2-7: Hoshikuma and Priestley (2000) Specimen HF1 Force-Displacement Response (1 mm = 0.0394 inch, 1 kN = 0.225 kips)

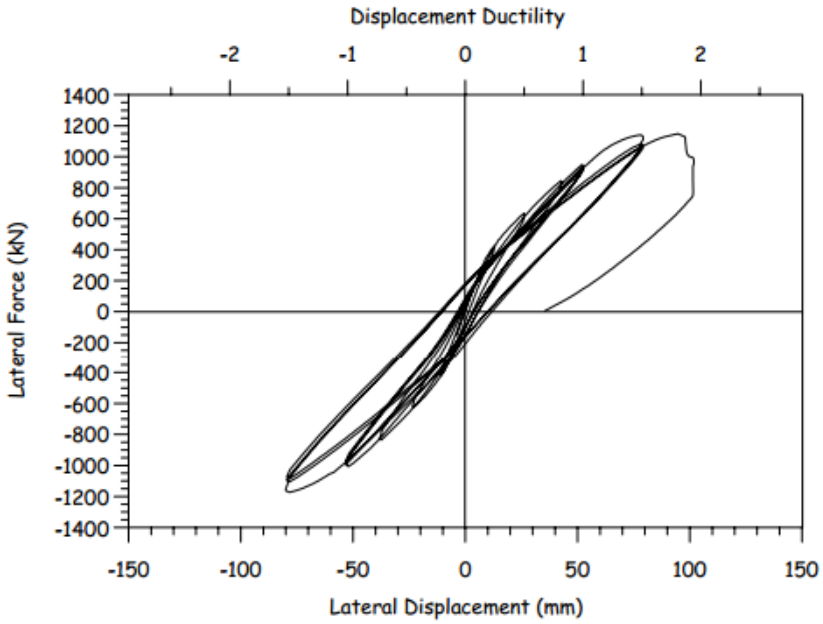

Figure 2-8: Hoshikuma and Priestley (2000) Specimen HF2 Force-Displacement Response (1 mm = 0.0394 inch, 1 kN = 0.225 kips)

The authors concluded that ductile behavior can be achieved when keeping the neutral axis within or near the inner face of the concrete wall, in order to prevent high compression strains at the inside face. They also recommend that the limit to ductility for a safe design of hollow columns with one layer of transverse reinforcement should be taken at a strain in the inside face concrete of 0.0035. Additionally, it was suggested that the confinement effectiveness should be reduced by using 1000 microstrain as the transverse steel strain for calculating the confinement pressure, since this was approximately the strain measured in the transverse reinforcement during testing.

The main focus of the research performed by Ranzo and Priestley (2001) was to study the shear strength of thin-wall circular hollow columns with one layer of transverse reinforcement. Although this topic is outside the scope of this research, it has been included due to the similarity and the flexural results of their test specimens. The research studied the accuracy of existing models in predicting the shear capacity of hollow columns. To determine the accuracy of these models, three full-size experimental columns were tested. The first column (labeled HS1) was designed to fail due to flexure and had a low amount of longitudinal reinforcement as well as low axial load. The remainder of the columns were designed with low shear reinforcement and were designed to fail in shear.

All of the specimens were cast on top of a rectangular footing, and the columns had a height of 152.8 inches. The first column was 61.4 inches in diameter with a wall thickness of 6 inches, and the next two were 60 inches in diameter with wall thicknesses of 5.5 inches. This corresponded to a wall thickness ratio of 0.098 for the first specimen and 0.092 for the other two. All specimens had 68 longitudinal bars, with the bars in the first specimen having a diameter of 0.51 inches and those in the other two having a diameter of 0.63 inches. For the first specimen, this corresponded to a longitudinal reinforcement ratio of 0.0047 to the gross section (0.013 to the net section), and for the others, the longitudinal reinforcement ratio was 0.0075 to the gross section (0.023 to the net section). All specimens had identical transverse reinforcement of a spiral composed of a 0.24 inch diameter bar spaced at 2.76 inches, for a transverse reinforcement ratio of 0.001 to the gross section (approximately 0.005 to net

section). The axial load was 275 kips for the first two specimens and 718 kips for the last specimen, which corresponded to axial load ratios of approximately 1.7 percent to the gross section (5 percent to the net section) for the first two specimens and 5.1 percent to the gross section (15.2 percent to the net section) for the third specimen.

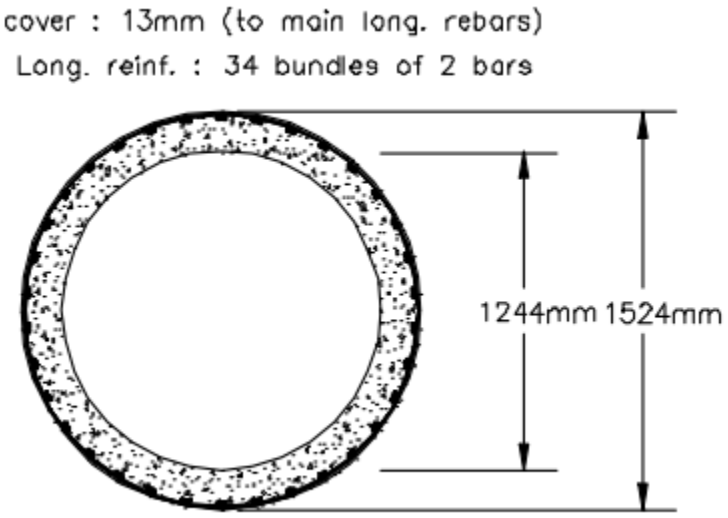

Figure 2-9: Ranzo and Priestley (2001) Specimen Dimensions (1 mm = 0.0394 inch)

The specimens were loaded cyclically under quasi-static loading until failure. The first specimen had a low longitudinal reinforcement ratio as well as low axial load ratio, and due to this fact, it experienced ductile behavior. Failure for this column occurred due to crushing of the inside face concrete at a displacement ductility of approximately six. Longitudinal reinforcement buckled near this ultimate point as well, which caused fracture at one point in the transverse reinforcement. The second specimen began to experience spalling of the inside face concrete at a ductility of three with a loss in applied lateral force of 25 percent. The inside face spalling led to reduced shear capacity and ultimately shear failure at ductility 3.5. The third specimen experienced significant inside face concrete spalling at a ductility of two, and ultimately failed due to crushing of the inside face concrete.

The measured force-displacement response of specimen HS1 is shown in Figure 2-10 as well as their analytical prediction. It is important to note that although the predicted failure point seems to coincide well with the actual failure point, the failure mode was incorrectly predicted. The failure point shown corresponds to tension strain in the longitudinal reinforcement of 0.06. Their analysis at this point indicated that the inside face concrete would be experiencing a tension strain of 0.001, indicating that the neutral axis would be within the wall. However, this was not the case as the actual test specimen failed due to crushing of the inside concrete face.

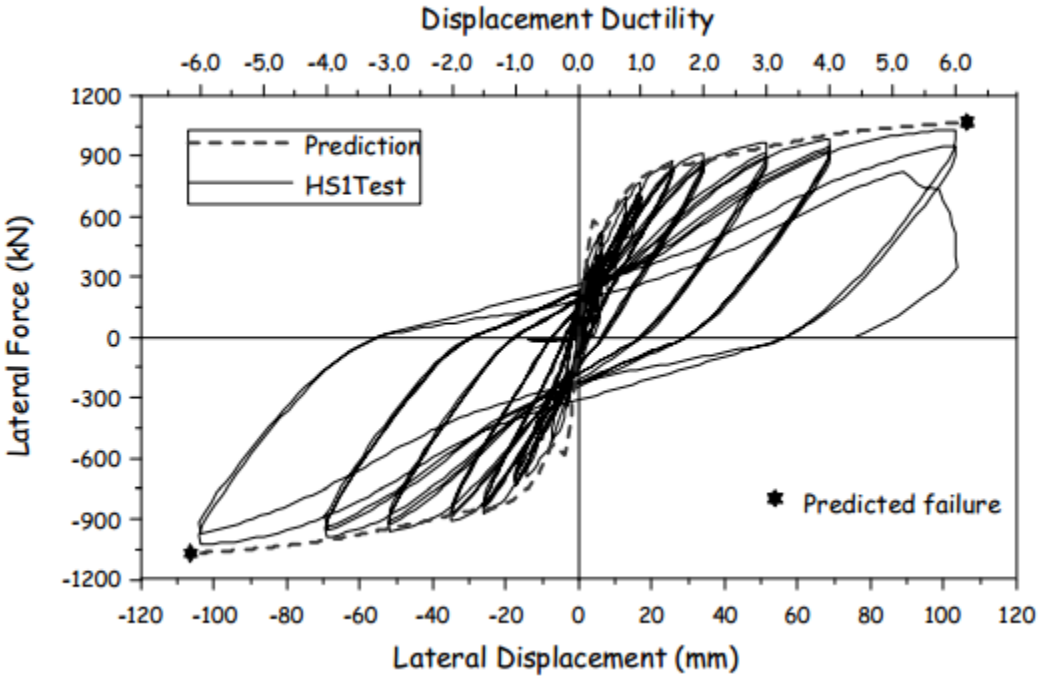

Figure 2-10: Ranzo and Priestley (2001) Specimen HS1 Force-Displacement Response (1 mm = 0.0394 inch, 1 kN = 0.225 kips)

The first specimen failed due to flexure, while the other two specimens seemed to have failed due to a combination of shear and flexure which caused failure of the inside concrete face. The research concluded that some shear models which estimate shear capacity based on transverse reinforcement yield can slightly overestimate the shear strength for hollow columns with one layer of transverse reinforcement, since they do not take into account the compression capacity of the inside face concrete. The report also suggests that a wall thickness

ratio of 0.1 can be a conservative design choice which avoids the possibility of buckling of the concrete tube.

An experimental program performed by Calvi et al. (2005) provides one of the only available sources of previous research into hollow square concrete columns with one layer of transverse reinforcement. The subject of this research was focused on the shear response of these specimens, and several different layouts of transverse reinforcement were tested. Several identical specimens were tested with outside dimensions of 17.7 inches square and wall thicknesses of 2.95 inches. The longitudinal reinforcement consisted of 24 bars 0.31 inches in diameter, and the transverse reinforcement was square hoops 0.12 inches in diameter and spaced at 2.95 inches. The section layout for these specimens can be seen labeled type 1 in Figure 2-11. Each specimen was subjected to a different amount of axial load. The axial loads were 56.2 kips, 112.4 kips, and 168.6 kips, corresponding to axial load ratios to the gross section (as if it were solid) of 3.6 percent, 10.4 percent, and 11.5 percent respectively. Columns with two layers of transverse reinforcement and similar axial loads were also tested, and the reinforcement arrangement of these columns is labeled as type two in Figure 2-11.

The research then compares several shear models to the results in order to determine which model most accurately predicts shear failure for hollow square columns. It was concluded that analytical methods for hollow columns are more accurate when flexure is governing the response, but when shear governs, it is difficult to accurately analyze the response. They also concluded that in the experimental program there was no indication of early flexural collapse at the inside face.

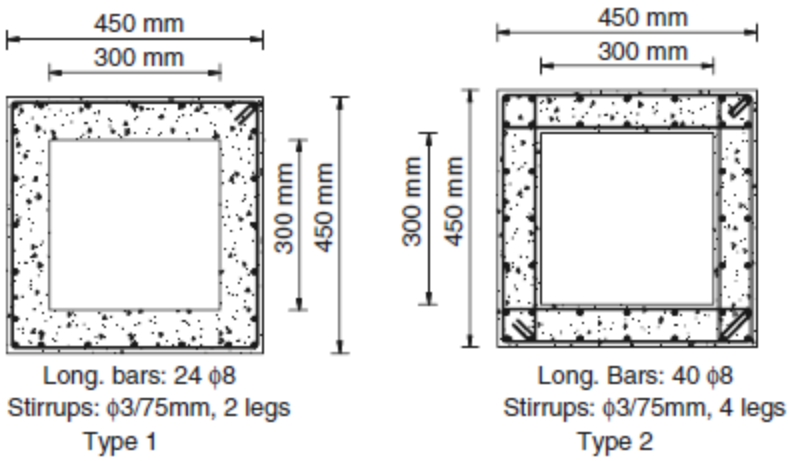

Figure 2-11: Calvi et al. (2005) Test Specimen Reinforcement Layouts (1 mm = 0.0394 inch)

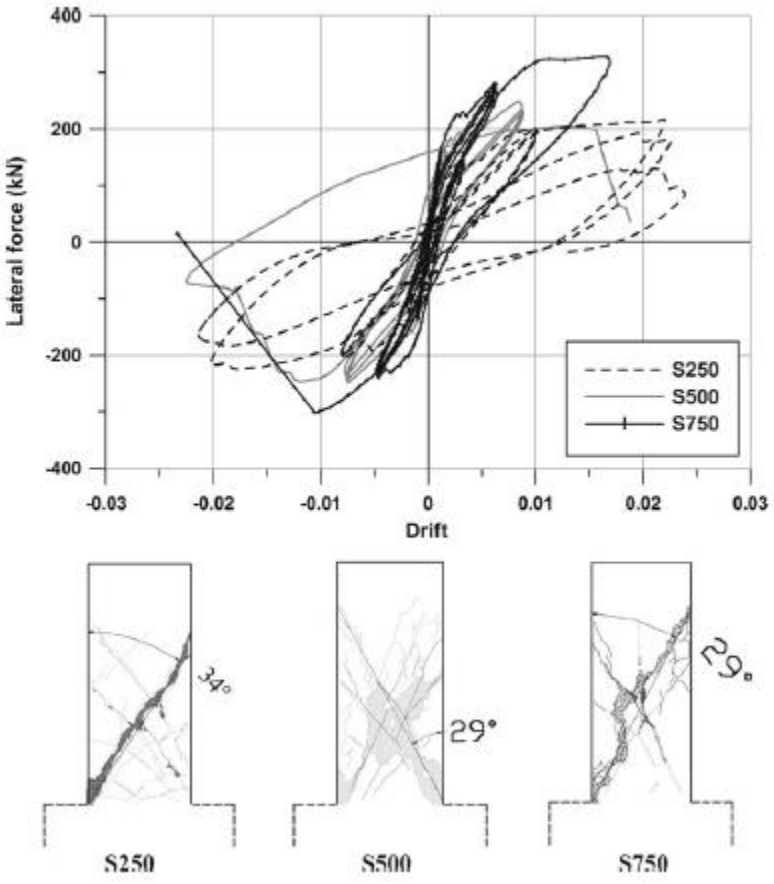

Figure 2-12: Calvi et al. (2005) Force-Displacement of Hollow Square Specimens with One Layer of Transverse Reinforcement (1 kN = 0.225 kips)

CHAPTER 3. ANALYSIS OF HOLLOW COLUMNS

3.1 Introduction

In order to ensure that bridge columns are able to resist the demand induced by the superstructure and earthquake motion, a section analysis is typically performed by bridge designers. The section analysis calculates the moment in the section at increments of curvature by determining the compression and tension forces in the section required to reach equilibrium. This process produces the overall moment-curvature response of the section. Since this process would be time-consuming to do by hand, bridge designers employ computer software to analyze the section. The software usually allows the designer to define a section composed of fibers or elements which represent steel and concrete material. Axial loads can then be applied to the section and the analysis is performed. The resulting moment-curvature analysis reflects the response at one section of the column. The displacement of the column at the top of the section is often needed in order to ensure code requirements are met. To determine the force-displacement response from the moment-curvature response, the curvature is integrated along the section or an empirical formula is used.

The method described above is commonly used since it is fairly simple to employ and not very time consuming. A similar method of analysis has been adopted by this research to ensure that the proposed modeling adjustments can produce accurate results for practicing engineers. This chapter will focus on the basis for the proposed method of modeling hollow columns as well as a comparison of the analysis method with previous test results. The next section will first propose a consistent terminology to use for hollow concrete columns to avoid confusion. The subsequent sections will describe the theoretical background, the modeling method, and the comparison of the analytical method to previous test results.

3.2 Definition of Key Variables

Before discussing the details of the analysis, it is important to define to how the section properties will be referred. In the past, there has been some confusion and disagreement

regarding a consistent way to define and describe parameters, such as the axial load ratio and reinforcing steel ratios. The main source of confusion is whether to define these ratios while ignoring the void (assuming that the void is filled and the column is solid) or including the void (using the net area of present concrete). The axial load ratio and reinforcing steel ratios may significantly increase if hollow sections are used for bridge columns based on net concrete area. Therefore, it is important to establish a standard to reduce confusion and to provide an appropriate way to compare hollow column behavior with that of solid columns.

As discussed in Chapter 1, hollow columns provide several benefits when compared to solid columns. These benefits are typically in the form of reduced mass and materials. In order for this to truly be a benefit, the hollow column must be approximately the same diameter as the solid column, or any reductions in mass and materials, due to the void, will be lost with the increase in mass and materials associated with increasing the diameter. For example, an axial load ratio of five percent is fairly typical for solid columns. If the axial load ratio for a hollow column is based on the net section, or the actual area of present concrete, then a five percent axial load ratio for a hollow column with a similar outside diameter to the solid column would mean that the axial load is significantly reduced for the hollow column. To hold the axial load of one column, it would be required to provide several hollow columns, and the reduction of mass would be negated. For this reason, it has been considered appropriate to define the section properties as if the hollow column was actually solid, in order to better compare between solid and hollow columns. The following terminology and variable definitions will be used throughout this paper.

Gross section = Area of section based on the outer diameter (as if section were solid)

Net section = Area of present concrete (gross section area with area of void subtracted)

$\rho_s = \frac{V_h}{V_{cg}} = \frac{4A_h}{d_s s}$ = Ratio of the volume of transverse reinforcement to the gross volume of concrete within transverse reinforcement.

$\rho_l = \frac{A_l}{A_g}$ = Ratio of area of longitudinal reinforcement to gross area of section

$\frac{P}{f_c' A_g}$ = Axial load ratio, the ratio of the axial load to the capacity of the section if it were solid

Defining the above variables in this manner will enable an easy comparison to the solid section in order to determine whether the hollow section can provide similar results. If desired, the above values can also be calculated to the net section in order to determine the ratio of axial load to the present concrete area. This can give a good idea of how much of the compressive strength of the concrete is being utilized by the axial load. However, using the gross section will enable easier comparison and determination of the viability of hollow columns relative to solid columns.

3.3 Simple Theoretical Investigation at Section Level

Several past research studies have been presented which study the behavior of hollow concrete columns with one layer of transverse reinforcement. This topic has not been investigated extensively, and available research is fairly limited. Experimental programs have been performed in the past, which have generally found that limited ductility can be achieved in hollow sections with the neutral axis located close to the concrete wall. This neutral axis location can be accomplished by providing a low axial load ratio and low amount of longitudinal reinforcement with a sufficiently thick wall. Several studies have attempted to provide a recommended wall thickness ratio, but this recommendation only holds for columns with similar dimensions and amounts of reinforcement, since the neutral axis location depends on the section properties as mentioned.

The previous research has also shown that the transverse reinforcement is not fully utilized, since low transverse reinforcement strains in the compression region have been reported. The experiment performed by Hoshikuma and Priestley (2000) found that the transverse

reinforcement only reached a maximum of 30 percent of the yield strain. This supports the work by Lignola et al. (2008), which suggested that hollow columns require less confining pressure to restrain the displacement. Previous testing of hollow columns with one layer of transverse reinforcement has also shown that in most cases, the transverse reinforcement does not fracture. In fact, the only reported fractures of transverse reinforcement of which the author is aware occurred in the testing by Ranzo and Priestley (2001), which was caused by outward longitudinal reinforcement buckling. This lack of hoop fracture seems to indicate that hollow columns are applying a much smaller demand to the confinement than solid columns typically do, and that failure of the inside face concrete usually controls. The lower confining pressure also suggests that the concrete near the transverse reinforcement may not be as well confined as that of concrete in solid columns, so the confinement might not be as effective as it is in solid columns. Currently it is unclear how to take this into account during the design and analysis of hollow columns with one layer of transverse reinforcement. It is also important to realize that past models, such as Mander's model, were developed for solid sections and were based on equilibrium equations, which hold true for solid sections. These models were verified based on pure axial compression tests of solid sections as well.

3.3.1 Equilibrium between concrete and transverse reinforcement

The development of confined concrete models by previous researchers has typically been based on the stresses that occur due to equilibrium between the concrete and transverse reinforcement. The theoretical background for Mander's model was developed by equating the stresses between concrete and steel under axial loading. The equilibrium equations enabled the determination of the stresses on the concrete, which could then be used with a triaxial confinement model to calculate the confined concrete properties. The equilibrium condition for hollow columns with one layer of transverse reinforcement can be calculated as well, and the equilibrium between concrete and transverse reinforcement for a circular column is shown in Figure 3-1.

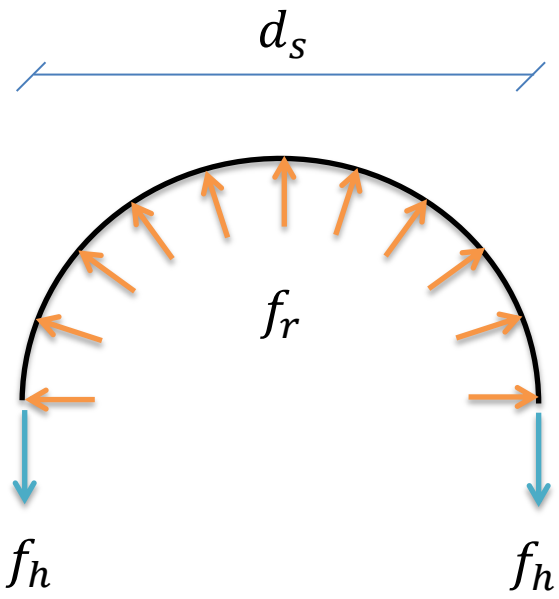

Figure 3-1: Radial Stress in Hollow Circular Columns with One Layer of Transverse Reinforcement

The dilation of the concrete induces strain in the transverse reinforcement and an associated hoop stress, f_h. This hoop stress is in equilibrium with the radial stress f_r. By equating the forces between the transverse reinforcement and the concrete, the following relationship can be found:

$$2f_h A_h = f_r d_s s \qquad \text{(Equation 3-1)}$$

$$f_r = \frac{2f_h A_h}{d_s s} \qquad \text{(Equation 3-2)}$$

Equation 3-2 relates the radial stress to the transverse reinforcement properties and the diameter of the confined concrete from the center of the hoop, d_s. This relationship does not depend on the diameter of the void, since it is simply a relationship between the concrete and steel at the location of the transverse reinforcement. This relationship is well known and has been used in the past by researchers such as Mander et al. in the development of the confined

concrete model. The radial stress is usually calculated at the yield stress of the transverse reinforcement, since this yield stress typically corresponds with the maximum stress of confined concrete, and since after yield, the transverse reinforcement stress can be assumed to remain constant.

A relationship for the circumferential stress in the concrete wall of circular hollow columns can also be found using equilibrium. As shown in Figure 3-2, the stress condition is similar to that of an arch, where the radial stress supplied by the transverse reinforcement must be supported at the base by the circumferential stress. Although it may not be entirely accurate the circumferential stress at the base of the arch can be assumed to be constant for simplicity. The circumferential stress can be related to the radial stress, as shown in Equation 3-3 through Equation 3-5.

$$2f_c t_s s = f_r d_s s \quad \text{(Equation 3-3)}$$

$$2t_s = d_s - d_i \quad \text{(Equation 3-4)}$$

$$f_c = \frac{f_r d_s s}{2t_s s} \quad \text{(Equation 3-5)}$$

Then using the relationship between the radial stress and the transverse stress given previously in Equation 3-2, the circumferential stress can be related to the hoop stress:

$$f_c = \frac{f_r d_s s}{2t_s s} = \frac{2f_h A_h}{2t_s s} = \frac{2f_h A_h}{(d_s - d_i)s} \quad \text{(Equation 3-6)}$$

As shown, this relationship depends on the diameter of the void. As the diameter of the void increases, the circumferential stress also increases. For a solid section, the diameter of the void is zero, and the relationship becomes:

$$f_c = \frac{2f_h A_h}{d_s s} \quad \text{(Equation 3-7)}$$

Equation 3-7 is identical to the equation given for radial stress in Equation 3-2, as it should be, since for a solid section, the in-plane stresses in perpendicular directions are assumed to be approximately equal. These relationships given above have been presented by several researchers in the past, including Hoshikuma and Priestley (2000).

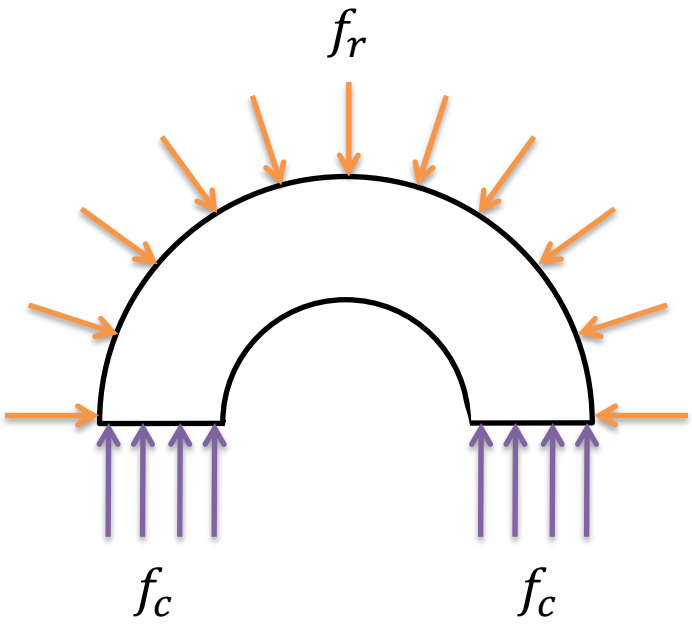

Figure 3-2: Circumferential Stress in Hollow Circular Columns with One Layer of Transverse Reinforcement

The radial and circumferential stress relationships indicate that for hollow circular columns with one layer of transverse reinforcement, the radial stress near the transverse reinforcement will be the same as that of a solid column for a given stress in the transverse reinforcement. However, for a hollow column, the radial stress will decrease when moving from the transverse reinforcement toward the void, until it must be zero at the free surface. The circumferential

stress will be larger for hollow circular columns than solid columns for a given transverse reinforcement stress.

For square hollow columns, the equilibrium is less straightforward and not as well understood, especially for square hollow columns with one layer of transverse reinforcement. The concept of confinement of solid square columns is similar to that of solid circular columns, where the concrete dilation is resisted by the transverse reinforcement. The matter becomes slightly more complicated due to the possibility of different arrangements of transverse reinforcement in square columns, where cross ties are often supplied in addition to the rectangular hoop around the perimeter. Despite this, equilibrium between the transverse reinforcement and the concrete can be estimated in a simplistic manner, as was done for the circular hollow columns. A simplistic representation of the equilibrium condition in hollow rectangular columns with one layer of transverse reinforcement is shown in Figure 3-3.

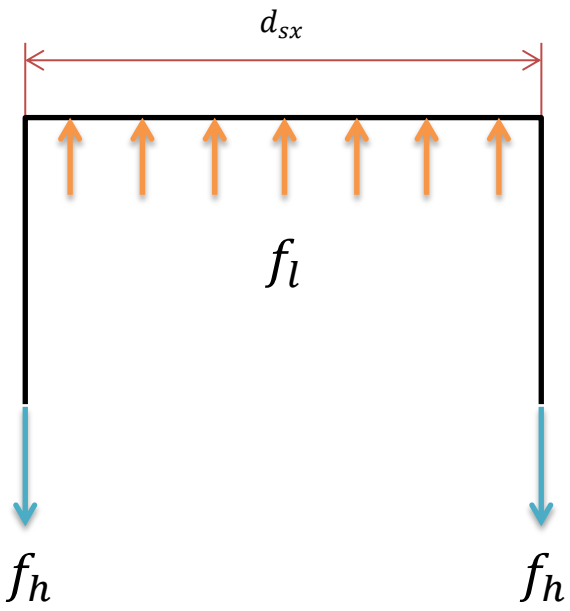

Figure 3-3: Approximate Equilibrium of Transverse Reinforcement in Hollow Rectangular Columns with One Layer of Transverse Reinforcement

An equilibrium equation can be written which relates the stresses in the transverse reinforcement to the lateral stress in the concrete, f_l. The resulting equations are similar to those presented for circular columns, and are as follows:

$$2f_h A_{hy} = f_{ly} d_{sy} s \quad \text{(Equation 3-8)}$$

$$f_{ly} = \frac{2f_h A_{hy}}{d_{sx} s} \quad \text{(Equation 3-9)}$$

Equation 3-9 presents a relationship which can be used to find the lateral stress applied to the concrete in the Y direction in the section by the transverse reinforcement. As shown, this stress depends on the yield stress of the transverse reinforcement, f_h, as well as the area of transverse reinforcement in the Y direction, A_{hy}. This stress is distributed over the area of the concrete surface, defined by the diameter from center to center of the transverse reinforcement at the perimeter of the section in the X direction, d_{sx}, as well as the spacing of the transverse reinforcement, s. The relationship presented above for the lateral stress has been presented previously by Mander et al. as the basis for determining the transverse stresses within a rectangular section. For a solid column, the lateral stress in the X direction would be calculated using the same relationship but with the dimensions in the X direction, as shown in Equation 3-10:

$$f_{lx} = \frac{2f_h A_{hx}}{d_{sx} s} \quad \text{(Equation 3-10)}$$

Equation 3-9 and Equation 3-10, presented above for f_{lx} and f_{ly}, are valid at the transverse reinforcement, essentially defining the lateral stresses around the perimeter of the confined concrete. These relationships do not depend on the dimension of the void and would hold true for both solid and hollow rectangular columns near the transverse reinforcement. However, in hollow rectangular columns, the lateral stress normal to the wall at the inside face must be zero, which means the lateral stress decreases from f_l at the transverse reinforcement to zero at the free surface.

Within a section of wall, there are two perpendicular stresses; one orthogonal to the transverse reinforcement, which has been defined as f_l. Equation 3-9 and Equation 3-10 have been provided to determine the approximate value of this lateral stress at the transverse reinforcement. The stress which occurs parallel to the transverse reinforcement within a wall section has been defined as f_p. Figure 3-4 illustrates this stress state within the wall of a hollow rectangular section. The stress f_p can be approximated in a manner similar to that of the circumferential stress f_c in hollow circular columns. If the section is cut in half, it can again be thought of as a structure similar to a frame, where the lateral loads applied to the concrete by the transverse reinforcement must be resisted by the supports, or the wall thickness in this case. In reality, there would likely be some stress concentrations and uneven stress distributions, especially at the corners. It has been assumed for simplicity that the stress is uniform across the wall thickness. The simplistic equilibrium state in the concrete, which has been assumed, is illustrated in Figure 3-5.

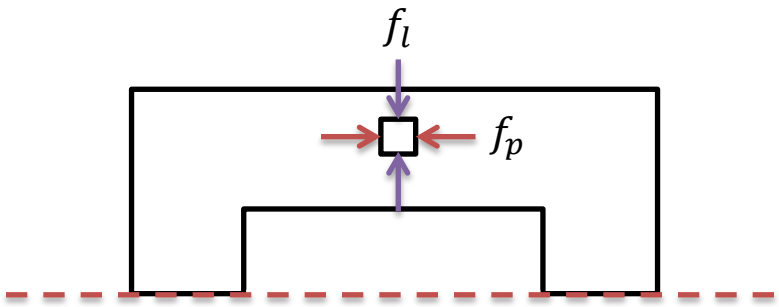

Figure 3-4: Stress State within Concrete Wall of Hollow Rectangular Columns

Using the equilibrium within the section, the stress parallel to the transverse reinforcement within a section of wall can be approximated. The resulting equations are similar to that of the circumferential stress in hollow circular specimens, and the equilibrium relationship for f_{py} is found in Equation 3-11:

$$f_{py} = \frac{f_{ly} d_{sx} s}{2 t_{sx} s} = \frac{2 f_h A_{hy}}{2 t_{sx} s} = \frac{2 f_h A_{hy}}{(d_{sx} - d_{ix}) s} \quad \text{(Equation 3-11)}$$

Similarly, the equilibrium relationship for f_{px} can be found as:

$$f_{px} = \frac{2 f_h A_{hx}}{(d_{sy} - d_{iy}) s} \quad \text{(Equation 3-12)}$$

As shown, the relationships for f_{px} and f_{py} depend on the dimensions of the void d_{ix} and d_{iy}. These equations indicate that as the void dimensions increase, so does the value of f_p. This means that hollow rectangular sections would theoretically have larger stresses parallel to the transverse reinforcement within the wall thickness than a solid section would in the same direction.

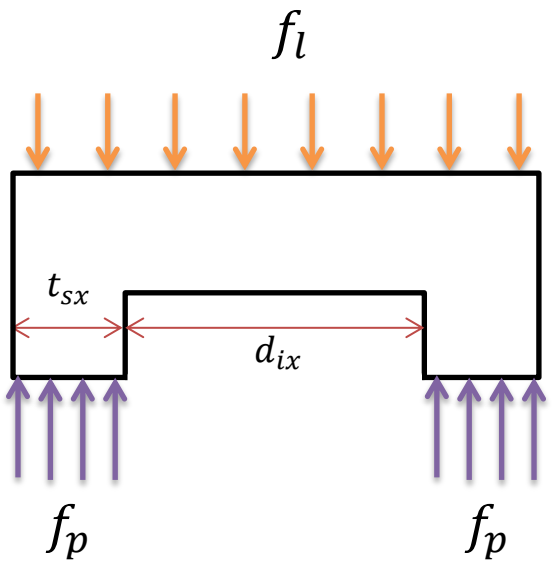

Figure 3-5: Stress Parallel to Transverse Reinforcement within the Concrete Wall of Hollow Rectangular Columns with One Layer of Transverse Reinforcement

It is important to note that these relationships for circular and rectangular columns are considered under pure axial compression. In reality, a column under flexure will only have a portion of the section experience compressive stress, and it is unclear if the same stresses will develop. Mander's model was developed based on pure axial compression, but it has been widely used and has been shown to produce safe design results for flexural tests of solid columns. Hollow columns under flexural conditions may not experience as large of transverse stresses as might be expected for hollow sections entirely under axial compression. Also, the circumferential stress distribution may not be uniform across the wall thickness, as was assumed. Additionally, as suggested by Lignola et al. (2008), since hollow columns require less confining pressure to limit radial displacement, it is not clear how much less radial stress is experienced by hollow columns since they have been shown to induce lower strains in the transverse reinforcement. The early failure of hollow columns at the inside face could also occur before the transverse reinforcement yields, causing further difficulty in predicting the confinement effects of hollow columns with one layer of transverse reinforcement.

3.4 Fiber-Based Analysis

The analysis of the hollow columns must be able to be performed using a method similar to the methods typically used in the engineering design process. For this reason, the Open System for Earthquake Engineering Simulation (OpenSees) was used for this type of analysis. OpenSees is a software framework developed by the Pacific Earthquake Engineering Research Center (PEER), which is capable of modeling and of analysis through the use of beam-column and other elements as well as uniaxial materials and section models. These modeling capabilities are combined with a wide range of algorithms and solution methods, which are capable of nonlinear analysis.

OpenSees is capable of performing both a fiber-based moment-curvature analysis as well as two and three dimensional analyses using beam-column elements. For this research, a two dimensional beam-column element analysis was chosen since this analysis is still based on a defined fiber section and since it directly calculates the force-displacement response. This was

more useful for modeling the results of the past research as well as the current experimental testing. Since the analysis is still based on a defined fiber-section, it will be comparable to the section analysis methods employed by practicing engineers.

The analysis was performed by creating the model geometry and defining a section or set of sections. The sections are made up of patched areas of uniaxial materials. Various material models are available within OpenSees, which represent different stress-strain models for materials such as concrete and steel. A section is patched with these uniaxial materials and the sections are then applied to the elements. The program then uses the section definition to apply stiffness and to determine the force-displacement response. It is able to analyze non-linear behavior by performing an iterative process between element deformation and the stress and strain behavior of the various section materials.

Since the program uses a 2D section to define the elements, this means it is able to model concrete and longitudinal steel, but is unable to model transverse reinforcement. Instead, the confined concrete material properties have to be applied directly. To achieve accurate results, the confined concrete model must be as realistic as possible. The stress state in the hollow section has been taken into account along with the findings of previous researchers in order to model the confinement effect of the concrete in hollow sections accurately.

To verify that the model was accurate, it was compared to previous experiments as well as the results of the current experiments discussed in Chapters 4 and 5. Due to the different experimentation types performed in previous literature and in this research, it was necessary to do both pushover analysis and beam loading analysis. The beam loading analysis was performed in order to model the experimentation presented in this research. Additionally, several different section types were modeled in order to better verify the model, including hollow and square columns with two layers of transverse reinforcement.

3.4.1 Section modeling and material properties

To produce accurate results, the inputs must be as accurate as possible. The section geometry and material stress-strain behaviors are key inputs that govern the analysis results. Section geometry can typically be defined fairly accurately due to the figures and information presented by past researchers and also using the design information for the experiments presented in this research. Providing accurate material stress-strain behavior is somewhat more challenging, especially due to the limited information presented in past research. Reinforcing steel especially plays an important role in these types of tests because it directly controls the section capacity, and also the ductility if tension steel failure occurs first. In order to ensure the experiments conducted in this report could be modeled accurately, tension tests were performed on the reinforcing steel to obtain the actual stress-strain behavior.

As mentioned previously, the program is unable to model transverse reinforcement, and the confined concrete properties must be input directly. Mander's model was used to define the confined concrete properties, with some adjustments made depending on the section geometry and configuration. These adjustments were based on the literature review and the findings of a finite element analysis performed in conjunction with this research Liang et al. (2015). Mander's model was then applied to the Concrete07 model (Chang & Mander, 1994) built into OpenSees by Waugh (2007). The Concrete07 model was used for all of the concrete, and the Steel02 (Filippou et al. 1983) model was used for all longitudinal reinforcing steel unless otherwise stated.

The section modeling method for hollow columns is discussed in this section. The modeling methods are discussed for hollow columns with both one and two layers of transverse reinforcement. Despite not being the focus of the research, the hollow columns with two layers of transverse reinforcement are discussed for comparison to the hollow columns with one layer of transverse reinforcement, and also due to the low amount of previous tests of hollow columns with one layer of transverse reinforcement. The modeling methods described in this section will be used in later sections to analyze and compare the response of previous experimental tests in order to verify the modeling and analysis methods. Four general modeling

arrangements were assumed based on the different confinement configurations and are discussed below.

3.4.1.1 One layer of transverse reinforcement

As discussed in the literature review, Mander's model calculates the confined stress-strain behavior based on the confinement stresses (confining pressure) in the transverse directions for sections under pure axial load. For a solid circular column, the radial and circumferential stresses are approximately equal throughout the section. The same is true for the lateral stresses of a solid square column, which has the same amount of transverse reinforcement in each direction. When the circular or square column has a void in the center these stresses are no longer equal.

3.4.1.1.1 Hollow circular columns

In Section 3.3.1 the calculation of the radial and circumferential confining stresses for circular columns was discussed. As shown, the radial stress at the transverse reinforcement does not depend on the void dimension, but the circumferential stress does depend on this void dimension. The radial stress will be the same between a solid and hollow circular section at the transverse steel yield point, since the transverse reinforcement will generate the same radial stress at yield. However, in the case of a hollow section, the radial stress will decrease in magnitude from the highest at where the transverse reinforcement is located to zero at the inside face since it is a free surface. This behavior has been demonstrated in a finite element analysis in collaboration with this research performed Liang et al. (2015), and can be approximated as a linear decrease from the transverse reinforcement to the void. The circumferential stress is caused by the radial stress acting on the concrete. The section can be cut along the centerline and thought of as an arch with a distributed load at the top coming from the transverse reinforcement confining pressure. This load is then distributed to the base of the arch. In the case of a solid column it is distributed along the entire base, but with a hollow section, the load is distributed along the wall thickness, creating larger stresses. This

concept is illustrated in Figure 3-6. The approximate stress distributions are illustrated in Figure 3-7.

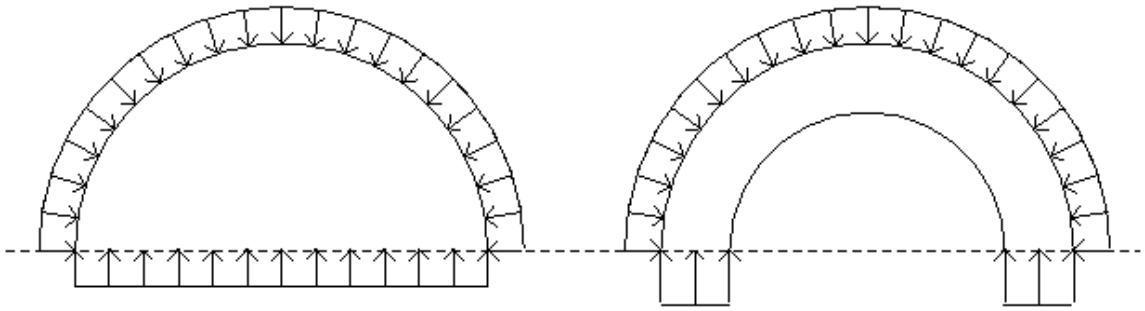

Figure 3-6: Circumferential Stress Distribution of Solid and Hollow Circular Columns

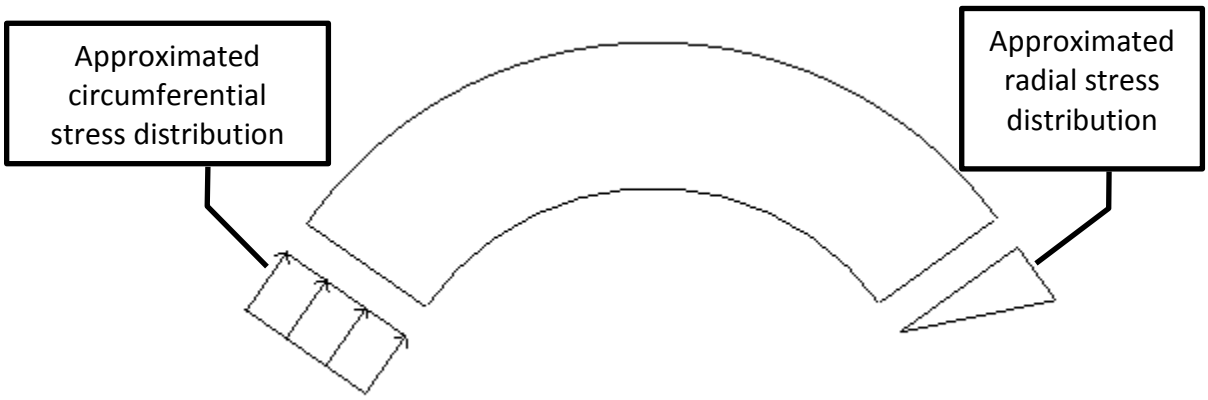

Figure 3-7: Approximated Stress Distributions in Hollow Circular Sections with One Layer of Transverse Reinforcement

Due to the fact that the radial stress decreases to zero at the void, previous researchers assumed the concrete was only biaxially confined, therefore neglecting the radial stress and only taking into account the axial and circumferential stress. However, this is a very conservative assumption. Essentially, the radial stress will be similar to a solid section near the

transverse reinforcement when the reinforcement yields, but decreasing to zero near the void. Additionally, the circumferential stress will be significantly higher for a hollow section, equating to an increase in circumferential stress of $\frac{d_s}{2t_s}$. The equations shown below illustrate this, based on the relationship for circumferential stress discussed previously.

$$f_c = \frac{2f_h A_h}{(d_s - d_i)s} \quad \text{(Equation 3-13)}$$

For a solid section d_i = 0:

$$f_{c,solid} = \frac{2f_h A_h}{d_s s} \quad \text{(Equation 3-14)}$$

The circumferential stress of a hollow section relative to a solid section can then be found as:

$$\frac{f_{c,hollow}}{f_{c,solid}} = \frac{2f_h A_h}{(d_s - d_i)s} * \frac{d_s s}{2f_h A_h} = \frac{d_s}{d_s - d_i} \quad \text{(Equation 3-15)}$$

This can be related to the wall thickness within the confinement instead of the difference in diameter:

$$2t_s = d_s - d_i \quad \text{(Equation 3-16)}$$

Substituting this into the circumferential stress ratio between solid and hollow specimens gives:

$$\frac{f_{c,hollow}}{f_{c,solid}} = \frac{d_s}{2t_s} \quad \text{(Equation 3-17)}$$

This ratio indicates that a hollow column under axial compression will experience larger circumferential stress than that of a similar solid column. For example, a specimen with a

diameter of confinement from center to center of 12 inches, and a wall thickness within the confinement of 2 inches, would experience $\frac{12}{2(2)}$ or 3 times the circumferential stress as a solid section with the same transverse reinforcement. The increase in stress indicates the concrete has high stress in the circumferential direction, but slightly lower stress in the radial direction. Near the inside face, the concrete is biaxially confined due to the high circumferential stress but lack of radial stress.

The conditions described hold true under pure axial compression. However, when subjected to flexure it becomes less clear how the stresses form. Only a portion of the transverse reinforcement will be restraining radial displacement, so only the compressed portion of the concrete will experience radial stress. This also means that the circumferential stress is likely not as high as under pure axial compression, since there is less overall radial stress when the specimen is under flexure. Therefore, it may not be accurate to account for large circumferential stresses in the concrete, since doing so may cause an overestimation of the confinement stresses.

An additional factor affecting the confinement of hollow columns is the increased deformability of the section. As discussed by Lignola et al. (2008) in the literature review, a hollow column requires less radial pressure to restrain displacement compared to a solid column. If solid and hollow columns with identical reinforcement are subjected to the same axial strain, the solid column will experience larger radial displacement, equating to larger hoop strain and larger radial stress. This idea is supported by the collaborative finite element analysis (Liang et al., 2015), which showed that the radial displacement for sections with identical reinforcement was higher for specimens with larger wall thicknesses at the same axial strains. This concept indicates that transverse reinforcement would not yield until higher axial strains when compared to a solid section with the same transverse reinforcement. The experimental testing performed by Hoshikuma and Priestley (2000) supports this claim, since their hollow test specimens showed that the transverse reinforcement had only reached 30 percent of the yield strain when the specimens failed due to the inside face crushing.

These observations have shown that for hollow columns, the concrete is well confined near the transverse reinforcement but not well confined near the inside face. Additionally, the axial strain at which yield of transverse reinforcement occurs is higher than that of a solid column. Essentially for the compression concrete, there are two controlling limits: failure of the confined concrete due to hoop fracture and failure of the concrete near the void. The location of the neutral axis, the transverse reinforcement quantity, and the concrete strength will control which occurs first. Since the radial stress changes over the wall thickness, it may be more accurate to divide the wall thickness into sections with different confined concrete properties to model the behavior. Ideally, a large number of sections would be used; however, the small increase in accuracy would not justify the significant increase in modeling and solution time, and it would not be feasible for design purposes. For this reason two sections have been used to approximate the radial stress distribution, which correspond to the controlling limits of the transverse reinforcement rupture and the inside face failure.

Figure 3-8 illustrates the two regions chosen. The thickness of each section corresponds to half the distance between the inside face and the center of the confinement reinforcement. The section near the inside face is conservatively modeled as unconfined concrete, neglecting the confinement contribution due to the circumferential stress as well as the small amount of radial stress near the inside face. The crushing of the inside wall has been shown to be brittle, so providing a conservative estimate has been deemed by this research to be appropriate, especially since it is unclear if high circumferential stresses actually develop under flexure. For the concrete near the transverse reinforcement, the confined concrete properties have been estimated using Mander's model with an adjustment factor to account for the reduced radial stress due to the lower radial displacement of hollow columns. Instead of explicitly calculating the stresses in both directions (circumferential and transverse), it has been assumed that the circumferential stress is equivalent to the adjusted radial stress. This assumption has been made since it is unclear how much circumferential stress develops under flexure.

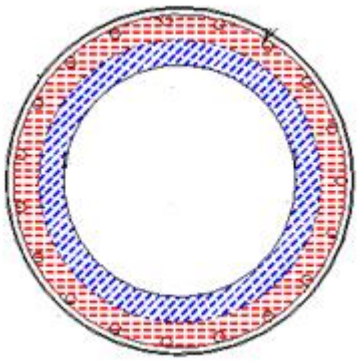

Figure 3-8: Regions for Unconfined and Confined Concrete for Circular Hollow Columns with One Layer of Transverse Reinforcement

Based on results of the finite element analysis of hollow columns (Liang et al., 2015), a simplified adjustment to Mander's model has been found for the outer layer modeled as confined concrete. The analysis showed that Mander's model more closely matched the stress-strain from the finite element analysis when a reduction in radial stress was used. This reduction in radial stress has been taken into account by a hollow column confinement effectiveness factor, similar to the confinement effectiveness factor k_e used by Mander's model. The hollow column confinement effectiveness factor proposed, k_h, can be found for circular columns using Equation 3-18.

$$k_h = \frac{t}{d} + 0.45 \qquad \text{(Equation 3-18)}$$

The calculation for the confined concrete properties in the layer of concrete near the transverse reinforcement is performed using Mander's model as if the column were solid. The factor adjusts the calculated radial stress for a solid column with the same outside dimensions and reinforcement details to estimate what the radial stress would be for the hollow column. The only difference in the standard Mander's model procedure occurs when calculating the effective radial stress f_l'. The calculation of f_l' for hollow columns would be done as shown in Equation 3-19.

$$f_l' = k_e k_h f_l \quad \text{(Equation 3-19)}$$

The confined concrete properties are then calculated in the usual manner using this adjusted effective radial stress. An example of this procedure is provided in Section 6.3.

3.4.1.1.2 Hollow rectangular columns

The theoretical calculation of the lateral stress near the transverse reinforcement, f_l, as well as the stress within the wall, which is parallel to the transverse reinforcement, f_p, has been demonstrated for rectangular columns in Section 3.3.1. As described, the lateral stress will be largest at the location of the transverse reinforcement and will decrease to zero at the inside face in a hollow rectangular column. The stress within the wall parallel to the transverse reinforcement will theoretically be higher for hollow rectangular sections than solid rectangular sections, due to the presence of the void. However, these relationships were described for pure axial compression, and it is unclear how well they describe the behavior when the columns are subjected to flexure. Additionally, it is not clear how much demand is actually applied to the transverse reinforcement due to the presence of the inner void. Other factors such as stress concentrations at corners or non-uniformity of stresses within the wall are not taken into account in the simple theory.

Due to the unknowns described for hollow rectangular columns with one layer of transverse reinforcement, additional finite element analysis was performed as part of this project (Liang et al., 2015). It was found that the lateral stress near the transverse reinforcement for hollow square columns with one layer of transverse reinforcement was significantly reduced when compared to solid square columns with the same reinforcement details and overall dimensions. It was also found that the dimension of the void had little effect on this lateral stress. Based on this, a constant hollow column confinement effectiveness factor, k_h, of 0.28 was proposed for hollow square columns with one layer of transverse reinforcement. This adjustment factor would then be applied, as described for hollow circular sections, as an adjustment to the calculation of the effective lateral stress in a solid rectangular column for use in Mander's

model. Mander's model would be used as if the column were solid, with the adjustment factor, k_h, of 0.28 applied when calculating the effective lateral stress. This hollow column effectiveness factor is applied in addition to the confinement effectiveness factor, k_e, proposed by Mander et al. The value of k_e for rectangular sections is typically used as 0.75 as suggested by Priestley et al. (1996).

The section modeling method proposed for rectangular columns with one layer of transverse reinforcement is similar to that of circular columns with one layer of transverse reinforcement. Since the lateral stress decreases to zero at the void, the changing stress state is approximated by two different regions of concrete, as shown in Figure 3-9. The hashed area near the void is modeled as unconfined concrete, while the hashed area near the transverse reinforcement is modeled as confined concrete with the adjustment to Mander's model applied, as described.

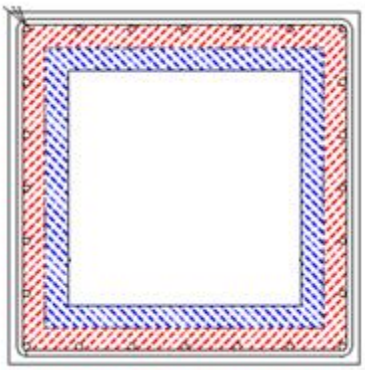

Figure 3-9: Regions for Unconfined and Confined Concrete in Rectangular Hollow Columns with One Layer of Transverse Reinforcement

3.4.1.2 Two layers of transverse reinforcement

Although the focus of this research is on hollow columns with one layer of transverse reinforcement, a discussion of hollow columns with two layers of transverse reinforcement has been included to illustrate the differences between the confinement methods, as well as to

provide further validation for fiber-based analysis. The more common confinement method for hollow columns is to provide two layers of transverse reinforcement, one near the outside face and one near the inside face. These layers are typically connected with cross-ties, and this type of arrangement does not experience the problem of zero radial stress at the inside face like hollow columns with one layer of transverse reinforcement do. Both circular and rectangular columns can be designed with this arrangement, and the calculation of confined concrete properties for these columns is described in this section.

3.4.1.2.1 Rectangular columns with two layers of transverse reinforcement

The confinement effect in solid rectangular hollow columns is calculated somewhat differently than that for circular columns, especially for rectangular solid columns with different amounts of transverse reinforcement in the X and Y directions. Additional interlocking hoops are often provided in these columns, as well as hoops which are oriented at an angle as shown in Figure 3-10.

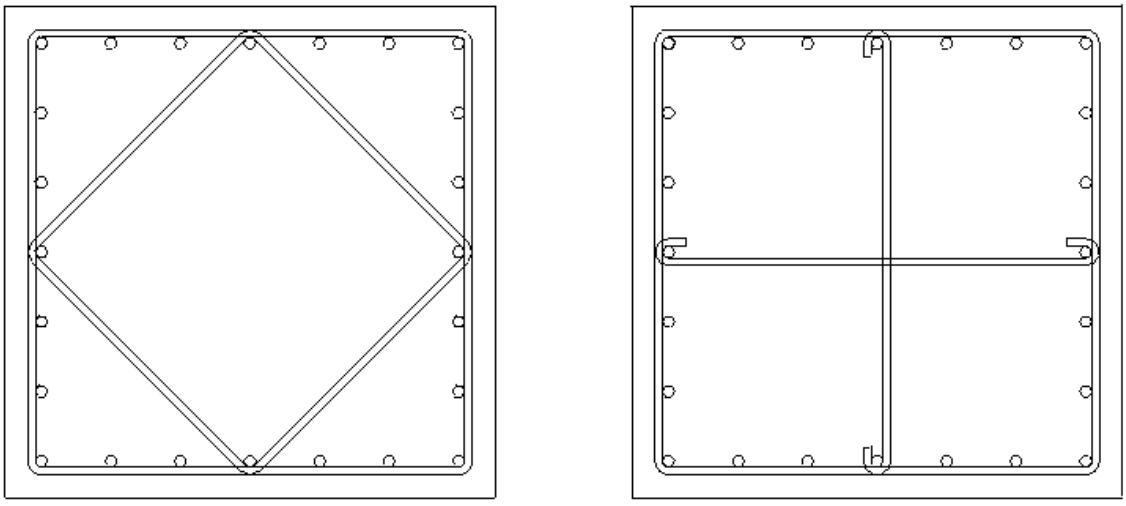

Figure 3-10: Possible Transverse Reinforcement Arrangements in Solid Rectangular Columns

When calculating the confined concrete properties for these columns using Mander's model, the procedure involves separating the amount of transverse reinforcement into X and Y components. These components are then used to calculate transverse reinforcement ratios in each direction, and then the stresses in each transverse direction. Finally, the stresses are used with Figure 3-11, which was provided by Mander et al. to determine the confined concrete properties, where f'_{l1} and f'_{l2} are the lateral stresses in orthogonal directions.

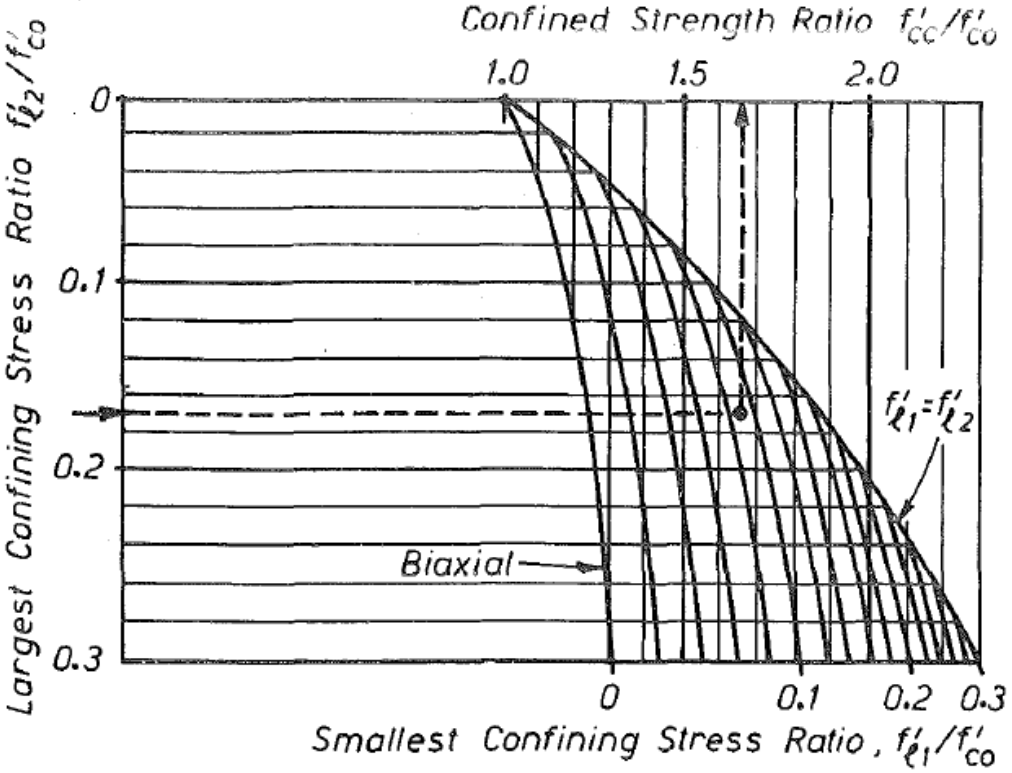

Figure 3-11: Confined Concrete Strength from Lateral Confining Stress [Mander et al. (1988)]

For hollow rectangular sections, the provision of two layers of steel is often achieved by providing rectangular hoops or multiple ties within each wall. A configuration of rectangular hollow columns where the transverse reinforcement is provided by overlapping hoops is shown in Figure 3-12. When estimating the confined concrete properties for these arrangements, the columns can be thought of as four separate wall sections. Once this assumption has been

made, the confined concrete properties can be estimated by treating each of these wall sections as a solid rectangular column, and calculating the confinement properties in each direction of this separate piece. See Figure 3-12 for an example of the separation of a hollow column with two layers of transverse reinforcement into individual wall sections.

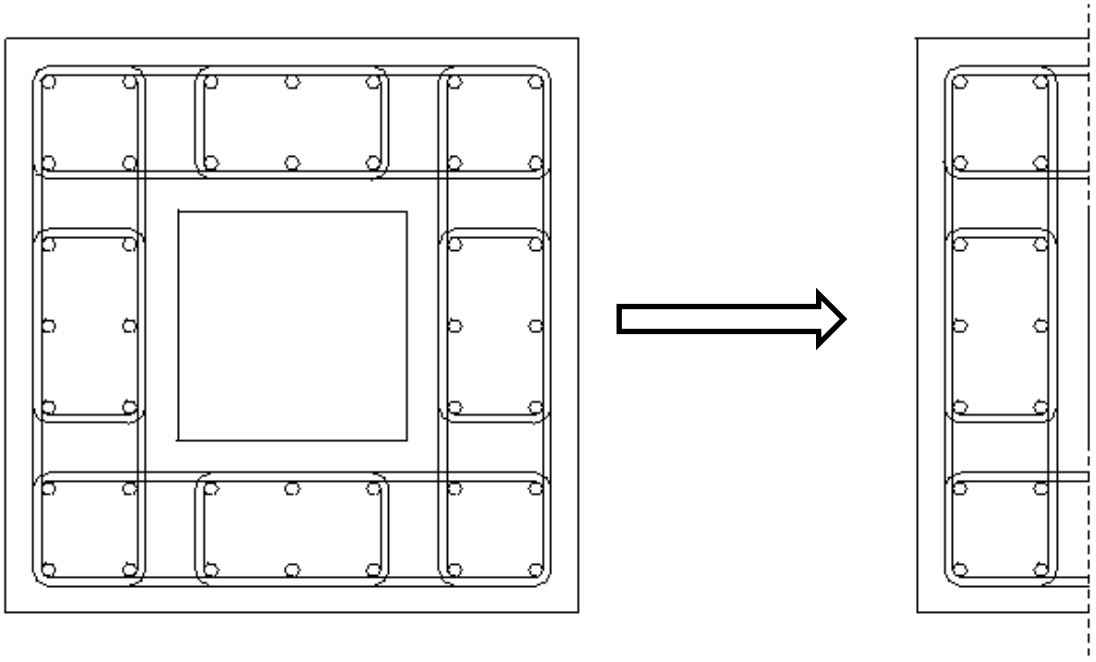

Figure 3-12: Hollow Rectangular Section Confined with Overlapping Hoops and Separation into Individual Wall Section

3.4.1.2.2 Circular columns with two layers of transverse reinforcement

The calculation of confined concrete properties in circular hollow columns with two layers of steel is not as well understood as that of rectangular hollow columns. The finite element analysis performed in collaboration with this research (Liang et al., 2015) has shown that the cross-ties between the inner and outer layer are essential to make the inner layer of confinement useful. These cross-ties have been assumed to transfer much of the demand to the outer layer of confinement. The finite element analysis suggests this is the case since two

layers of steel without cross-ties experiences early failure due to the inner layer of confinement pulling through the inner cover.

Since the cross-ties seem to transfer the demand to the outer layer of confinement, it has been deemed appropriate to model the confined concrete by using the area of both the inner and outer confinement hoop when calculating the transverse reinforcement ratio. Unlike for hollow columns with one layer of transverse reinforcement, the transverse reinforcement ratio is taken to the net area of concrete. This method has been used since it is similar to the square hollow columns with two layers of transverse reinforcement, where the wall can be thought of as an individual column. If you take a wall segment of a hollow circular column, it could similarly be thought of as an individual column of curved shape. The wall section is confined on both sides, so using the net area of concrete more accurately reflects the demands supplied to the transverse reinforcement.

3.4.2 Model verification

An analysis of previous test specimens was performed to verify that the suggested modeling methods can provide accurate results. Several previous experiments were selected in order to attempt to verify each type of arrangement (hollow sections with one layer of transverse reinforcement and hollow sections with two layers connected with effective cross-ties, both circular and square). Previous experiments were typically chosen for use if they experienced a flexural failure, since this would provide a more appropriate comparison to the model.

As discussed previously, providing accurate stress and strain behavior for the material models is very important to produce accurate results. Past researchers have often only reported tension steel yield stress and ultimate stress values without corresponding strain values, which cause difficulties in producing accurate analysis response in the nonlinear range. When using past research to check the accuracy of the analysis, the studies that provided more information about stress and strain of steel were used whenever possible.

3.4.2.1 Hollow circular with one layer of transverse reinforcement

Two specimens were tested by Hoshikuma and Priestley (2000), which were described previously in the literature review. A pushover analysis was performed for these specimens. The specimens were identical in section except for different amounts of longitudinal reinforcing steel. The sections can be seen below in Figure 3-13.

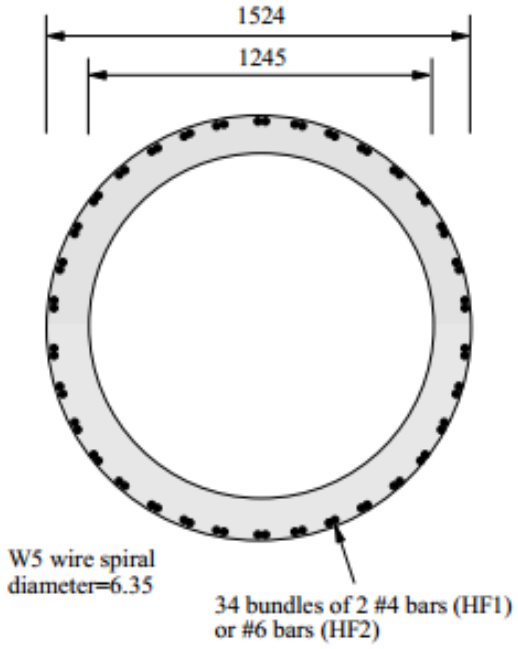

Figure 3-13: Cross-Section Dimensions (in mm) of the Hollow Column Tested by Hoshikuma and Priestley (2000), (1 mm = 0.0394 inch)

The specimens were cast as a hollow column with a foundation block at the base. A steel tube was attached to the top of the column to extend the column further, and the load was applied near the end of this steel tube. The steel tube was designed to remain in the elastic range during testing. The column was modeled with a nonlinear beam-column element, and the column to foundation interface was modeled using a section with a strain penetration model [i.e. using Bond_SP01 in OpenSees (Zhao & Sritharan, 2007)]. The base of the column below the strain penetration section was modeled as a fixed end. The loading steel tube was modeled using an elastic beam-column element. Two specimens were tested, with the same geometry and materials except for a differing amount of longitudinal steel. Sets of two bundled bars were

used for longitudinal steel, and each of these was modeled as a single bar of equivalent area. Axial load was also applied identically to that applied in the experiment, with axial load of 654.9 kips being applied to specimen HF1 and axial load of 673.8 kips applied to HF2.

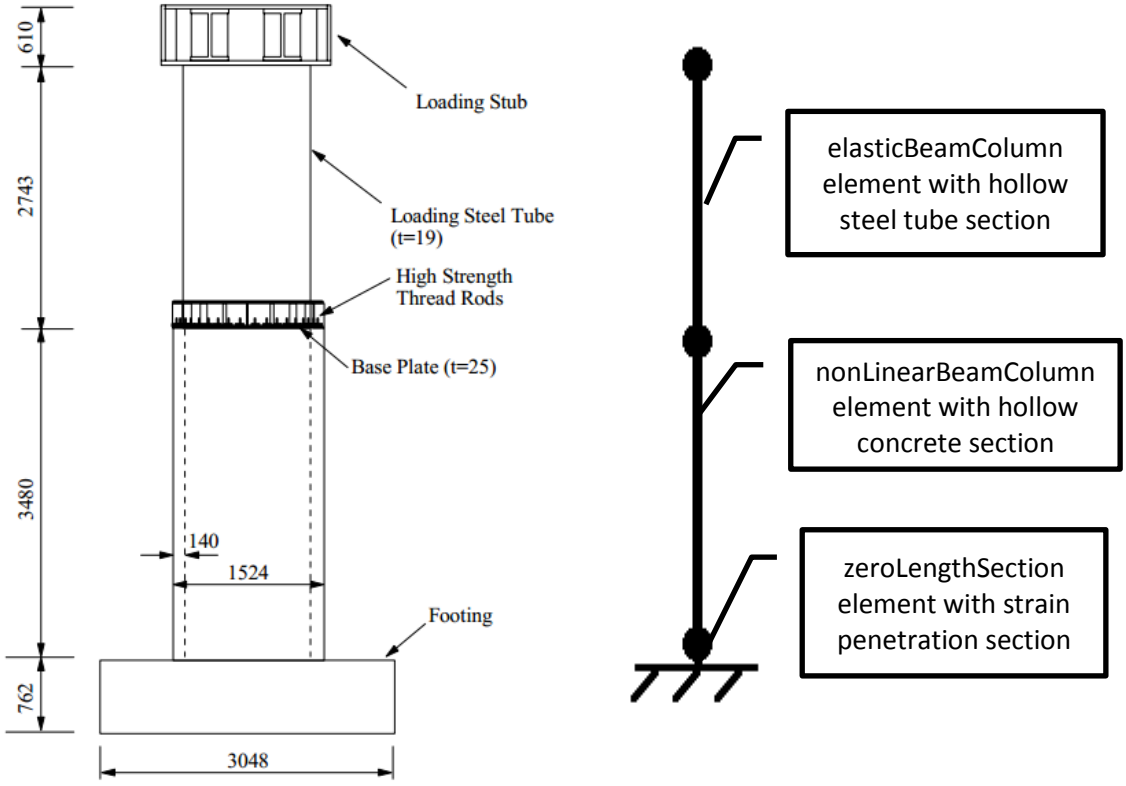

Figure 3-14: Test Setup of Hoshikuma and Priestley (2000) and Corresponding Model Configuration (Dimensions in mm), (1 mm = 0.0394 inch)

The section material models were defined, as described in Section 3.4.1.1, with two layers of concrete used to represent the inner unconfined layer and the outer confined layer. A pushover analysis was then performed for the modeled properties. The results of the analysis of the two test units can be seen in Figure 3-15. The experimental results are reported using a plot digitzer to extract the force-displacement envelope from the cyclic force-displacement presented in their research.

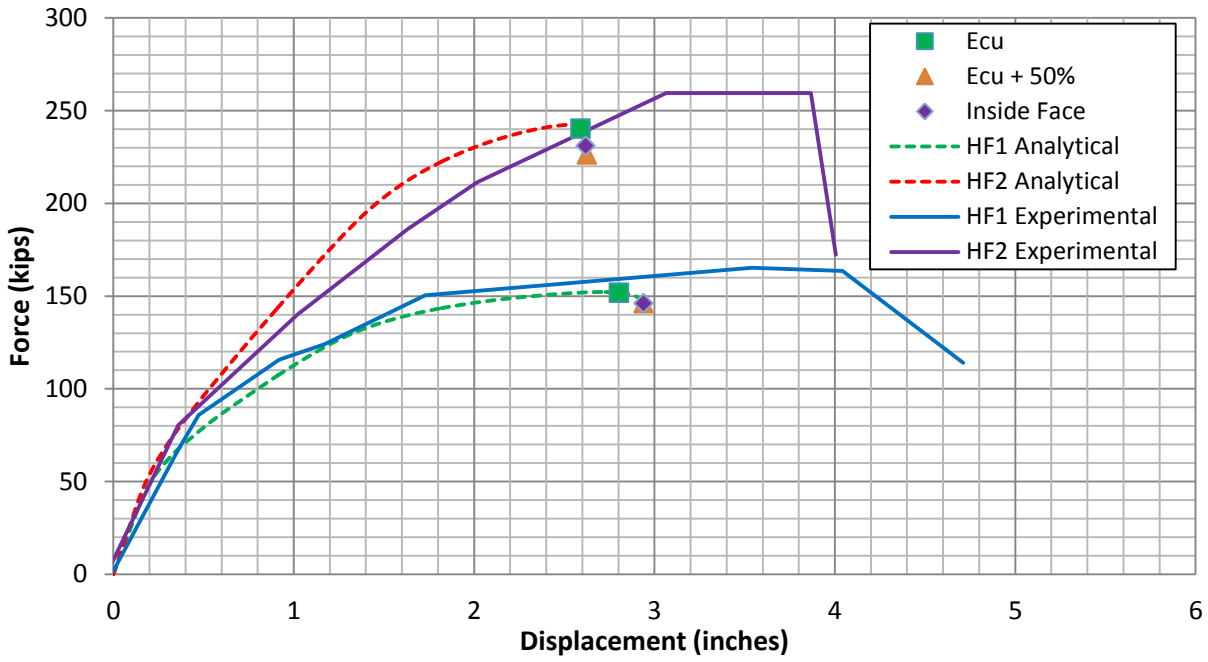

Figure 3-15: Comparison between Current Analysis and Experimental Results of Specimens HF1 and HF2 Tested by Hoshikuma and Priestley (2000)

The analysis matches fairly well with the experimental results, except for the early failure of the analytical columns. Shear deformation was not accounted for in the analysis, and this may be contributing to the difference in the ultimate failure prediction. The predicted failure modes are plotted on the analysis as well. The actual specimens failed due to crushing of the concrete at the inside face. The analysis predicts that the confined concrete near the transverse reinforcement reaches the ultimate strain, which is calculated by the following equation proposed by Priestley et al. (1996):

$$\varepsilon_{cu} = 0.004 + \frac{1.4\rho_s f_{yh} \varepsilon_{su}}{f'_{cc}}$$

Priestley et al. (1996) also state that this equation can often be conservative by at least 50 percent. For this reason, the ultimate strain of confined concrete predicted by this equation has been increased by 50 percent and has been considered as another possible failure point plotted in Figure 3-15 as well. The possible failure points predicted by the ultimate strain of confined

concrete, and the ultimate strain of confined concrete increased by 50 percent, have been labeled in this and future plots as “Ecu” and “Ecu + 50%”, respectively.

The next failure mode predicted is the crushing of the inside face concrete, which agrees with the failure mode of the tested columns. Crushing of inside face concrete was considered to occur at a strain of 0.005 at the inside face, as suggested by Hoshikuma and Priestley (2000). The last point shown indicates the point where the ultimate confined concrete failure is considered, when increased by 50 percent to account for the conservatism of the ultimate estimate.

It is interesting to note that the equation proposed by Priestley et al. (1996) predicts failure of the confined concrete at approximately the same displacement as that of the prediction of the failure of the inside concrete face in Figure 3-15. Even when the prediction of failure of the confined concrete is increased by 50 percent, to account for conservatism in the estimate, this predicted failure still occurs at a similar displacement as that of the inside concrete face crushing. The experimental results of these tests showed that the confinement had only reached 30 percent of the yield strain when inside concrete face crushing occurred. This seems to indicate that estimates of the ultimate confined concrete strain are extremely conservative for hollow columns, due to the lower demand applied to the transverse steel by hollow columns.

3.4.2.2 Hollow square with one layer of transverse reinforcement

Several specimens were tested by Calvi et al. (2005) which were described previously in the literature review. The testing performed in the reported research is some of the only testing of hollow rectangular columns with one layer of transverse reinforcement available in the literature. Although this reported research focused on the shear response of the specimens, it has been used as an approximate verification of the analysis method due to the lack of previous testing of these columns.

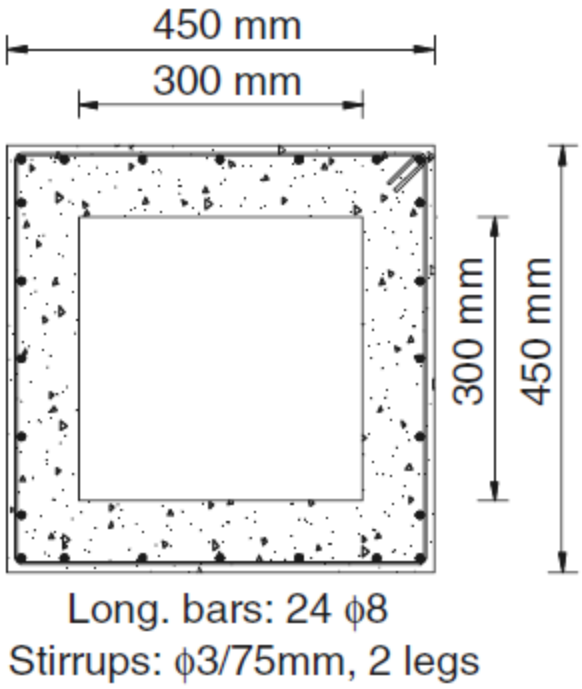

Figure 3-16: Cross-Section Dimensions and Reinforcement Layout of Square Hollow Columns with One Layer of Transverse Reinforcement Tested by Calvi et al. (2005), (1 mm = 0.0394 inch)

Several different transverse reinforcement layouts were tested by Calvi et al., but the analysis was compared to the sections with one layer of transverse reinforcement, which had the dimensions and reinforcement configuration pictured in Figure 3-16. One of the tested specimens was chosen to be analyzed using the described analysis method. The specimen was labeled S250, and was subjected to 56.2 kips of axial load. The axial load was held constant throughout the testing. The research reported that the longitudinal and transverse reinforcement used in the specimen had yield stresses of 80 ksi, with ultimate stresses of approximately 97 ksi. A corresponding ultimate strain was not reported, so a fairly typical value of 0.08 was assumed. The concrete compressive strength was reported to be approximately 5 ksi. The test unit was 35.4 inches tall and cast on top of a foundation block. The specimen was tested under cyclic lateral loading at the top of the column with constant axial load applied.

The described section dimensions and properties were modeled using the procedure described in Section 3.4.1.1.2, including the use of two layers of concrete within the transverse reinforcement. The layer near the void was modeled as unconfined concrete, and the layer near the transverse reinforcement was modeled as confined concrete. The concrete properties for the layer of confined concrete were estimated using Mander's model, with the hollow column confinement effectiveness factor of 0.28 applied. Due to convergence issues for this specimen, the concrete was modeled using the Concrete02 model (Mohd Yassin, 1994) built into OpenSees. The analysis was then performed, and the resulting force-displacement response of the test unit and analysis are shown in Figure 3-17, along with several possible failure modes predicted by the analysis.

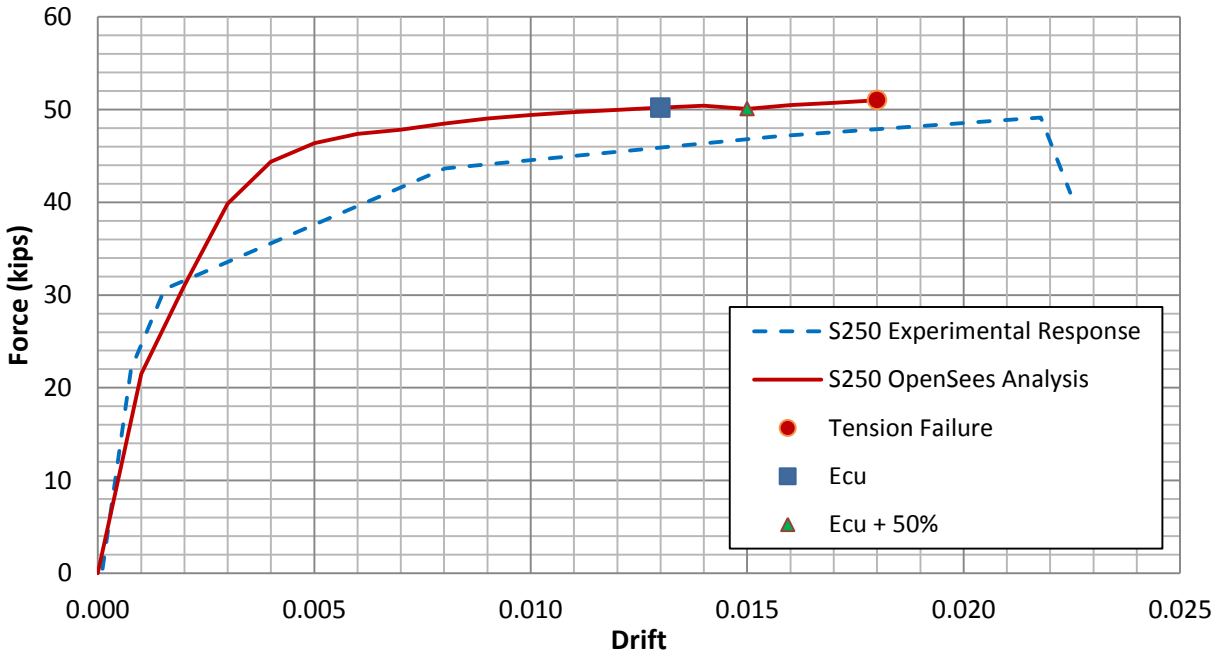

Figure 3-17: Force-Displacement Response Comparisons between Test Unit S250 by Calvi et al. (2005) and Analytical Results

As shown, the analytical response agrees fairly well with the experimental response. The initial stiffness is captured closely, but the displacement of the test unit begins to increase more

rapidly than the analytical displacement does. This rapid increase in displacement may be due to the contribution of shear deformation. Test unit S250 was designed and tested to fail in shear, and the shear failure caused the failure of the test unit. This also could be the reason that the experimental test unit experienced a larger ultimate displacement than what was predicted by the analysis, since the shear displacement would have been significant since the specimen failed in shear. It is also important to realize that the ultimate tensile strain of the longitudinal reinforcement was not reported, and a value of 0.08 was assumed. If the ultimate strain of the longitudinal reinforcement was actually higher than 0.08, this could also explain why the ultimate displacement of the test unit is higher than that predicted by the OpenSees analysis.

Also plotted on the figure is the failure point predicted by the ultimate concrete compressive strain, labeled Ecu, which was found using the equation given by Priestley et al. (1996). As discussed previously, this equation is often conservative by 50 percent, so the failure point predicted by the ultimate concrete strain, increased by 50 percent, is plotted on the figure as well. As shown, even with the additional 50 percent, this estimate of the ultimate strain is very conservative for the hollow square column.

3.4.2.3 Hollow circular with two layers of transverse reinforcement

There are few previous tests performed on hollow circular columns with one layer of transverse reinforcement in the literature. Due to the limited previous testing information available, an analysis of sections with two layers of transverse reinforcement has been provided to further demonstrate the ability of the analysis to produce accurate results. An analysis of previous testing of hollow circular columns with two layers of transverse reinforcement by Yeh et al. (2001) has been performed. Three specimens were tested, and of those three only one specimen experienced flexural failure. This specimen was analyzed to further verify the analysis method as well as to determine the accuracy of the calculated confined concrete properties for this configuration. The modeling method for circular hollow columns with two layers of

transverse steel which was discussed in the previous section was utilized for this column. The section layout can be seen in Figure 3-18.

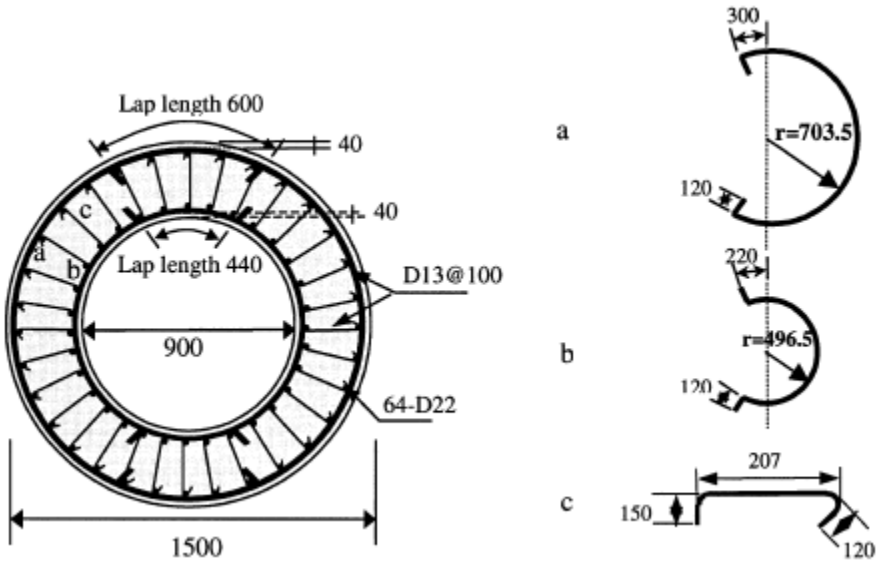

Figure 3-18: Cross-Section Dimensions and Lateral Reinforcement Details of Hollow Columns Tested by Yeh et al. (2001), (Dimensions in mm, 1 mm = 0.0394 inch)

The specimen was tested and analyzed under an axial load of 809.3 kips. The analysis compared to the experimental results can be seen in Figure 3-19. As shown, the analysis is very close to the experimental specimen results. The experimental specimen failed due to rupture of the tensile steel. The predicted tensile steel failure strain of 0.15 is plotted on the analysis and corresponds well with the experimental failure point. Although the ultimate strain was not explicitly stated in the study, the strain of 0.15 corresponds well with the failure point for this test performed by Yeh et al. (2001) as well as the square column tests performed by Yeh et al. (2002), and it was assumed that this is approximately the steel failure strain. Additionally, the ultimate compression concrete strain as predicted by the equation given by Priestley et al. (1996) has been plotted as well as the ultimate concrete compression strain, with an additional 50 percent added due to the conservativeness of the estimate. This illustrates that the prediction of the ultimate compressive strain of the confined concrete is very conservative for hollow columns with two layers of transverse reinforcement.

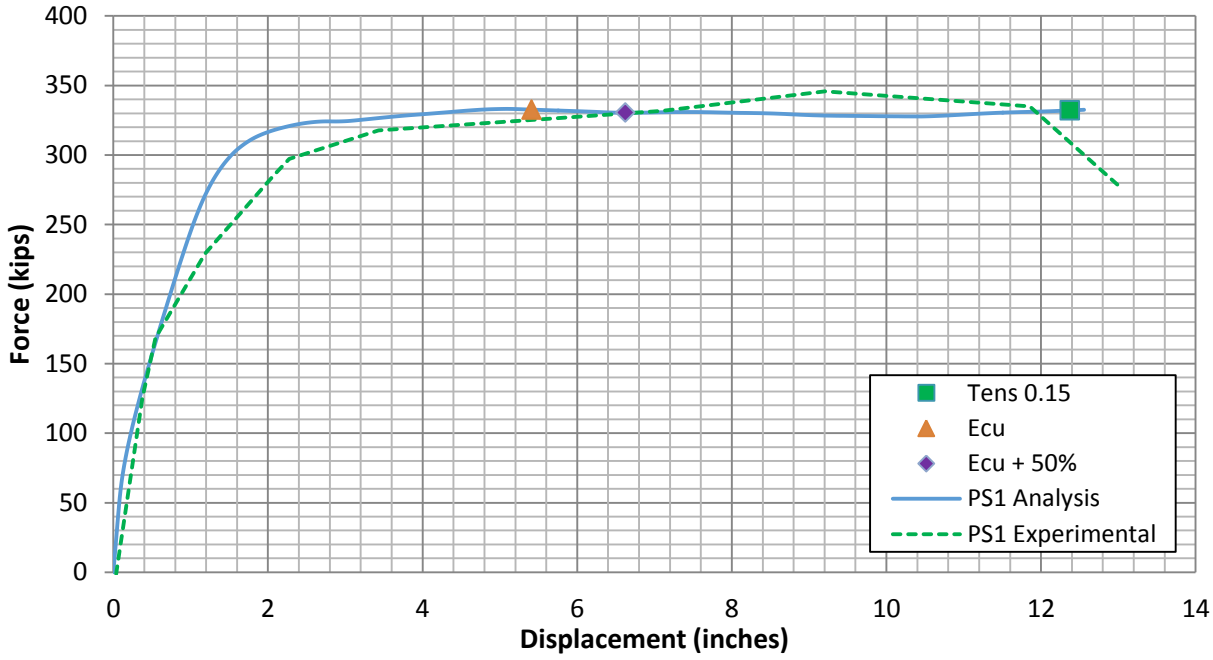

Figure 3-19: Comparison between Analytical Results and Experimental Results of Specimen PS1 Tested by Yeh et al. (2001)

3.4.2.4 Hollow square with two layers of transverse reinforcement

Yeh et al. (2002) tested two square hollow columns which contained two layers of transverse reinforcement and cross-ties. The columns were connected to foundation blocks, and the cyclic loading was applied at the top of the column horizontally. The specimens had similar cross-section dimensions and the same longitudinal steel arrangement with different transverse reinforcement sizes and spacing. Different axial loads were applied to each column as well, with specimen PS1 having 301.2 kips of axial load applied, and specimen PI1 having 436.1 kips of axial load applied. These axial loads were included in the analysis. The section dimensions and reinforcement configuration of specimens PS1 and PI1 can be seen in Figure 3-20 and Figure 3-21, respectively.

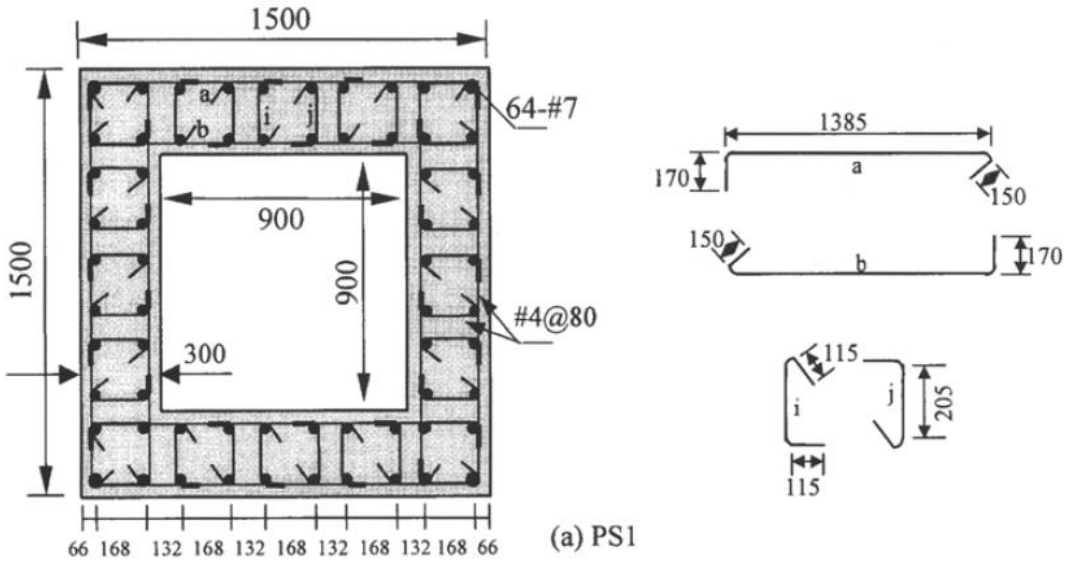

Figure 3-20: Cross Section Dimensions of Specimen PS1 Tested by Yeh et al. (2002) (Dimensions in mm, 1 mm = 0.0394 inch)

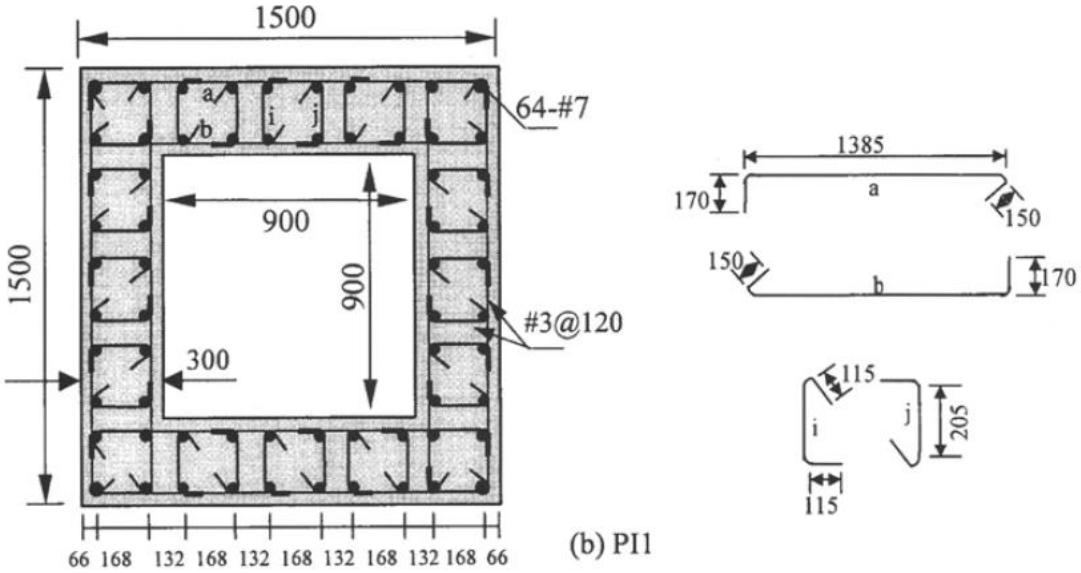

Figure 3-21: Cross-Section Dimensions of Specimen PI1 Tested by Yeh et al. (2002) (Dimensions in mm, 1 mm = 0.0394 inch)

The column was modeled as a nonlinear beam-column with a strain penetration section at the column-foundation interface. The base of the column was modeled as a fixed end. The

concrete and steel properties were based on those reported in the research. The confined concrete was modeled using the previously described method for square columns with two layers of transverse reinforcement, involving treating each wall as a separate rectangular column. The pushover analysis was performed, and the results are shown in Figure 3-22, comparing the digitized force displacement envelope of the experiment to the pushover analysis. Several possible predicted ultimate points are also shown on the graph. The ultimate tension steel strain of 0.15 was not explicitly stated. The research paper reported that both specimens fail due to rupture of tension steel, and a tension steel strain of 0.15 corresponds fairly well with the failure points as well as the failure points of the circular specimen tested by Yeh et al. (2001).

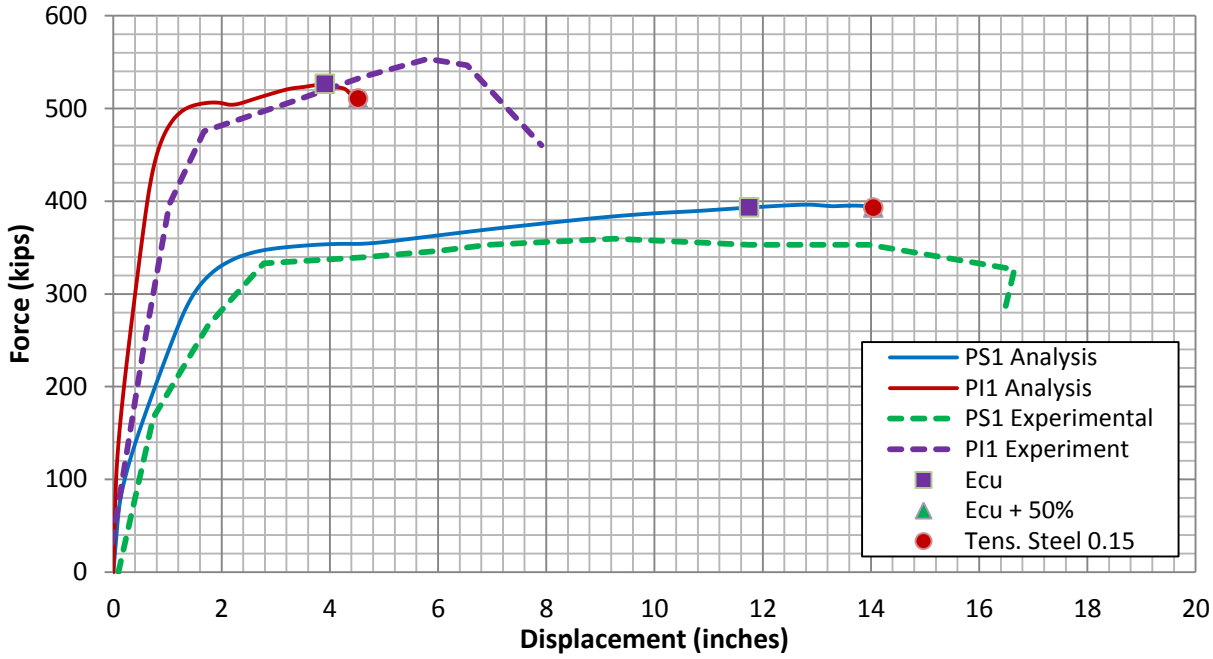

Figure 3-22: Comparison between Analytical Results and Experimental Results for Hollow Square Specimens with Two Layers of Transverse Reinforcement Tested by Yeh et al. (2002)

As shown in Figure 3-22, the analysis corresponds fairly well to the test results, including the predicted failure region. The ultimate displacement of the test results is somewhat higher, and the initial stiffness is somewhat lower, but this may be because shear was not accounted for in

the flexural analysis. As shown, the predicted ultimate compressive strains of concrete (Ecu and Ecu + 50%) are fairly conservative, since the ultimate strain, with an additional 50 percent added, is predicted to occur almost simultaneously with tensile rupture of longitudinal steel. The tests were controlled by tensile steel rupture without crushing of confined concrete.

3.4.3 Applicability of model

The methods utilized for modeling the confined concrete properties have been developed based on methods used by previous researchers with some modifications to account for the void, which is present in hollow columns. The comparisons to previous experimental work illustrate that these methods are able to conservatively model confined concrete. When utilized in the OpenSees analysis, the material models have been able to predict the response of the specimens to a reasonable degree of accuracy.

Comparing the analysis results to the experimental results and to descriptions of the experimental behavior has shown that the analysis is also fairly capable of predicting the cause of failure and the ultimate force and displacement points. It can be seen that in many cases, the ultimate concrete compressive strain prediction provided by Priestley et al. (1996) is very conservative for hollow columns, even when increased by 50 percent. This discrepancy is likely due to the increased deformability of hollow columns, as discussed by Lignola et al. (2008). Since the hollow specimens require less pressure to restrain the radial displacement of the column, less demand is supplied to the transverse reinforcement. This causes the transverse reinforcement to experience low strains, which means that the prediction of the ultimate compressive strain of confined concrete will be very conservative, since this prediction was based on hoop fracture in solid columns.

The prediction of crushing of the inside concrete face in hollow columns with one layer of transverse reinforcement has also been found to be conservative, as illustrated in the comparison to tests by Hoshikuma and Priestley (2000). The early prediction of the inside concrete face crushing may be caused by neglecting the influence of circumferential stress in the confined concrete model, as well as neglecting the small amount of radial stress near the

inside concrete face. These stresses were conservatively neglected, but in reality the concrete strength near the inside face would likely have some increase in strength and ductility due to the confinement effect. An approach is discussed later in Section 5.5 which accounts for these stresses.

CHAPTER 4. EXPERIMENTAL INVESTIGATION

4.1 Overview

Small-scale solid and hollow concrete columns were tested under various conditions in order to determine the accuracy of the analytical method for hollow columns with one layer of transverse reinforcement, described in Section 3.4.1.1. They were also tested to provide further information about the behavior of hollow columns. A total of 16 columns were tested, with 8 circular and 8 square cross sections. The specimens had similar reinforcement details, with the main test parameters being wall thickness and axial load ratio. A test frame was prepared in order to test the specimens under pure bending without the influence of shear in the critical region. Both monotonic and cyclic tests were performed.

4.2 Test Specimens

Eight circular columns were tested. The columns were 48 inches tall with an outer diameter of 12 inches, representing a 6 foot diameter column at $1/6^{th}$ scale. The smaller scale was selected in order to increase the number of test units. Although such a scale is typically avoided as it introduces challenges in finding suitable small diameter reinforcement and adds construction difficulties, it is expected that some large-scale tests will follow this study.

Two of the circular columns were solid sections, and six were hollow. Of the six hollow sections, two different wall thicknesses were used. Three specimens had a two-inch thick wall and the other three had a one-inch thick wall, corresponding to wall thickness to section diameter ratios of 0.17 and 0.08, respectively. The steel reinforcement in all eight columns was identical, with one layer of reinforcement placed near the outside concrete wall. The longitudinal reinforcement consisted of 20 #2 bars. The transverse reinforcement was provided by a continuous spiral of 0.208 inch diameter wire, spaced at 1.2 inches in the critical region. Outside of the critical region, the spiral spacing was shortened to one inch to ensure failure occurred near the critical region. These quantities of reinforcing steel correspond to gross reinforcement ratios (i.e, ratio to solid section, ignoring the void in the hollow section) of 0.87

percent for longitudinal steel and 0.97 percent for transverse steel. If calculated using the net section of present concrete for the one-inch thick specimens, the longitudinal reinforcement ratio would be 2.84 percent, and the transverse reinforcement ratio would be 3.5 percent. For the two-inch thick section using the net section, the longitudinal reinforcement ratio would be 1.56 percent, and the transverse reinforcement ratio would be 1.8 percent. The amount of longitudinal reinforcement provided is somewhat low for bridge columns, but the gross section longitudinal reinforcement ratio is still greater than the minimum value of 0.5 percent recommended for circular columns by Priestley et al. (1996). This low amount of longitudinal reinforcement was provided since ductility would be reduced with more longitudinal reinforcing steel, because this would cause the neutral axis to move toward the void. An additional reason that a small amount of longitudinal reinforcement was provided was because of the limited space available due to the small wall thickness. The specimens were designed to have minimal cover concrete, resulting in a concrete cover of approximately 0.35 inches that was measured to the center of main longitudinal steel. This minimal amount of cover concrete resulted in narrow shrinkage cracks on the specimens prior to testing. The location of these cracks coincided with the transverse reinforcement, and the cracks occurred throughout the length of the specimens.

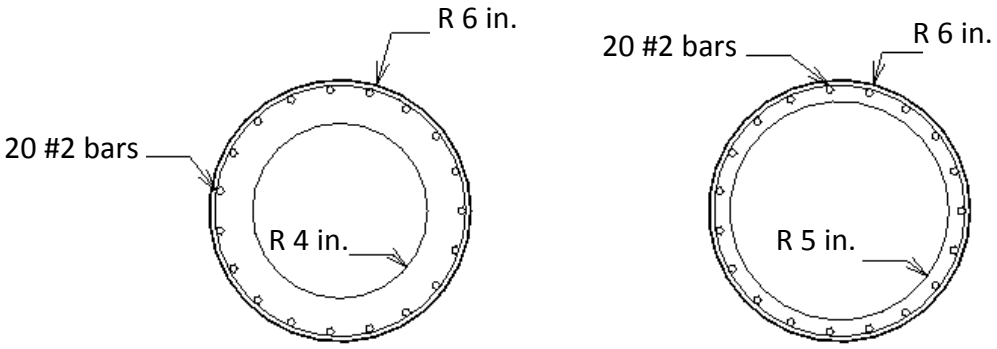

a) Two-inch wall thickness **b) One-inch wall thickness**

Figure 4-1: Cross-Sections of Circular Hollow Columns

Eight square columns were also tested, with only minor changes in the general details of the circular columns in order to provide similar reinforcement ratios to the circular sections. These columns were also 48 inches tall with 12 inch by 12 inch section dimensions. Of these eight columns, two were solid sections, three were hollow with a two-inch wall thickness, and three were hollow with a 1.25-inch wall thickness. The 1.25-inch wall thickness was provided instead of the 1-inch wall thickness used for the circular sections in an effort to allow the concrete to fill the section more easily. The hollow columns with a 2-inch thick wall and a 1.25-inch thick wall had wall thickness to section diameter ratios of 0.17 and 0.1, respectively. Similarly to the circular sections, one layer of steel reinforcement was used near the outside concrete wall, except with 24 longitudinal #2 bars. The confinement was provided by a 0.208 inch diameter continuous square wire spiral, spaced at 1.2 inches in the critical region and 1 inch outside of the critical region. Using continuous square shaped spiral transverse reinforcement is uncommon in square columns, since it is not commonly manufactured, and individual hoops are typically used. However, due to the small section size of the specimens, this was the most readily available confinement configuration. The longitudinal and transverse reinforcement ratios to the gross section (ignoring the void for hollow sections) were 0.82 percent and 1.0 percent, respectively. If calculated using the net section of present concrete for the 1.25-inch thick specimens, the longitudinal reinforcement ratio would be 2.19 percent, and the transverse reinforcement ratio would be 2.89 percent. For the two-inch thick section using the net section the longitudinal reinforcement ratio would be 1.47 percent, and the transverse reinforcement ratio would be 1.84 percent. The amount of longitudinal reinforcement provided for the square columns is also fairly low, but the gross section longitudinal reinforcement ratio is still slightly over the minimum of 0.8 percent recommended for rectangular columns by Priestley et al. (1996). The square specimens also had minimal concrete cover, with a depth to the center of longitudinal reinforcing steel of 0.4 inches.

The test units have been given a naming system for easy referral. The first letter can be either S or H, indicating solid or hollow. If hollow, there will be a number immediately following the first letter representing the thickness of the wall. For example, a hollow specimen with a one-inch wall thickness would start with H1, while a solid specimen would just start with S. The

second letter can either be C or S, for circular or square. The next character is a number indicating which test unit it is. Each type of specimen has an individual numbering system, so the second solid section would be labeled test unit 2 for solid sections, and the second hollow two-inch thick specimen would be labeled test unit 2 for hollow two-inch thick specimens. The last letter in the naming convention is either M or C for monotonic or cyclic loading. For example, of the three circular hollow one-inch thick specimens, the second one tested would have the designation H1C2-C if tested cyclically.

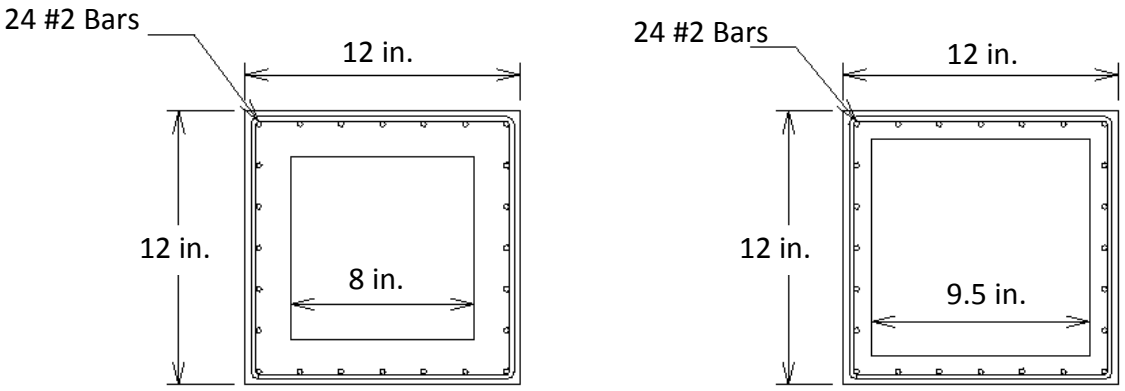

a) Two-inch wall thickness **b) 1.25-inch wall thickness**

Figure 4-2: Cross-Sections of Square Hollow Columns

4.3 Material Properties

The tables below summarize the steel and concrete properties for the test units. Table 4-1 shows the tested steel properties of the longitudinal and transverse reinforcement, while Table 4-2 gives the concrete strength on the day of testing for each unit. The steel used in the specimens for both longitudinal and transverse reinforcement had much higher yield strengths than typical reinforcing steel, as well as much lower ultimate strains. Though not expected, this seems to be true for the small diameter longitudinal reinforcement. This steel was used due to the limited options available for the small specimen size. At the time it was acquired, the ultimate tensile strain of the steel was expected to be significantly higher than what was found

during material testing. The smaller steel ductility has an impact on the test results; however, the specimen behavior and the effects of using one layer of transverse reinforcement can still be studied effectively.

Table 4-1: Measured Steel Reinforcement Properties

Steel	Diameter (inches)	Yield Stress (ksi)	Yield Strain (in/in)	Ultimate Stress (ksi)	Ultimate Strain (in/in)
Longitudinal	0.25	95	0.0033	100	0.02*
Transverse	0.208	95	0.0033	105	0.012*

*Significantly lower than expected

Table 4-2: Measured Concrete Strength on Day of Testing

Specimen	f'_c (psi)	f'_c of patched concrete (psi)	f'_c of grout (psi)
SC1-M	6309		
SC2-C	6248		
H1C1-M	5792	7000	7112
H1C2-C	6549	6738	
H1C3-C	6549	6738	
H2C1-M	6015		
H2C2-C	5677		
H2C3-C	5677		
SS1-M	7496		
SS2-C	7390		
H1.25S1-M	7573	7160	6016
H1.25S2-C	7283	7004	5603
H1.25S3-C	7283	7004	5603
H2S1-M	7573	7160	6016
H2S2-C	7594	7122	5557
H2S3-C	7594	7122	5557

4.3.1 Concrete quality

The small wall size of the hollow specimens presented a challenge when attempting to achieve good concrete fill in the specimens. The reinforcement cage further reduces the area which concrete can fill and restricts the ability to vibrate the concrete. For this reason, the concrete used was a self-consolidating concrete mix with a target strength of 5,000 psi. Aggregate size was limited to 3/8 inch in the concrete in an effort to achieve better fill between the reinforcement. These procedures helped to achieve good concrete fill for all solid sections as well as the circular two-inch thick specimens. However, this procedure did not help for the remainder of the specimens, which ended up needing some patches. The concrete and grout used for patching was intended to match as closely as possible to the initial mix, especially in strength and aggregate size. The patching was able to fill the voids which the initial concrete pour had left.

4.4 Test Setup

A specialized loading frame was designed for the experiment in order to examine the effects of flexure independently, and the layout of this frame can be seen in Figure 4-3. Examining the effects of flexure independently was accomplished by placing the columns horizontally and loading them laterally at two points near the center of the column. This loading arrangement creates a constant moment region over the central portion of the columns, allowing the flexural effects to be examined with no shear present. The column supports were 42 inches apart, and the two lateral load points were applied 11 inches apart in each direction using an actuator for each direction. The actuators applied load to loading beams, which transferred the load to the two point loads. The point loads and support points were applied using one-inch thick curved steel plates for circular columns and 1.5 inch thick flat plates for square column. A layer of neoprene rubber was provided between the plates and the test specimens to help distribute the load more evenly. The lateral load applied by the bottom actuator was resisted by structural tube sections on top of the specimen and threaded rods which transferred the load to a bottom beam. The bottom beam was attached to the strong floor using structural tubes at

each end and DYWIDAG bars. Lateral load applied by the top actuator was resisted by the beam assembly frame above the specimen, which was tied down to the strong floor by DYWIDAG bars, which ran through the square structural tube columns. The described setup can be seen in Figure 4-3. The various components are colored for better visualization, and some of the described components are labeled.

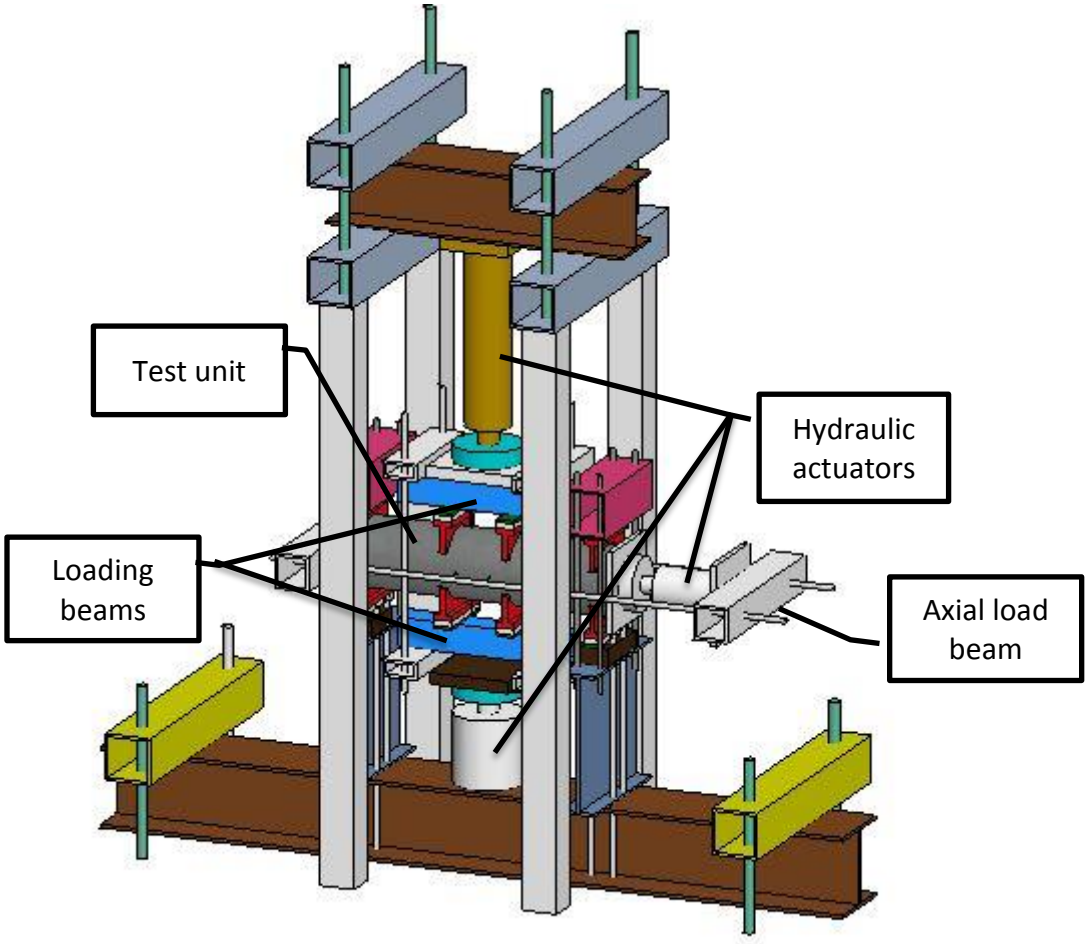

Figure 4-3: Overall Test Frame

The axial load was applied through the use of two threaded rods connected by structural tube sections on either end to transfer the axial load to the column. Steel plates were used on

either end to distribute the load. The columns were capped on each end with a layer of hydrostone to ensure even loading. A hydraulic actuator and load cell was used at one end between the structural tube and plate in order to apply the axial load, and was also used to keep the axial load constant throughout the testing, since the increasing specimen deformation would cause the axial load to increase. All specimens except for specimen SC1-M were held at constant axial load. The test frame setup is shown in Figure 4-3 through Figure 4-5.

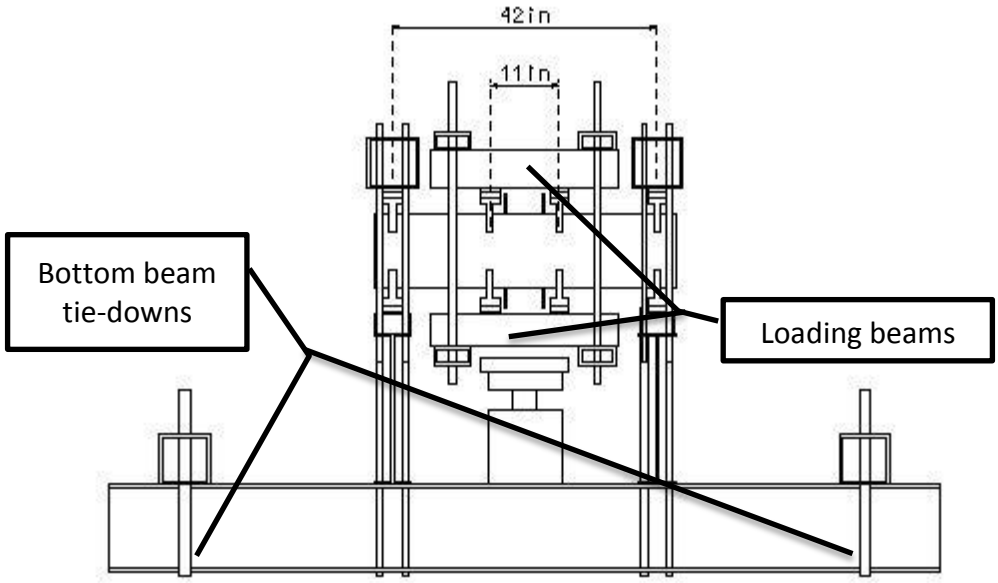

Figure 4-4: Frame Cutaway Showing Test Specimen Setup

Figure 4-5: Picture of Experimental Testing Setup

4.5 Test Instrumentation

Steel strain gauges were mounted to the longitudinal and hoop reinforcement, with 12 steel strain gauges being used on the circular specimens and 17 being used on the square specimens. The strain gauges are labeled according to the format SGLongL#H#. It can be SGLong or SGHoop, representing whether the gauge was on the longitudinal steel or the transverse steel. The term L# represents which longitudinal steel bar the gauge was located on or near, with the longitudinal bars being numbered around the circumference. Bar one was located at the extreme fiber of the section, which would experience the largest tension and compression strains under cyclic loading. For monotonic loading, bar one is always at the most extreme compression fiber. The term H# can either be H20 or H25, for which hoop the strain gauge was located on or near, counting up from the bottom. Figure 4-6 shows the location of the hoop sections and the spacing of the transverse reinforcement along the column height. For

example, SGHoopL11H25 would be the gauge located on the hoop near longitudinal bar 11 at the bottom of the specimen, on the 25th hoop up counted upwards from the base.

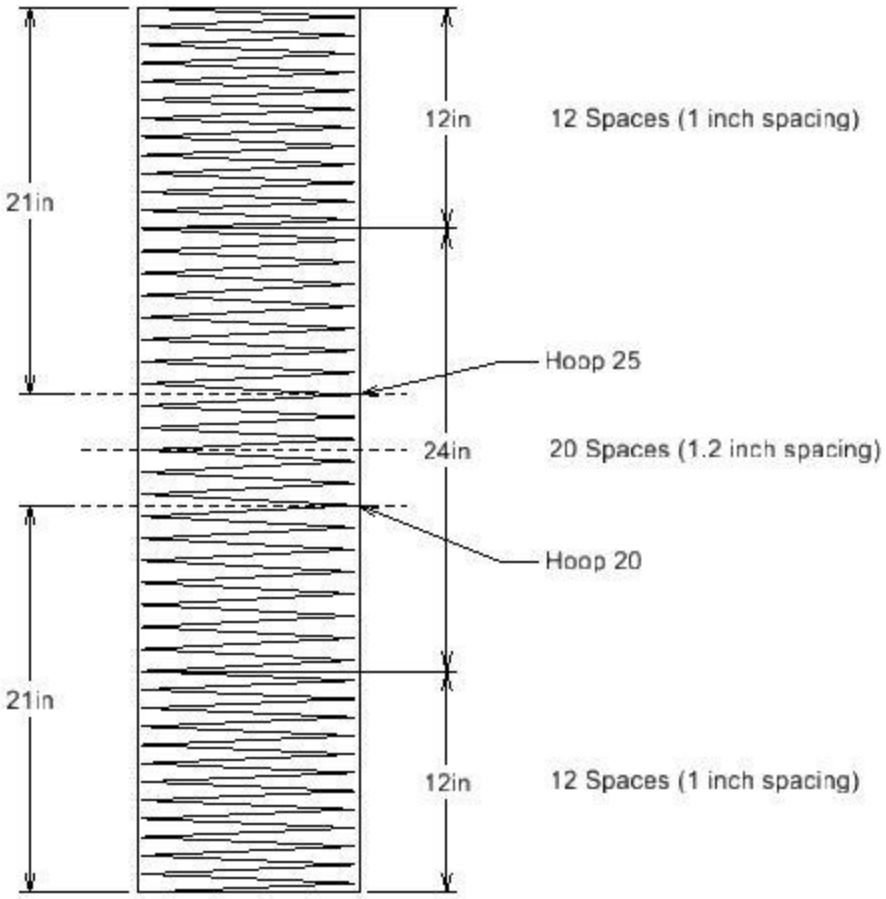

Figure 4-6: Transverse Reinforcement Spacing for Both Circular and Square Columns

The circular section has six strain gauges on the longitudinal steel and six on the hoop steel. The section labeled H20 is approximately 21 inches from the bottom of the specimen. Eight strain gauges are located near this hoop, consisting of four longitudinal and four hoop gauges. The section labeled H25 is approximately 27 inches from the bottom, and it has only four gauges, two longitudinal and two hoop gauges. Fewer gauges were used in this section because the response should ideally be symmetric. The square section has nine strain gauges on the longitudinal steel and eight strain gauges on the hoop steel. The section labeled H20 is

approximately 21 inches from the bottom of the specimen and has 11 strain gauges, and the section labeled H25 is 27 inches from the bottom of the specimen and has six strain gauges. The circular strain gauge section layout is shown in Figure 4-7. The gauges not marked with an asterisk exist at both sections, H20 and H25, while the gauges which are marked with an asterisk only appear at section H20. The square strain gauge section layout is shown in Figure 4-8, and the same notation is used for the strain gauges in the square section.

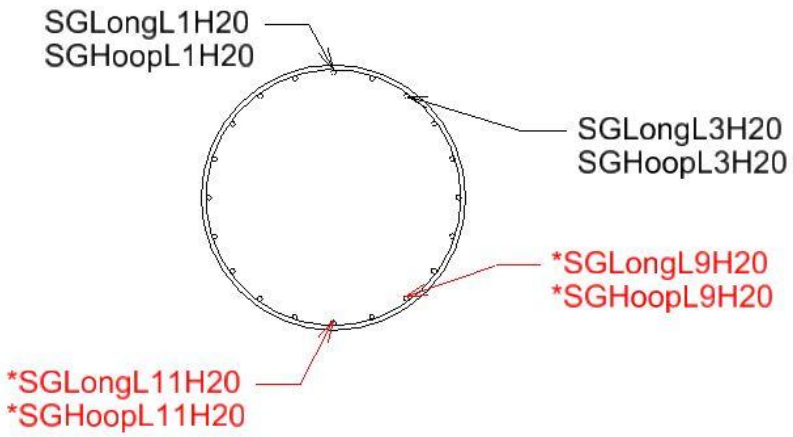

Figure 4-7: Strain Gauge Layout of Circular Section

In addition to the strain gauges, linear-variable-displacement-transducers (LVDTs) were used to measure both the column displacement as well as the curvature. Four LVDTs were attached at the center of the specimen, spaced at 90 degrees around the specimen circumference. These LVDTs spanned approximately six inches. These curvature LVDTs were anchored to the specimen using threaded rods which were either cast into the specimen or drilled into the specimen. The threaded rods extended into the void of the hollow sections. The hollow circular sections had the threaded rods cast integrally with the section, while all other sections had holes drilled and threaded rods inserted and held in place using epoxy. In addition to the curvature LVDTs, three LVDTs were used to measure the specimen displacement. An LVDT was placed at each support, and an LVDT was placed at the center of the specimen. See

Figure 4-9 for the layout of the LVDTs. One attached curvature LVDT is not shown in the figure and is attached to the side opposite of the side shown, similar to the other three attached LVDTs.

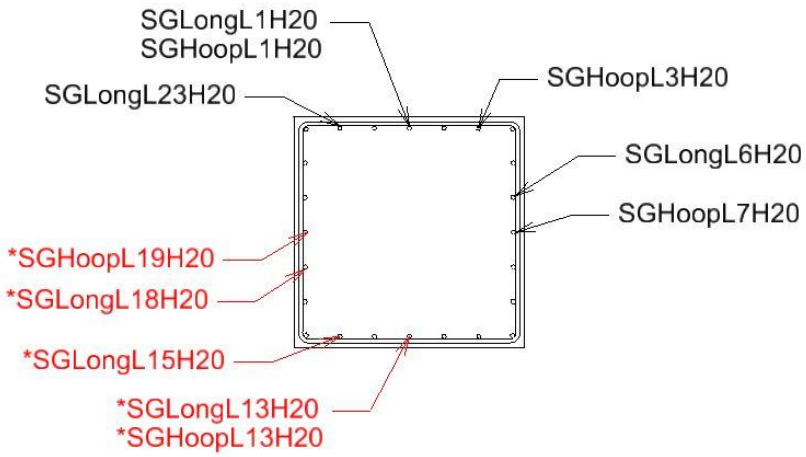

Figure 4-8: Strain Gauge Layout of Square Section

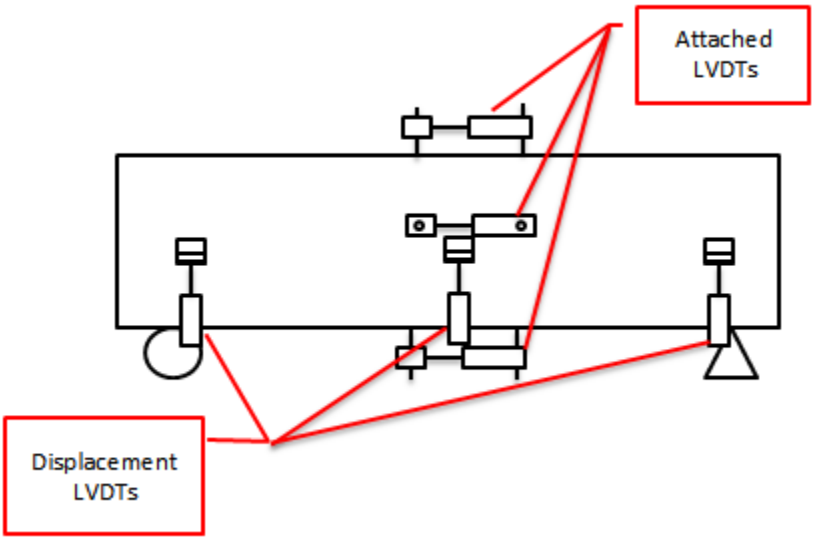

Figure 4-9: LVDT Locations

In addition to the gauges and LVDTs, a 3D motion capture system was used to measure the displacement of points in space in real time. The Optotrak Certus Motion Capture System was used, which finds displacement of certain points using strobing LEDs. The LED arrangement consisted of 38 LEDs, and the general locations of these LEDs are shown in Figure 4-10, with each number representing an LED, according to the numbering scheme given to the LEDs. Several LEDs are not pictured, and these LEDs were either attached to the frame as a point of reference or were used as indicators. The system was set to output at 5 frames per second, and the outputs are given as the X, Y, and Z location of each LED, relative to a defined coordinate system. These coordinates were then used to calculate values such as displacement, axial strain, and shear contribution. LEDs 35 through 38 were used particularly for the shear displacement calculations, with LEDs 11, 12, 25, and 26 also used to check these shear calculations. LEDs 1, 2, 11, 12, and the central column of LEDs (vertically from 6 to 19) were used to calculate displacement values. The LEDs in the critical region (5 through 10 and 15 through 20) were also used to calculate axial strains.

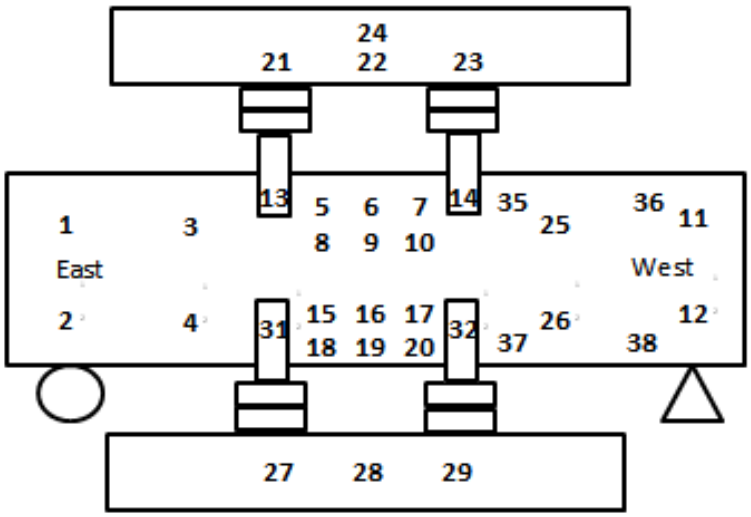

Figure 4-10: General LED Layout

4.6 Loading Protocol

The specimens were subjected to constant axial load and increasing flexural load until failure. The loading plan and amount of axial load for each specimen can be seen in Table 4-3 and Table 4-4**.** Axial load was applied for all specimens, and was held constant using a hydraulic actuator for all specimens except specimen SC1-M, which experienced increasing axial load due to flexure during the test. Flexural load was applied through the use of two manually controlled actuators. Increments in the force controlled range were applied under load control, with certain loads targeted, and the remainder of the test was performed under displacement control. The displacement control was performed by manually controlling the actuator and loading the test unit until targeted displacements were achieved, which were monitored constantly throughout the test.

Table 4-3: Summary of the Test of Circular Specimens

Circular					
	Thickness (inches)	Axial Load (kips)	Axial Load Ratio (ALR) (%)	ALR to Net Area (%)	Loading
SC1-M	Solid	22.6	3%	3%	Monotonic
SC2-C	Solid	45.2	6%	6%	Cyclic
H1C1-M	1	22.6	3%	10%	Monotonic
H1C2-C	1	22.6	3%	10%	Cyclic
H1C3-C	1	45.2	6%	20%	Cyclic
H2C1-M	2	22.6	3%	6%	Monotonic
H2C2-C	2	22.6	3%	6%	Cyclic
H2C3-C	2	45.2	6%	11%	Cyclic

Specimens loaded cyclically were subjected to four equal load increments in the linear range, with the fourth increment corresponding to the target first yield point found through OpenSees analysis of the test column. The increments in the force controlled range were load controlled. Each increment was one full cycle, with loads applied alternately in the lateral

directions. The longitudinal steel strain was monitored during the linear loading, and the linear loading phase was stopped when yield strain was reached in the longitudinal steel, even if the target yield load was not attained. This point was then used to calculate the approximate ductility levels, and the loading then entered the nonlinear stage. In this stage, three cycles were performed at each increment, with the increments occurring on ductility levels 1, 1.5, 2, 3, 4, and so on. Increments in the force controlled range were labeled F1, -F1, and so on through –F4. Increments in the nonlinear range were labeled A, B, C and so on, with a number following each label, such as A1 or –A2, to represent which cycle was being applied at a certain displacement level and which direction the load was being applied. Increment A corresponded with theoretical ductility 1, B with ductility 1.5, C with ductility 2, and D with ductility 3, continuing in this pattern until failure. The loading history used for each specimen is shown in Figure 4-11. Specimens loaded monotonically were loaded in one direction until failure occurred. The loading was paused in the same increment levels as the cyclic specimens in order to observe and mark cracking.

Table 4-4: Summary of the Test of Square Specimens

Square					
	Thickness (inches)	Axial Load (kips)	Axial Load Ratio (ALR) (%)	ALR to Net Area (%)	Loading
SS1-M	Solid	28.8	3%	3%	Monotonic
SS2-C	Solid	57.6	6%	6%	Cyclic
H1.25S1-M	1.25	28.8	3%	8%	Monotonic
H1.25S2-C	1.25	28.8	3%	8%	Cyclic
H1.25S3-C	1.25	57.6	6%	16%	Cyclic
H2S1-M	2	28.8	3%	6%	Monotonic
H2S2-C	2	28.8	3%	6%	Cyclic
H2S3-C	2	57.6	6%	11%	Cyclic

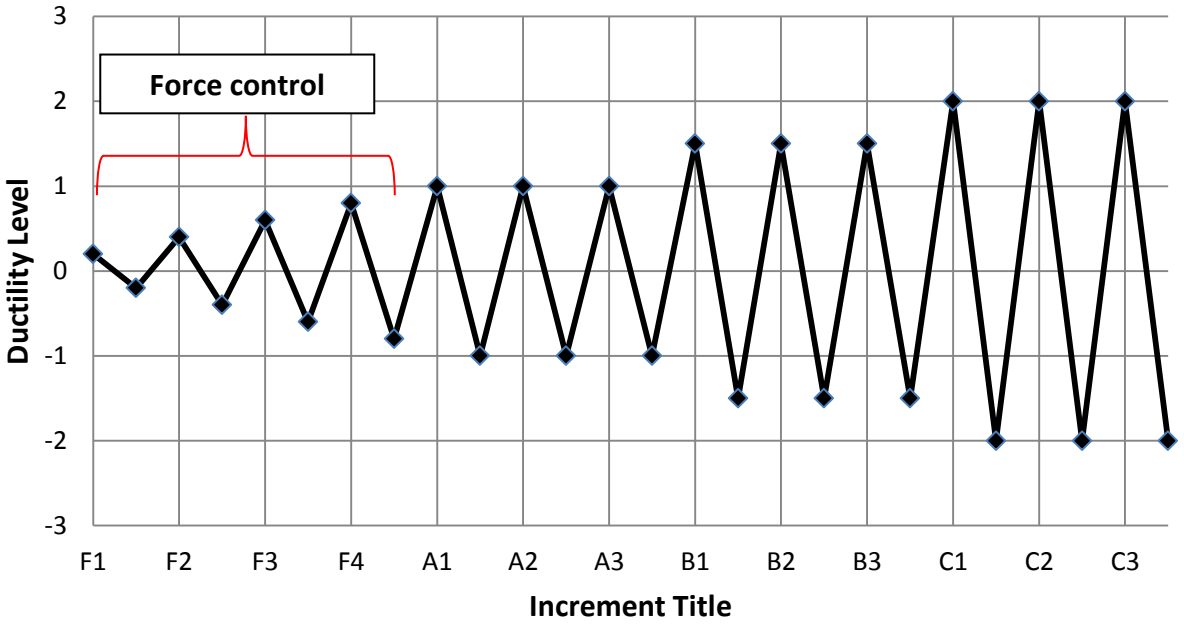

Figure 4-11: Loading History Selected for Testing

CHAPTER 5. EXPERIMENTAL AND ANALYTICAL RESULTS

5.1 Analytical Modeling

All test specimens were modeled using OpenSees (McKenna et al., 2000) to further determine the ability of the modeling method to accurately describe the response of the specimens. A general description of the analysis and modeling methodology is described in Section 3.4.1.1. The element geometry and loading used in this analysis are intended to model the actual testing setup as closely as possible. The element geometry is shown in Figure 5-1, with four force-based nonLinearBeamColumn elements which are capable of modeling nonlinear behavior. Forces were applied at the node locations (shown by arrows in the figure), with the axial load held constant and equal to the applied axial load in the test, and the lateral loads constantly increasing, to represent monotonic loading. Supports were modeled as a roller and pin, allowing axial deformation but restraining all other directional forces.

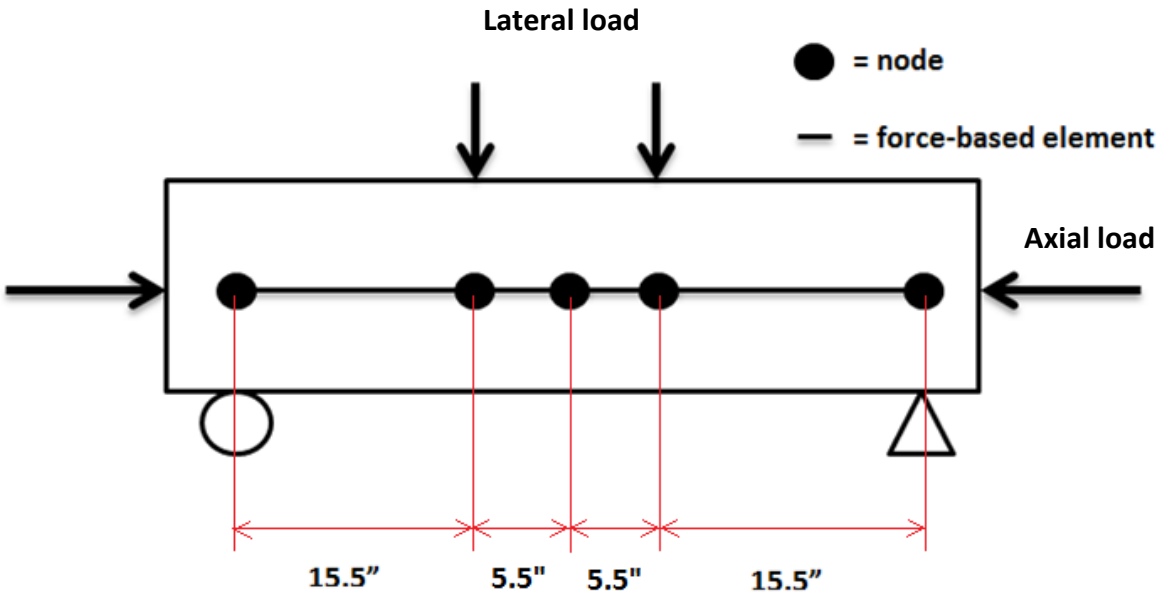

Figure 5-1: Schematic of the OpenSees Model Representing the Test Units

For all hollow specimens, two concrete types were considered, which were confined and unconfined concrete. The model by Mander et al. used to determine the confined concrete behavior, and Concrete07 within OpenSees, was chosen to accurately represent this behavior. Unconfined concrete was provided for the concrete cover and also for the concrete at the inside face near the void if the column was hollow. Near the void the unconfined concrete was only provided half the distance to the location of the transverse reinforcement, with the other half being modeled as confined concrete for hollow columns, as discussed in Section 3.4.1.1. Solid columns were modeled as entirely confined concrete within the transverse reinforcement. For hollow columns, the confined concrete was modeled using the adjustment suggested to Mander's model, which was described in Section 3.4.1.1. The normal Mander's model procedure was used for solid columns. Longitudinal steel in all cases was modeled using the measured steel properties, and the Steel02 material model was used to apply these properties to the longitudinal reinforcement.

5.1.1 Hollow column section layout

The circular and square hollow columns were modeled using the procedure which was discussed and described in Section 3.4.1.1. Figure 5-2 and Figure 5-3 illustrate the general section geometry used, with the hashed areas showing the differentiation of confined and unconfined concrete within the transverse reinforcement. Solid columns had an identical steel layout corresponding to their shape, but the entire area within the transverse reinforcement was modeled as confined concrete. Although shown in the diagrams, transverse steel could not be modeled in OpenSees and the confined concrete properties were instead calculated and defined.

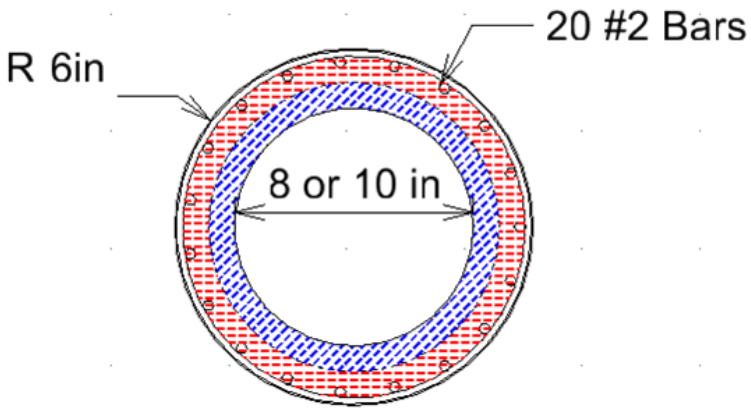

Figure 5-2: General Section Model for Tested Hollow Circular Specimens

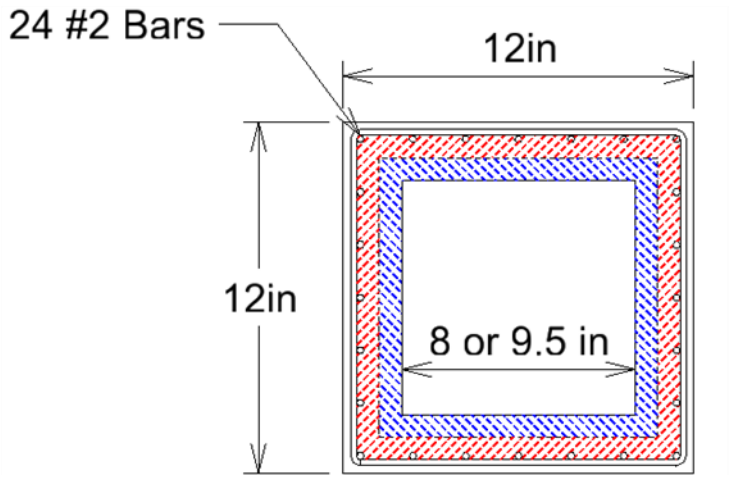

Figure 5-3: General Section Model for Tested Hollow Square Specimens

5.2 Experimental Results and Comparison to Analytical Results

5.2.1 Circular section

The results of the circular tests are described in the following sections. The solid specimens and the two-inch thick specimens had satisfactory results, while the one-inch thick specimens experienced premature local and shear failures. These local and shear failures are suspected to be due to the small wall thickness combined with some of these areas needing concrete patching or due to poor consolidation within the small wall thickness. The solid and two-inch thick specimens had good concrete and did not require any patching, and thus the focus is placed more on these specimens.

5.2.1.1 Visual observations of circular specimens

SC1-M

Specimen SC1-M was loaded monotonically until failure. This specimen is the only specimen which was loaded using a SATEC uni-axial testing machine and therefore used a different setup than the other specimens. Additionally, the axial load was applied to this specimen through manual tightening of the nuts on each threaded rod through the end beams. The axial load was applied to all other specimens through the use of a hydraulic actuator. For this reason, the axial load for this specimen did not remain constant and crept up from 22.6 kips to approximately 40 kips by the end of the testing.

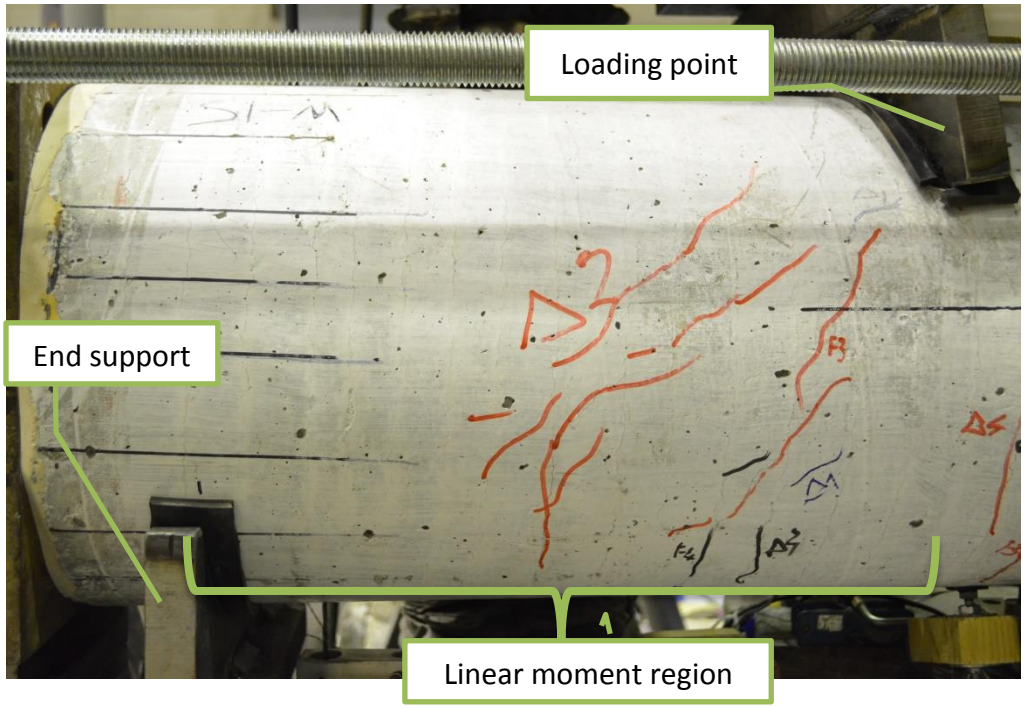

Figure 5-4: Specimen SC1-M Shear Cracking at Peak Displacement

The load was applied monotonically, with pauses at predetermined points in order to inspect the critical region and mark cracks. Minor shear cracks first appeared in the linear moment region at approximately 36 kips of applied load as well as minor flexural cracks in the constant moment region. The shear cracks gradually continued to increase in number and length throughout the testing, although they remained fairly small. Several flexural cracks appeared in the tension region, following the shrinkage cracks which were present after casting due to the small amount of concrete cover over the transverse reinforcement. These cracks continued to widen throughout the test. As the specimen failed, one of the flexural cracks widened a large amount, and the specimen lost load capacity due to rupture of longitudinal reinforcement. The specimen failure occurred due to rupture of the longitudinal reinforcement, which was not unexpected due to the lower tensile ultimate strain of the reinforcement. The axial load was maintained throughout failure and did not drop. The cover concrete near the compression face crushed slightly after failure of the specimen occurred.

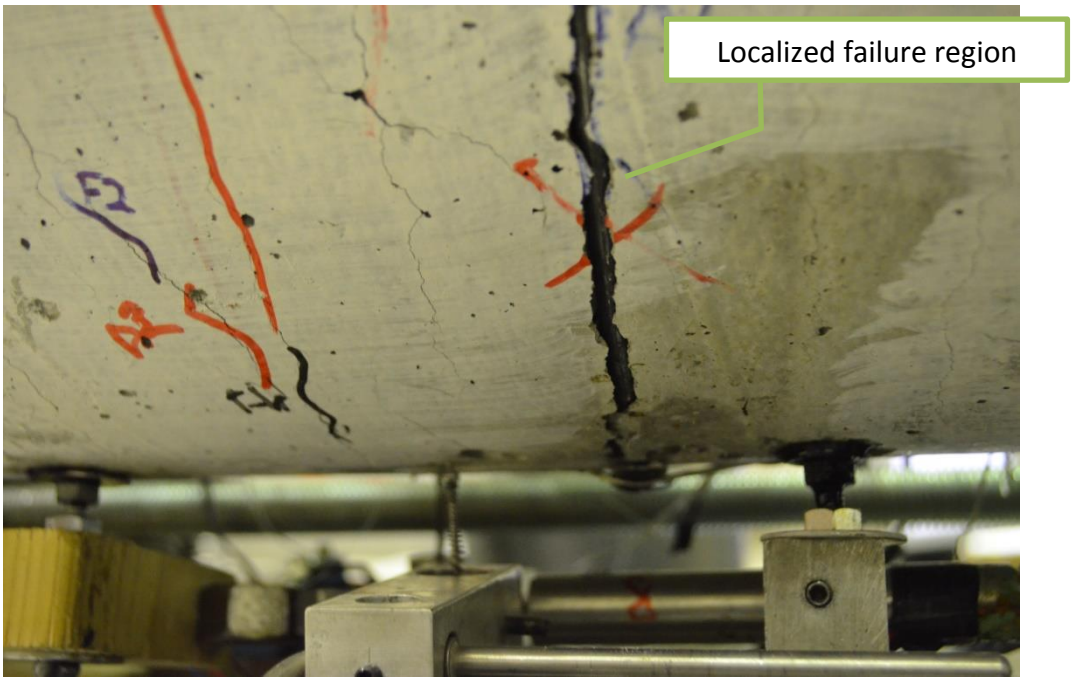

Figure 5-5: Large Flexural Crack in Specimen SC1-M at End of Test

SC2-C

Specimen SC2-C was loaded cyclically using the frame which was specifically designed for this testing. Three cycles were performed in the linear range in equal force increments until first yield of the longitudinal reinforcement was observed. After the first yield, three cycles were performed at increments based on ductility levels until specimen failure occurred. The specimen was tested under the target axial load of 45.2 kips, which was held constant during the test. Slight shear cracking in the linear moment region and flexural shrinkage crack widening in the constant moment region occurred near the first yield of the tension steel. More shear cracks appeared and flexural cracks continued to widen as the loading continued, and these crack patterns can be seen in Figure 5-6. The cover concrete crushed slightly during the second cycle near displacement ductility level 1.5. During the cycles near displacement ductility level two, the cover concrete began spalling and flexural cracks grew much wider. During the first cycle to displacement ductility level three the specimen failed due to tension steel rupture,

and a large flexural crack opened up. This failure was not unexpected due to the low ultimate tensile strain of the longitudinal reinforcement.

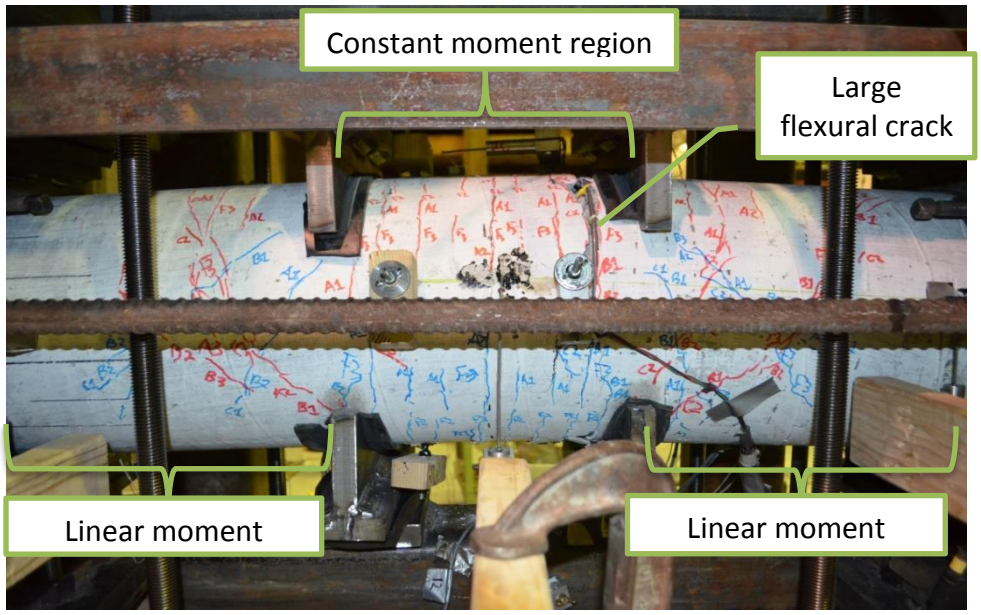

Figure 5-6: Specimen SC2-C after Flexural Failure

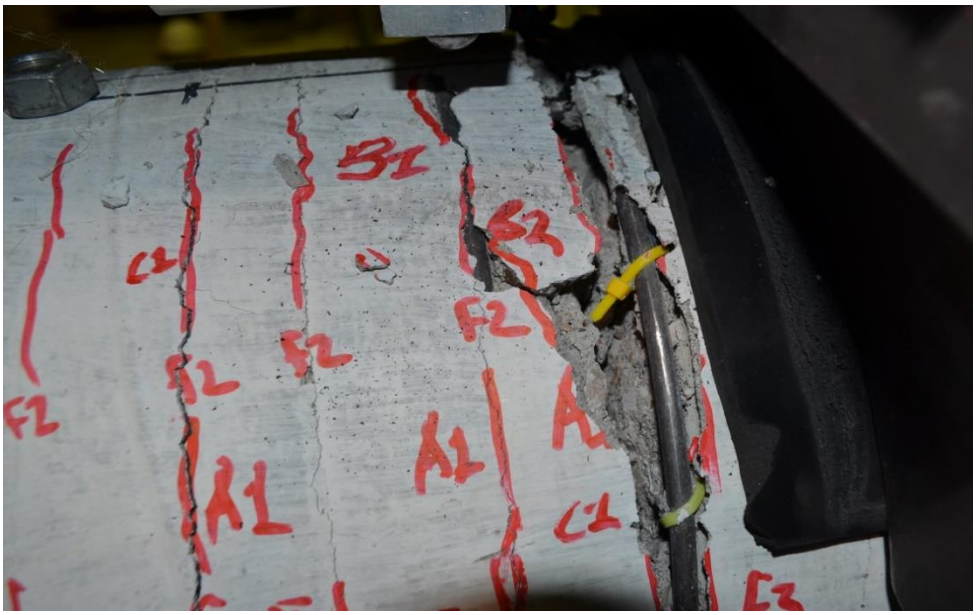

Figure 5-7: Close-Up View of Large Flexural Crack in Specimen SC2-C

H2C1-M

Specimen H2C1-M was tested monotonically until failure under the target axial load of 22.6 kips, which was held constant throughout the test. In the second increment in the force controlled cycles, shear cracks began to appear in the linear moment region, and flexural crack widening occurred in the constant moment region. The length and amount of small shear cracks continued to grow throughout the testing. The flexural cracks followed the shrinkage crack locations and continued to widen these cracks. The specimen failed on the push to displacement ductility three, and one of the flexural cracks widened significantly as the tension steel failed due to the low ultimate steel strain. Minor crushing of concrete cover was seen at the compression face after failure.

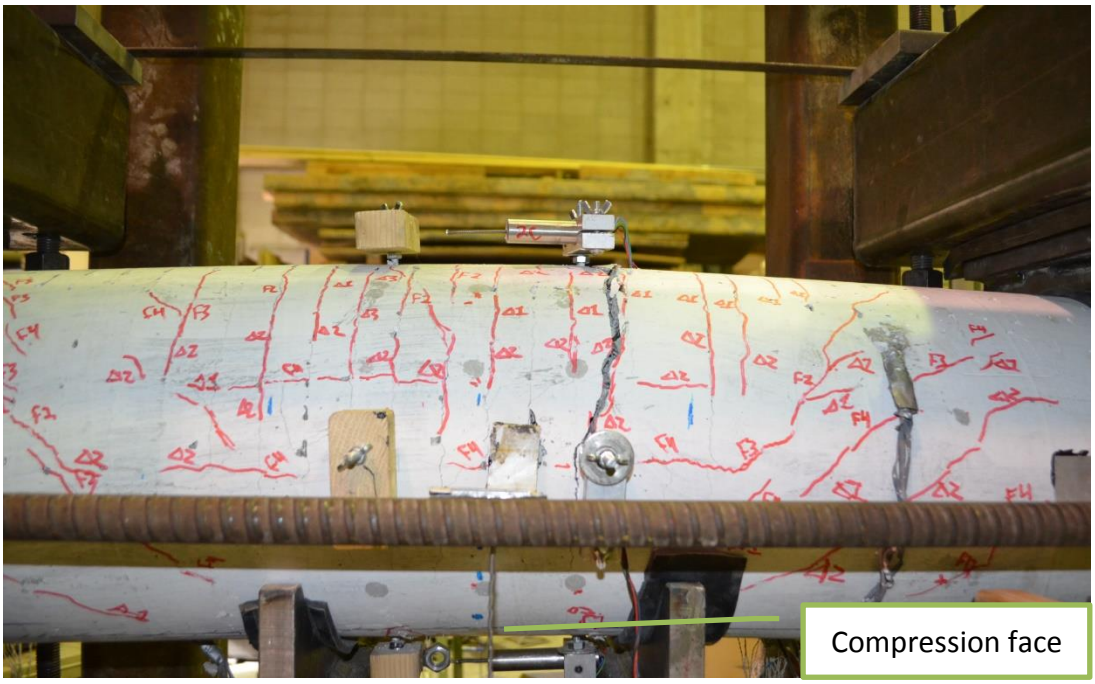

Figure 5-8: Specimen H2C1-M after Tension Steel Failure

The inside face concrete remained undamaged due to compression after the specimen failed. The inside face concrete before and after testing is shown in Figure 5-9. The images show the inside face concrete in the constant moment region at the extreme compression face.

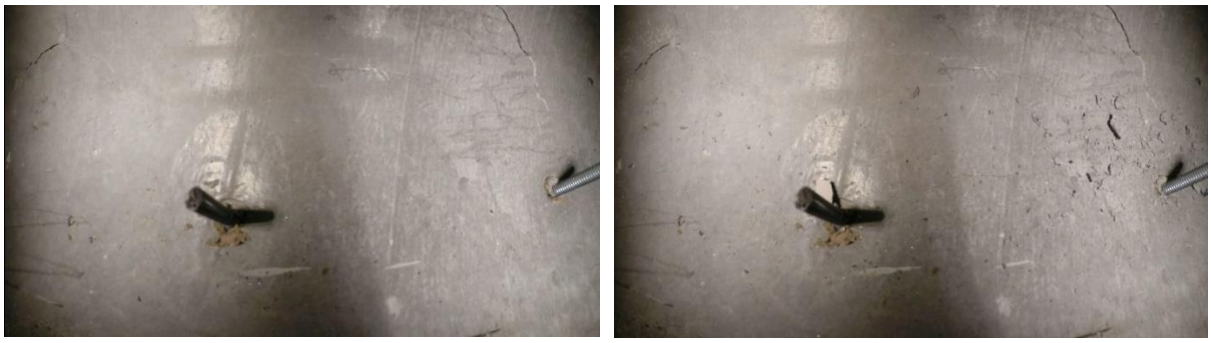

a) Before Testing **b) After Specimen Failure**

Figure 5-9: Inside Face at the Compression Face in the Constant Moment Region of Specimen H2C1-M Before and After Testing

H2C2-C

Specimen H2C2-C was tested cyclically until failure under 22.6 kips axial load, which was held constant throughout the test. Minor shear cracks began to appear in the second cycle in the linear range as well as flexural widening of the shrinkage cracks. The amount and length of the shear cracks continued to increase, and the flexural cracks widened. Slight cover concrete crushing occurred in the first cycle at ductility one. Tension steel rupture occurred on the first push to ductility 1.5, and one of the flexural cracks widened significantly. The inside face extreme compression concrete did not experience damage for either loading direction.

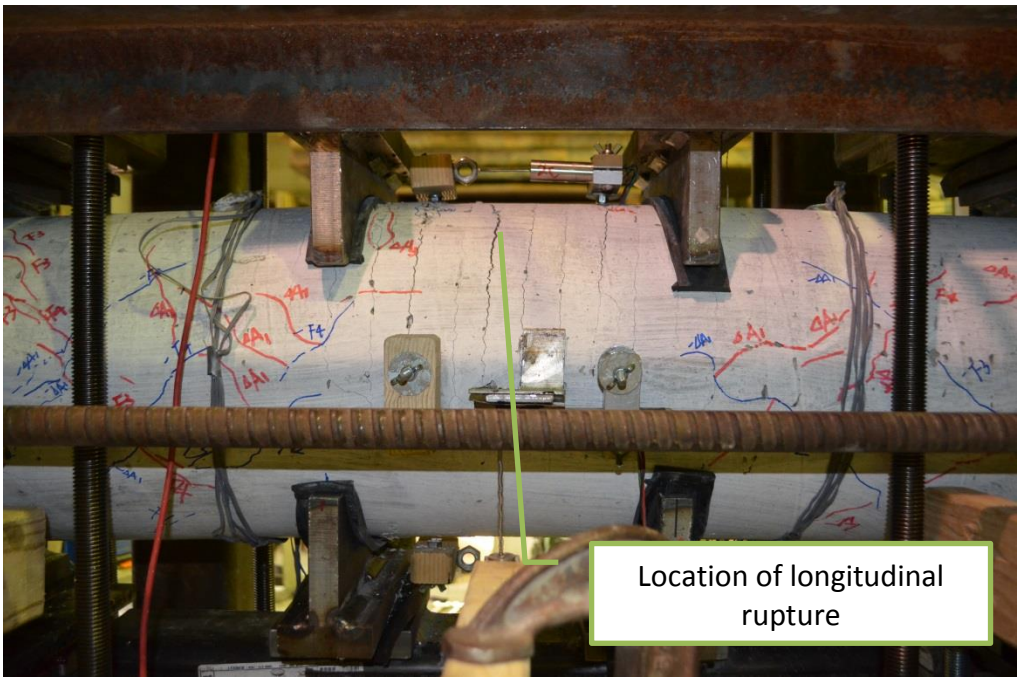

Figure 5-10: Specimen H2C2-C after Failure

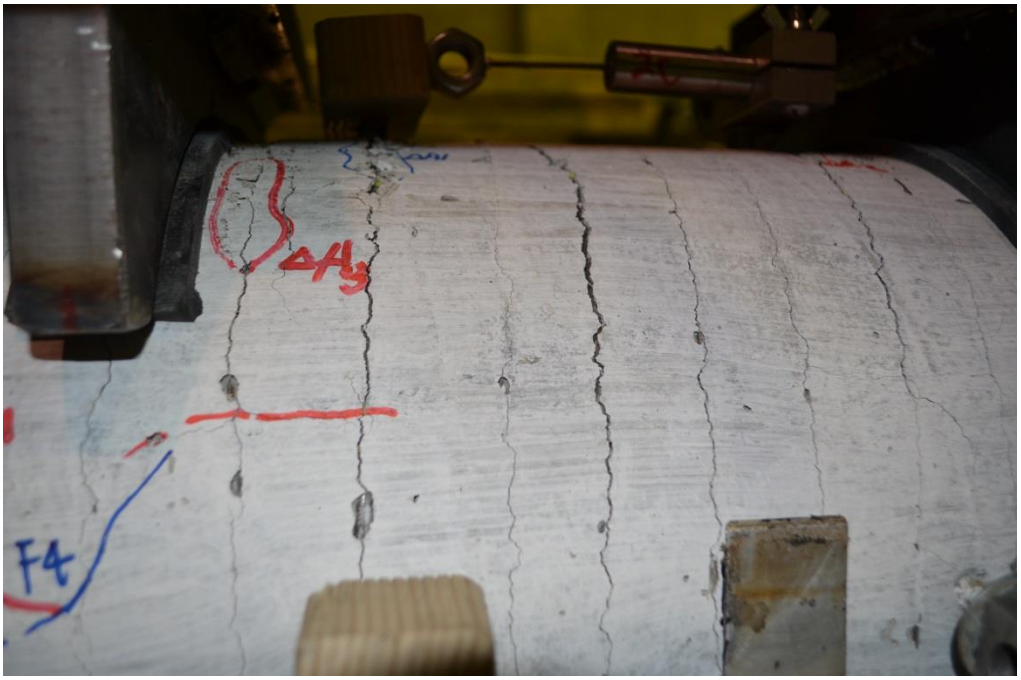

Figure 5-11: Close-Up View of Flexural Cracks in Specimen H2C2-C after Failure

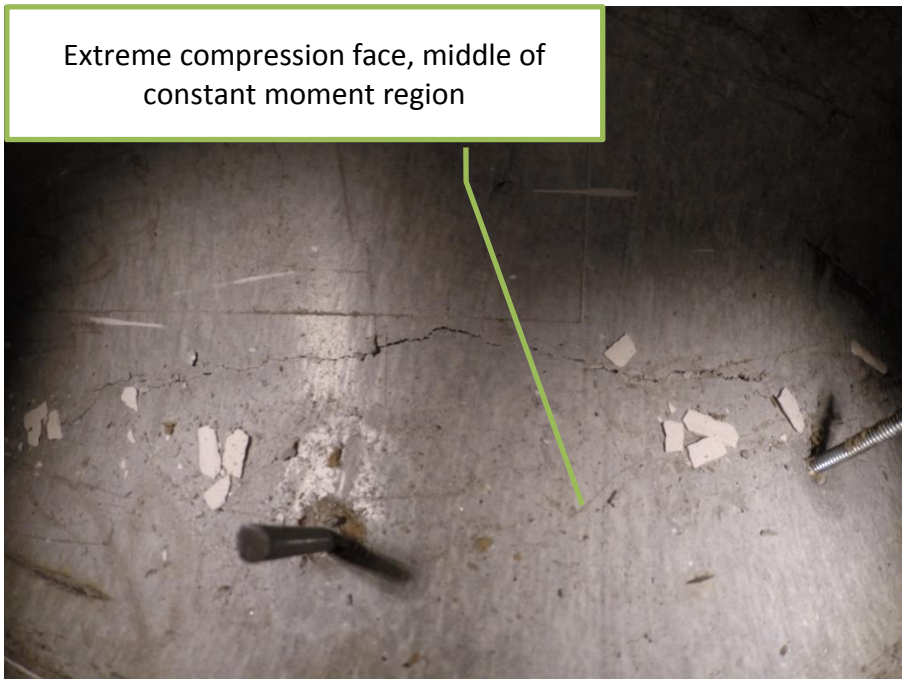

Figure 5-12: Inside Face of Specimen H2C2-C in Constant Moment Region under Compression

H2C3-C

Specimen H2C3-C was tested under lateral cyclic loading and subjected to the targeted axial load of 45.2 kips, which was held constant until the specimen failed. Minor shear cracking appeared in the linear moment region in the second cycle increment in the force controlled range. Shear cracking continued to increase as loading continued, and the shrinkage cracks began to widen under flexure in the constant moment region. Slight cover concrete crushing occurred in the first cycle at ductility one. Some spalling of cover concrete occurred by the end of the third cycle at displacement ductility one. The specimen failed on the first push to displacement ductility 1.5 due to rupture of tension steel. The inside extreme compression face remained undamaged for both loading directions.

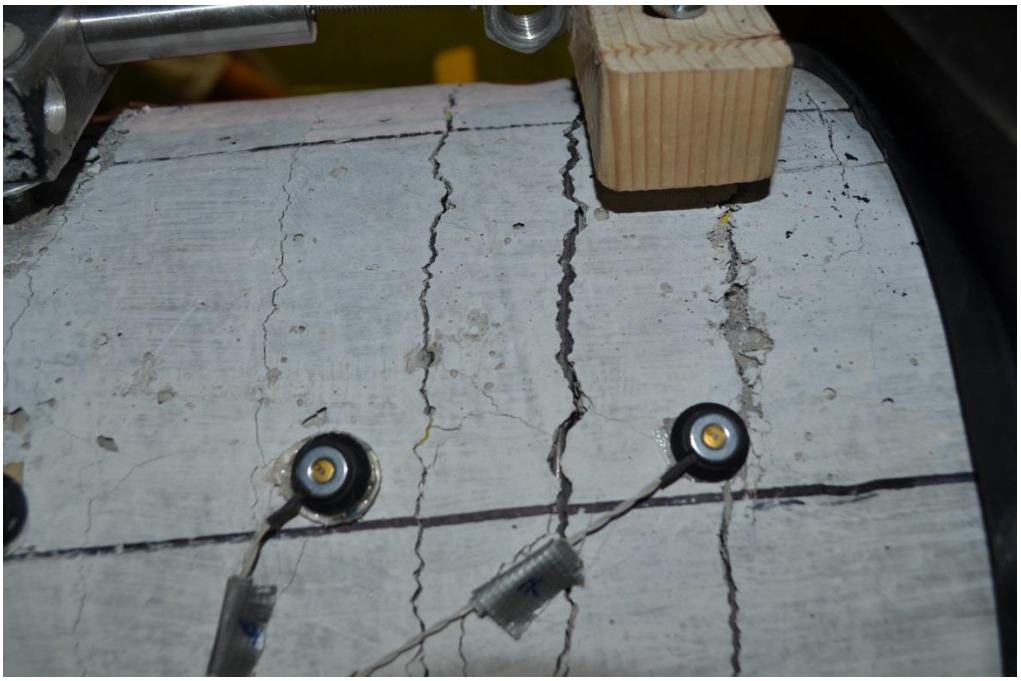

Figure 5-13: Close-Up View of Flexural Cracks in Specimen H2C3-C after Failure

H1C1-M

Specimen H1C1-M was tested monotonically under the target axial load of 22.6 kips, which was held constant until the specimen failed. Shear cracking occurred in the linear moment region during the second push prior to first yield. Shear cracking continued to grow until failure, with little flexural cracking visible in the constant moment region. On the way to the predicted first yield point, the specimen failed suddenly near one of the points of load application. There was some local failure near the loading plate which seems to have led to a shear failure at that location. The plate may have begun to punch through the wall which weakened the specimen and contributed to a shear failure at that location. This punching is suspected to be a result of the very small wall thickness of the specimen. The inside compression face appeared undamaged before the sudden failure of the loading plate pushing through the wall.

Figure 5-14: Specimen H1C1-M Shear/Local Failure at West Point of Load Application

H1C2-C

Specimen H1C2-C was tested under lateral cyclic loading and subjected to the targeted axial load of 22.6 kips, which was held constant until failure. Four pieces of wood were added inside the specimen at the points where the loads were applied as well as the supports in an effort to distribute the load more effectively and avoid local failure, as witnessed in H1C1-M. Some slight shear cracking appeared in the linear moment region in the second cycle before reaching the first yield strength. In the third cycle, there was some slight concrete crushing near the support. At the first yield, there was a large amount of cover spalling in the linear moment region as well as a large number of shear cracks. In the second part of the first yield cycle, the specimen underwent a premature shear type failure, which can be seen in Figure 5-17. The inside face concrete in the constant moment region remained undamaged during the testing.

Figure 5-15: Specimen H1C2-C Wooden Braces Located at Load Points and Support to Avoid Punching Failure

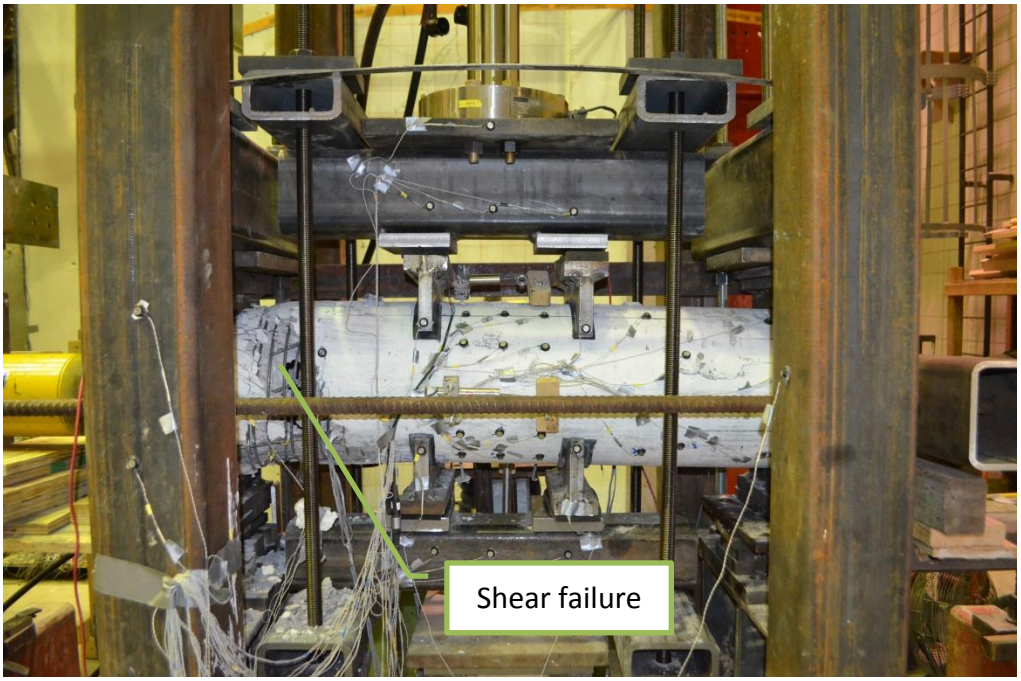

Figure 5-16: Specimen H1C2-C after Shear Failure

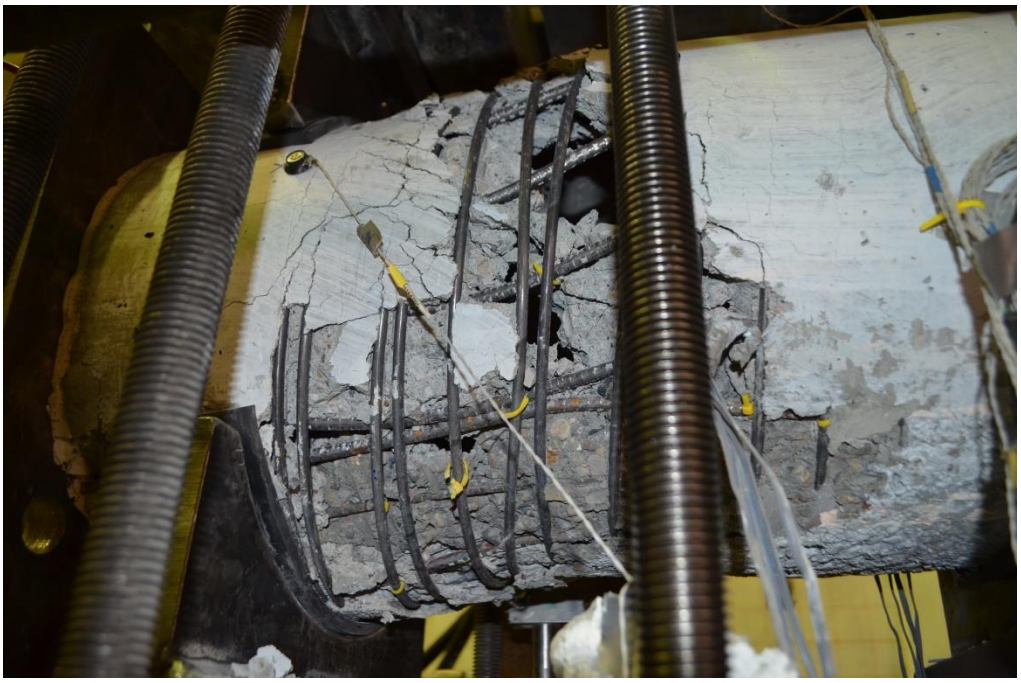

Figure 5-17: Specimen H1C2-C Shear Failure Region

H1C3-C

Specimen H1C3-C was tested under lateral cyclic loading with the target axial load of 45.2 kips applied. Wooden braces were not placed inside this specimen at the loading and support locations because this specimen was tested prior to specimen H1C2-C, and it had not yet been made clear that punching failure could occur commonly for the small wall size. Some minor shear cracking began to appear in the linear moment region during the second cycle in the force-controlled range. On the second half of the second cycle, the specimen experienced a sudden local failure near one of the points of load application, as shown in Figure 5-18. This local failure again appeared to be caused by the loading plate punching through the thin wall of the specimen. There was no damage to the inside face of concrete under compression before this local failure occurred.

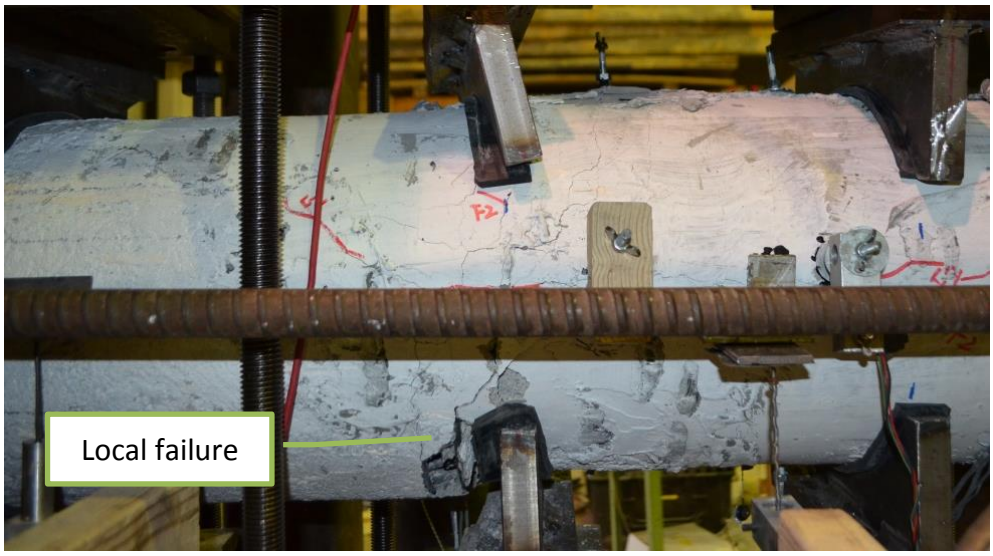

Figure 5-18: Specimen H1C3-C Local Failure near Loading Point

Figure 5-19: Specimen H1C3-C Close-Up of Local Failure on LED Side after Clearing Damaged Concrete

5.2.1.2 Circular section experimental results and comparison to analytical results

5.2.1.2.1 Overall force-displacement response

Using the recorded values from the load cells and the measured displacements, the force-displacement response of each test unit was evaluated. The force-displacement response of each specimen can be seen in the figures below, as measured by the LEDs. The force reported is the lateral force supplied to the loading beam by the actuator. For the monotonic tests, only the overall envelope is shown. All of the LED data has been processed to remove outliers and noise. The experimental results shown in this portion include shear deformation as well.

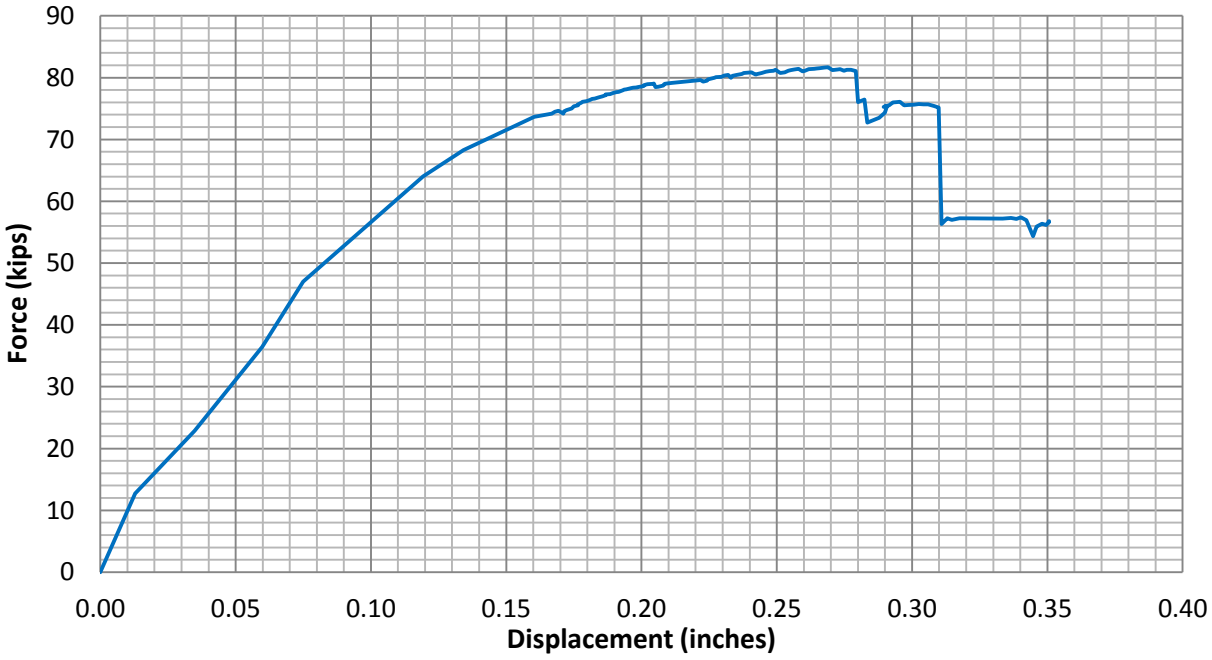

Figure 5-20: Force-Displacement Response of Test Unit SC1-M

Specimen SC1-M is the only specimen for which the axial load increased during testing as it was tested using a uniaxial machine. This specimen was tested without using a hydraulic actuator to control the axial load levels, so the lateral deformation during loading caused the

axial load to increase. It started out at 22.6 kips of axial load, which corresponds to an axial load ratio of 3 percent, and had reached approximately 40 kips of axial load by the end of the testing, corresponding to an axial load ratio of 5.4 percent. This increase in axial load has been taken into account in analysis comparisons, which are presented and discussed in later sections.

The large displacement imposed in Figure 5-24 occurred due to rupture of the longitudinal reinforcement, which resulted in a slight loss of strength capacity and a sudden deformation. As previously described in Section 4.6, the loading applied in the nonlinear region was done by manually targeting displacements. This meant that loss of strength was often associated with a significant increase in displacement as the pressure in the actuator balanced out.

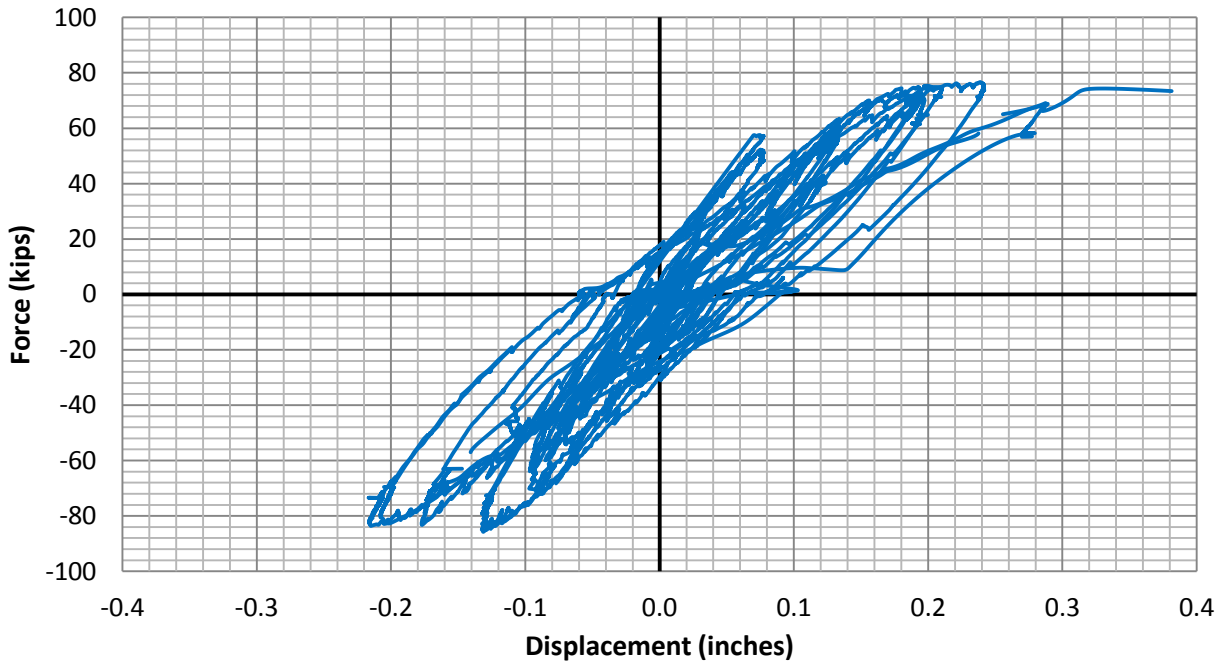

Figure 5-21: Force-Displacement Response of Test Unit SC2-C

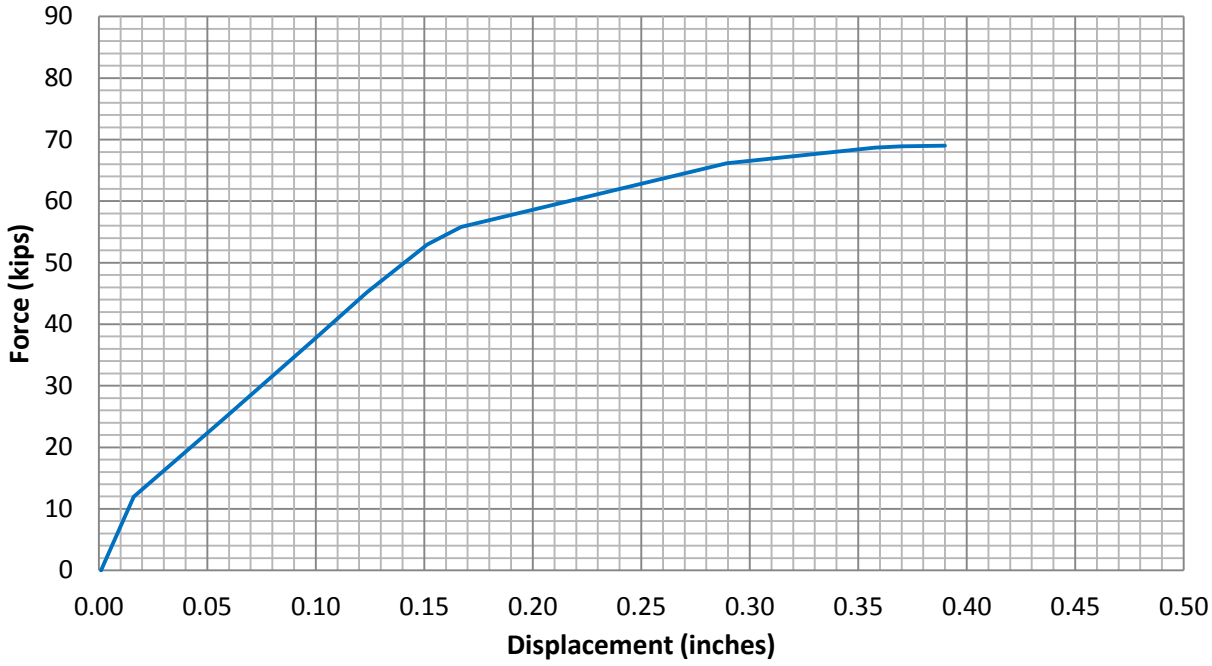

Figure 5-22: Force-Displacement Response of Test Unit H2C1-M

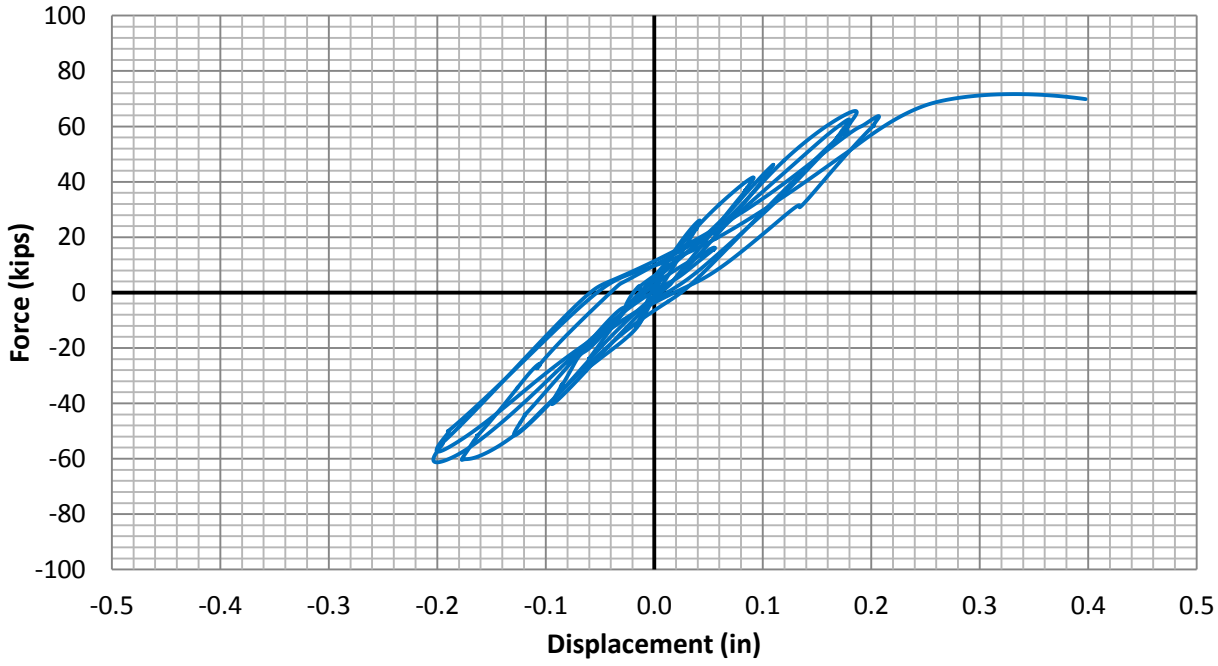

Figure 5-23: Force-Displacement Response of Test Unit H2C2-C

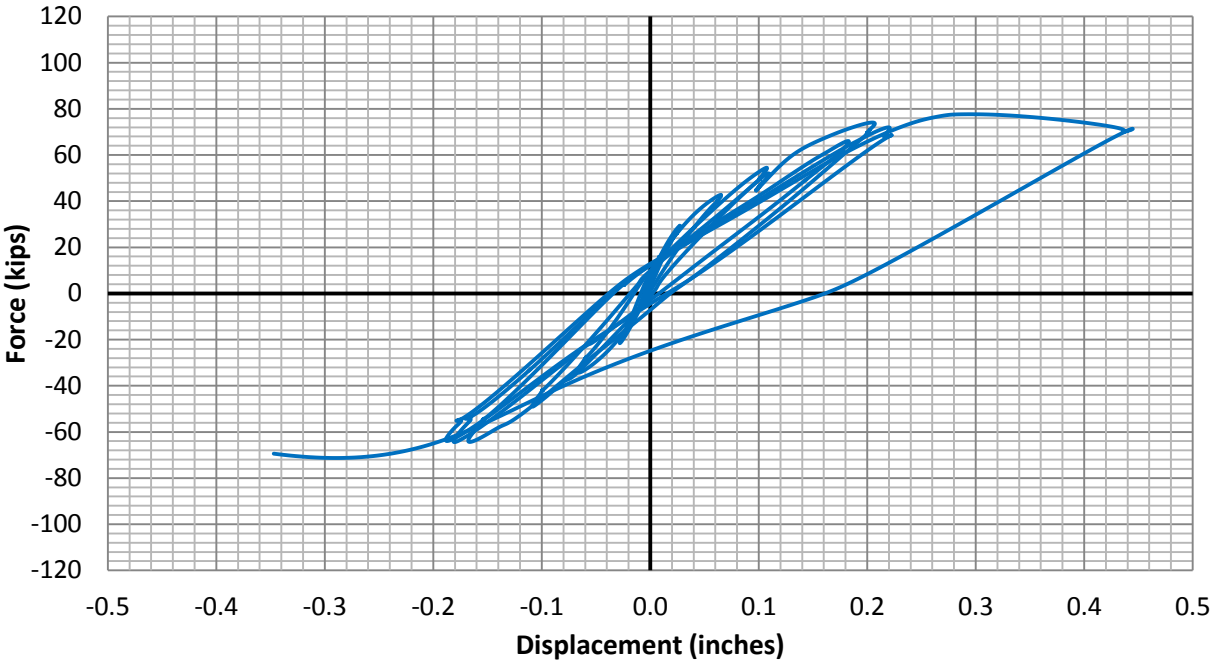

Figure 5-24: Force-Displacement Response of Test Unit H2C3-C

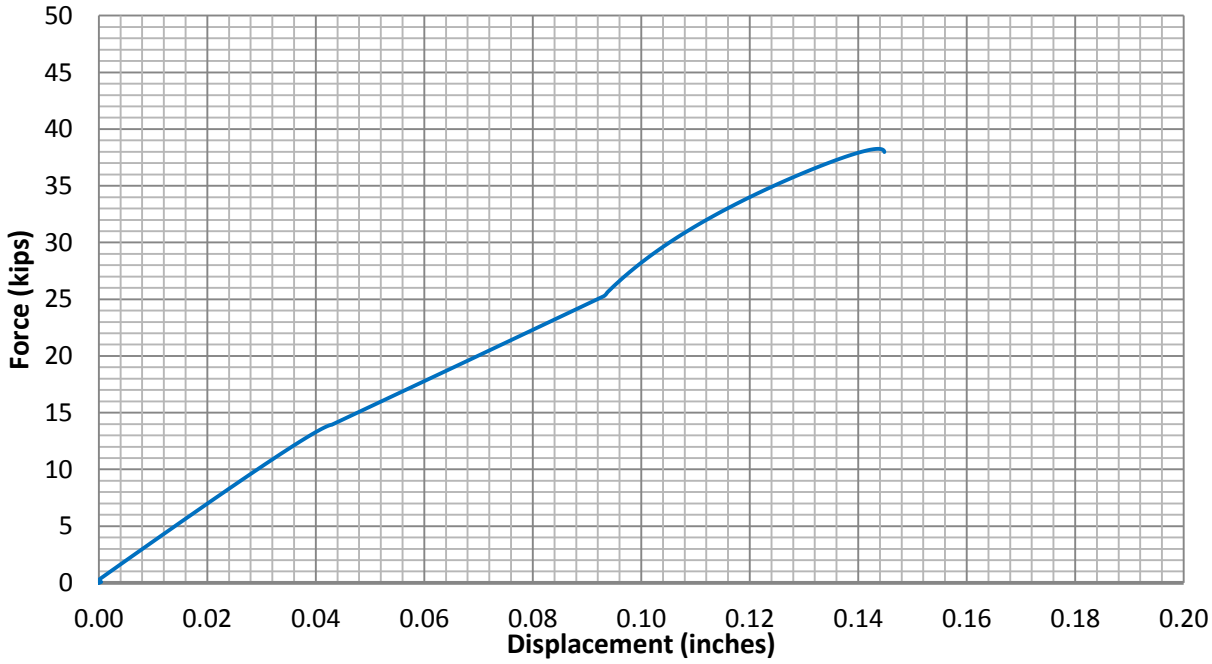

Figure 5-25: Force-Displacement Response of Test Unit H1C1-M

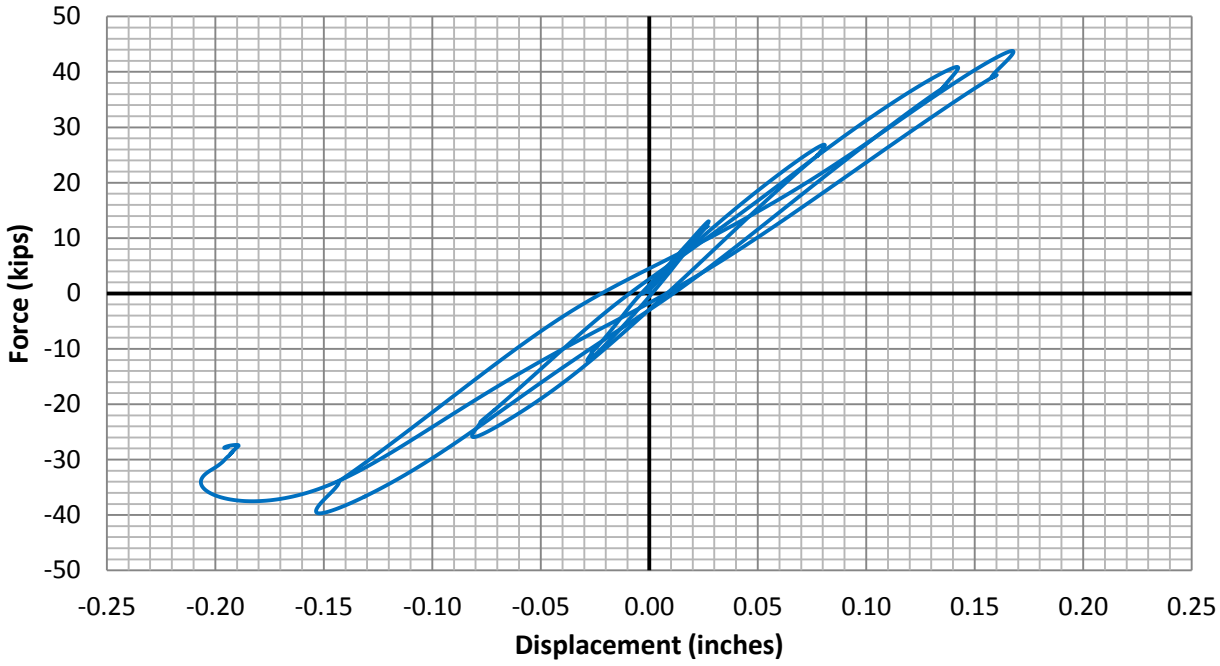

Figure 5-26: Force-Displacement Response of Test Unit H1C2-C

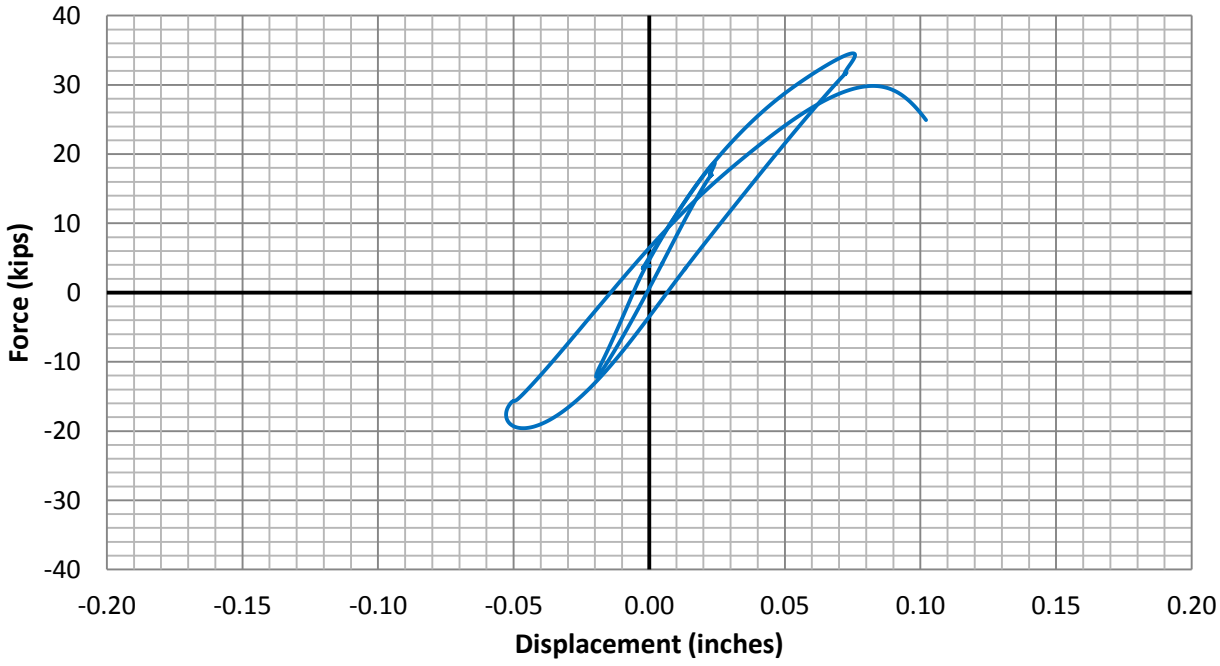

Figure 5-27: Force-Displacement Response of Test Unit H1C3-C

Figure 5-28 shows the force-displacement response comparisons for the solid, two-inch wall and one-inch wall hollow columns under 22.6 kips axial load. As shown, the solid column presents a higher capacity and higher stiffness compared to the hollow specimens. Although the capacity of the solid section was higher, this specimen also had an increasing axial load, which likely contributed to the lateral load capacity of the specimen. The two-inch wall hollow specimen experienced a larger ultimate displacement compared to the solid specimen, which was attributed to the greater shear deformation experienced in the hollow columns. The shear deformation experienced by the hollow specimens will be discussed in detail in the next section.

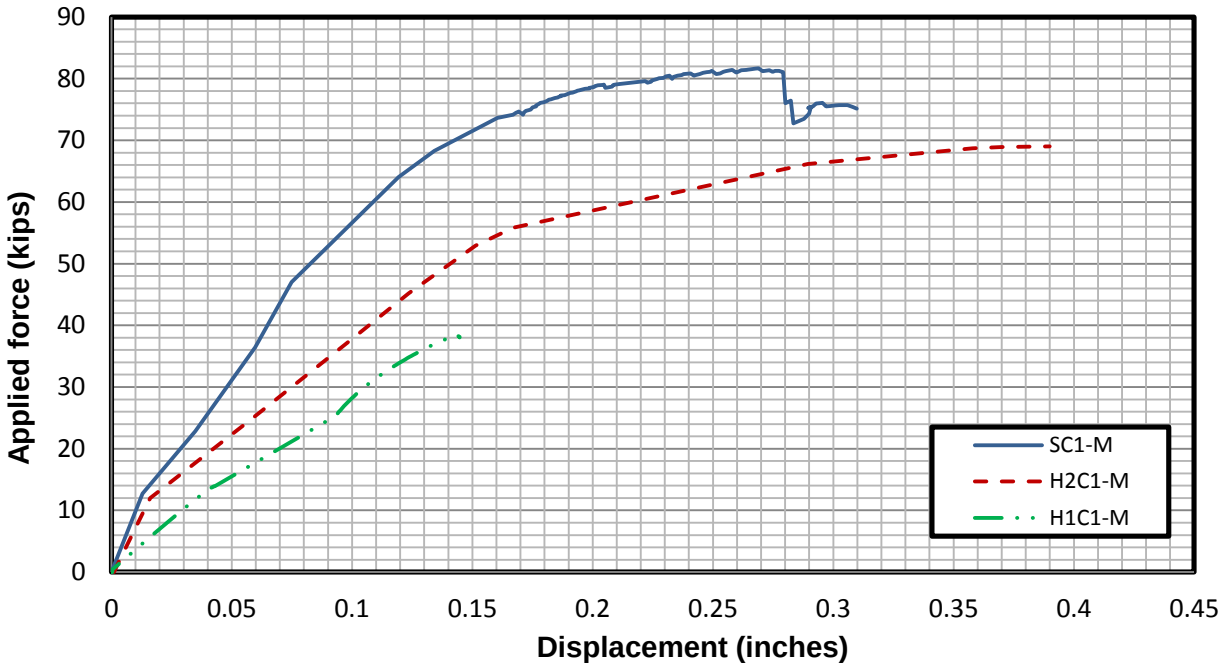

Figure 5-28: Force-Displacement Response Comparisons for Solid, Two-Inch Wall, and One-Inch Wall Hollow Circular Columns under 22.6 kips Axial Load

Figure 5-29 displays a comparison between montonic and cyclic loading response. The specimens used for comparison are the hollow specimens with two-inch thick walls, both of which were subjected to 22.6 kips of axial load. As shown, there is little difference between the

responses of the two units. Cyclic testing can often experience earlier failure due to material fatigue. However, the cyclic specimens in this experimentation were only subjected to a relatively small amount of cycles before longitudinal steel failure occurred, due to the small ultimate strain of the steel. For this reason, it is likely that not enough cycles were performed for material fatigue to have a significant effect, causing the response to be very similar between cyclic and montonic testing.

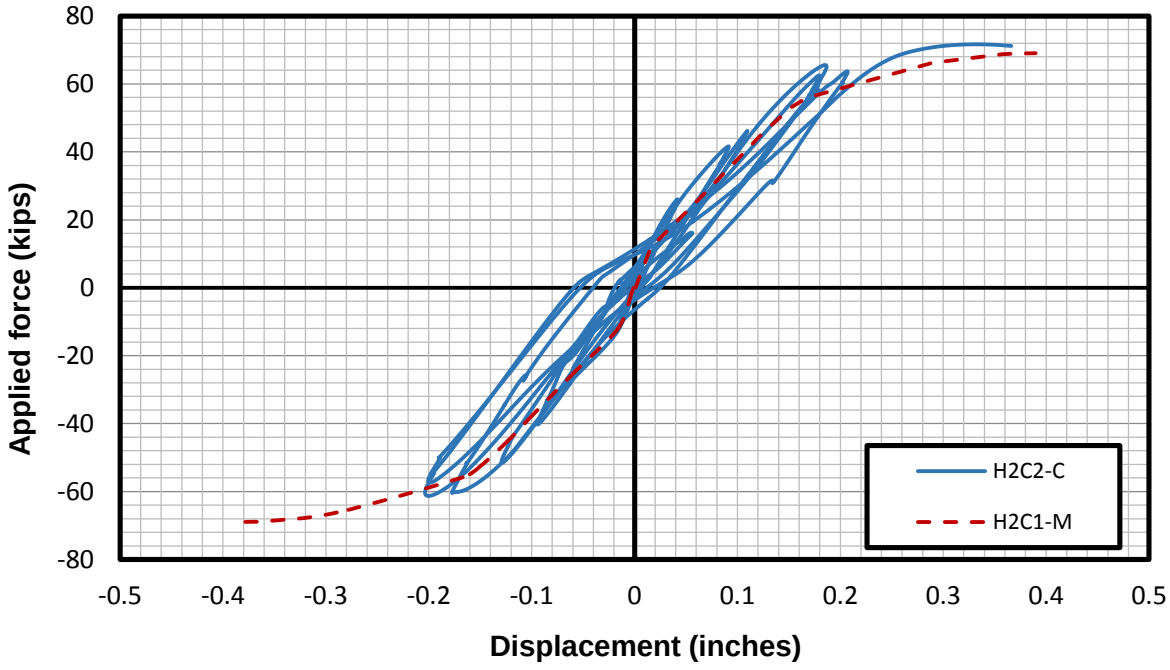

Figure 5-29: Force-displacement response comparisons of two-inch wall hollow columns under monotonic and cyclic loadings

5.2.1.2.2 Shear contribution

It became apparent when testing the hollow columns that the hollow columns experienced a larger percentage of shear displacement than the solid columns did. Typical analysis methods used in design, as well as the OpenSees analysis used in this research, do not account for shear displacement, and thus it became necessary to estimate the amount of shear displacement experienced by the columns. A method was utilized using a set of LEDs in the shear region to

estimate the shear displacement. The method has been adopted, which was used previously by Sritharan (1998), and in this case a grid of LEDs was used to determine the various deformation components.

The shear contribution of the solid specimens was unable to be measured during testing since shear had not been identified as an issue and vision of key LEDs was blocked in many cases. However, the shear contribution of the hollow columns was able to be estimated well in most cases. The following plots show the shear displacement plotted against the applied load for all specimens as well as the force-displacement response of each specimen with shear included and with shear subtracted for comparison. For monotonic plots only, the envelope is shown for clarity.

The response shown in Figure 5-30 gives the overall force-displacement response as well as the force-displacement response with the shear deformation subtracted for specimen H2C1-M. The shear deformation is fairly significant for this specimen, and accounts for approximately 30 percent of the overall displacement of the specimen. The shear deformation is plotted against the applied load in Figure 5-31. As shown in the figure, the shear deformation increases linearly with increased loading in the measured portion of the specimen, indicating that shear capacity was not reached within the linear moment region of the specimen. This agrees with the observed test results which found some minor shear cracking in the linear moment region, and that the specimen ultimately failed due to flexure in the constant moment region.

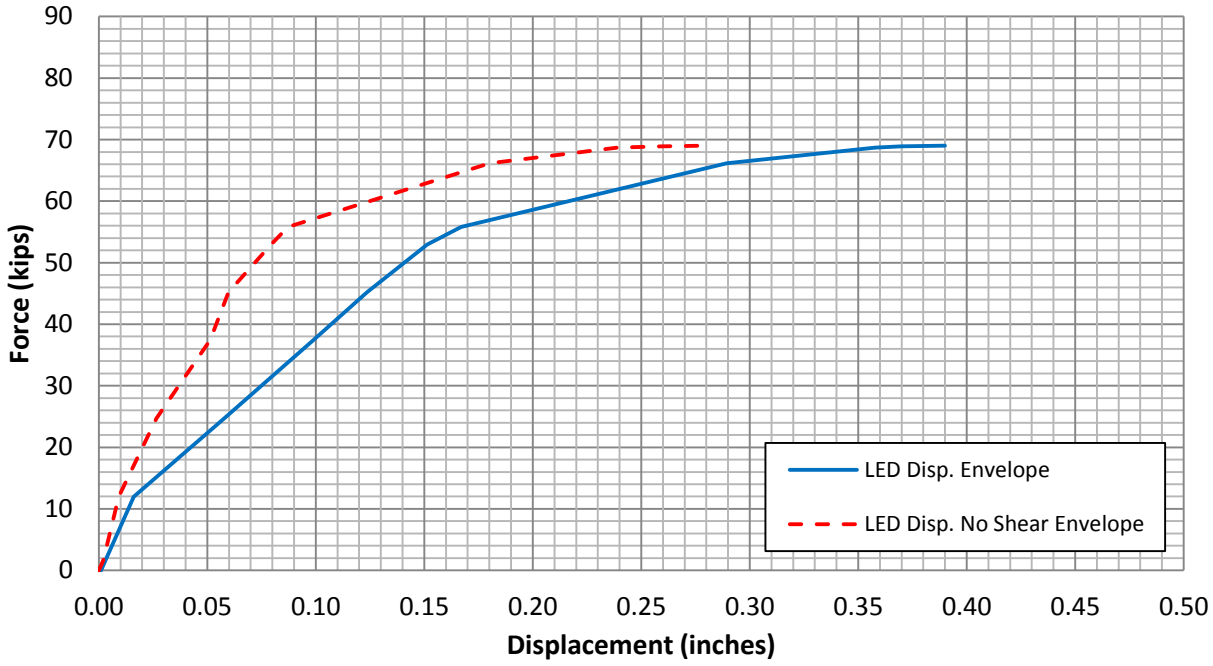

Figure 5-30: Force-Displacement of Specimen H2C1-M with and without Shear Deformation

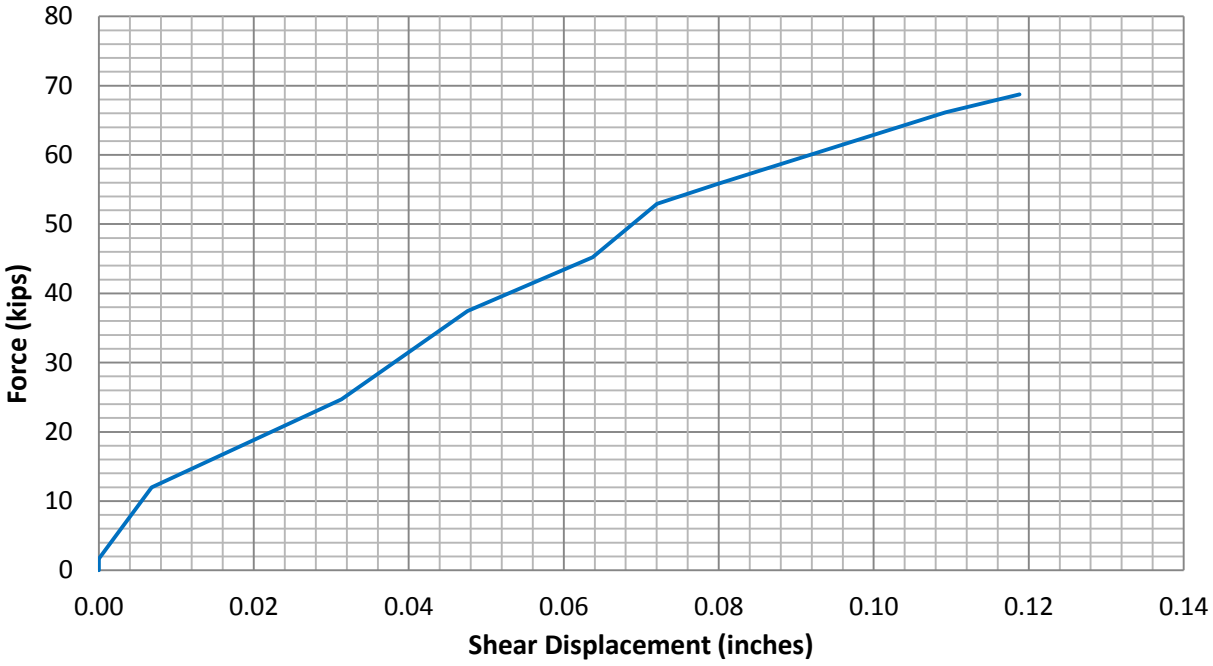

Figure 5-31: Force vs. Shear Displacement of Specimen H2C1-M

The response with and without shear deformation for specimen H2C2-C is shown in Figure 5-32. Again, shear was fairly significant for this specimen, contributing 20 to 30 percent of the overall displacement, depending on which lateral loading direction was used. The difference in measured shear displacement in each loading direction may be due to local effects or possibly by some minor asymmetry in the column. The shear deformation is plotted against the applied load for this specimen in Figure 5-33. The shear deformation of this specimen also increases linearly as the applied load increases, as was the case for almost all of the specimens. For this reason, the plots of shear deformation against the applied load are not shown for the remainder of the specimens. Specimen H1C3-C experienced some nonlinearity due to the local punching failure at one of the load application points. This point was near the linear moment region where the shear displacement was measured, which is why this local punching failure caused nonlinearity in the measured shear.

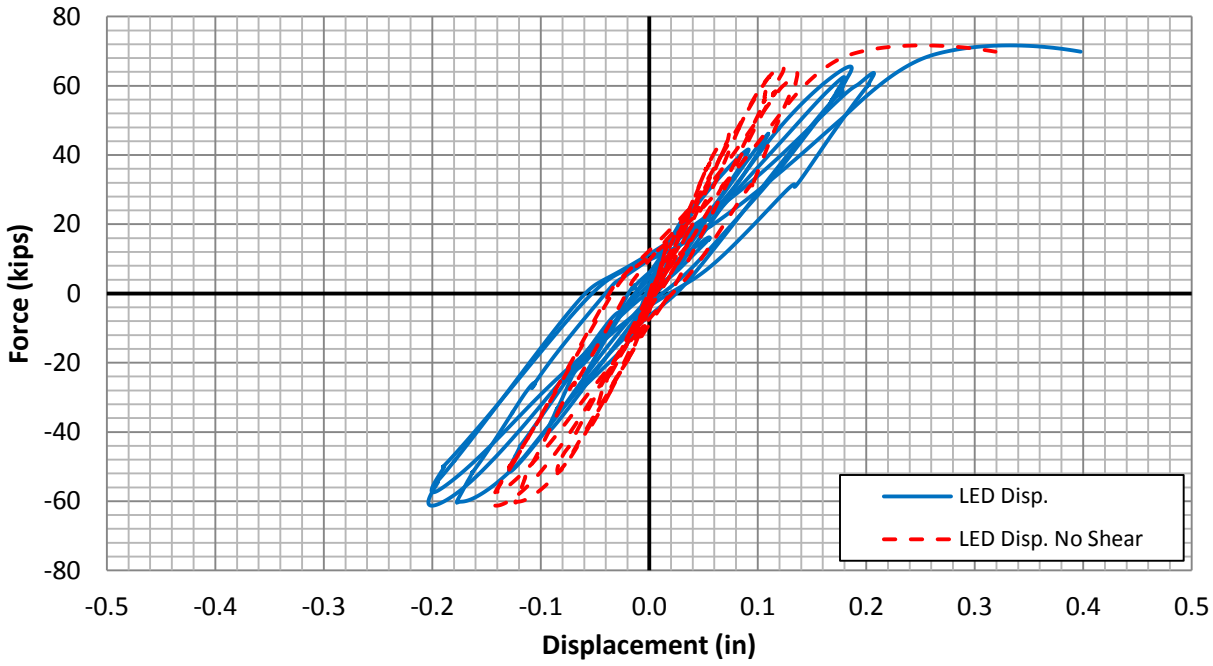

Figure 5-32: Force-Displacement of Specimen H2C2-C with and without Shear Deformation

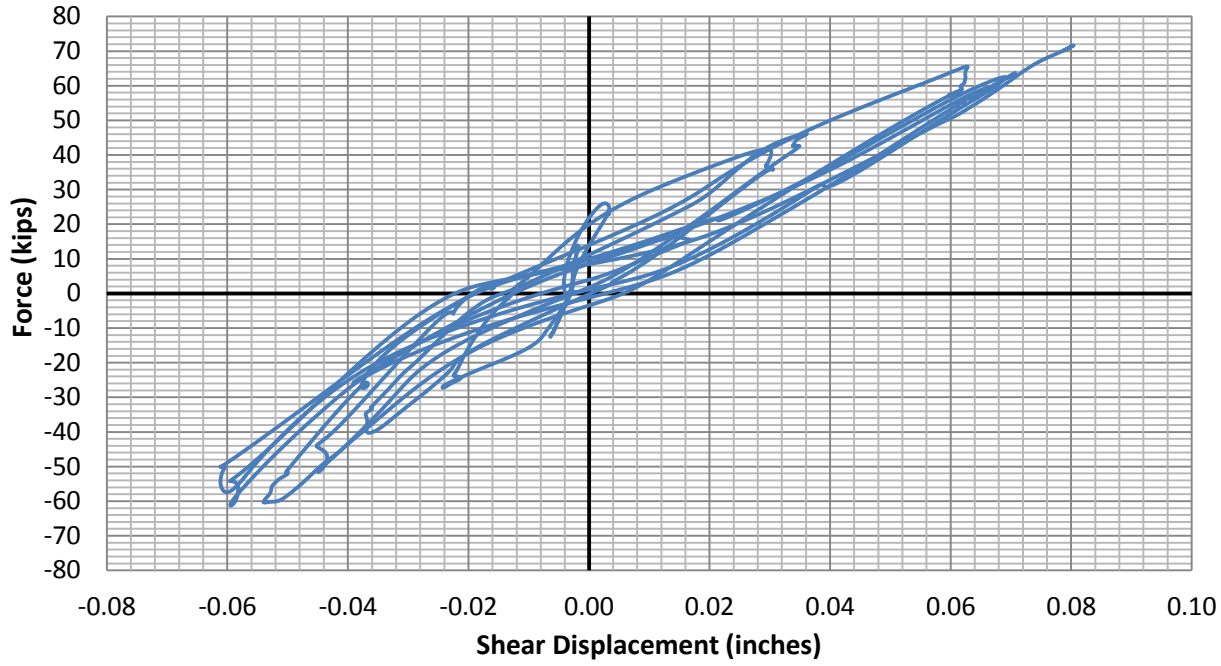

Figure 5-33: Force vs. Shear Displacement of Specimen H2C2-C

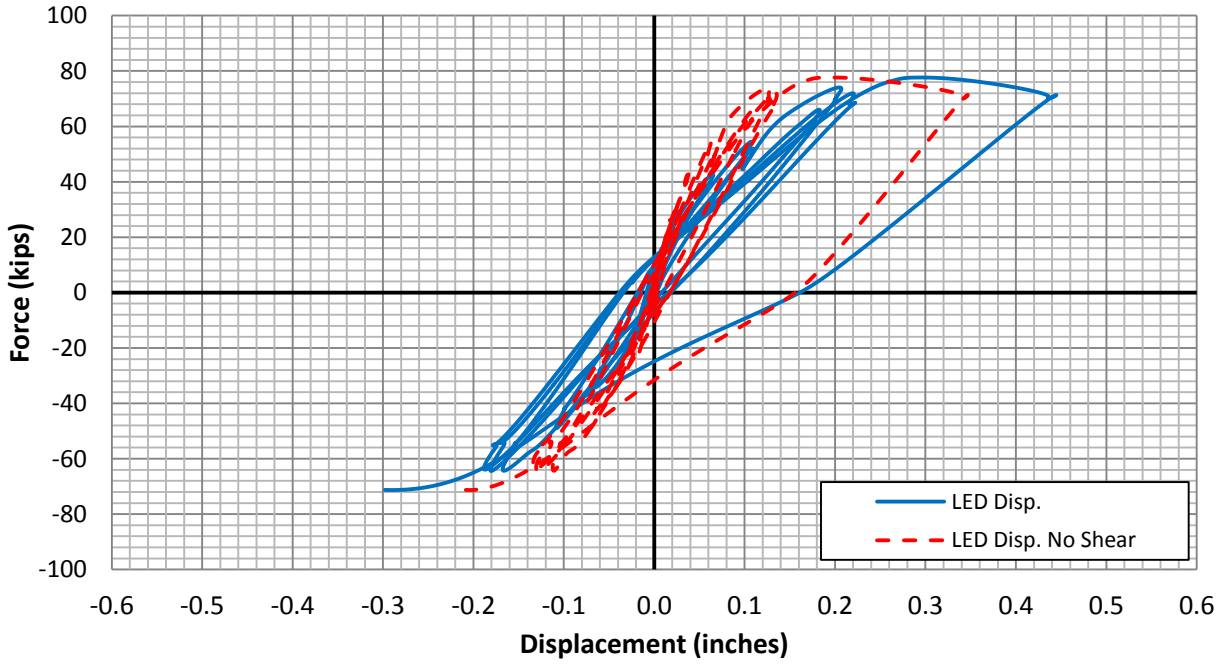

Figure 5-34: Force-Displacement of Specimen H2C3-C with and without Shear Deformation

Figure 5-35 through Figure 5-37 present the specimen force-displacement responses with and without shear for the one-inch thick specimens. It can be seen that for the one-inch thick specimens, the shear deformation is more significant than that of the two-inch thick specimens. For the one-inch thick specimens, the shear deformation typically accounted for between 40 and 60 percent of the overall displacement at the peak displacement.

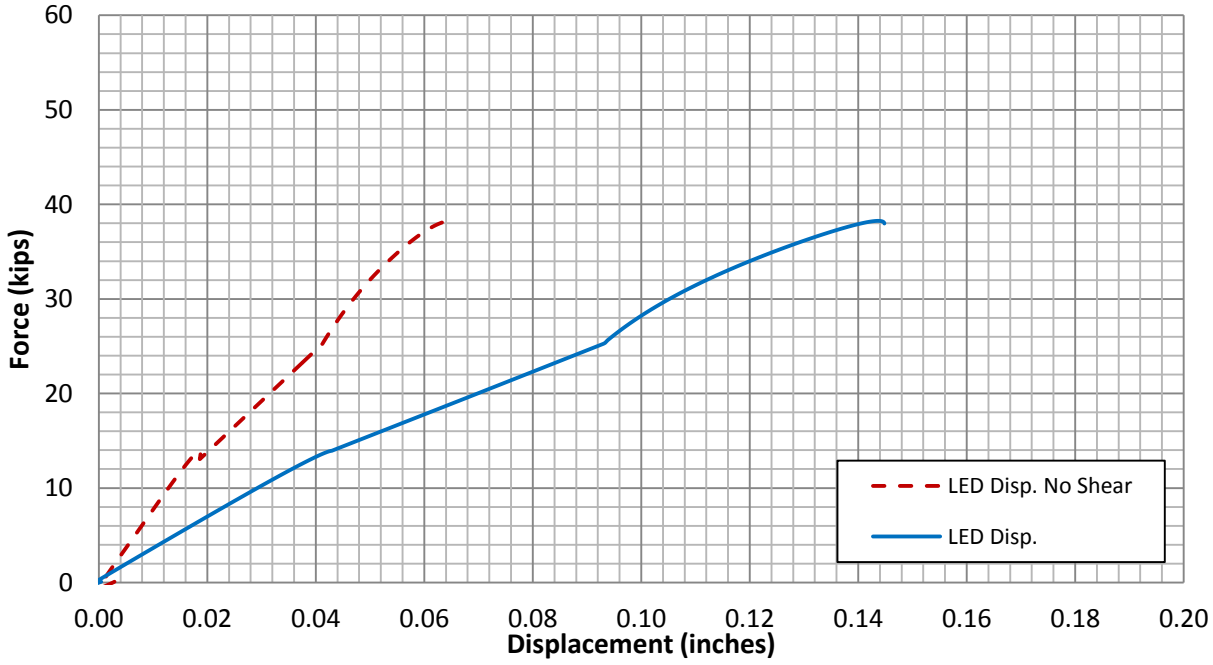

Figure 5-35: Force-Displacement of Specimen H1C1-M with and without Shear Deformation

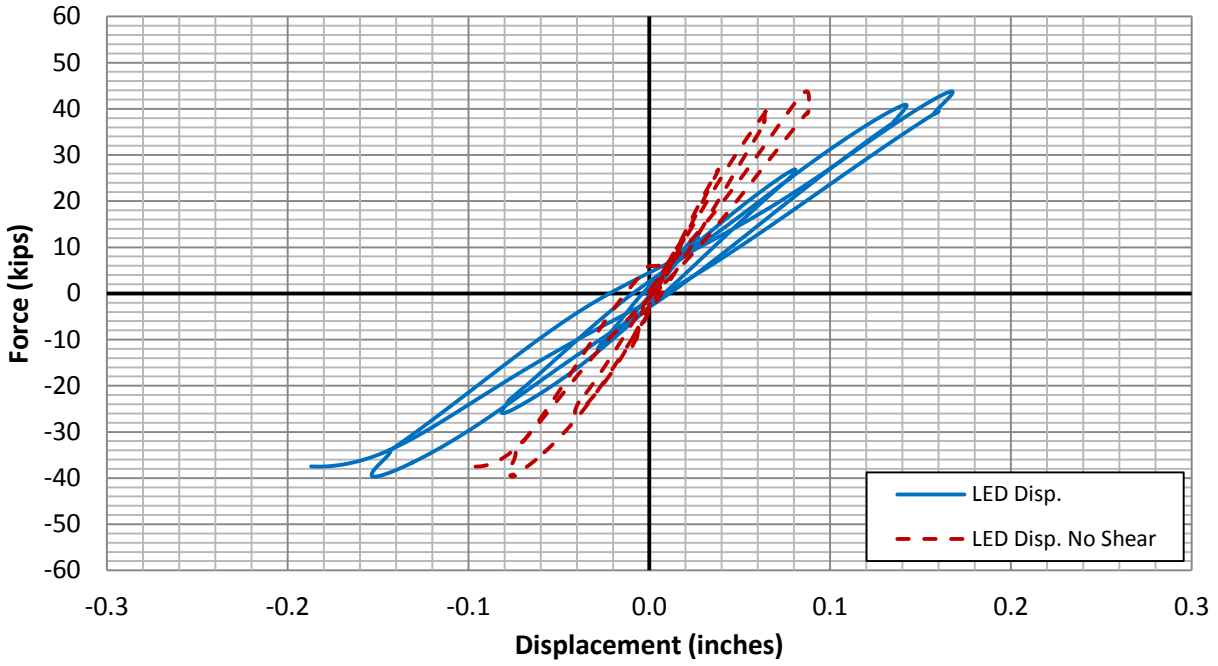

Figure 5-36: Force-Displacement of Specimen H1C2-C with and without Shear Deformation

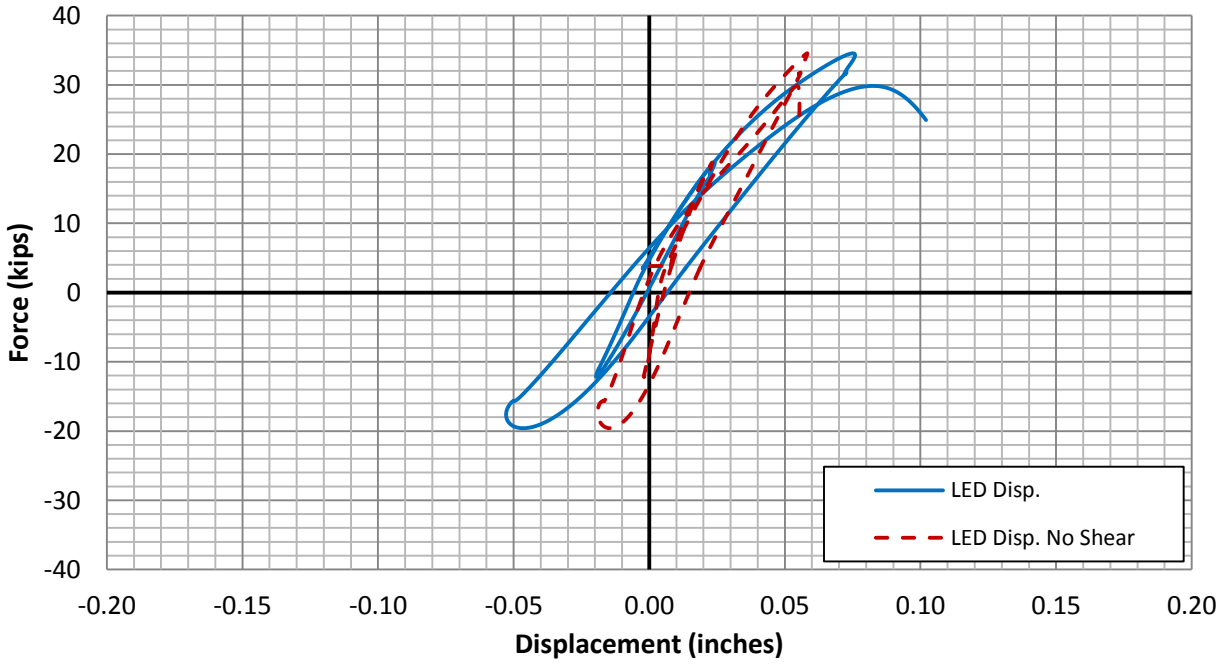

Figure 5-37: Force-Displacement of Specimen H1C3-C with and without Shear Deformation

5.2.1.2.3 Force-displacement response without shear

Due to the fact that the OpenSees analysis method used in the research did not incorporate shear effects, the force-displacement response of the hollow test specimens with the shear component removed has been compared to the OpenSees analysis. For the solid sections, the shear component was not able to be measured during the testing, so the overall specimen displacement has been compared to the OpenSees analysis. An estimate of the shear component has also been provided for the solid columns using a model provided by Beyer et al. (2011), which is based on the curvature and geometry of the section. The model was developed for slender reinforced concrete walls but has been applied to the current testing in order to provide an estimate of the shear contribution. The model has been shown in results for the solid section and has also been provided for the monotonically tested hollow section with a two-inch thick wall, in order to determine how applicable the model is to hollow columns.

The force-displacement response of specimen SC1-M is shown in Figure 5-38. As mentioned, the shear response of this specimen was not measured during testing, so the test results provided in the figure give the overall displacement of the specimen. The shear component of the response has also been estimated using the shear model mentioned in the previous paragraph (Beyer et al., 2011). This estimated shear component has been added to the flexural component provided by the OpenSees analysis and has been included in the figure. As shown, the analytical response including shear seems to match the test results more accurately than the flexural response from the OpenSees analysis alone but also greatly overestimates the displacement at which longitudinal steel failure occurs.

It is also important to recall that specimen SC1-M experienced a steady increase in axial load throughout the test. The initial axial load was 22.6 kips, and the axial load had increased to 40 kips by the end of the test. This increase in axial load was accounted for in the OpenSees analysis to ensure the comparison would be accurate. The axial load during the testing, with the approximated axial load used in the OpenSees analysis, can be seen in Figure 5-39.

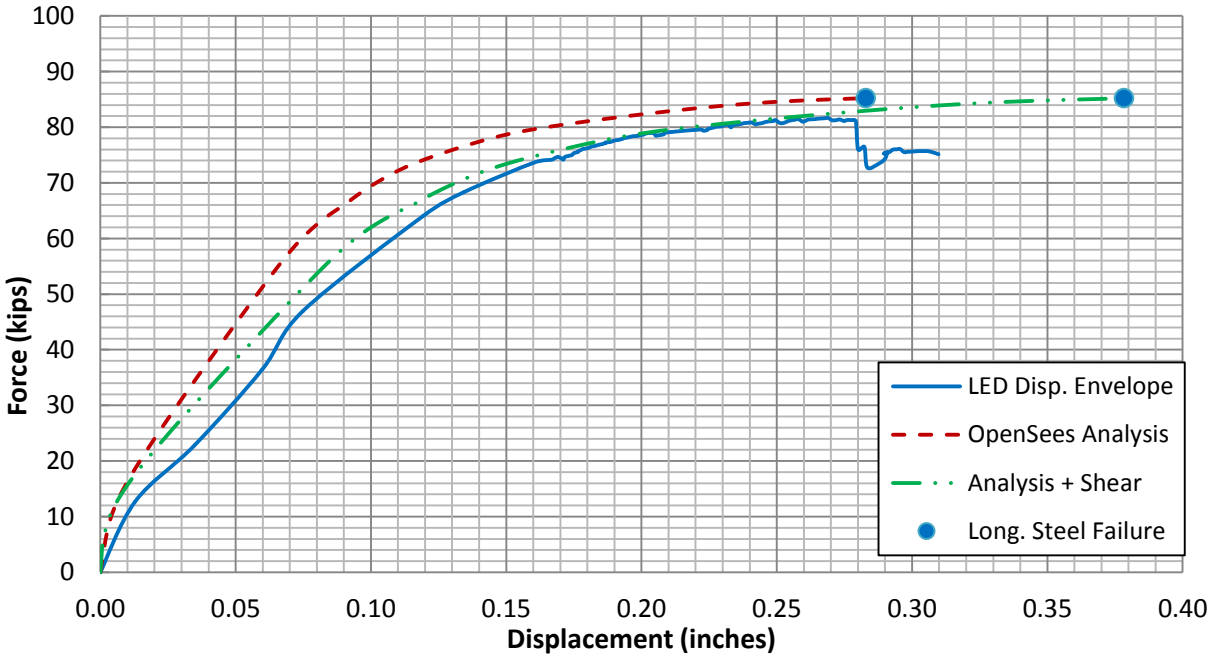

Figure 5-38: Measured Force-Displacement Response of Specimen SC1-M Compared to Analytical Envelope Response

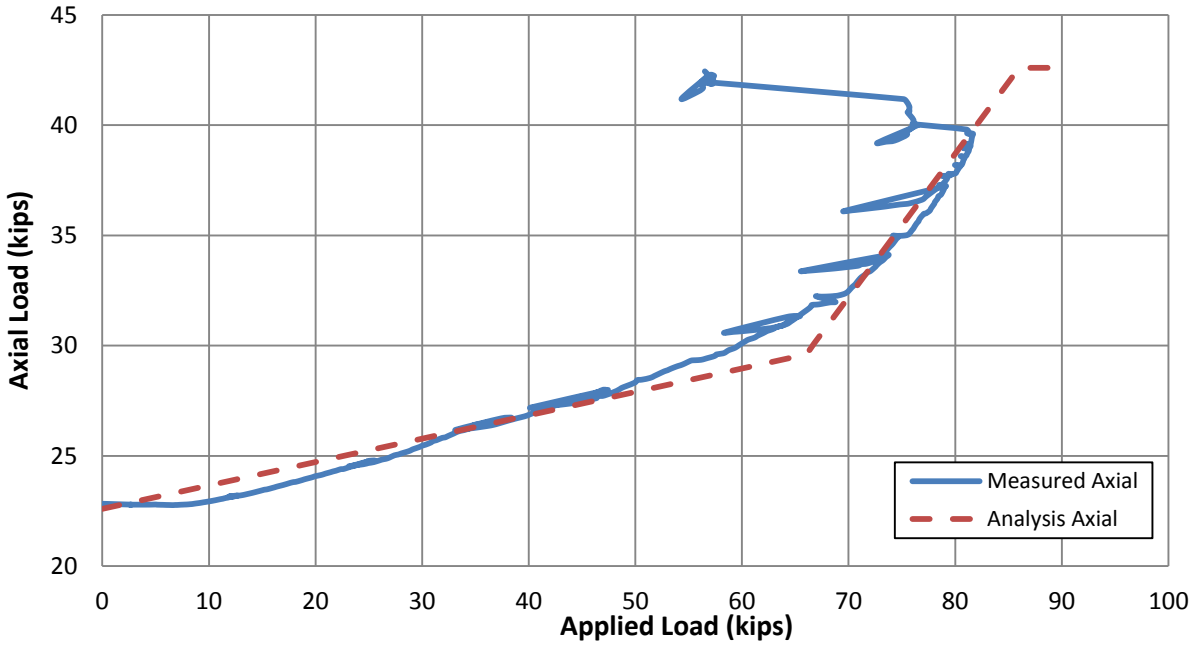

Figure 5-39: Specimen SC1-M Experimental and Analytical Axial Load vs. Applied Load

Figure 5-40 shows the results of specimen SC2-C plotted with the OpenSees analytical response. Similarly to the plot shown for specimen SC1-M, the estimated shear component has been added to the OpenSees flexural component and has been included in the figure. As noted for specimen SC1-M, the shear response for specimen SC2-C is fairly similar to the flexural response, although it provides a much higher estimate of the displacement at the longitudinal steel failure.

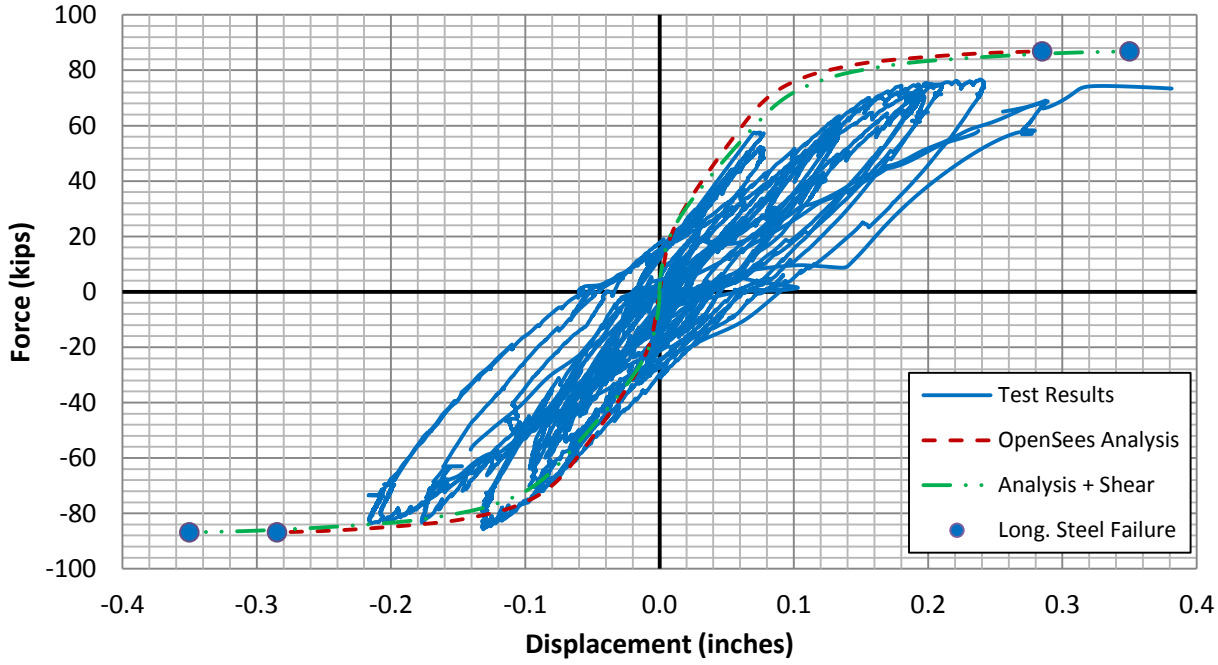

Figure 5-40: Measured Force-Displacement Response of Specimen SC2-C Compared to Analytical Envelope Response

The experimental and analytical response of specimen H2C1-M, with the shear deformation removed, is shown in Figure 5-41 as well as the total experimental response and the analytical flexural response with the estimated shear component added. In this case, the response with the analytical flexure and shear components combined significantly underestimates the overall measured response. This is most likely because the shear model was developed for shear walls and not for hollow columns. As demonstrated in Section 5.2.1.2.2, shear in hollow columns

seems to be significantly higher than for solid columns, and current shear models have not taken this into account.

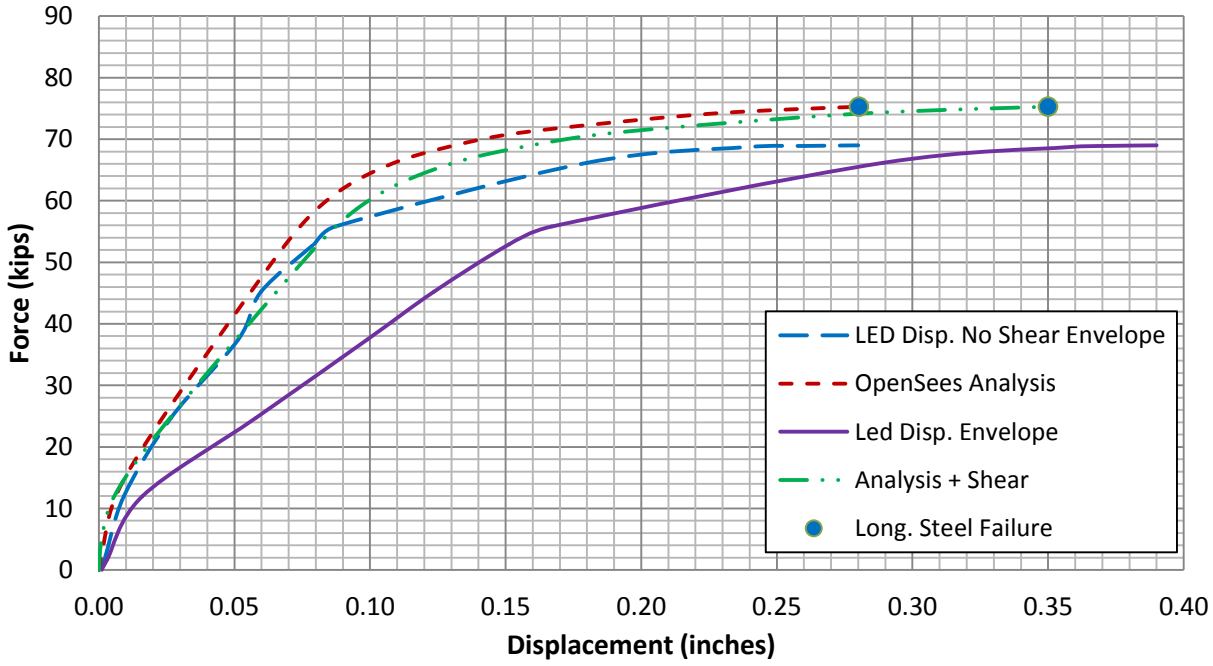

Figure 5-41: Measured Force-Displacement Response of Specimen H2C1-M with Shear Deformation Removed Compared to Analytical Envelope Response

The remainder of the force-displacement plots shown in this section have shear subtracted from the measured response and also show only the analytical flexural response for comparison. The expected failure mode, as determined from the analytical response, is also plotted in the figures. As shown, the analytical response compares well to the measured experimental response without shear deformation for the solid specimens and for the two-inch thick specimens, including the failure mode and ultimate displacement at this failure point. For the one-inch thick specimens, the analytical response does not match the experimental response due to the early failure of the specimens caused by local and shear failures.

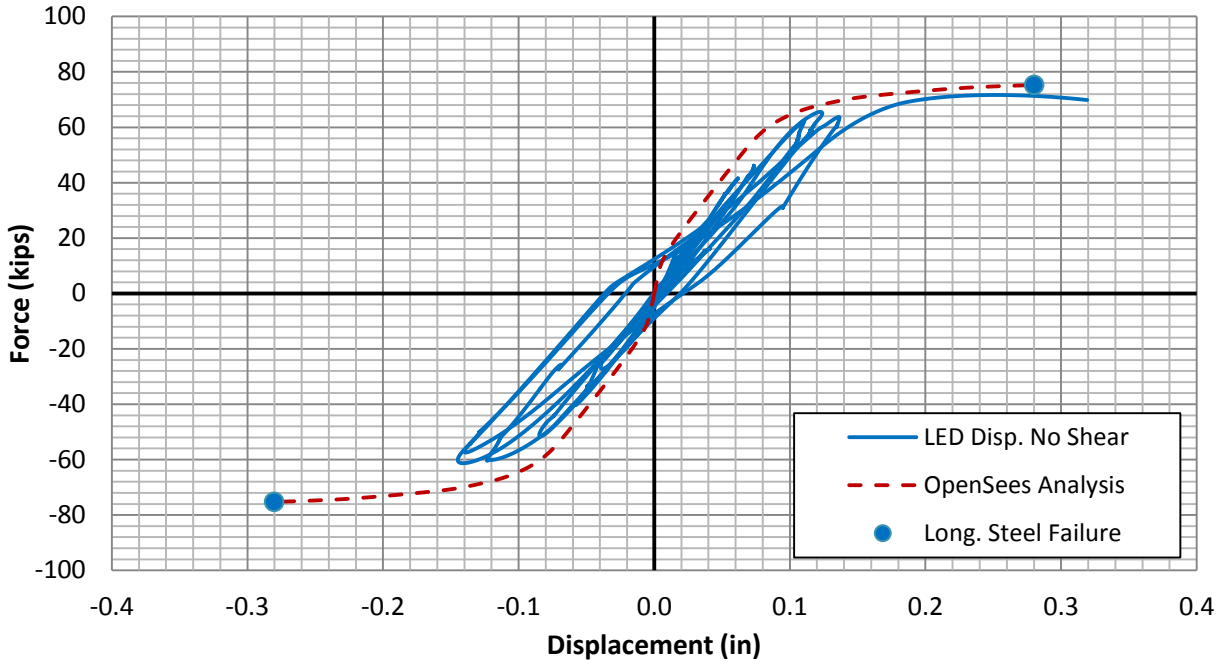

Figure 5-42: Measured Force-Displacement Response of Specimen H2C2-C with Shear Deformation Removed Compared to Analytical Envelope Response

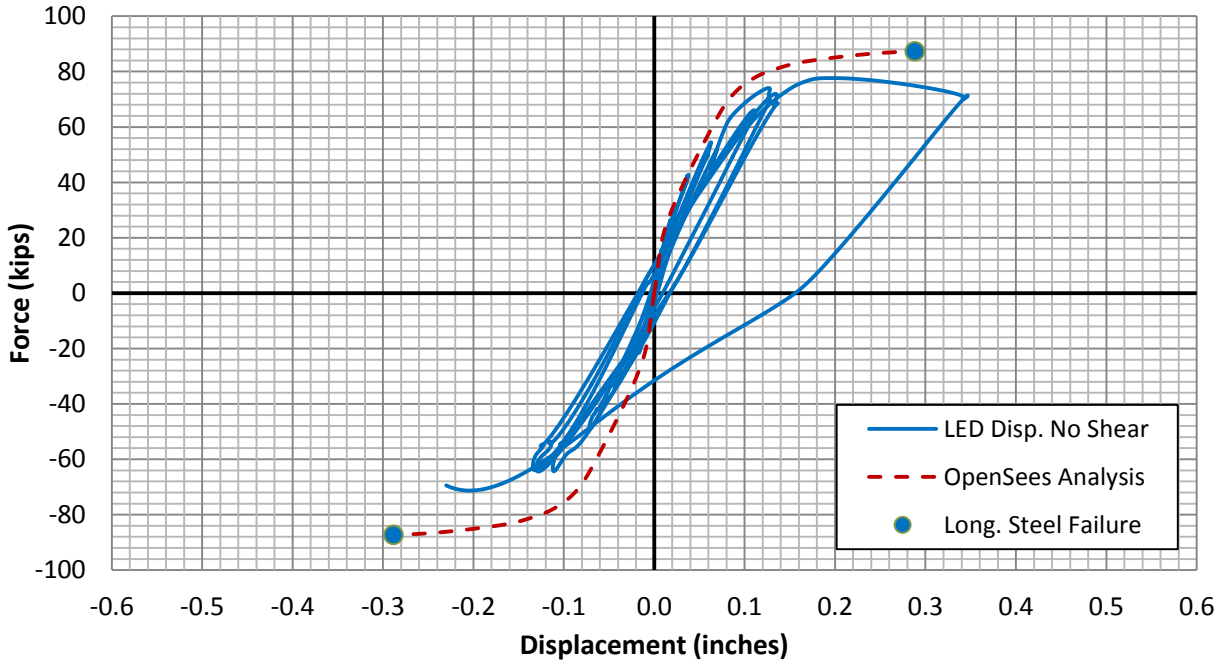

Figure 5-43: Measured Force-Displacement Response of Specimen H2C3-C with Shear Deformation Removed Compared to Analytical Envelope Response

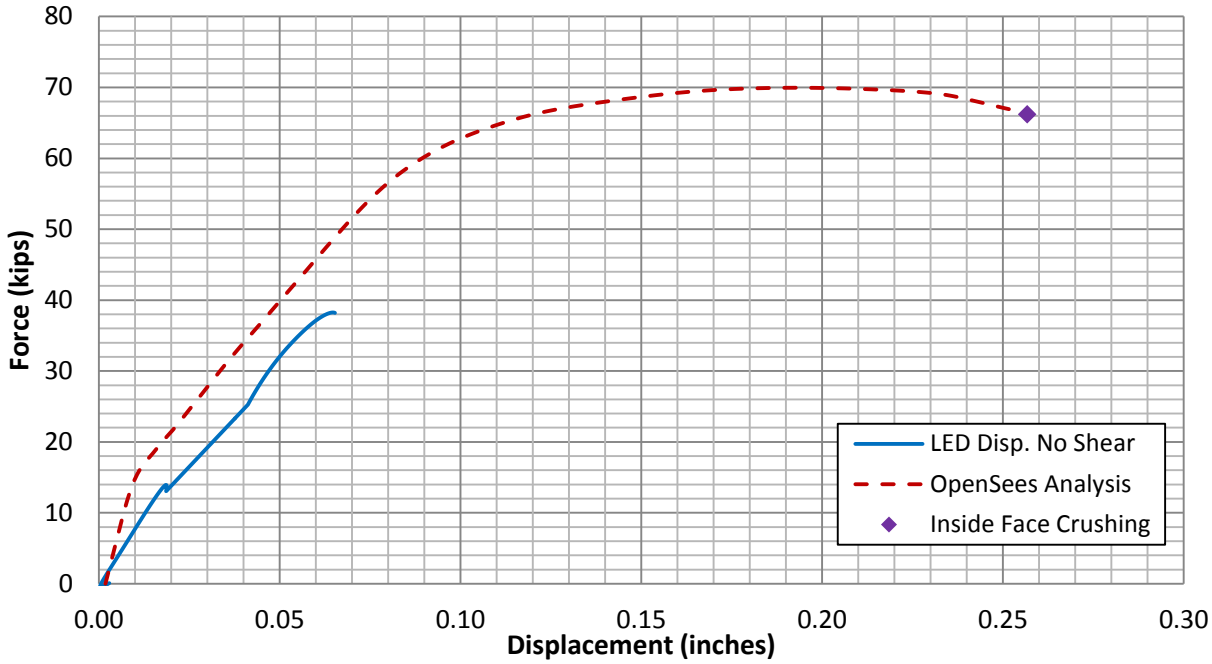

Figure 5-44: Measured Force-Displacement Response of Specimen H1C1-M with Shear Deformation Removed Compared to Analytical Envelope Response

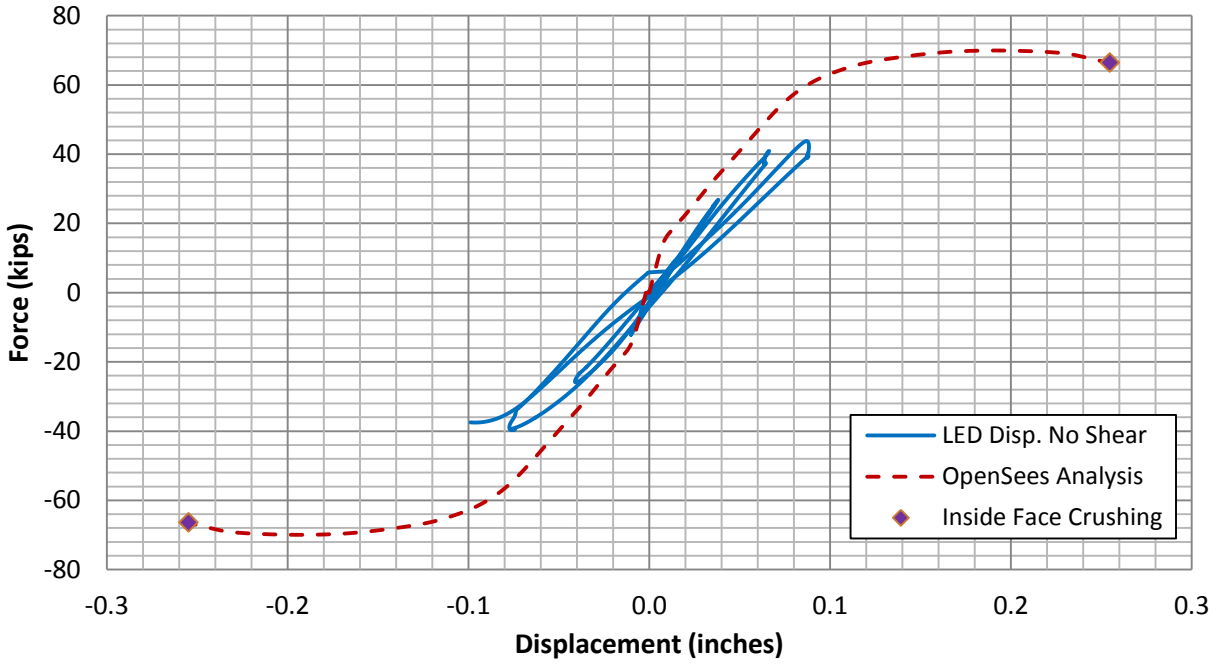

Figure 5-45: Measured Force-Displacement Response of Specimen H1C2-C with Shear Deformation Removed Compared to Analytical Envelope Response

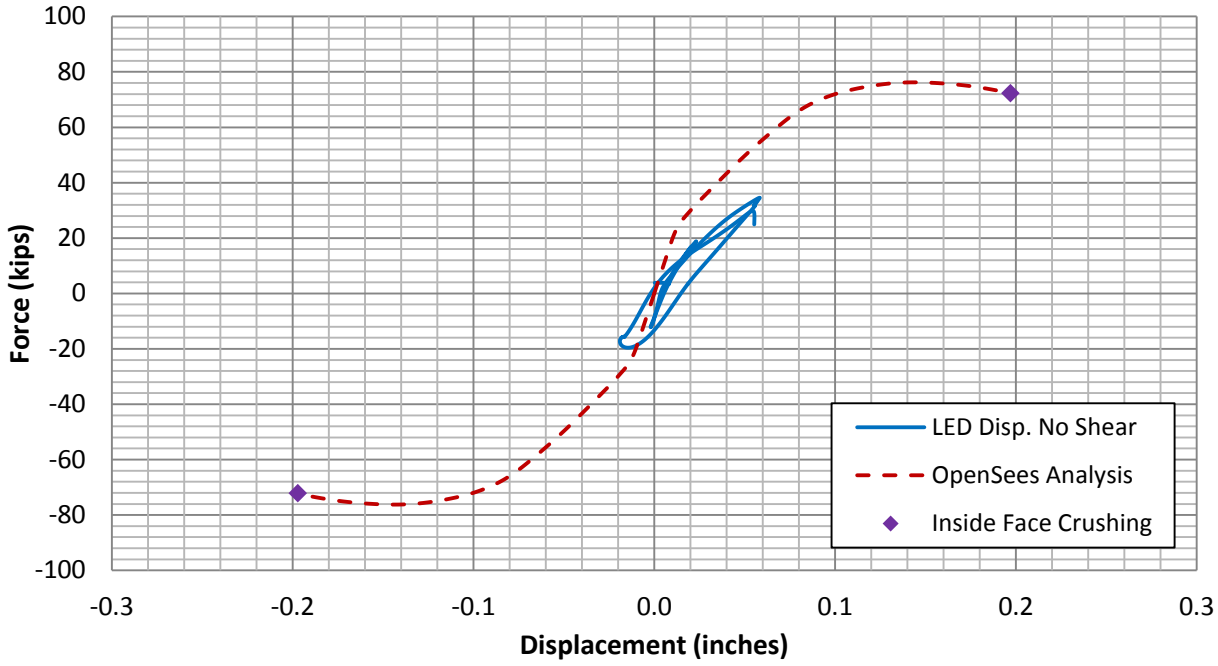

Figure 5-46: Measured Force-Displacement Response of Specimen H1C3-C with Shear Deformation Removed Compared to Analytical Envelope Response

5.2.1.2.4 Longitudinal bar strain

The longitudinal steel strain was measured during the testing, and plots of some of the measured strains compared to the applied load are shown in this section. The figures show longitudinal strains for the bars close to the extreme tension and compression edge in each section, which were measured by strain gauges attached to the longitudinal reinforcement. The strains presented are from the cyclic tests, and the figures are labeled as either near longitudinal bar 1 or longitudinal bar 11. The longitudinal steel strains provided by the OpenSees analysis are also shown in each of these plots to compare to the measured values. The analytical longitudinal steel strains are given at the extreme tension and compression reinforcing bars. The analytical steel strains are reported up until the predicted analytical failure occurs. For the solid and two-inch thick specimens the analytical failure occurred due to tensile steel rupture. For the one-inch thick specimens, the predicted failure mode was crushing of the inside face concrete.

Only some of the measured strains have been presented, since in general the test results and comparison to analytical results are similar to what is shown in the figures below. The OpenSees analysis was in fairly good agreement with the measured steel strains for all of the solid specimens and hollow two-inch thick specimens.

The circular specimen strain gauge locations have been provided again in Figure 5-47 for quick reference. The gauges marked with an asterisk only appeared at one section in the specimen, while all other gauges were at both sections. A more in-depth discussion of strain gauge locations was provided in Section 4.5. The measured response compared to analytical response for certain longitudinal bars is provided in Figure 5-48 through Figure 5-52.

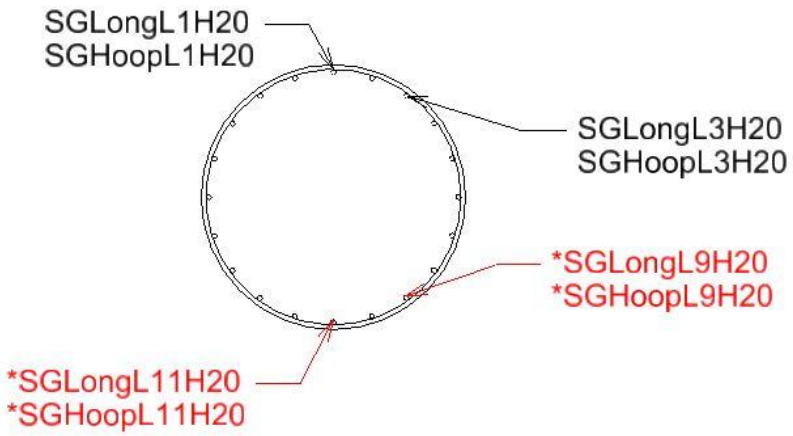

Figure 5-47: Circular Section Strain Gauge Locations

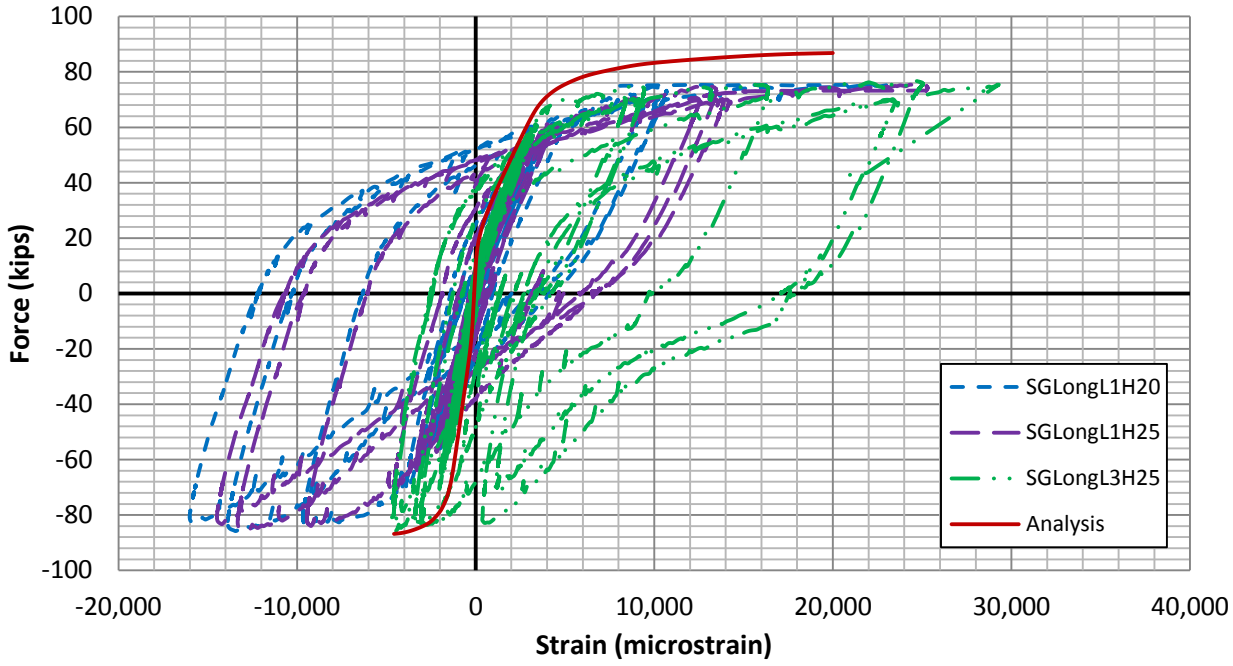

Figure 5-48: Specimen SC2-C Longitudinal Strain near Longitudinal Bar One vs. Applied Load

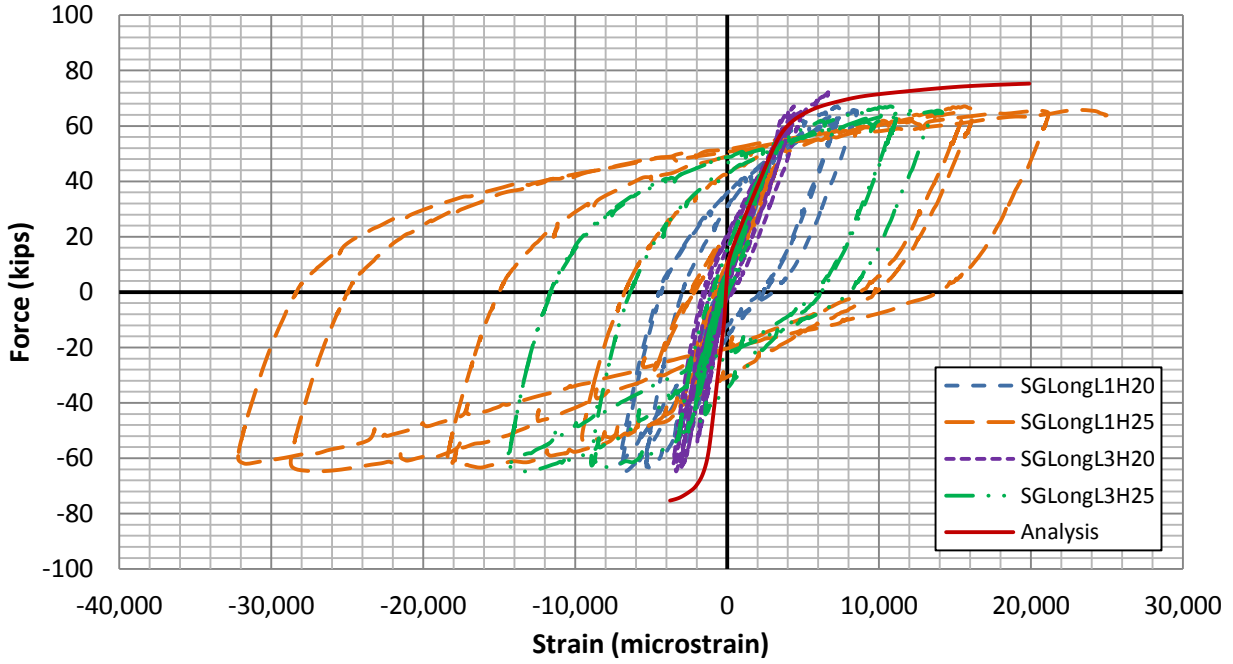

Figure 5-49: Specimen H2C2-C Longitudinal Strain near Longitudinal Bar One vs. Applied Load

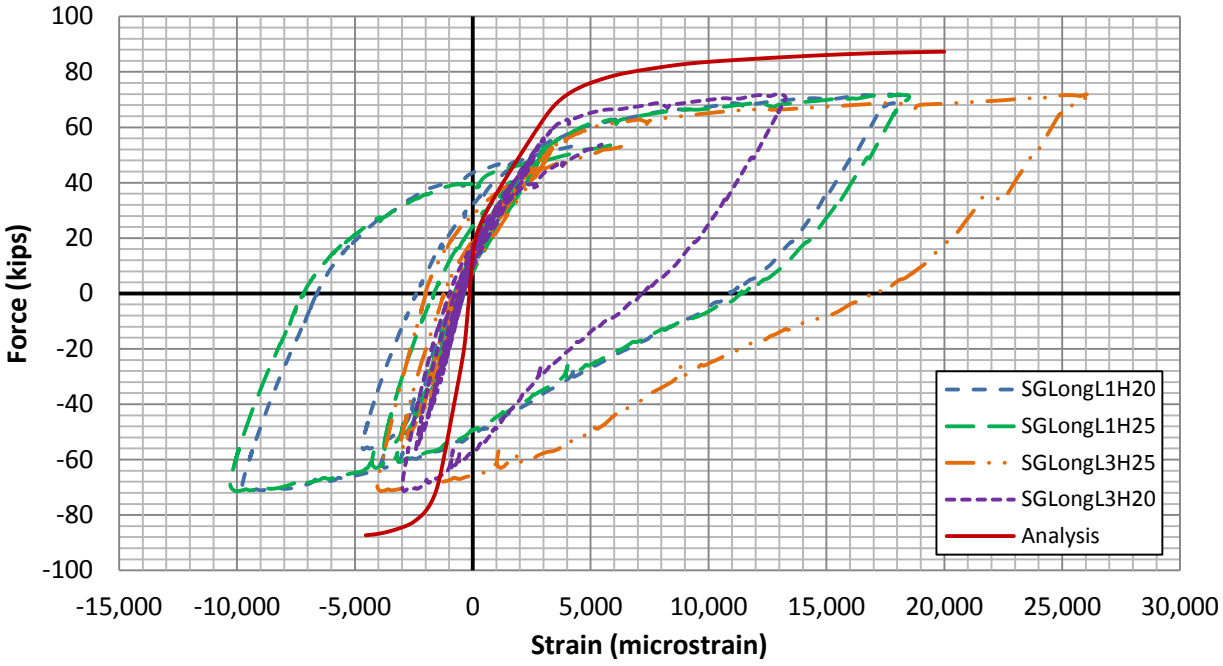

Figure 5-50: Specimen H2C3-C Longitudinal Strain near Longitudinal Bar One vs. Applied Load

The analytical longitudinal steel behavior in the plots for the one-inch thick specimens below show the analytical steel behavior up to the point of specimen failure. These specimens were predicted to fail due to high inside face compression strain, and the analytical longitudinal steel has been plotted up until this predicted failure point. These one-inch thick specimens experienced early failure during the testing due to local and shear effects. The analysis only measured the flexural response, and thus the ultimate displacement and force predicted by the analysis are very different than what was seen during the testing. Despite this, the analysis was still able to agree with the measured strains in the linear range.

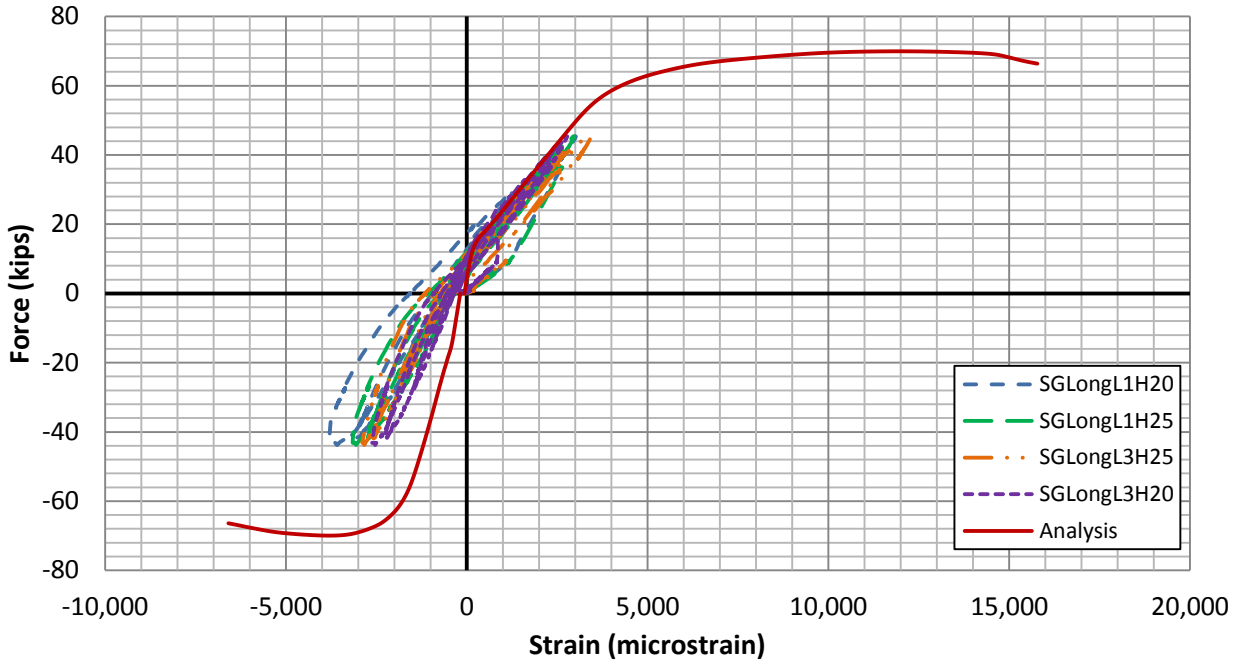

Figure 5-51: Specimen H1C2-C Longitudinal Strain near Longitudinal Bar One vs. Applied Load

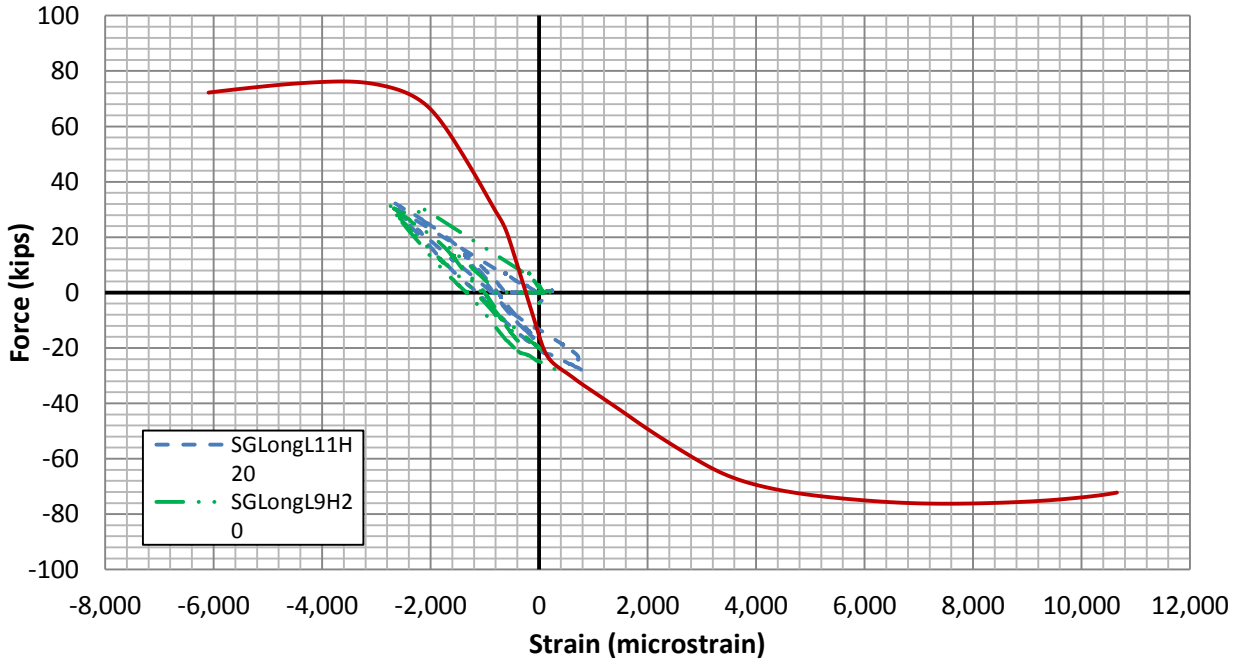

Figure 5-52: Specimen H1C3-C Longitudinal Strain near Longitudinal Bar 11 vs. Applied Load

As shown in Figure 5-48 through Figure 5-52, the analysis is able to match fairly closely to the actual measured values. The compressive strains measured by the strain gauges during testing appear very high in some cases. These high strains are likely caused by gauge errors, since these large compressive strains would have been visible due to increased damage to the concrete in the compressive region. Despite larger measured compressive strains, the measured tensile strains agree closely with the analytical tension steel strains. The next section presents the strains measured by LEDs attached to the concrete surface and compares them with analytical strains in order provide additional verification of the analytical method, as well as to give another estimate of the extreme fiber compressive strains experienced by the test units.

5.2.1.2.5 Concrete strain

The concrete strains near to the top and bottom of the sections were found using the LED grid in the constant moment region. The location of the presented LEDs was fairly close to the extreme compression and tension faces, so the longitudinal reinforcement strains from the extreme tension and compression reinforcement found in the OpenSees analysis has been plotted for comparison. The tension and compression strains are presented in the same plot, as well as the analytical strains. The measured strains are labeled either “Strain57” representing the strain measured between LEDs 5 and 7, or “Strain1820” representing the strain measured between LEDs 18 and 20.

The layout of the LEDs used during testing is shown in Figure 5-53 for reference. The measured LED strains presented in this section were measured in the constant moment region. The strain gauge sets, which were used in the plots, are highlighted in the figure.

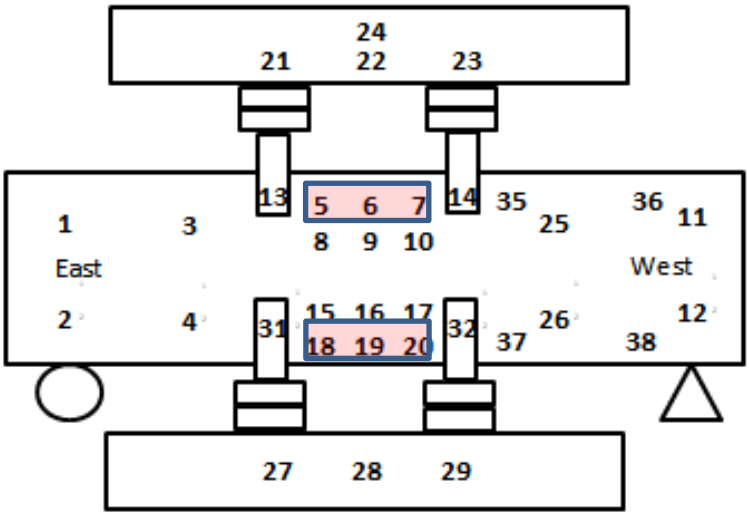

Figure 5-53: LED Layout with Highlighted Strain Locations

The measured and analytical strains are plotted against the applied lateral load for the solid and two-inch thick specimens in Figure 5-54 through Figure 5-56. The plots show good agreement between the measured and analytical strains. Additionally, the compressive strains measured by the LEDs are not as large as was shown by the strain gauges, and agree better with the visual results of the test specimens. The test specimens did not show signs of high compressive strains, since there was not a large amount of crushed concrete near the extreme compression region. Similar behavior and agreement was found for all circular, solid, and two-inch thick specimens, so only a few of the cyclic test results have been shown for brevity.

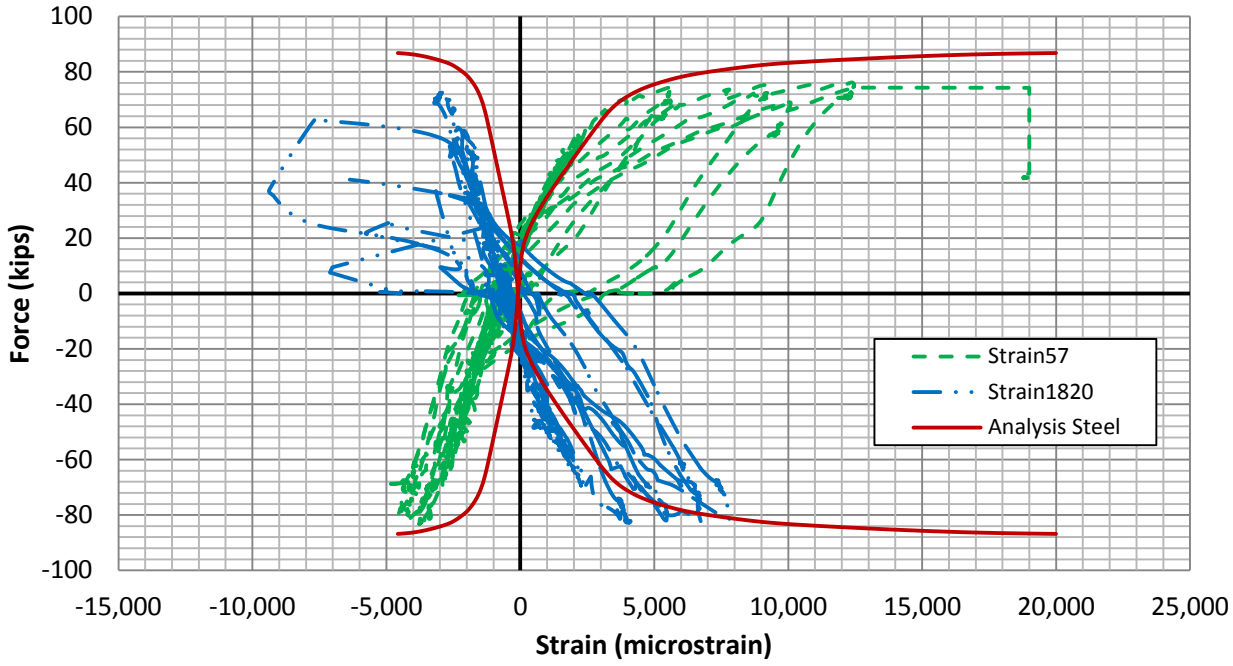

Figure 5-54: Attached LED Concrete Strain Measured During Testing and Analytical Steel Strain vs. Applied Lateral Load for Specimen SC2-C

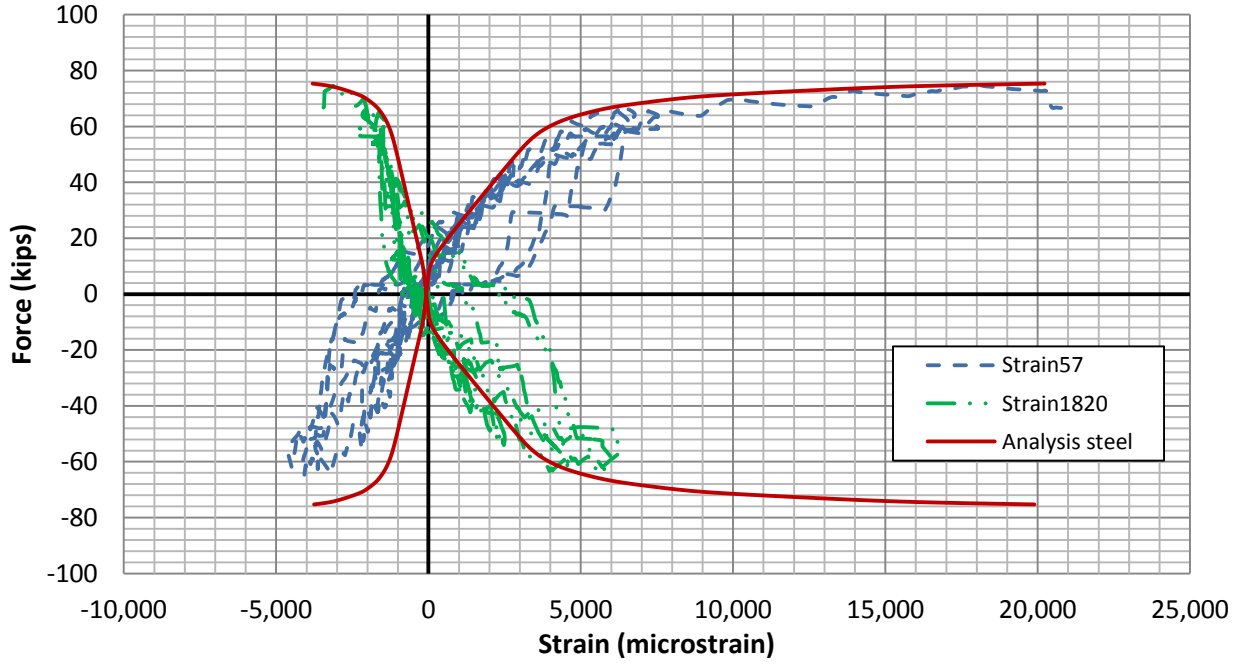

Figure 5-55: Attached LED Concrete Strain Measured During Testing and Analytical Steel Strain vs. Applied Lateral Load for Specimen H2C2-C

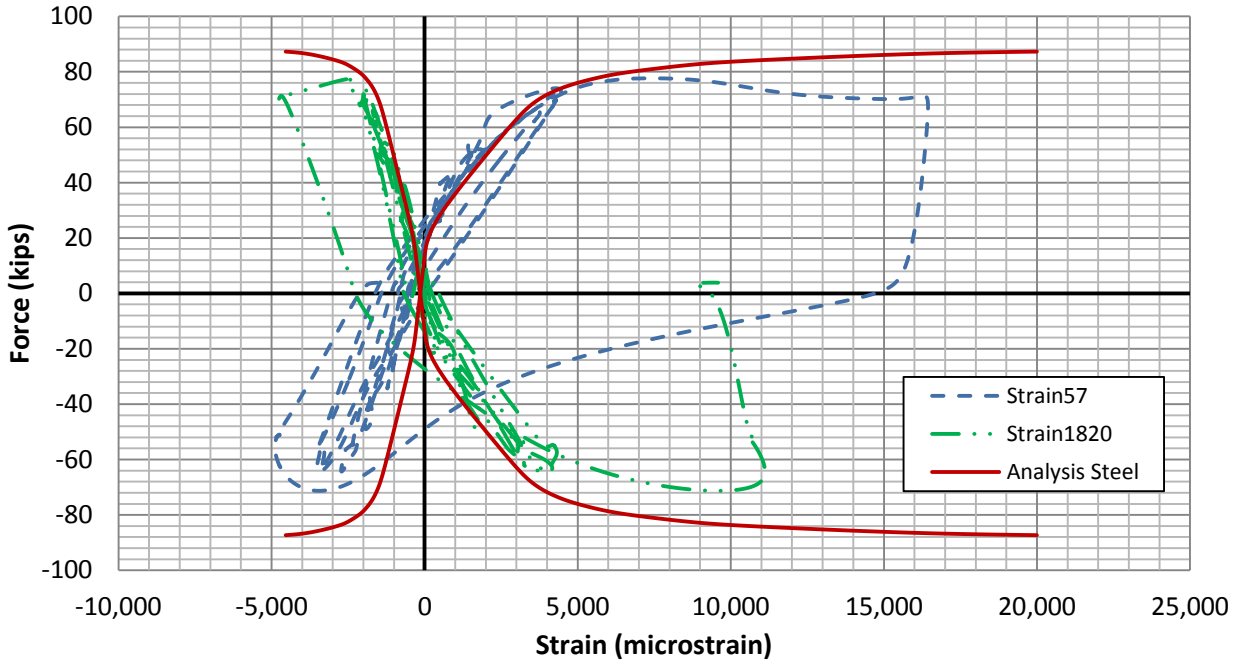

Figure 5-56: Attached LED Concrete Strain Measured During Testing and Analytical Steel Strain vs. Applied Lateral Load for Specimen H2C3-C

Figure 5-57 shows the LED strains attached to the concrete for one of the one-inch thick specimens. The analytical failure mode for these specimens was inside concrete face crushing, and thus the analytical tension steel strains are plotted up to the point of inside concrete face crushing. These specimens experienced early failure due to local and shear effects, which the analysis did not account for. For this reason the analysis results predicted much higher capacities and ultimate displacements than found through experimental testing. Despite the differences, the strains measured by the LEDs prior to failure still match closely with the strains at these force levels, which the analysis provided.

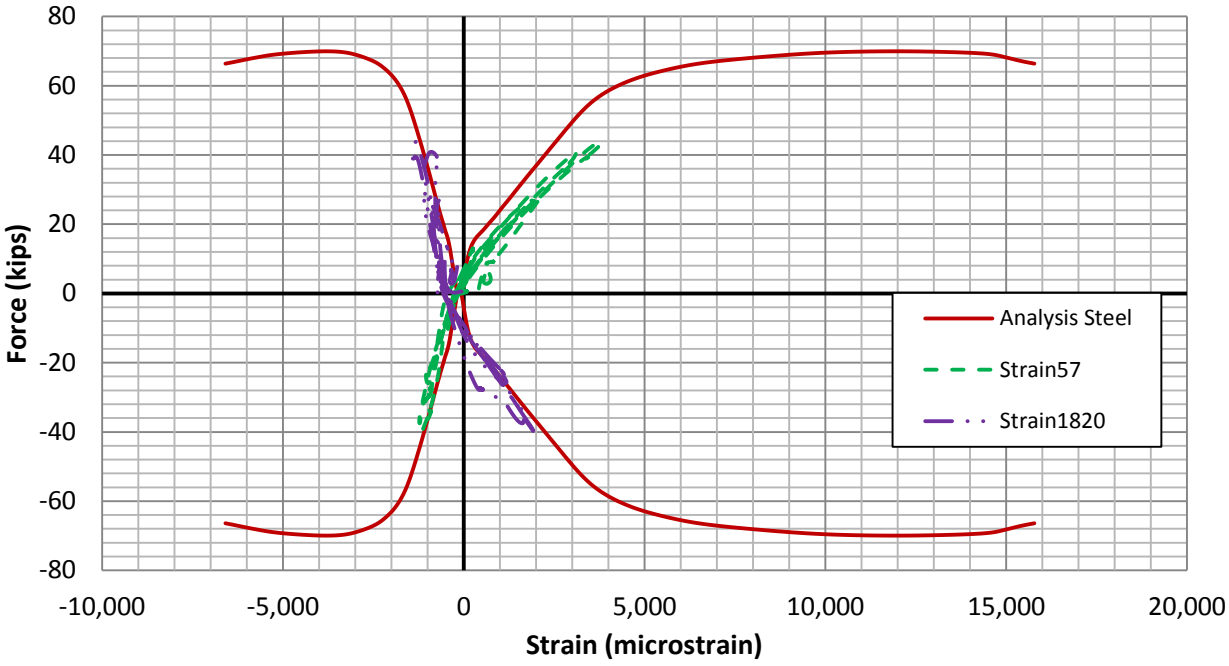

Figure 5-57: Specimen H1C2-C Attached LED Concrete Strain and Analytical Strain vs. Applied Load

As shown in Figure 5-54 through Figure 5-57, the strains measured by the LEDs near the extreme tension and compression faces agree very closely with the extreme tension and compression analytical steel strains. The LED strains seem to provide a better estimate of the extreme fiber compression strain in the concrete when compared to the compression strains measured by strain gauges on the longitudinal reinforcement, which were presented in Section 5.2.1.2.4. The analytical strains match up well with the measured LED strains, even for the one-inch thick specimens, which experienced early failure.

5.2.1.2.6 Circular hoop strain

During testing, the strains were also measured in the transverse reinforcement using strain gauges. These measured strains can provide information about the demand on the confinement, as well as providing an indication of if the transverse reinforcement was close to fracture. For the circular test specimens, the failures occurred due to longitudinal steel rupture

at low steel strain for the solid and two-inch thick specimens and due to local failure for the one-inch thick specimens. These failures occurred at a fairly low ductility, which means that the confinement most likely was not subjected to high demand. This was found to be true based on the measured transverse steel strains, which at the most only reached close to 1500 microstrain prior to specimen failure out of all the specimens.

Specimen SC2-C experienced the highest transverse steel strain, which did not even reach the yield strain of the transverse reinforcement. For this specimen, a fairly clear pattern was noticed, where the transverse reinforcement reached higher tensile strains when that section was under compression, as would be expected. This pattern is illustrated in Figure 5-58 and Figure 5-59. The pattern is clearer in Figure 5-59, where the two gauges on the transverse reinforcement agree very closely.

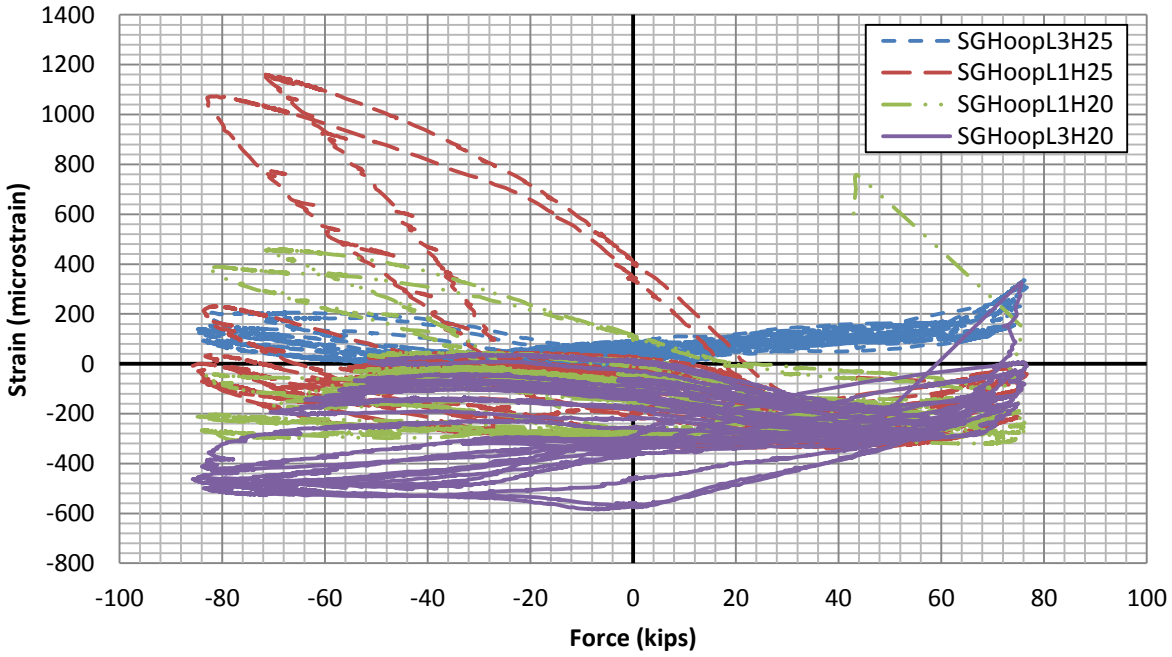

Figure 5-58: Specimen SC2-C Hoop Strain Near Longitudinal Bar 1 vs. Applied Load

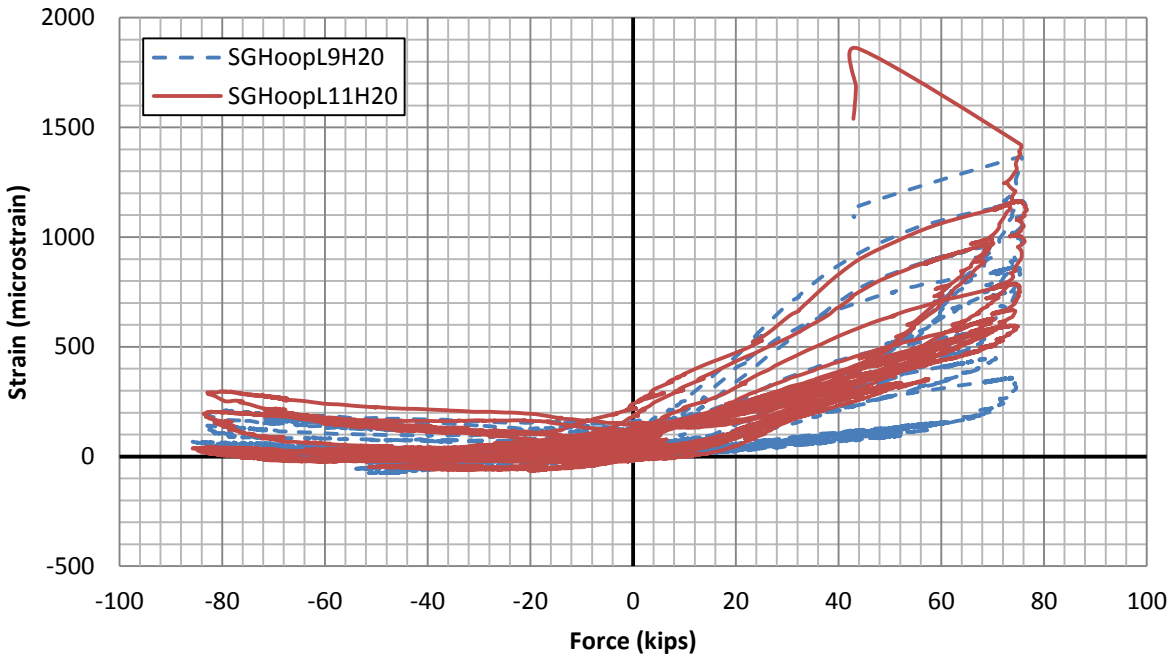

Figure 5-59: Specimen SC2-C Hoop Strain Near Longitudinal Bar 11 vs. Applied Load

For the hollow sections, the pattern was typically much less clear, partly due to the fact that the transverse steel strains remained very low, usually under 1000 microstrain. These low strains for the hollow sections illustrate that the failure of transverse reinforcement was not a concern and that very little demand was induced in the transverse reinforcement. Even for specimen SC2-C, which experienced higher transverse tensile strains, the transverse reinforcement did not yield, which showed that the specimen was confined adequately. This observation is consistent with the analytical findings reported in Liang et al. (2015).

5.2.2 Square section

The results of the square column tests are described in the following sections. The solid test specimens had satisfactory results, while the hollow specimens experienced premature local and shear failures. These local and shear failures seem to have been caused by small wall thickness, poor quality concrete resulting from tight spacing in some areas although these

regions were patched, and possibly inapplicability of shear design procedure developed for solid members to hollow concrete members.

5.2.2.1 Visual observations of square specimens

SS1-M

Specimen SS1-M was loaded monotonically under 28.8 kips of axial load until failure. The loading was paused at predetermined targets to mark cracking. Flexural cracking began appearing at $0.75F_y$, where F_y is the force at first yield. Slight shear cracking began to occur when the specimen was pushed to the first yield point. Cracks continued to widen and the amount and length of the shear cracks gradually increased. The specimen failed due to tension steel rupture on the way to displacement ductility three. Crushing of cover concrete at the compression face was observed after failure, especially at the specimen compression corners.

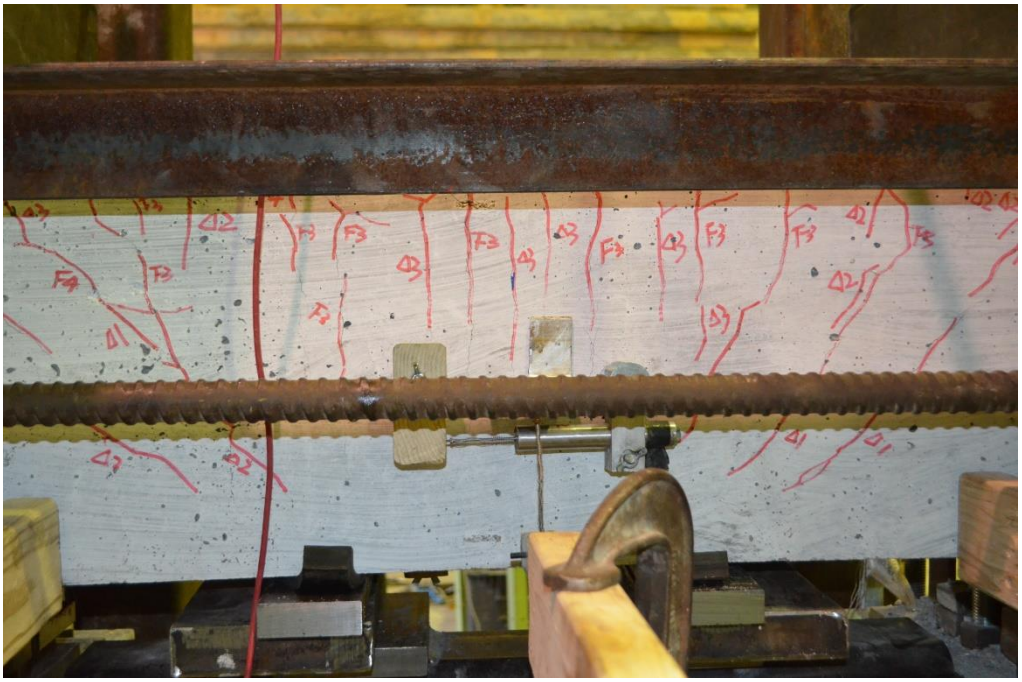

Figure 5-60: Specimen SS1-M Specimen Prior to Failure

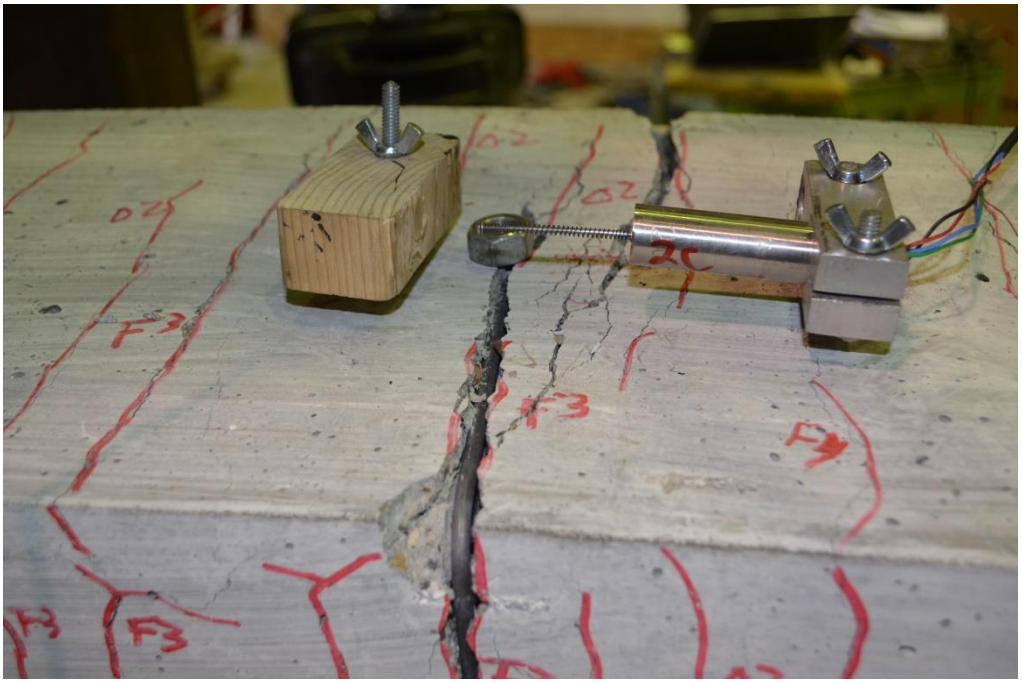

Figure 5-61: Specimen SS1-M Close-Up of Large Flexural Crack after Failure

SS2-C

Specimen SS2-C was loaded cyclically under 57.6 kips of axial load until failure. Slight flexural and shear cracks first appeared at $0.75F_y$, as observed for the monotonic loading case. The amount of flexural cracks gradually increased as loading continued, with the flexural crack spacing seeming to coincide with the transverse reinforcement spacing. The amount and length of shear cracks also gradually increased as loading continued. In the cycles near displacement ductility two, the cover concrete at the specimen corners under the central loading points began to crush slightly, most likely due to local stresses due to loading. The specimen failed during the first cycle at displacement ductility three due to tension steel reinforcement rupture, and a large flexural crack opened up. The cover concrete at the compression face was crushed after failure.

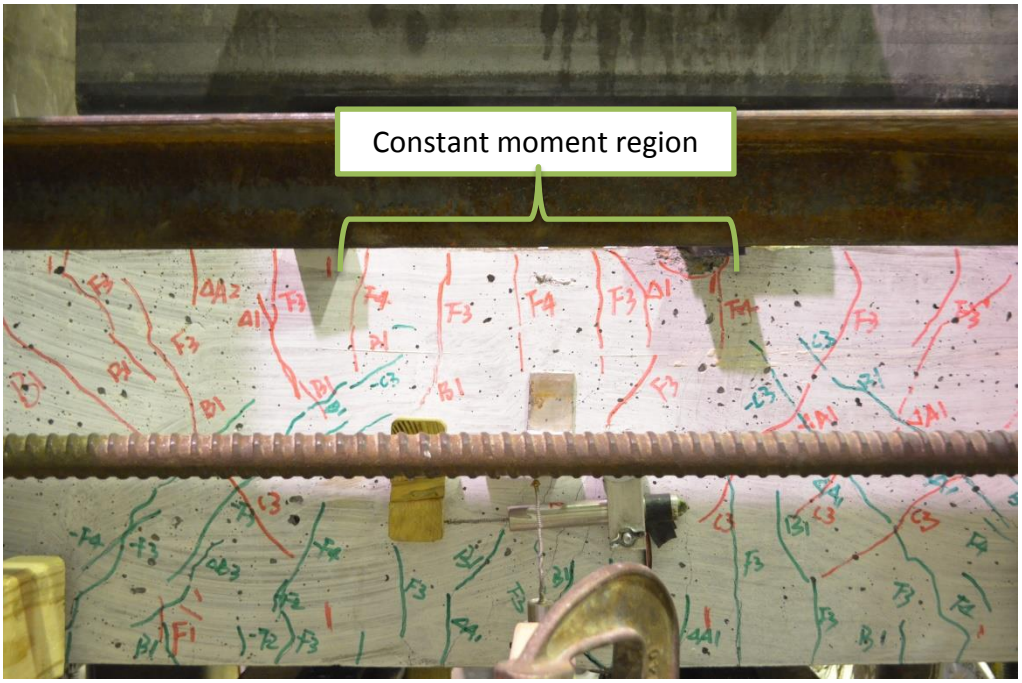

Figure 5-62: Crack Pattern of Specimen SS2-C at Ductility Three Prior to Failure

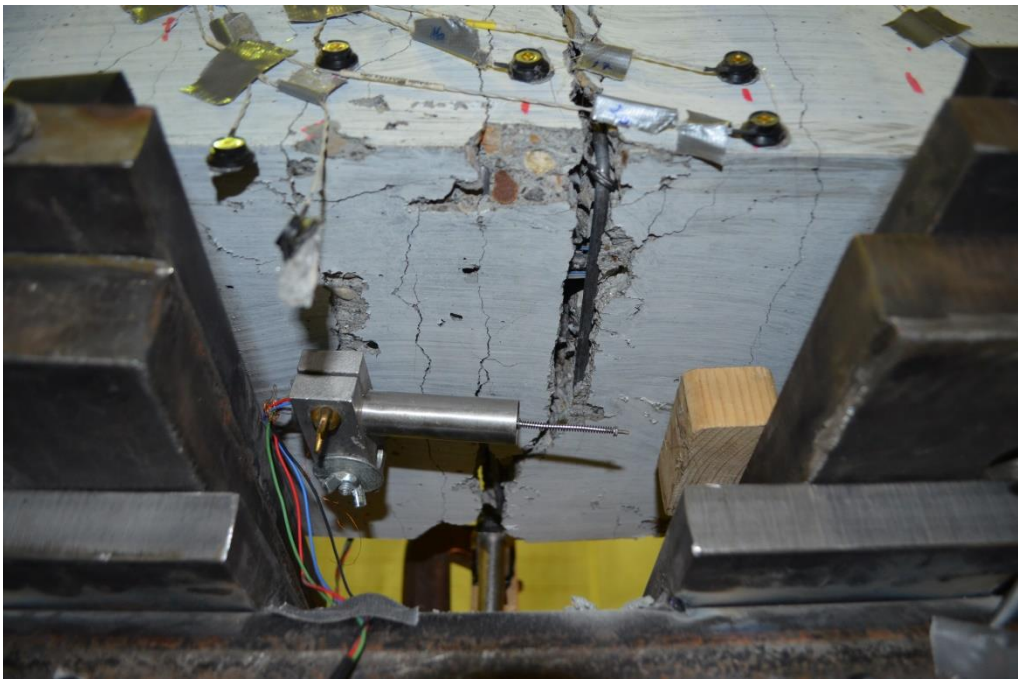

Figure 5-63: Specimen SS2-C Large Flexural Crack in Constant Moment Region after Failure

The hollow square specimens presented in the remainder of this section experienced premature local and shear failure, as previously noted. The early failures may be due to the small wall thickness combined with local effects at the loading and support points. Additionally, these specimens had been patched to fix poor concrete fill, and the early failure seemed to coincide with patched locations, although it is unclear what the primary cause of failure may have been for these specimens.

H2S1-M

Specimen H2S1-M was loaded monotonically under 28.8 kips axial load until failure occurred. Minor shear cracks first appeared in the second increment in the linear moment region, followed by many small shear cracks appearing in the third increment. Flexural cracks began appearing in the constant moment region at F_y in the linear phase. As displacement ductility one was approached, some local concrete cover crushing appeared near the corners by the point of loading, followed by significant crushing as shown in Figure 5-64. After continuing loading, the specimen failed due to what appeared to be a combination of local failure at a point of load application and wall buckling occurring inward. The compression wall between the loading points appeared to fail with a section of the wall failing inward, causing the longitudinal reinforcing bars to buckle inward as well. Some longitudinal reinforcing bars on the side of the specimen near the compression face in the constant moment region were seen to be buckled shortly after failure as well, as shown in Figure 5-66. The amount of transverse reinforcement provided was above the minimum recommended in order to prevent the longitudinal reinforcing steel from buckling. It is likely that when the compression wall buckled inward, the sudden loss of compression area resulted in high compressive stresses in the longitudinal reinforcement, which may have caused the buckling to occur.

Flexural cracks could be seen to have widened presumably as a result of the observed failure. After removal of the load, it was seen that significant indentations in the concrete under the points of load application were visible. Photos of the inside face prior to failure shows some cracking before the inner compression wall suddenly failing inward.

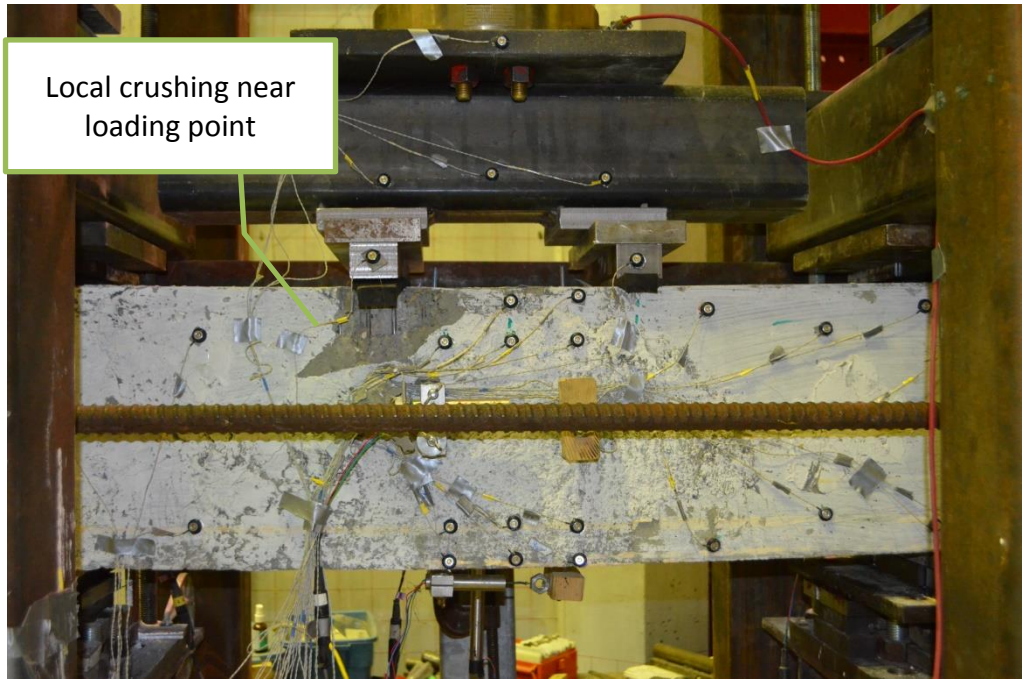

Figure 5-64: Local Crushing and Spalling of Cover Concrete in Specimen H2S1-M at Displacement Ductility One

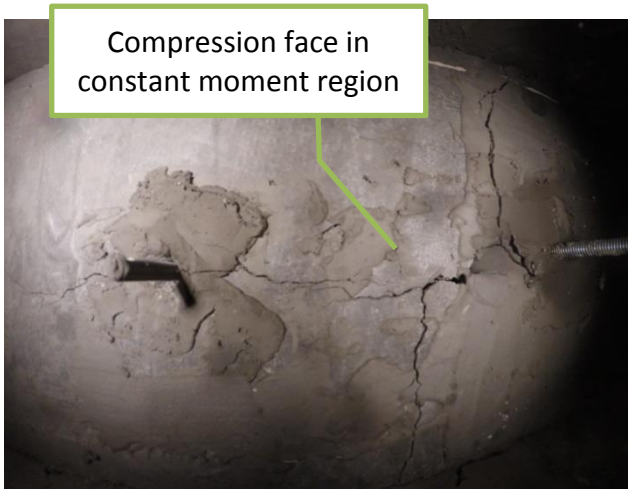

a) Prior to failure on the inner surface **b) Inward pushing after failure**

Figure 5-65: Compression Face Prior to Failure and Inward Failure of the Compression Face Concrete in the Wall of Specimen H2S1-M

Figure 5-66: Specimen H2S1-M Longitudinal Reinforcement Buckling after Failure

H2S2-C

Specimen H2S2-C was tested cyclically under 28.8 kips of axial load until failure. After witnessing the local failure of specimen H2S1-M and following the experience from the hollow circular column testing, wooden support blocks were added inside the column at the support locations in an effort to brace this region and avoid local failure. Shear cracks first appeared in the linear moment regions at the cycle at $0.5F_y$, with more shear cracks appearing in the cycle at $0.75F_y$. Some concrete spalling in the linear moment region began appearing in this cycle as well. In the first part of the cycle at F_y, shear failure occurred with significant spalling of concrete in the linear moment region at one end of the specimen. On the front side, a large shear crack was visible, as shown in Figure 5-69. The inside face of the specimen in the central region experienced some cracking, but remained mainly undamaged.

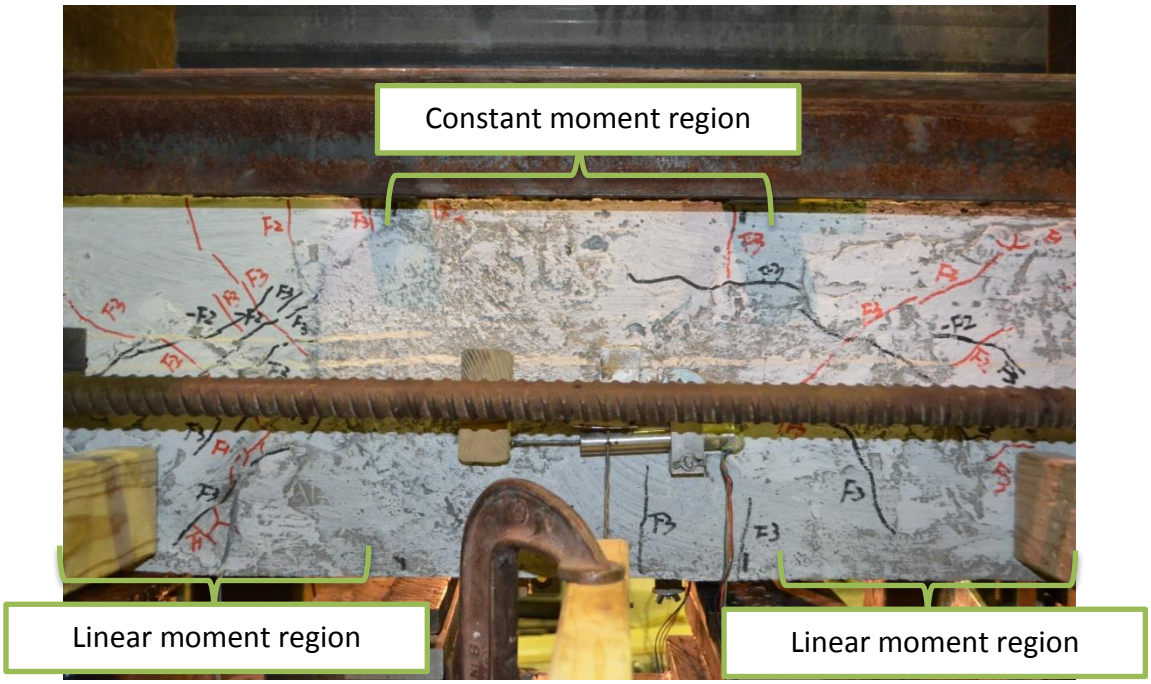

Figure 5-67: Crack Pattern of Specimen H2S2-C in the Cycle at $0.75F_y$

Figure 5-68: Specimen H2S2-C Shear Failure in the Linear Moment Region

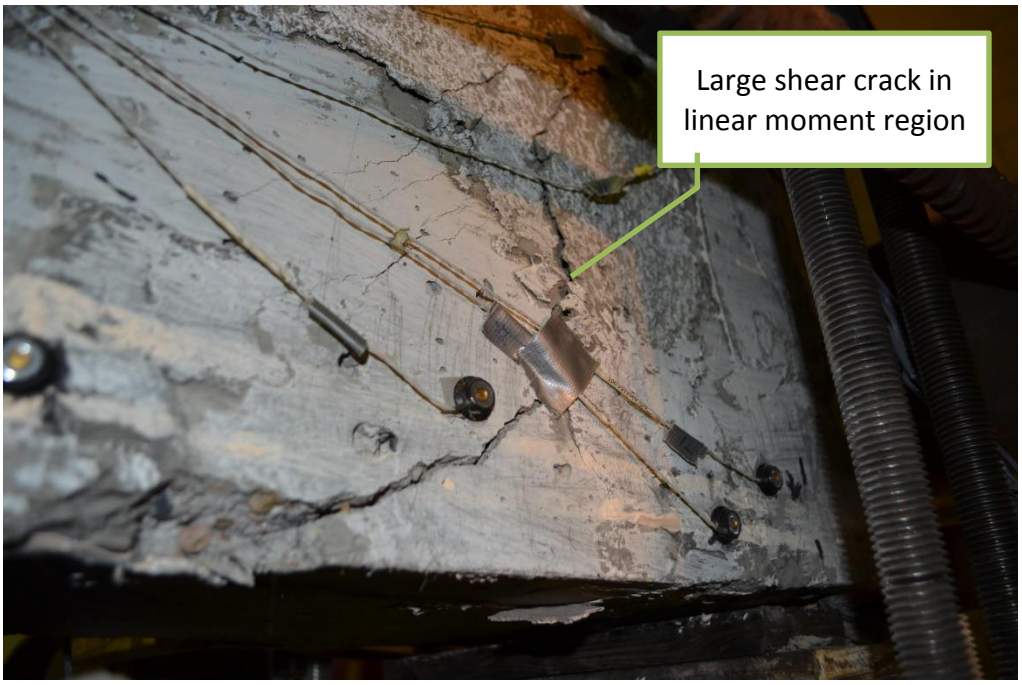

Figure 5-69: Large Shear Crack in the Linear Moment Region on LED Side of Specimen H2S2-C after Failure

H2S3-C

Specimen H2S3-C was tested cyclically under 57.6 kips of axial load until failure. This specimen also contained wooden braces inside the column at the loading and support points in an effort to avoid local failure. Slight shear cracking appeared in the second cycle in the linear moment region with the number and length of the shear cracks increasing significantly into the cycles at $0.75F_y$ and F_y. Local cover concrete crushing began occurring at the loading points in the second cycle and continued to increase with some significant cover concrete spalling occurring in the cycle at $0.75F_y$. The specimen failed in the second part of the cycle at F_y, due to shear failure. The inside face experienced some slight cracking prior to failure but otherwise was mainly undamaged.

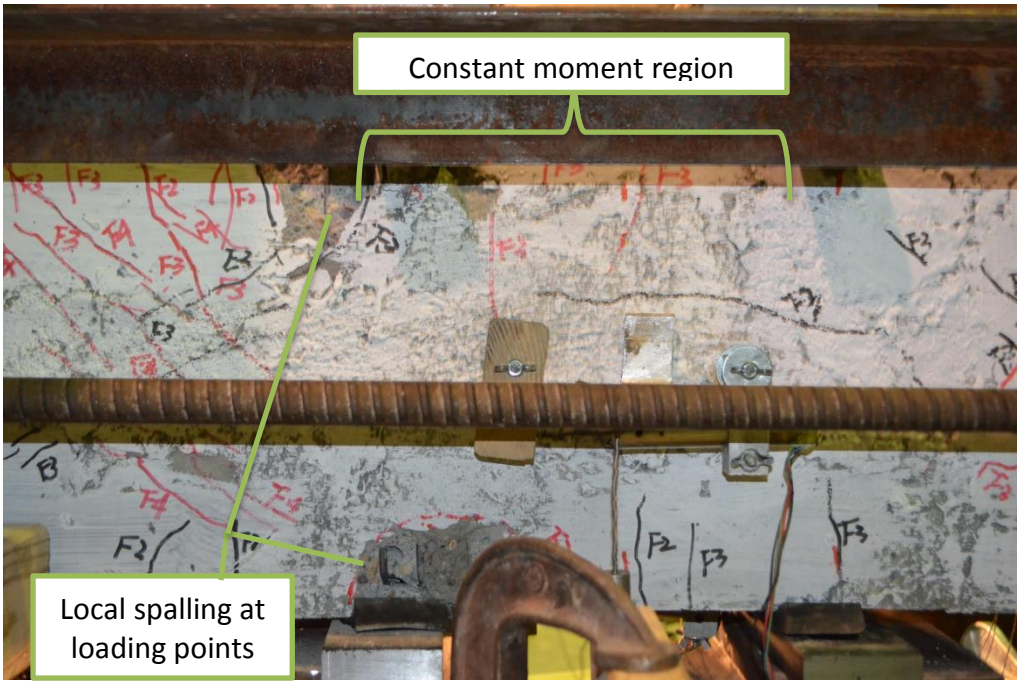

Figure 5-70: Specimen H2S3-C Local Spalling and Crack Pattern in the First Part of Cycle at F_y

It was clear that shear effects were contributing significantly to the behavior of hollow columns. The measured displacements found during testing were much higher than anticipated based on the preliminary OpenSees analysis performed for these specimens. In order to quantify the effect of shear on the specimens, the shear component of the displacement needed to be estimated. A measurement of the shear component of displacement was able to be taken by using a grid of LEDs, and the results of this investigation are further discussed in Section 5.2.2.2.2.

Figure 5-71: Specimen H2S3-C Close-Up of Local Cover Crushing at Load Point while Unloaded Prior to the Second Part of the Cycle at F_y

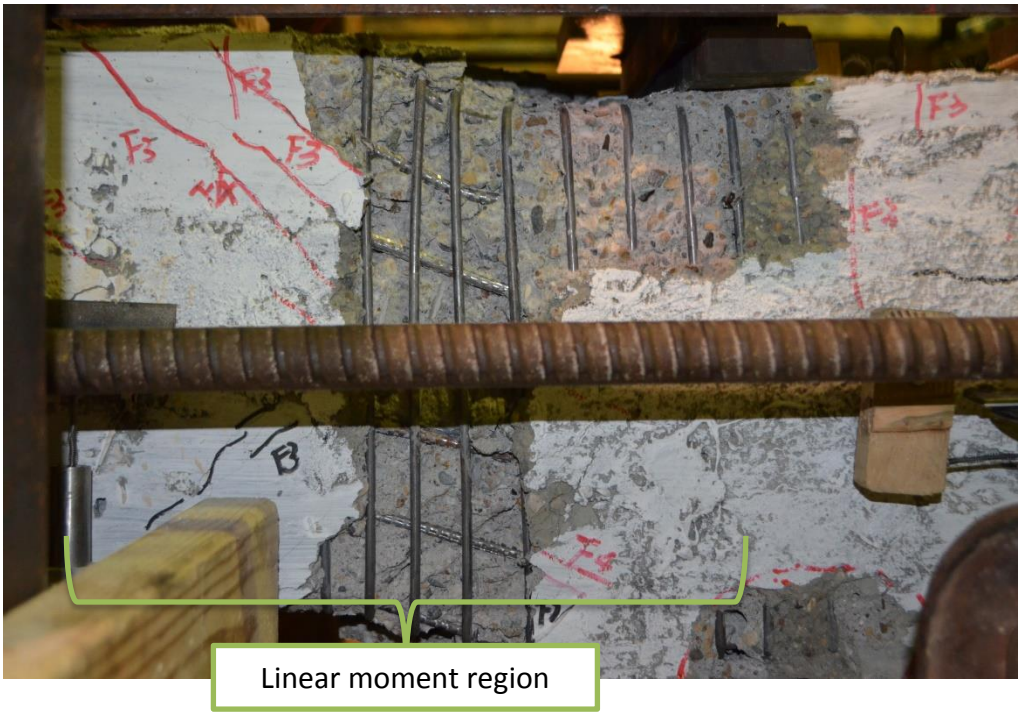

Figure 5-72: Specimen H2S3-C Shear Failure in the Linear Moment Region

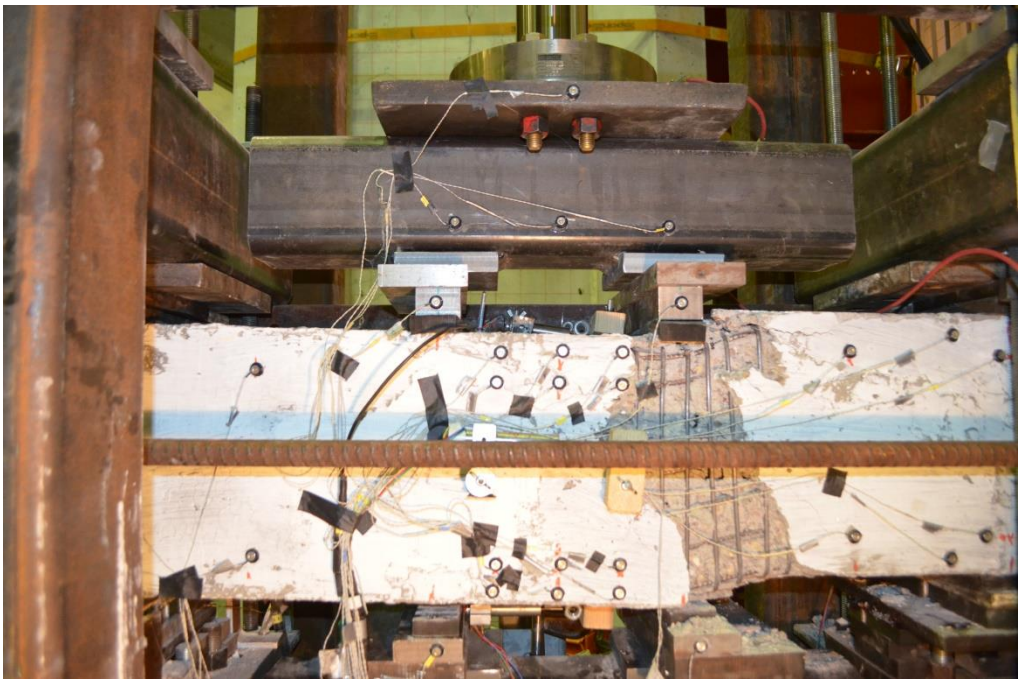

Figure 5-73: Specimen H2S3-C LED Side after Failure

H1.25S1-M

Specimen H1.25S1-M was loaded monotonically under 28.8 kips of axial load. It also had wooden braces on the inside near the support and load locations in an effort to avoid local failure. The specimen experienced shear cracking in the linear moment region at $0.5F_y$. On the way to $0.75F_y$, the specimen experienced premature shear failure in the linear moment region at one end of the specimen. The shear failure was somewhat lopsided, and a large damage region was visible on the backside of the specimen but not on the LED side. The inside compression face was mainly undamaged.

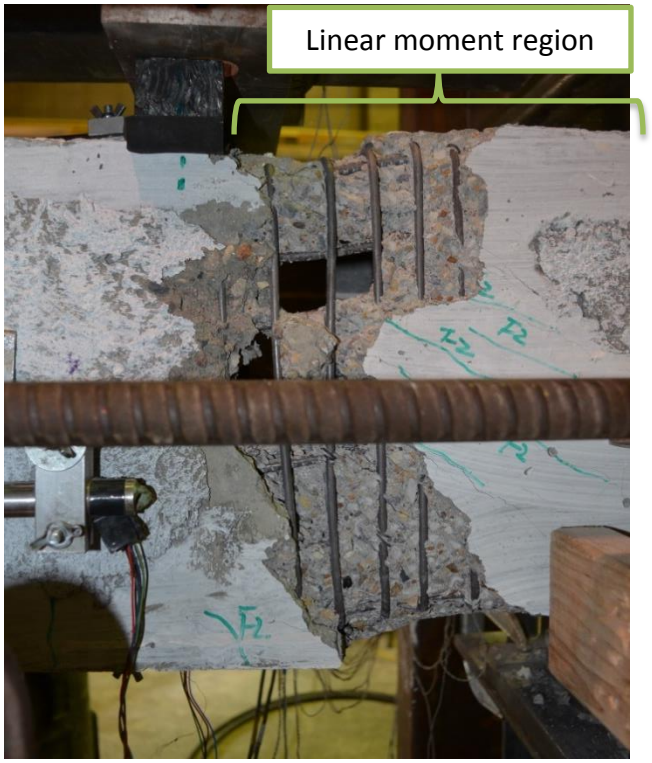

Figure 5-74: Specimen H1.25S1-M Shear Failure in the Linear Moment Region

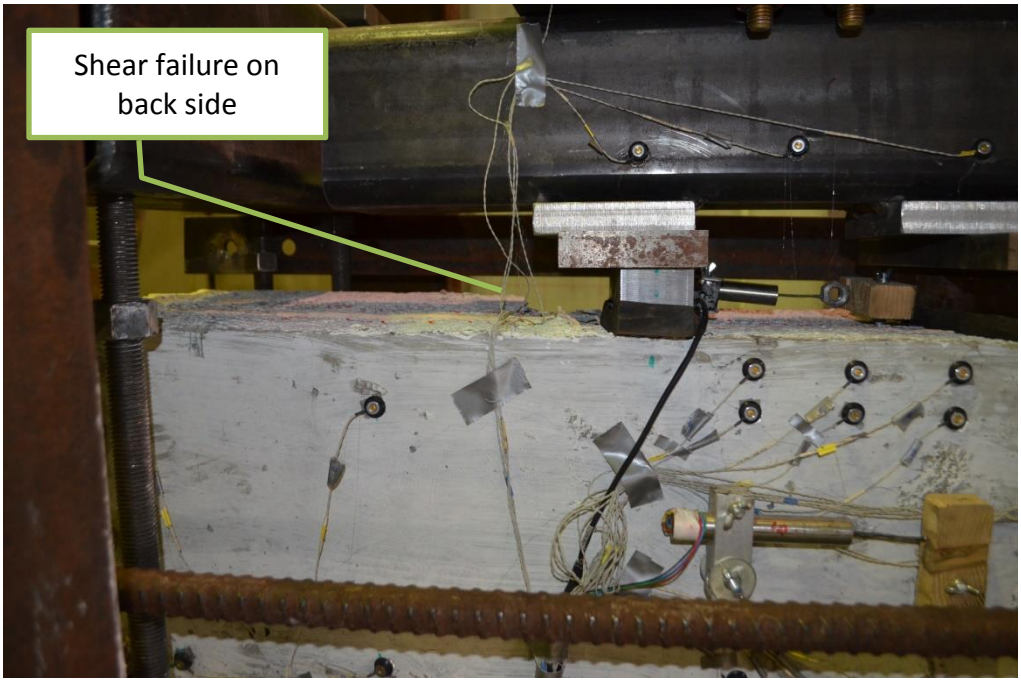

Figure 5-75: Specimen H1.25S1-M LED Side of Damaged Linear Moment Region after Failure

H1.25S2-C

Specimen H1.25S2-C was tested cyclically under 28.8 kips axial load until failure and contained wooden braces at the loading and support points. During the cycle at $0.5F_y$, some slight shear cracks appeared in the linear moment region as well as some cover concrete spalling at one of the points of load application. In the second part of the cycle at $0.5F_y$ a local failure occurred at the support, as shown in Figure 5-76. The inside face compression concrete was not damaged during the testing.

Figure 5-76: Specimen H1.25S2-C Support after Failure

H1.25S3-C

Specimen H1.25S3-C was tested under 57.6 kips axial load until failure. This specimen also had wooden braces near the loading and support points. The specimen experienced premature failure in the cycle at $0.5F_y$. The failure occurred near the support as shown in Figure 5-77 due to local crushing and loss of concrete. The concrete spalled off entirely from the wall on the

side of the specimen near the end plate where the axial load is applied. The specimen quickly lost both lateral and axial load capacity after failure. No damage occurred to the inside compression face in the constant moment region of the column.

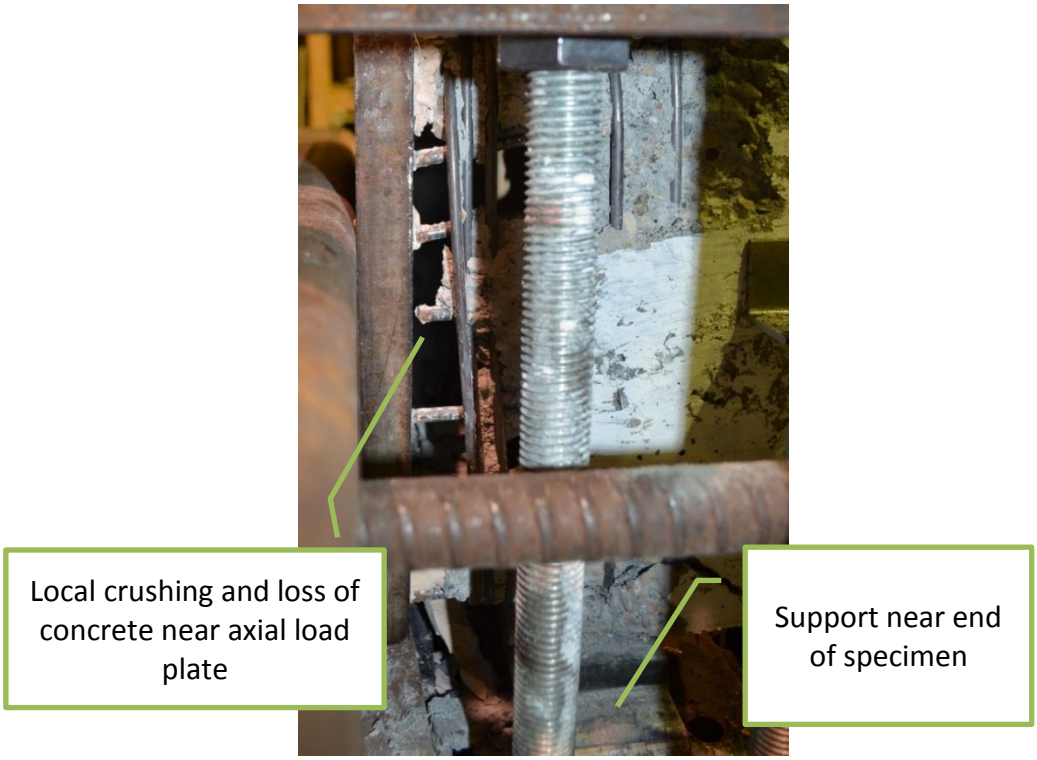

Figure 5-77: Local Failure Near the End Support of Specimen H1.25S3-C

5.2.2.2 Square section experimental results and comparison to analytical results

5.2.2.2.1 Overall force-displacement response

The recorded values from the load cells and the measured displacements, has been used to determine the force-displacement response of each specimen. The force-displacement response of each test unit is shown in the figures below. The experimental results shown in this section include the effects of shear. The displacement response was found using the LEDs, and the data has been processed for to remove outliers and noise. For the monotonic tests, the

envelope response has been provided to avoid noise and load drops, which occurred when the loading was paused for crack marking.

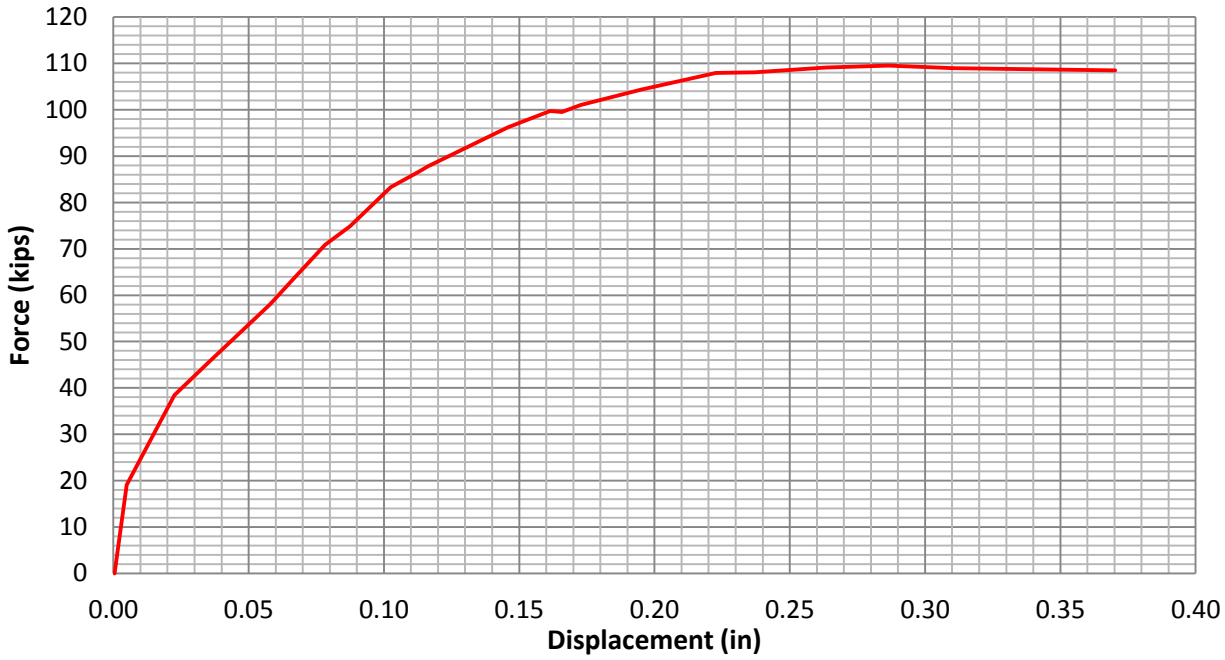

Figure 5-78: Force-Displacement Response of Test Unit SS1-M

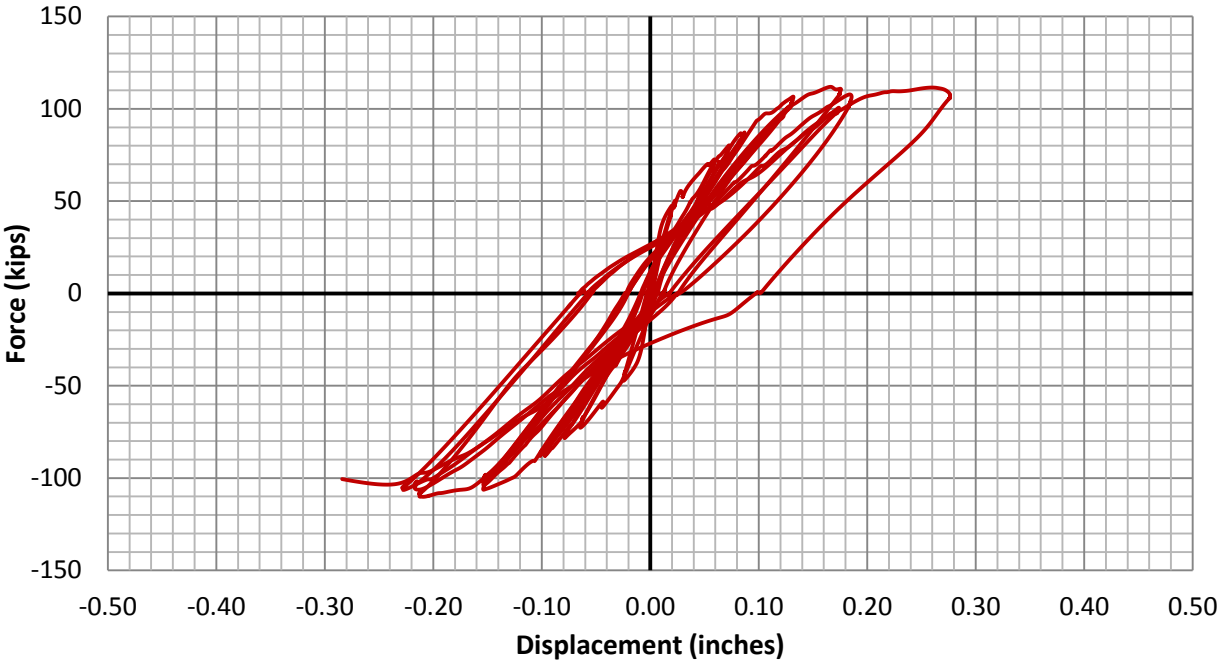

Figure 5-79: Force-Displacement Response of Test Unit SS2-C

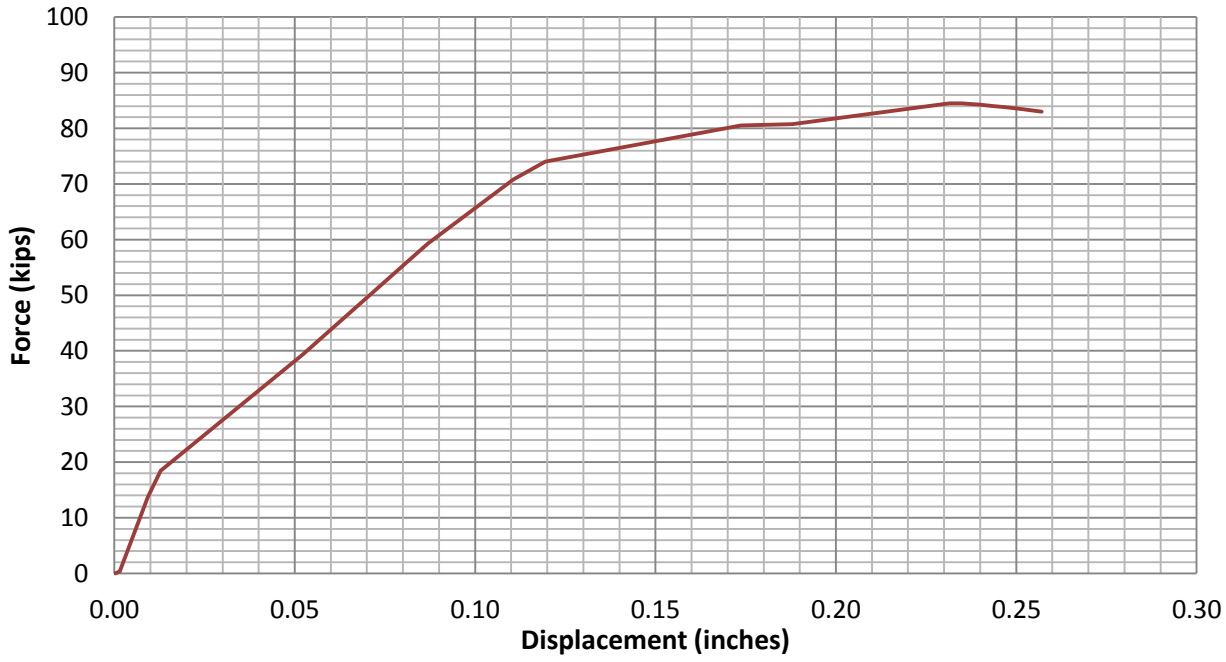

Figure 5-80: Force-Displacement Response of Test Unit H2S1-M

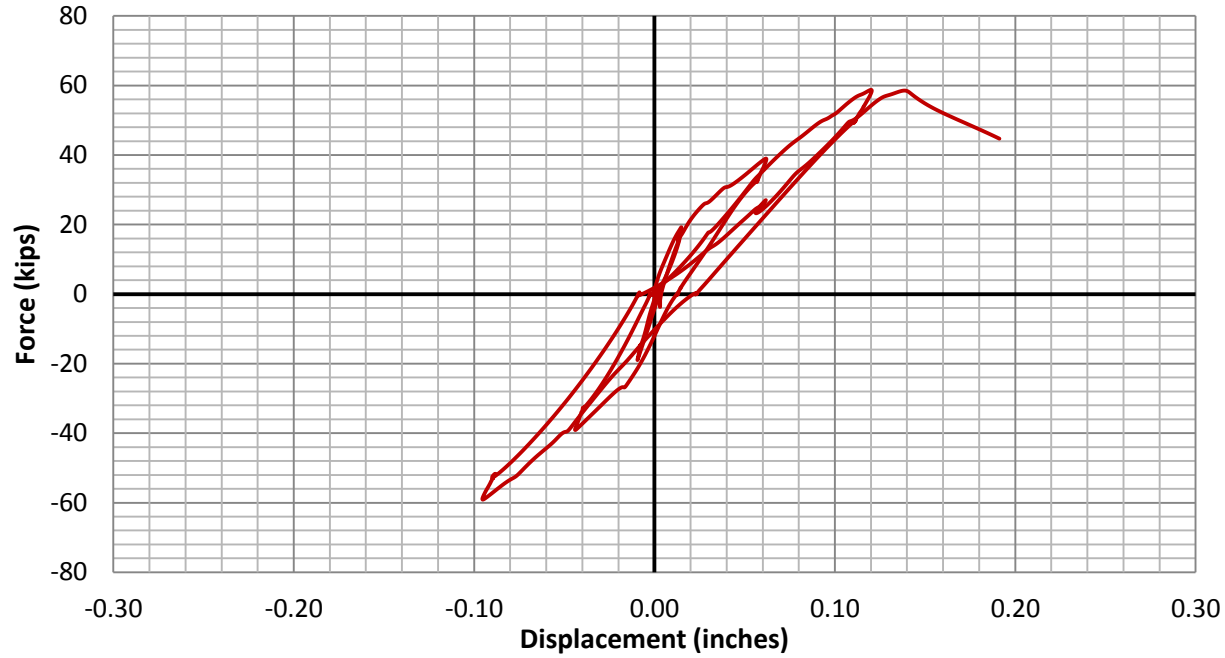

Figure 5-81: Force-Displacement Response of Test Unit H2S2-C

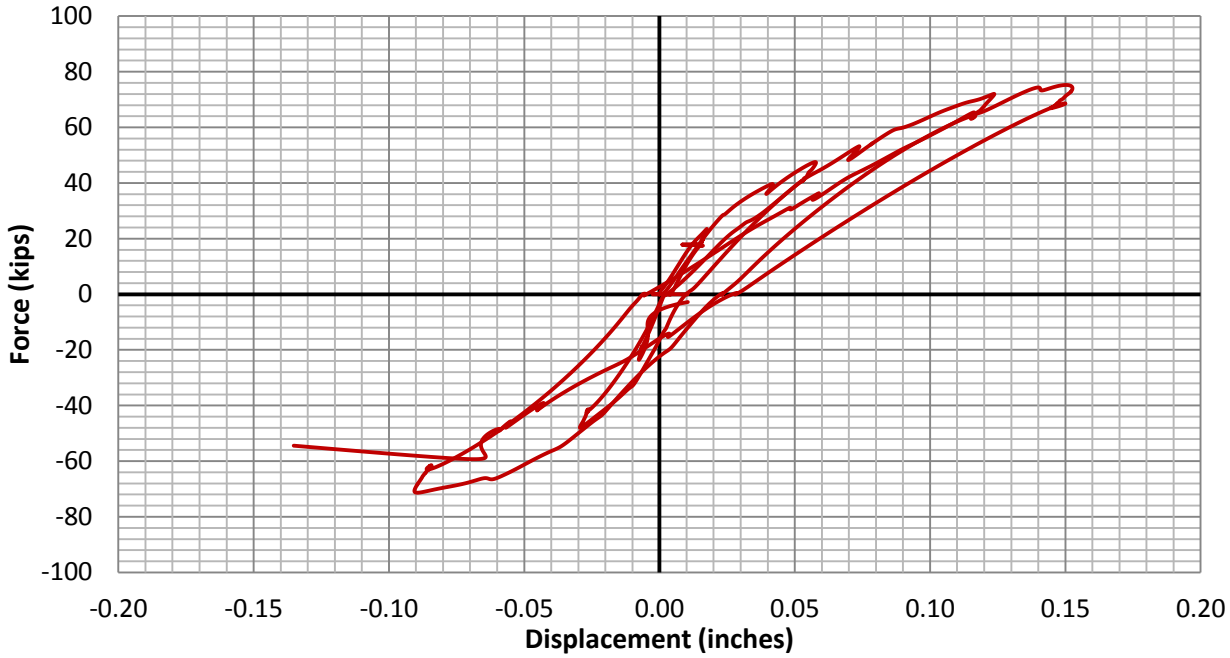

Figure 5-82: Force-Displacement Response of Test Unit H2S3-C

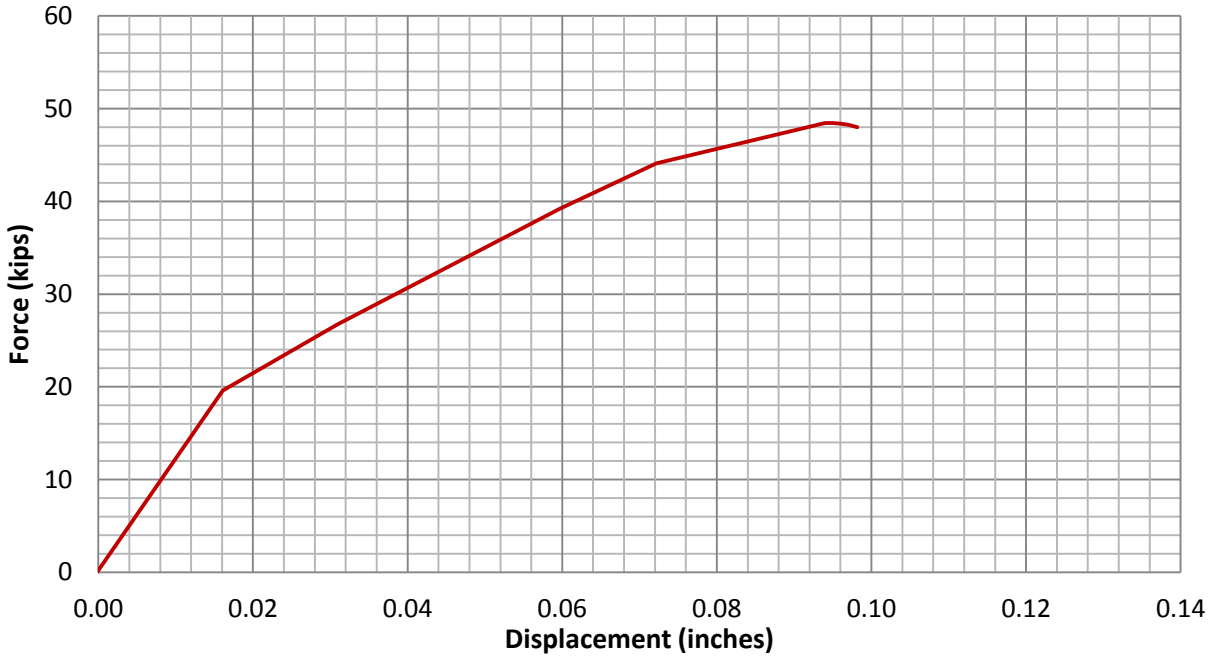

Figure 5-83: Force-Displacement Response of Test Unit H1.25S1-M

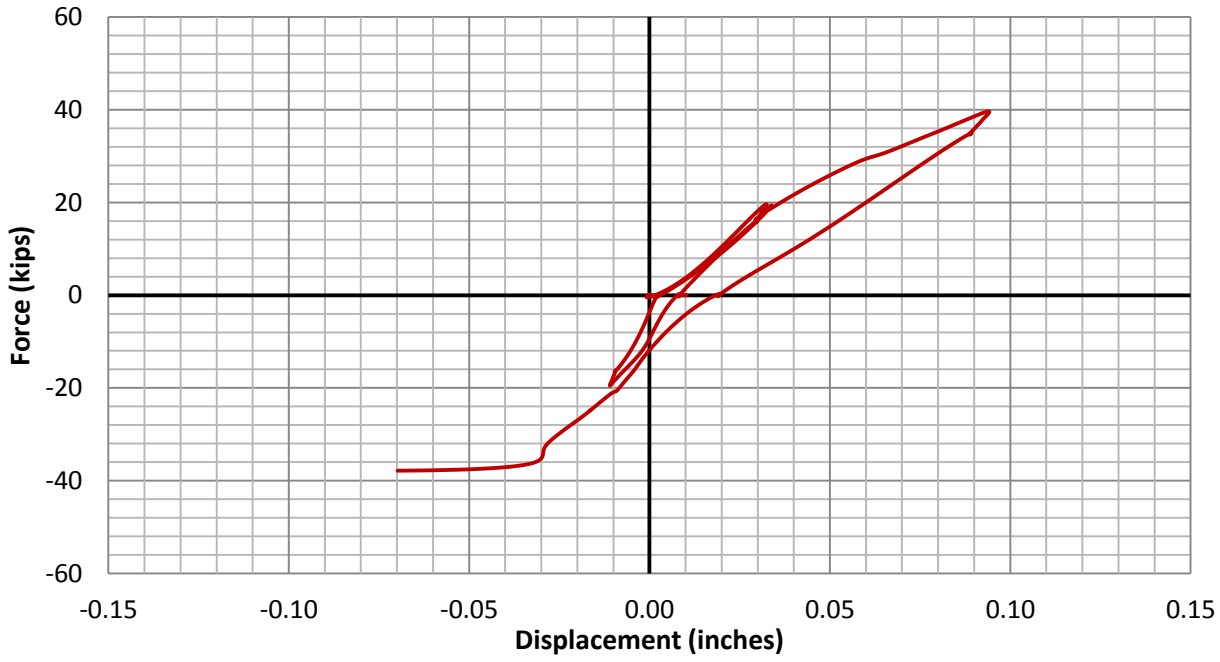

Figure 5-84: Force-Displacement Response of Test Unit H1.25S2-C

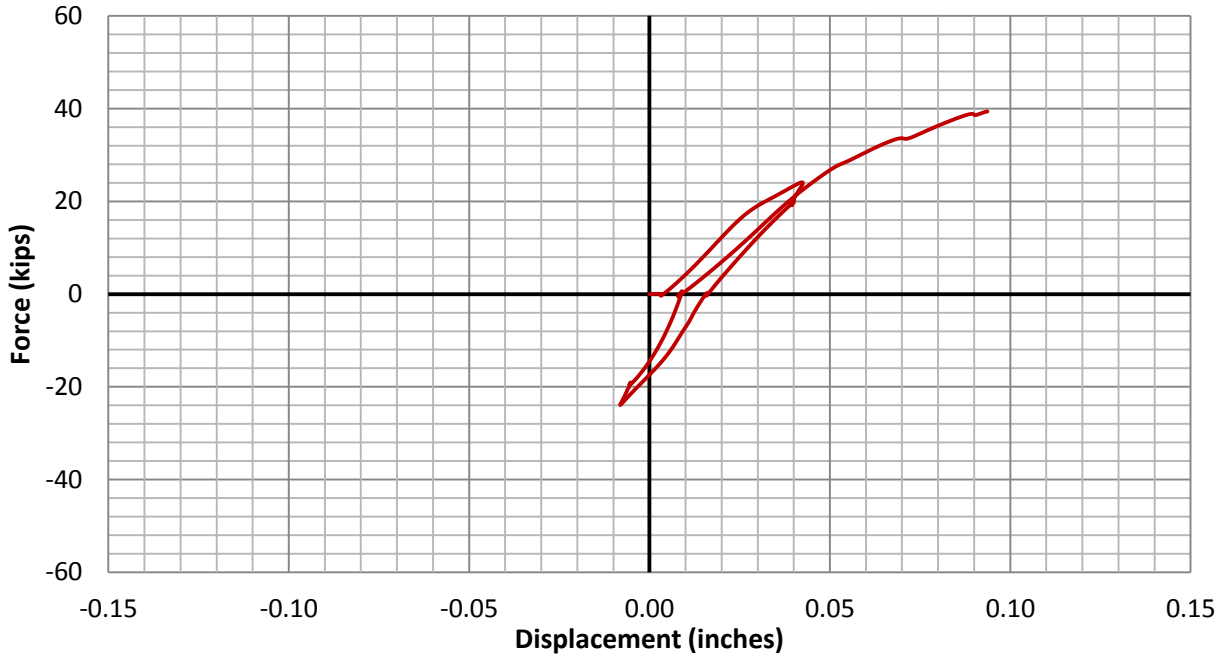

Figure 5-85: Force-Displacement Response of Test Unit H1.25S3-C

Figure 5-86 shows a comparison of the force-displacement response for the solid, two-inch, and 1.25-inch wall hollow columns under 28.8 kips axial load. As shown by the figure, the hollow columns experience larger displacements than the solid column. Additionally, it can be seen that the displacement seems to increase slightly for the thinner wall. The two hollow square specimens failed early due to local and shear effects, which is why their lateral load capacity is not as high as that of the solid column. The two hollow columns experienced similar stiffness early on, which is likely because there was not a very large difference in wall thickness between them.

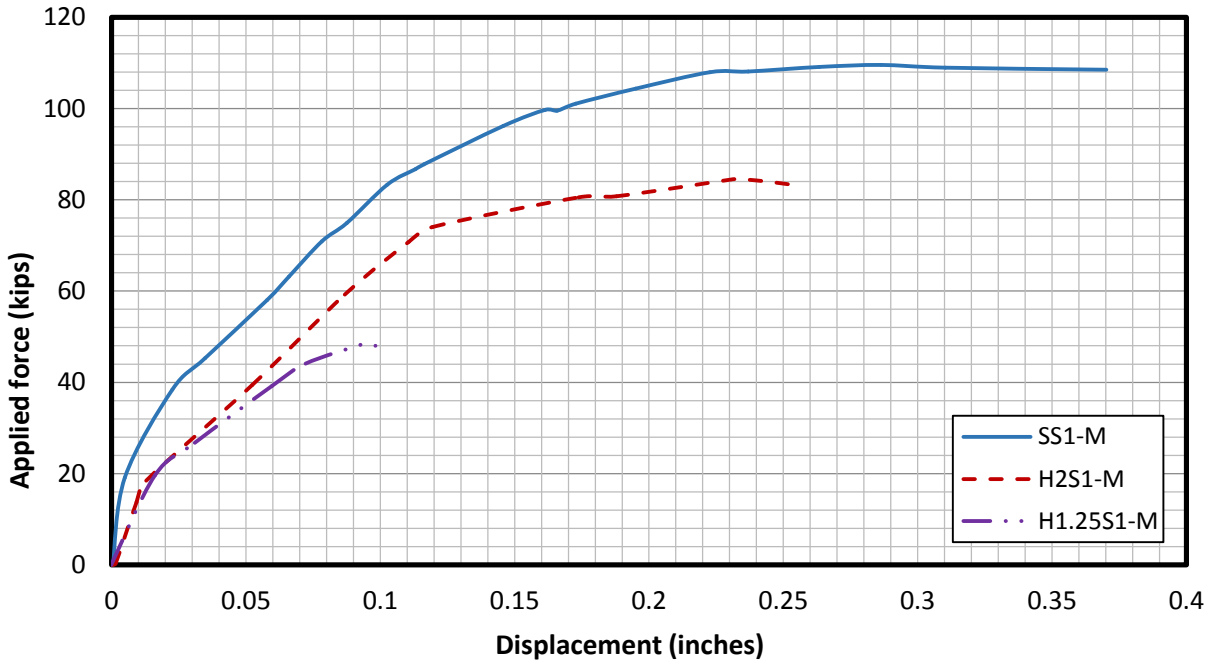

Figure 5-86: Force-Displacement Response Comparisons for Solid, Two-Inch Wall, and One-Inch Wall Hollow Columns under 22.6 kips Axial Load

5.2.2.2.2 Shear contribution

It became obvious during the testing that shear deformation was having a large effect on the test results for the hollow columns, which was evident in the fact that many of the square hollow columns failed in shear. The OpenSees analysis method used does not account for shear effects, and typical analysis methods used in design do not account for these effects either. Therefore, the shear contribution has been estimated in order to quantify the effect of shear on the square specimens and to provide a better comparison to the OpenSees analysis. The method has been adopted which was used previously by Sritharan (1998), and in this case, a grid of LEDs was used to determine the various deformation components. The following plots show the shear displacement plotted against the applied load for all specimens as well as the force-displacement response of each specimen with shear included and with shear subtracted for comparison. The LED data has been processed to remove noise and outliers, and the envelope has been provided for the specimens tested monotonically. Figure 5-87 gives the overall force-displacement response as well as the force-displacement response with the shear

deformation subtracted for specimen SS1-M. The shear deformation for this specimen accounts for approximately 25 percent of the overall force-displacement response.

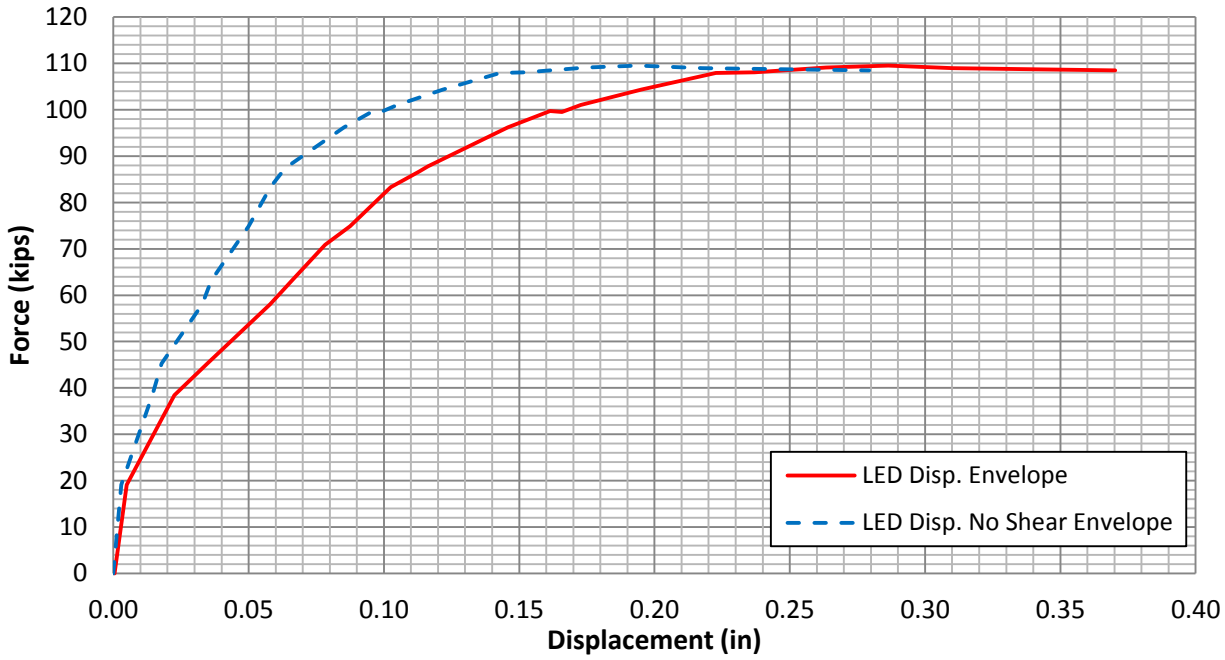

Figure 5-87: Force-Displacement of Specimen SS1-M with and without Shear Deformation

Figure 5-88 gives the applied load plotted against the shear deformation for specimen SS1-M. As shown, the shear deformation maintains a mostly linear relationship with the applied load. The shear displacement response shown in the figure has been adjusted and zeroed. An initial negative shear displacement was measured before load was applied, and during the early loading, so this initial shear displacement has been zeroed.

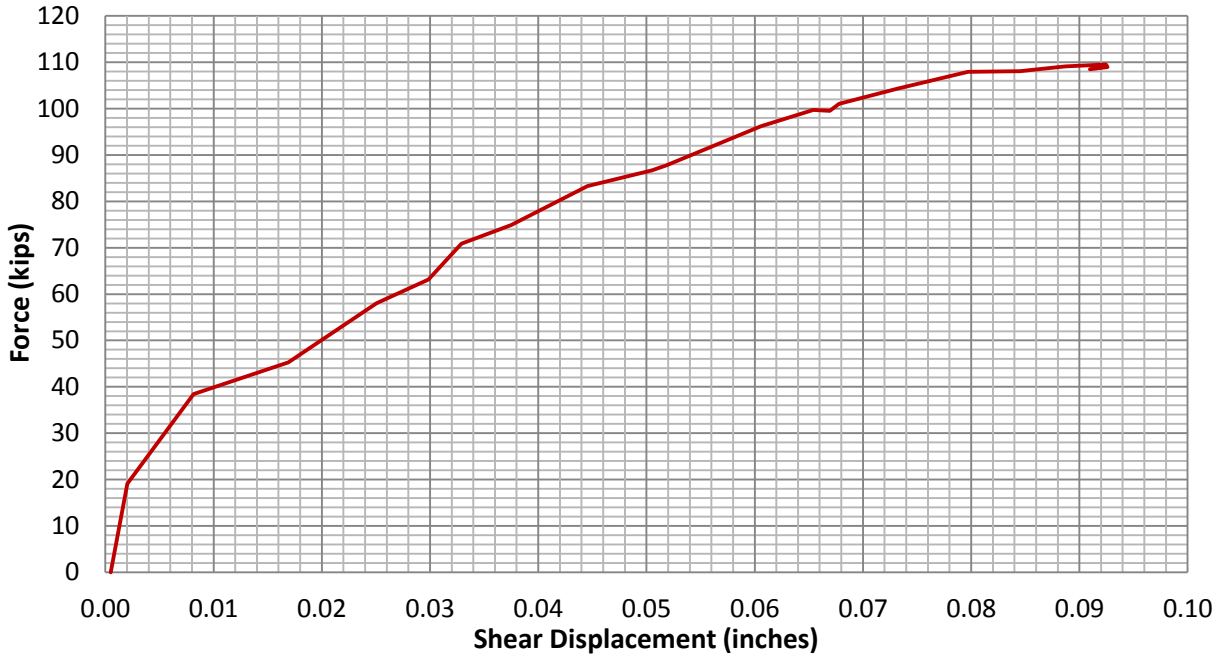

Figure 5-88: Specimen SS1-M Force vs. Shear Displacement

The force-displacement response of specimen SS2-C with and without the shear deformation can be seen in Figure 5-89. The shear component has a smaller contribution to the overall displacement for this specimen. The shear deformation is also somewhat uneven in each loading direction, with shear contributing approximately 20 percent of the overall displacement in the positive loading direction but only 8 percent in the negative loading direction. The shear deformation is plotted against the applied load for this specimen in Figure 5-90. As shown, in the positive loading direction, the shear response is linear, while in the negative loading direction, there is very little shear deformation, and the shape does not coincide as well with linear behavior.

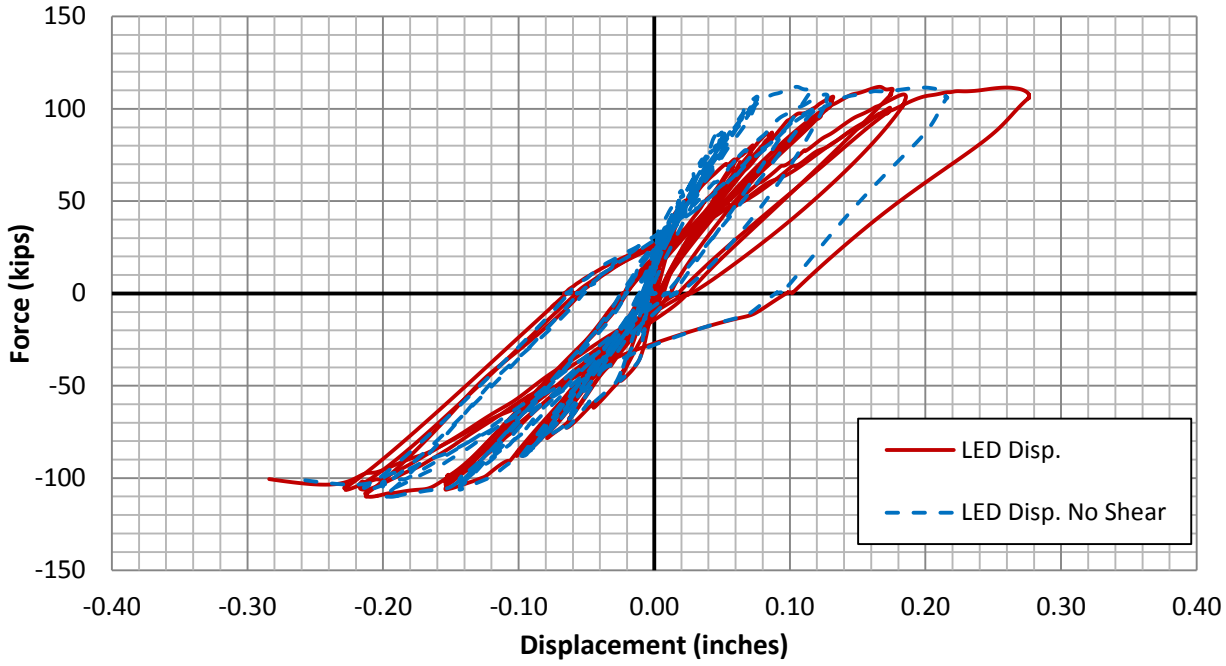

Figure 5-89: Force-Displacement of Specimen SS2-C with and without Shear Deformation

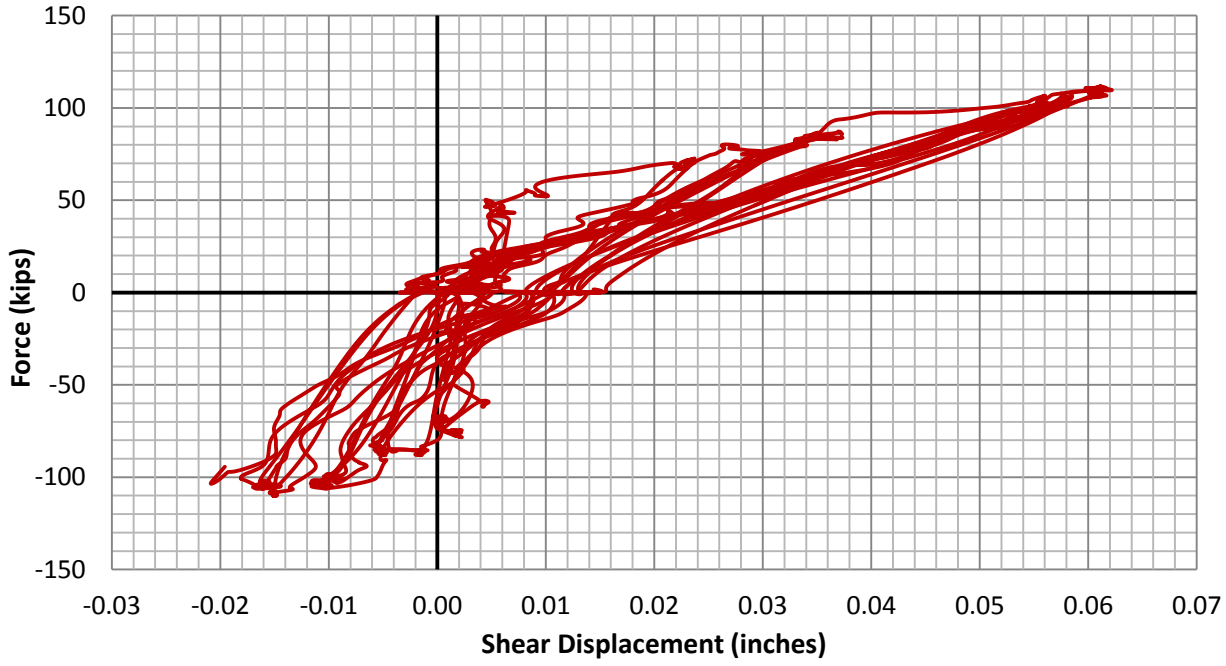

Figure 5-90: Specimen SS2-C Force vs. Shear Displacement

The shear displacement measured for specimen H2S1-M accounts for approximately 20 percent of the overall displacement response, which is very similar to that of the solid sections. The force-displacement response with and without the shear deformation included can be seen in Figure 5-91, and the applied load is plotted against the shear deformation in Figure 5-92. The shear deformation response of this specimen is fairly linear as well. This specimen ultimately failed due to inward compression wall buckling and local effects at the load application points.

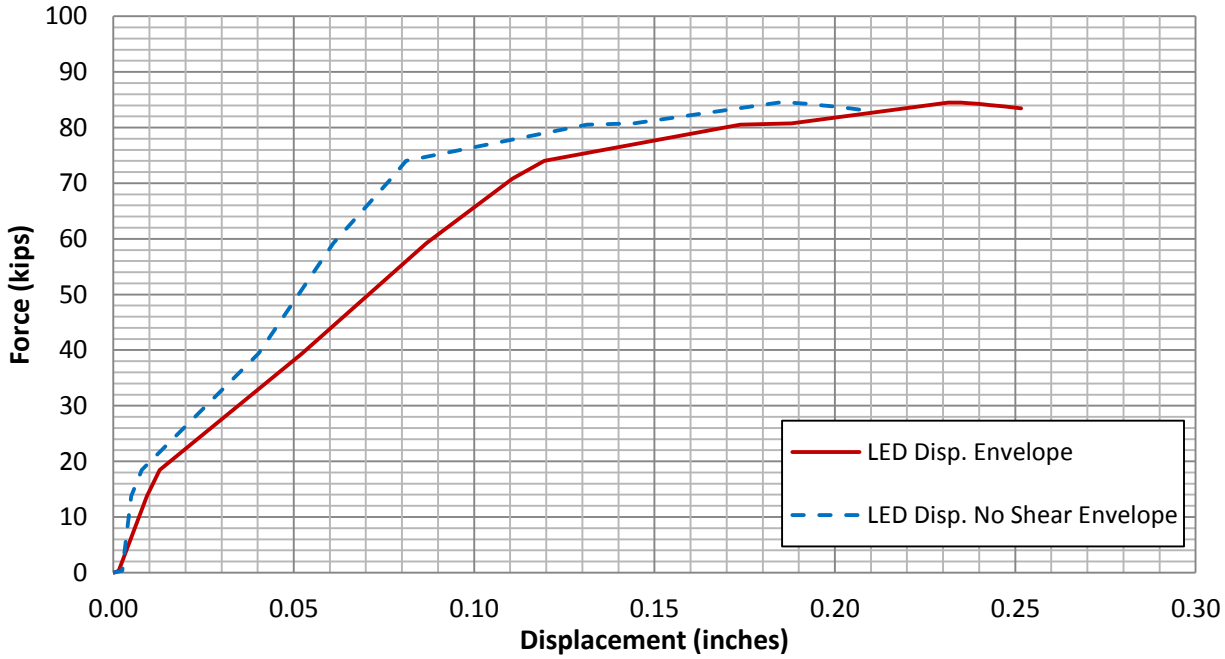

Figure 5-91: Force-Displacement of Specimen H2S1-M with and without Shear Deformation

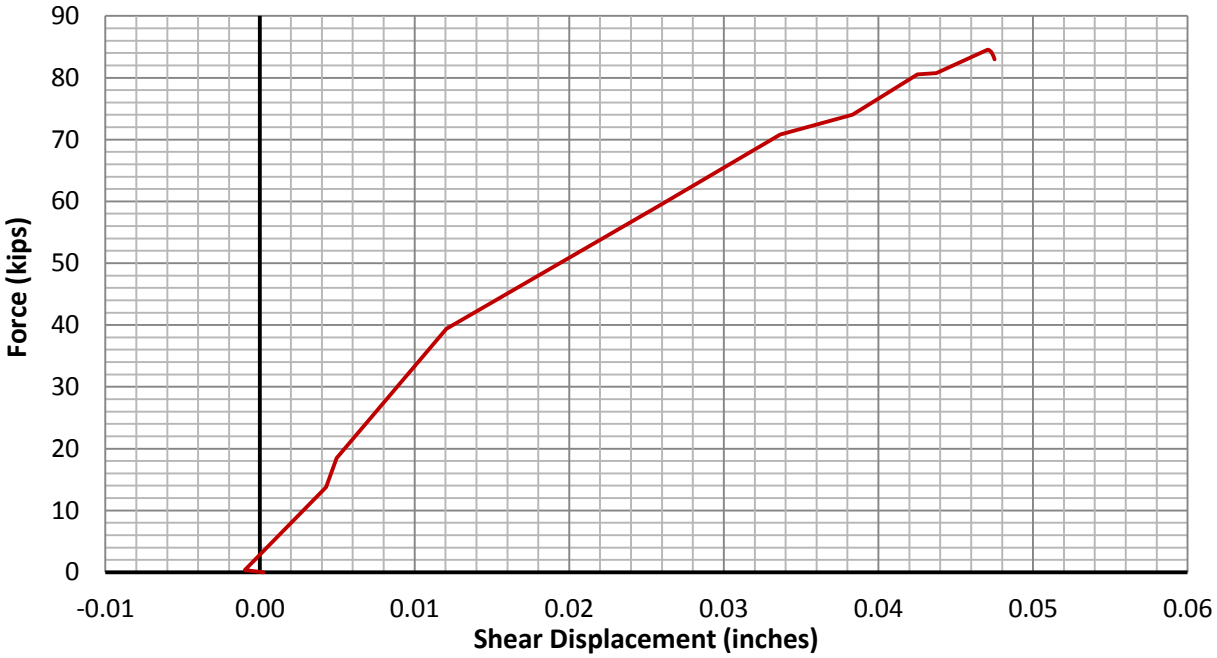

Figure 5-92: Specimen H2S1-M Force vs. Shear Displacement

The remainder of the specimens experienced premature failure caused by shear or by local effects at the loading and support points. Despite some of these specimens failing in shear, the shear deformation at the failure point was not typically captured for the specimens, since the shear failure usually occurred outside the measured region. If the shear failure did occur in the measured region, the LEDs typically spalled off with the concrete in the region. Therefore the measured shear deformation maintains a fairly linear relationship with the applied load for all of the specimens, since the actual shear nonlinear deformation was unable to be captured. The force-displacement responses of these specimens with and without the shear deformation can be seen in Figure 5-93 through Figure 5-97.

Similarly to the circular hollow columns, it can be seen that for the square hollow columns, the shear deformation seems to increase with smaller wall thickness. For the two-inch thick specimens, the shear deformation seems to range from approximately 20 to 30 percent of the overall deformation, with contributions up to around 50 percent in the case of specimen H2S2-

C. For the 1.25-inch wall specimens, the shear deformation is more consistently around 40 to 50 percent.

The response with the shear deformation removed shown in Figure 5-97 for specimen H1.25S3-C indicates that when negative load was applied, the specimen did not achieve negative displacement, and the displacement remained positive. This is most likely due to the early local and shear failure in this specimen, which may have caused nonlinear displacement in the specimen or possibly some local movement in the LEDs.

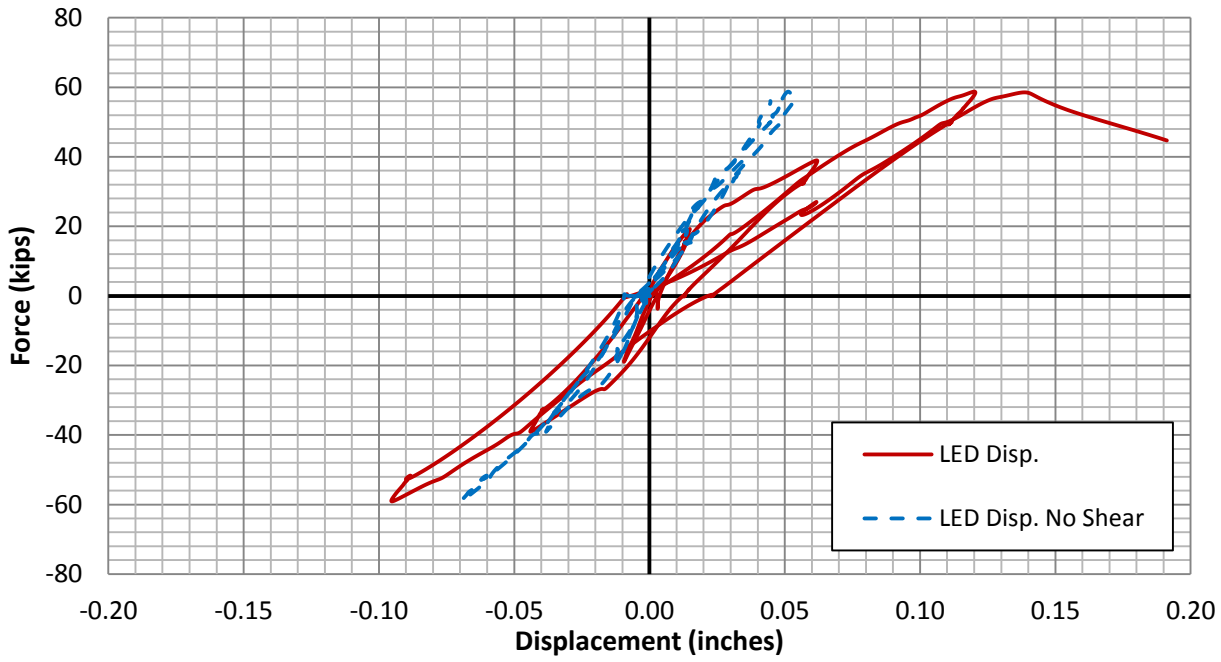

Figure 5-93: Force-Displacement of Specimen H2S2-C with and without Shear Deformation

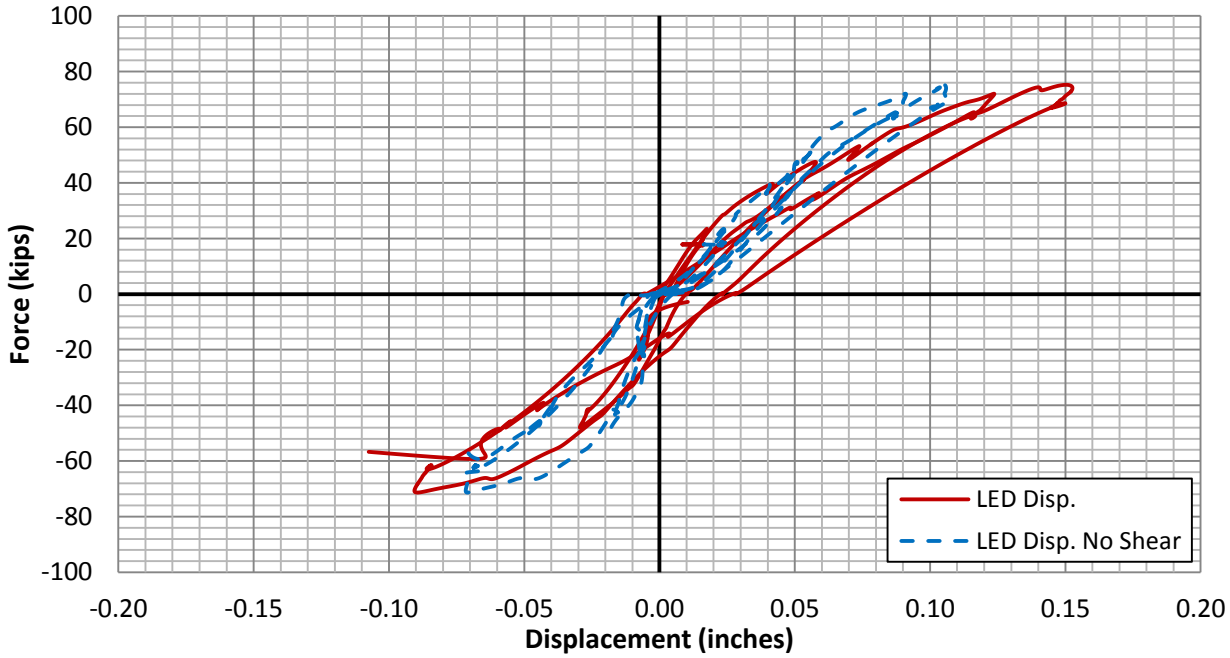

Figure 5-94: Force-Displacement of Specimen H2S3-C with and without Shear Deformation

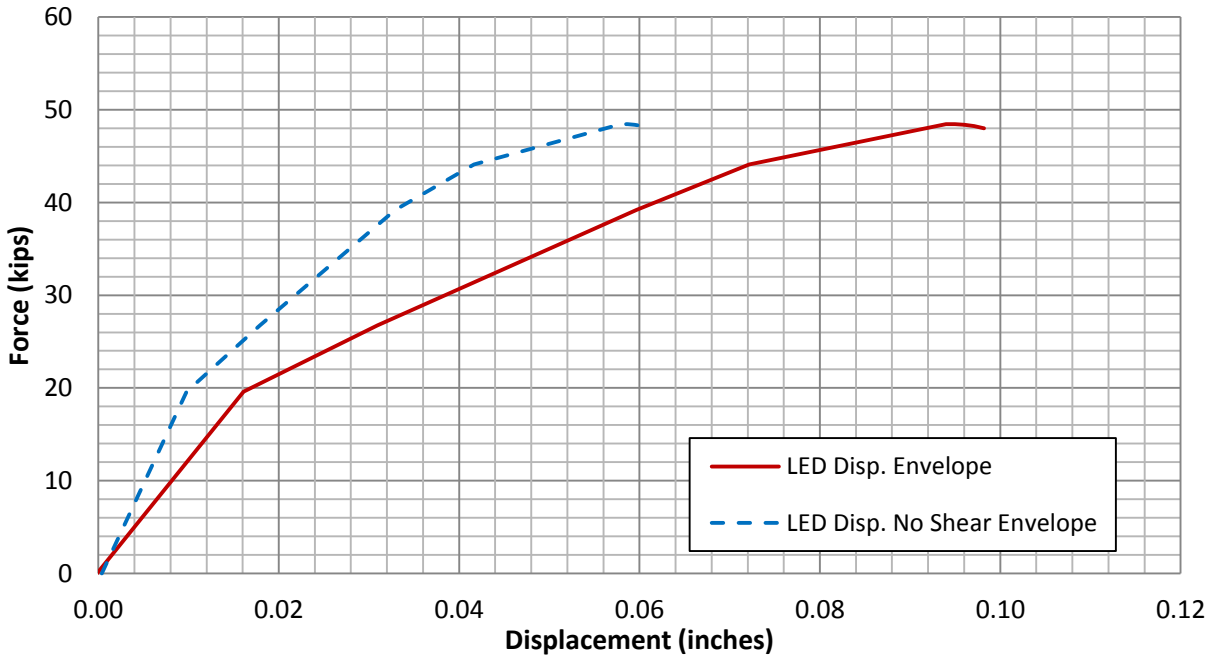

Figure 5-95: Force-Displacement of Specimen H1.25S1-M with and without Shear Deformation

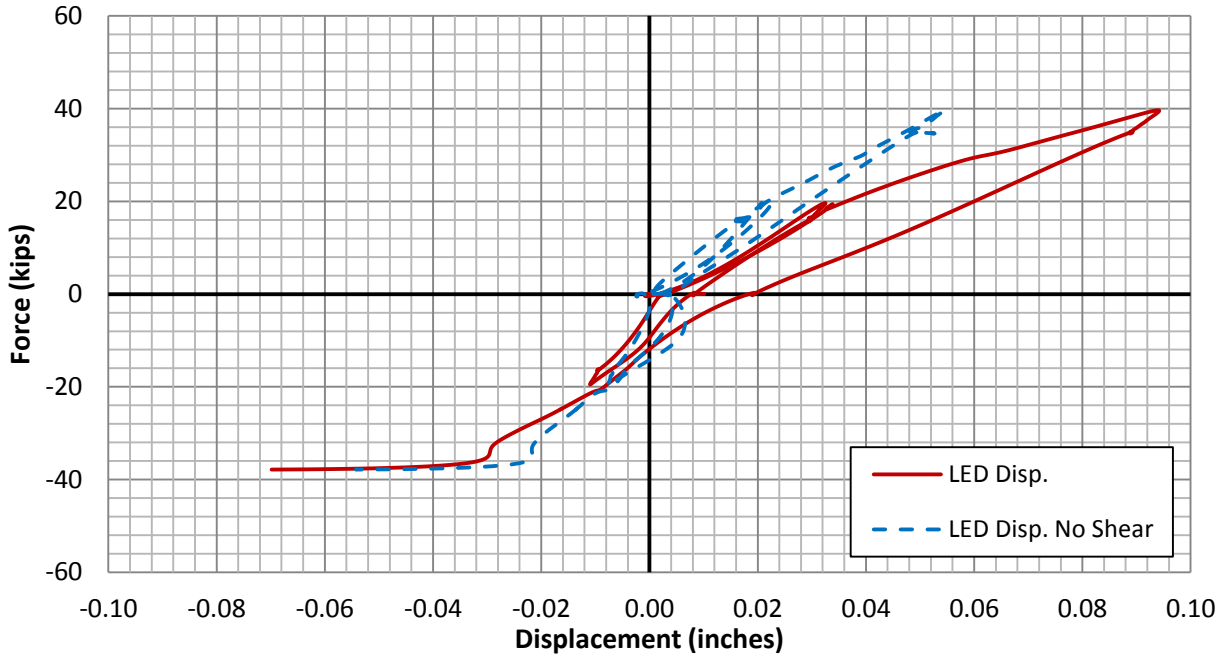

Figure 5-96: Force-Displacement of Specimen H1.25S2-C with and without Shear Deformation

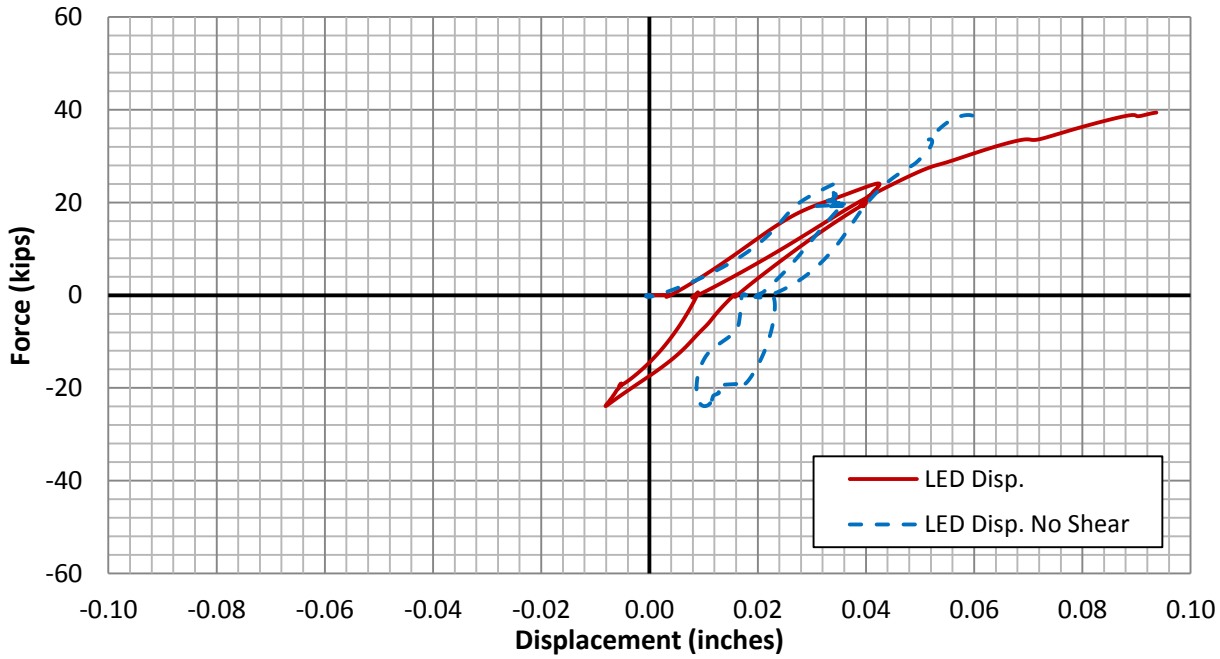

Figure 5-97: Force-Displacement of Specimen H1.25S3-C with and without Shear Deformation

5.2.2.2.3 Force-displacement response without shear

The figures below show the force-displacement response of each specimen with the shear deformation subtracted as well as the OpenSees analysis force-displacement response. The OpenSees response does not include shear effects, so it has been compared to the experimental results with the shear component subtracted. Included in the figures is the predicted failure mode based on the OpenSees response. The predicted failure mode for all specimens was rupture of longitudinal reinforcement. Despite the early failure of the hollow specimens due to shear and local effects, it can be seen that the OpenSees analysis can often capture the initial stiffness of these specimens fairly accurately.

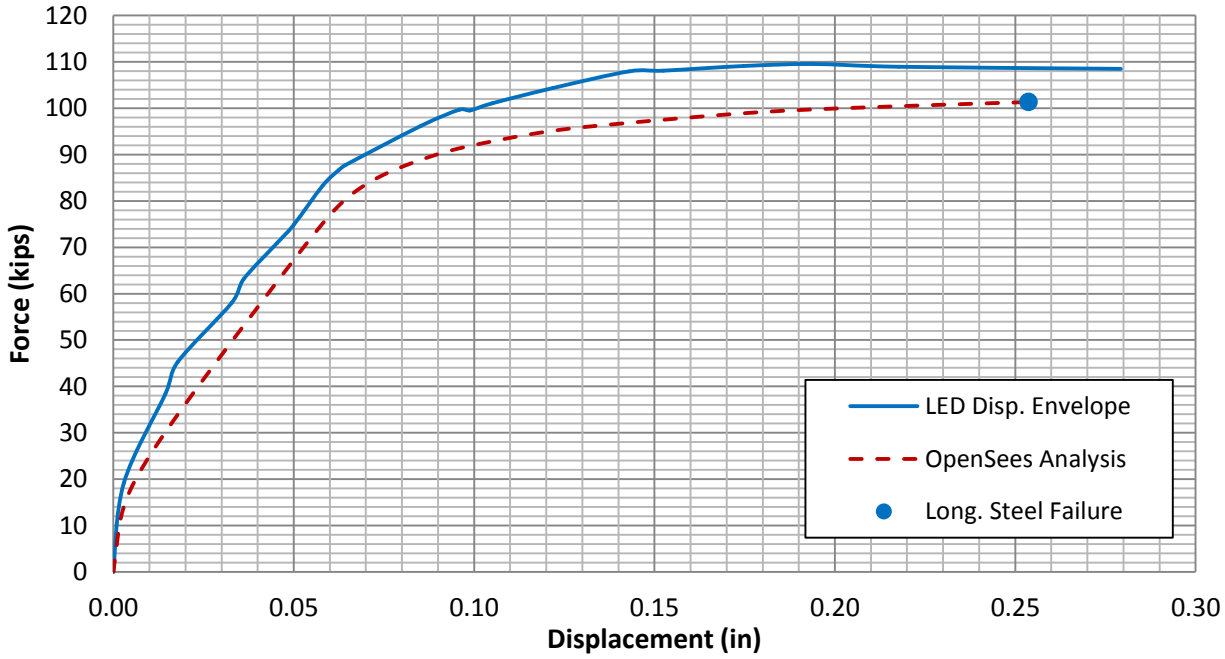

Figure 5-98: Measured Force-Displacement Response of Specimen SS1-M with Shear Deformation Removed Compared to Analytical Envelope Response

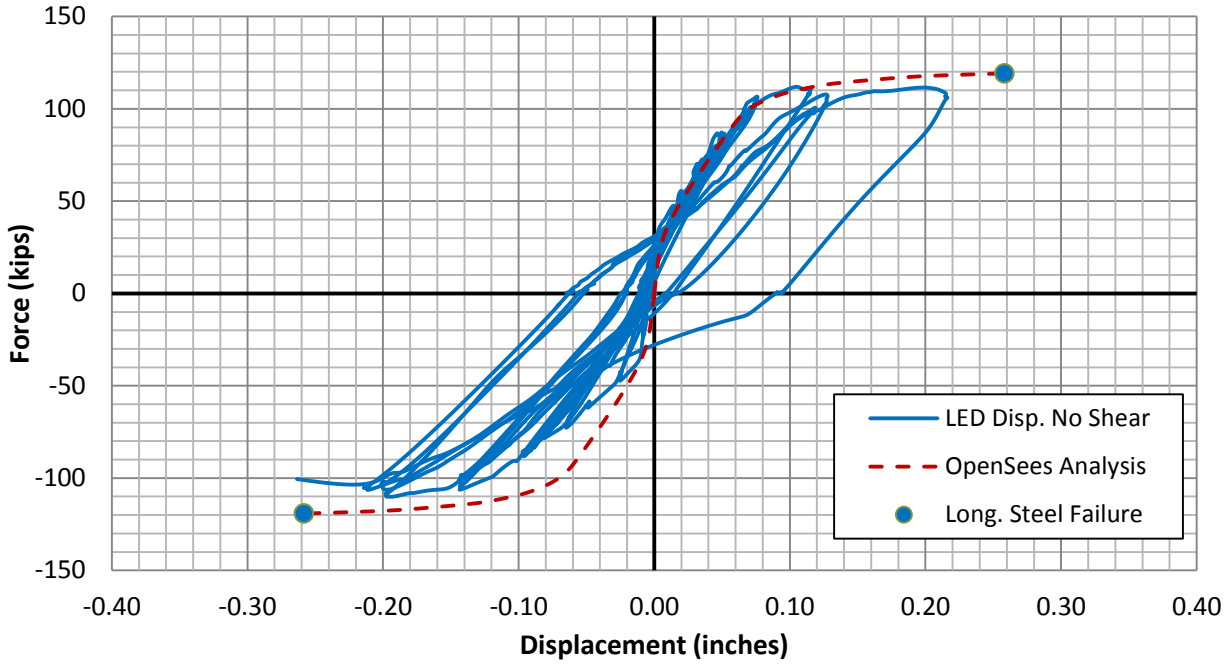

Figure 5-99: Measured Force-Displacement Response of Specimen SS2-C with Shear Deformation Removed Compared to Analytical Envelope Response

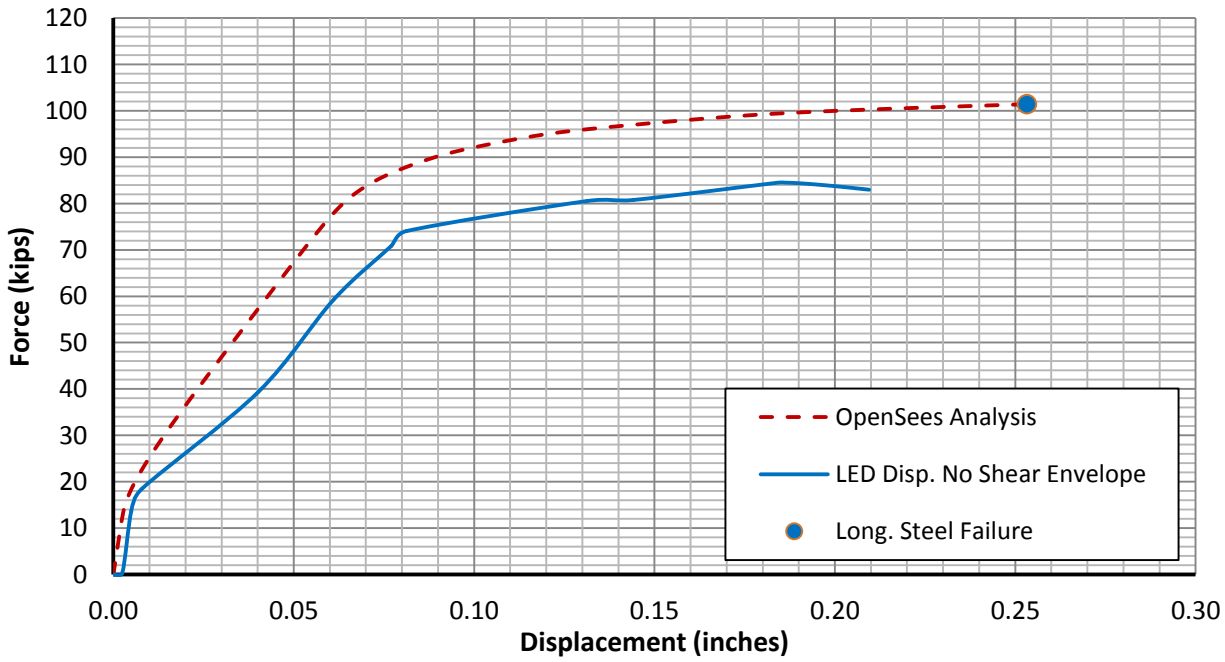

Figure 5-100: Measured Force-Displacement Response of Specimen H2S1-M with Shear Deformation Removed Compared to Analytical Envelope Response

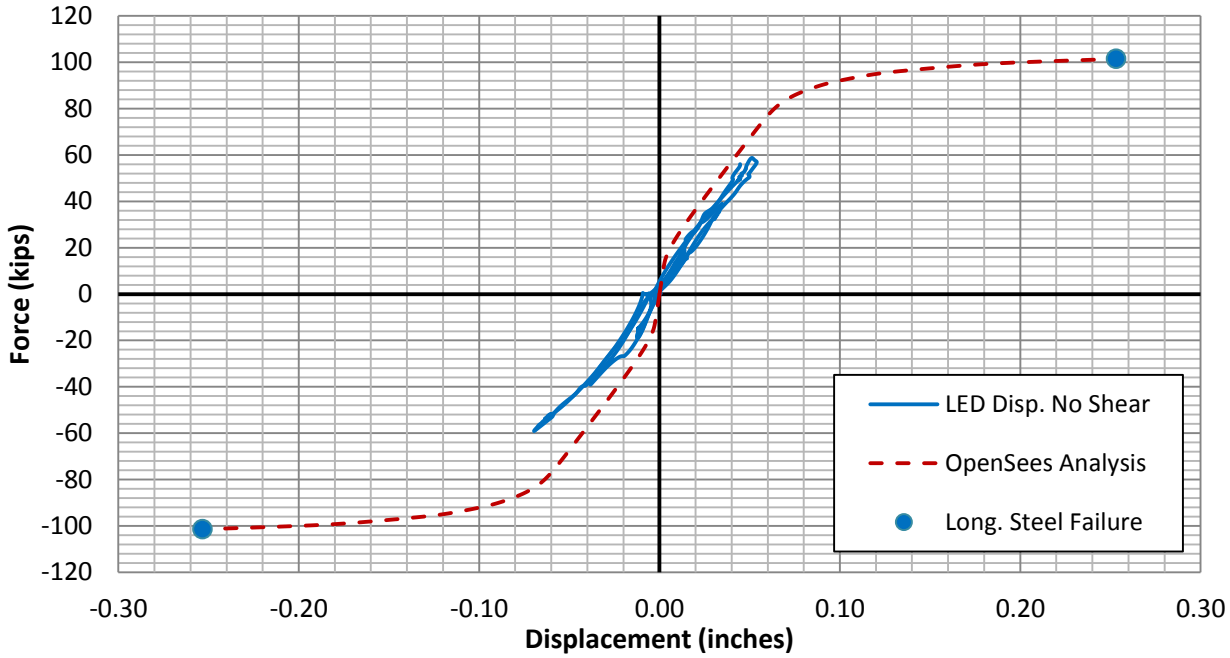

Figure 5-101: Measured Force-Displacement Response of Specimen H2S2-C with Shear Deformation Removed Compared to Analytical Envelope Response

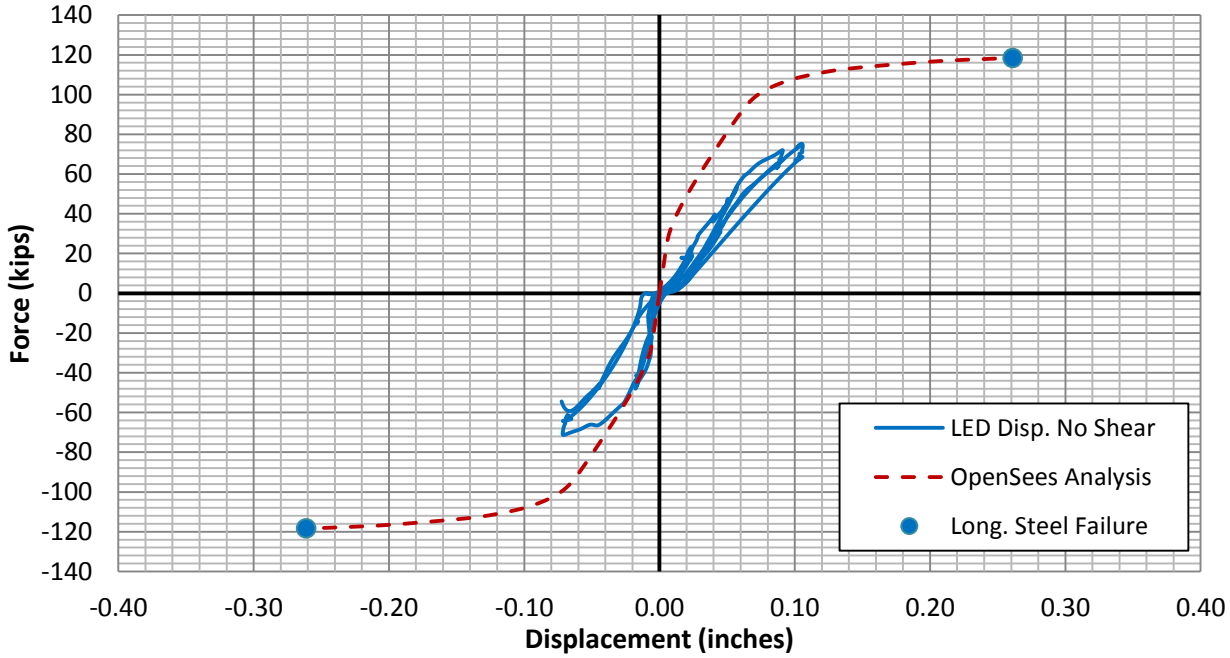

Figure 5-102: Measured Force-Displacement Response of Specimen H2S3-C with Shear Deformation Removed Compared to Analytical Envelope Response

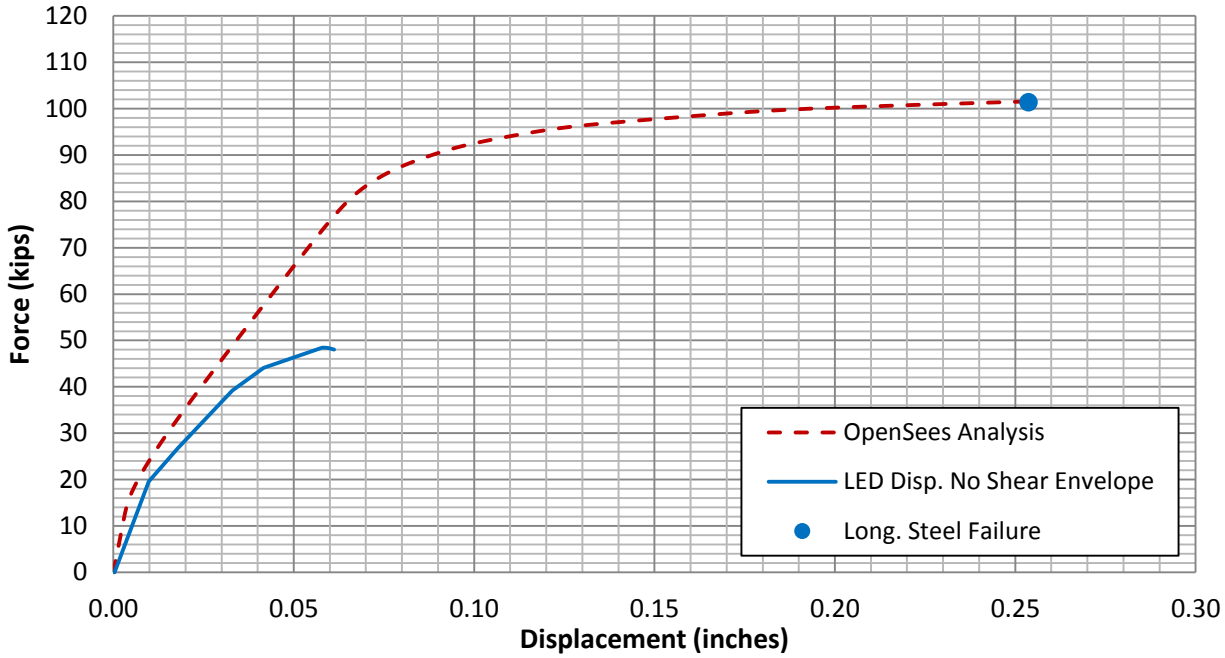

Figure 5-103: Measured Force-Displacement Response of Specimen H1.25S1-M with Shear Deformation Removed Compared to Analytical Envelope Response

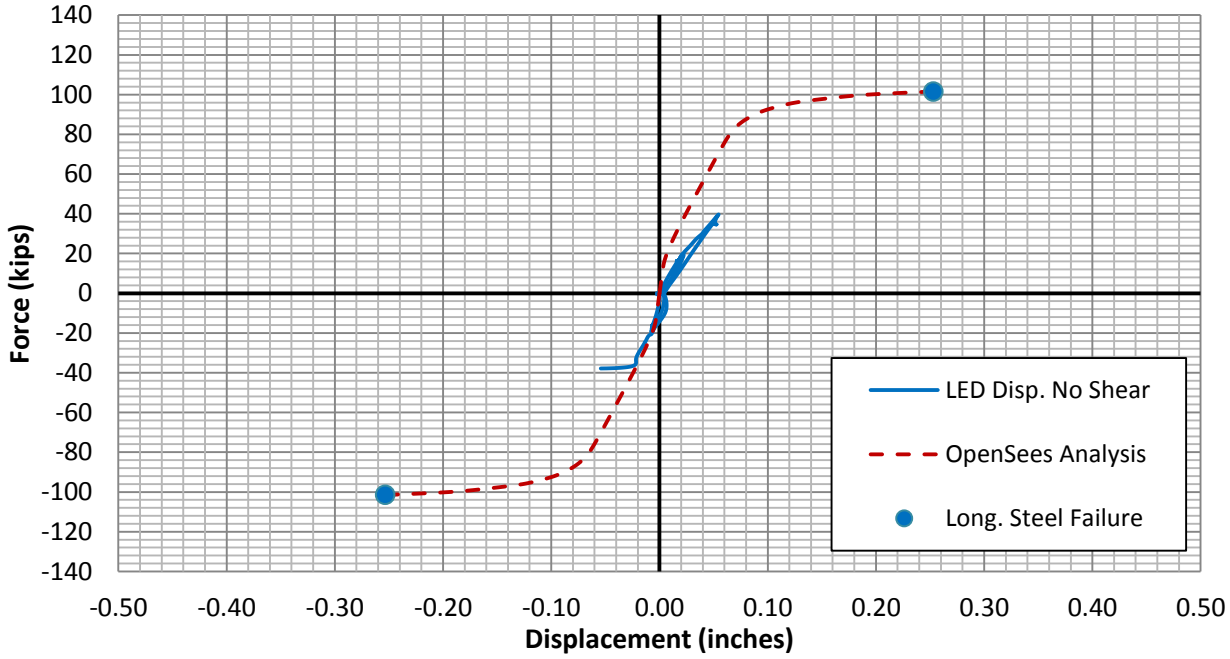

Figure 5-104: Measured Force-Displacement Response of Specimen H1.25S2-C with Shear Deformation Removed Compared to Analytical Envelope Response

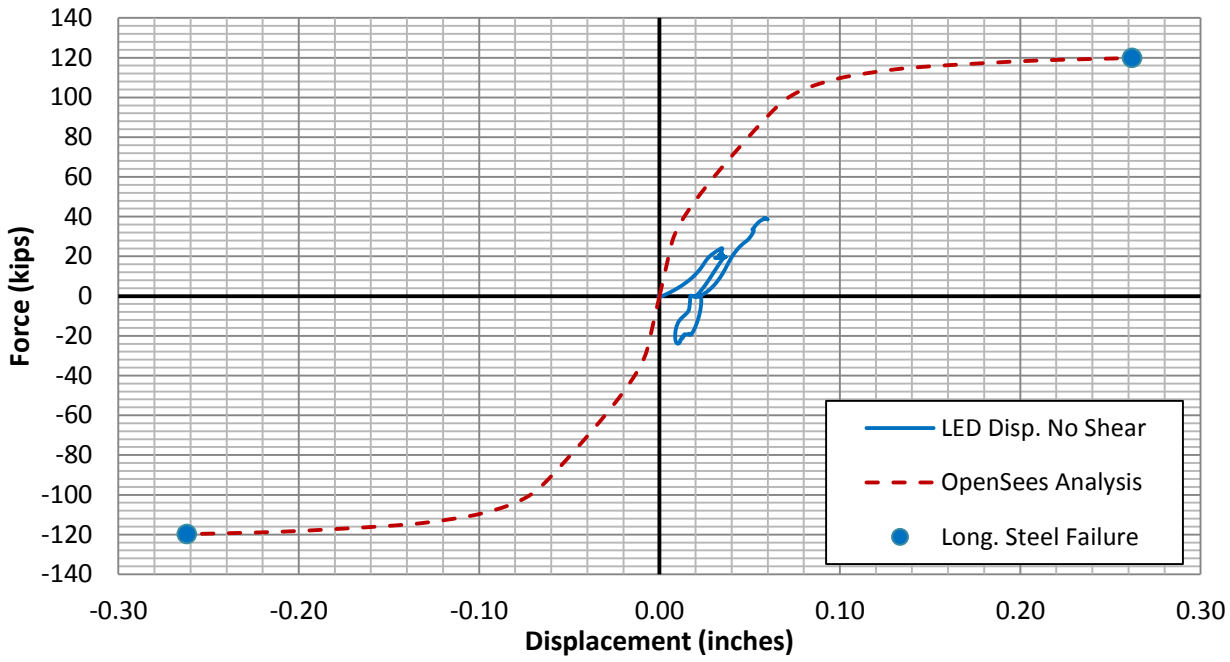

Figure 5-105: Measured Force-Displacement Response of Specimen H1.25S3-C with Shear Deformation Removed Compared to Analytical Response

5.2.2.2.4 Longitudinal bar strain

The following section gives the longitudinal bar strains of each specimen, measured by strain gauges attached to the bars. The longitudinal bar strain from the OpenSees analysis for each specimen is also shown for comparison. The analysis strains shown are from either the extreme tension or compression longitudinal steel bars. The measured and analytical strains are presented for the cyclically loaded specimens, with strains from one of the sides, which experienced extreme tension and compression strains being shown. The figures are labeled as either near longitudinal bar 1 or longitudinal bar 12. The response from the OpenSees analysis is plotted up until the point where failure was predicted in the analysis. The predicted analytical failure mode was longitudinal steel rupture for all specimens.

Only some of the measured strains have been presented, since the comparisons are fairly similar for most specimens. The solid specimens show very good agreement to the analytical results, including the prediction of the ultimate failure mode. The hollow specimens agreed well

with the predicted results for the most part in the force-control range of testing. However, the hollow specimens experienced early failure due to local and shear effects, while the analysis indicated these specimens would experience failure due to longitudinal bar rupture at similar force levels to the solid specimens.

The square specimen strain gauge locations have been provided again in Figure 5-106 for quick reference. The gauges marked with an asterisk only appeared at one section in the specimen, while all other gauges were at both sections. See Section 4.5 for more details of the strain gauge locations. The measured response compared to analytical response for certain longitudinal bars is provided in Figure 5-107 through Figure 5-111.

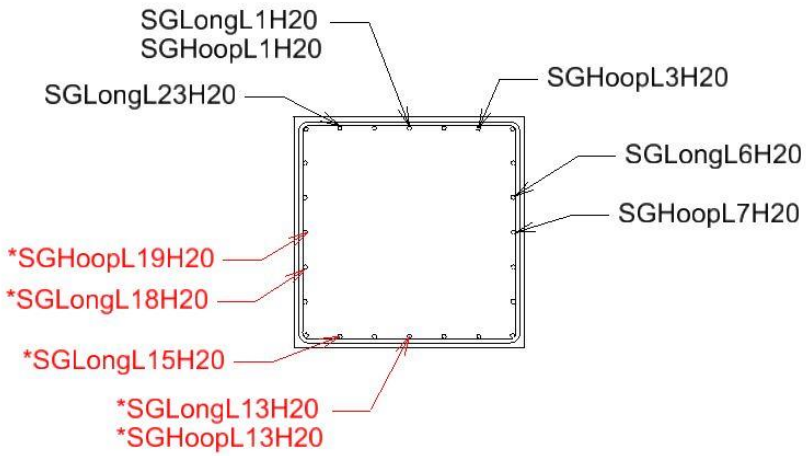

Figure 5-106: Square Section Strain Gauge Locations

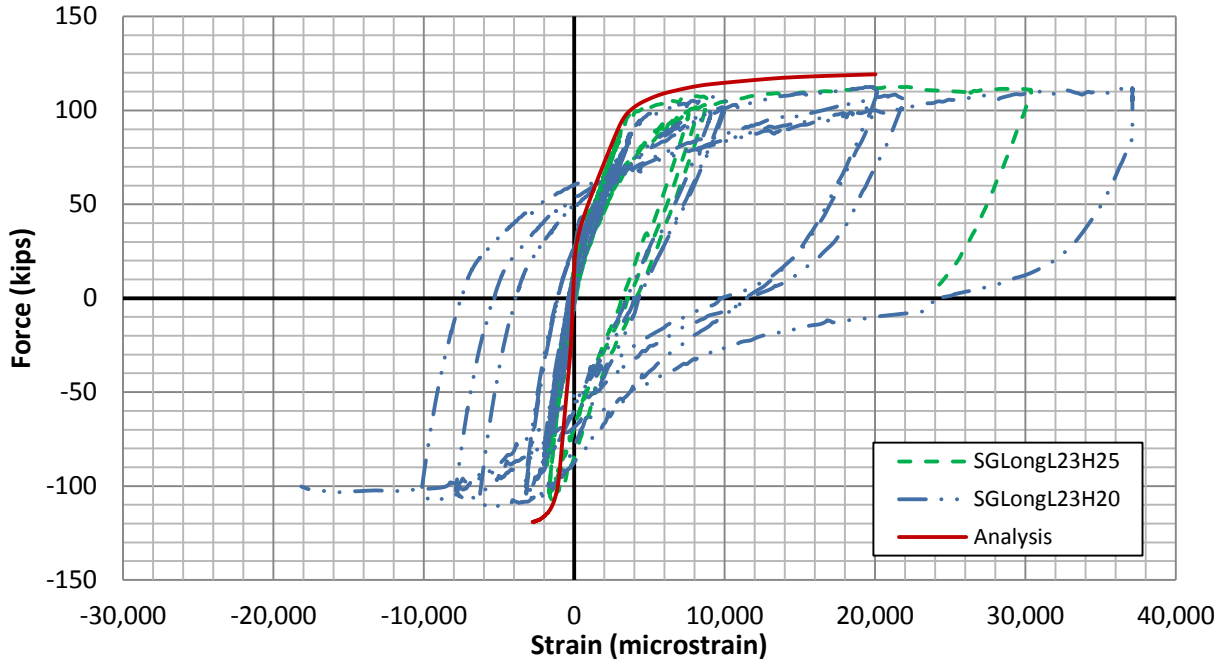

Figure 5-107: Specimen SS2-C Longitudinal Strain near Longitudinal Bar One vs. Applied Load

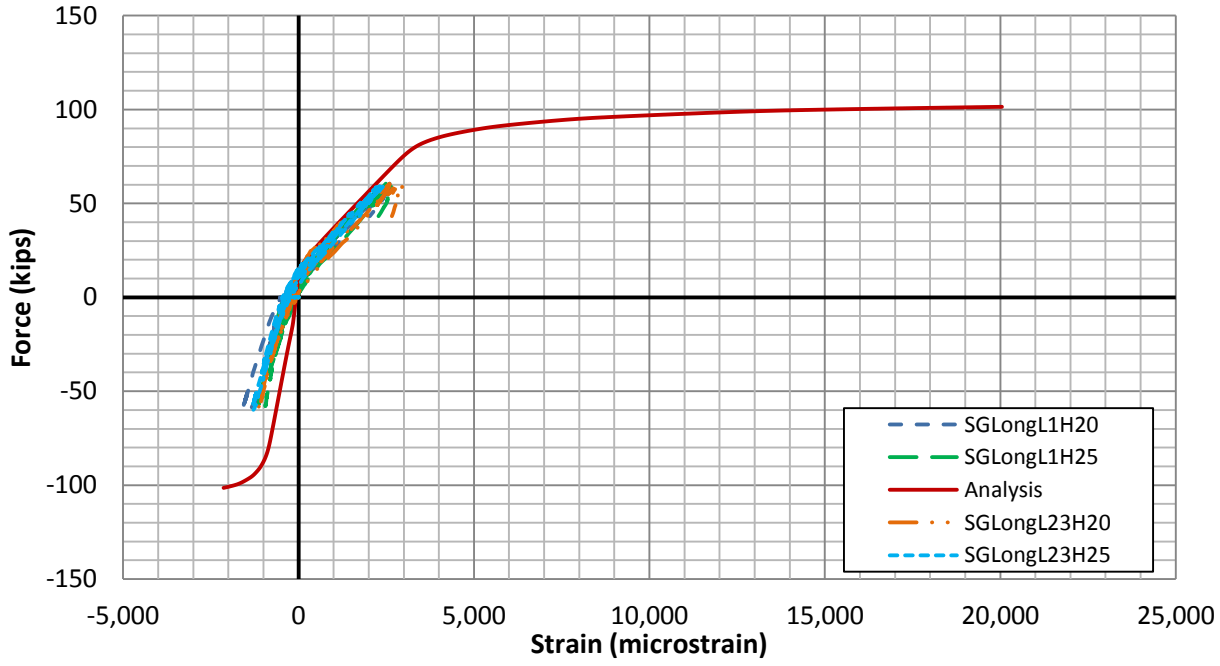

Figure 5-108: Specimen H2S2-C Longitudinal Strain near Longitudinal Bar One vs. Applied Load

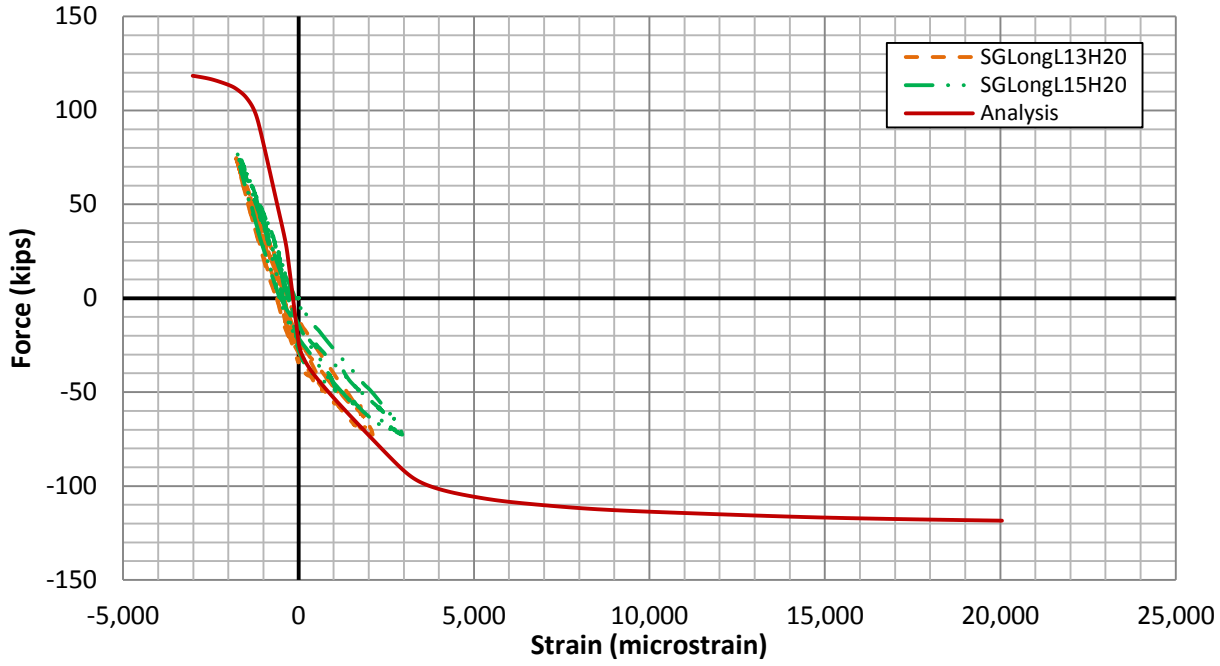

Figure 5-109: Specimen H2S3-C Longitudinal Strain near Longitudinal Bar 12 vs. Applied Load

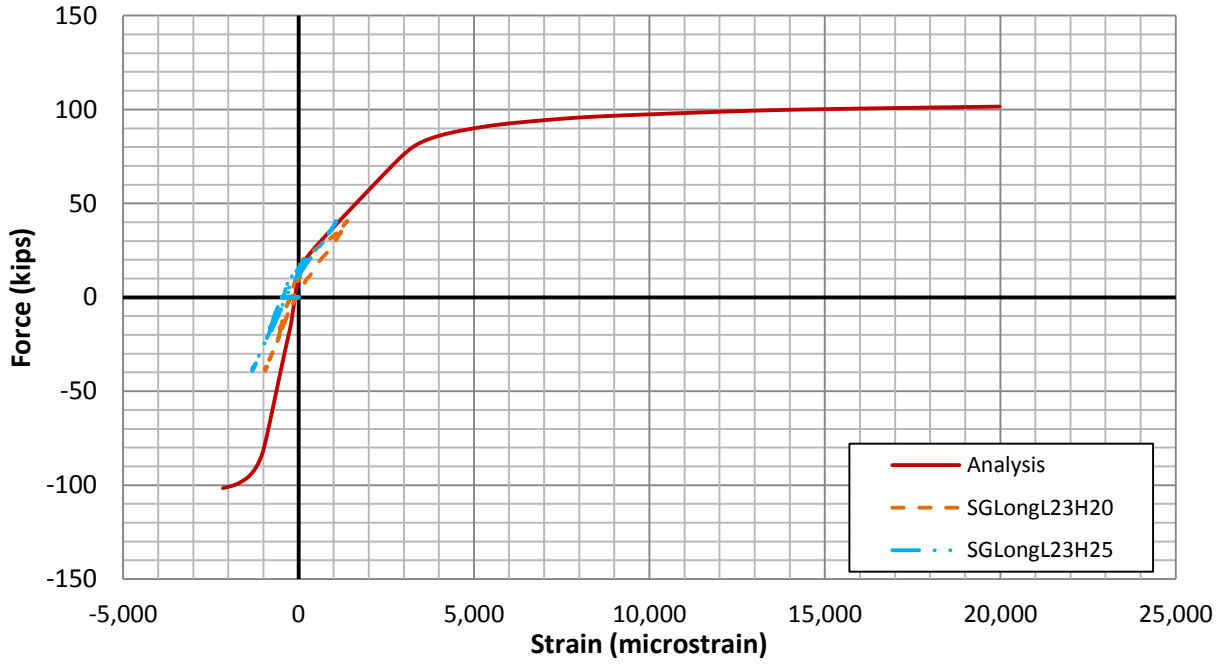

Figure 5-110: Specimen H1.25S2-C Longitudinal Strain near Longitudinal Bar One vs. Applied Load

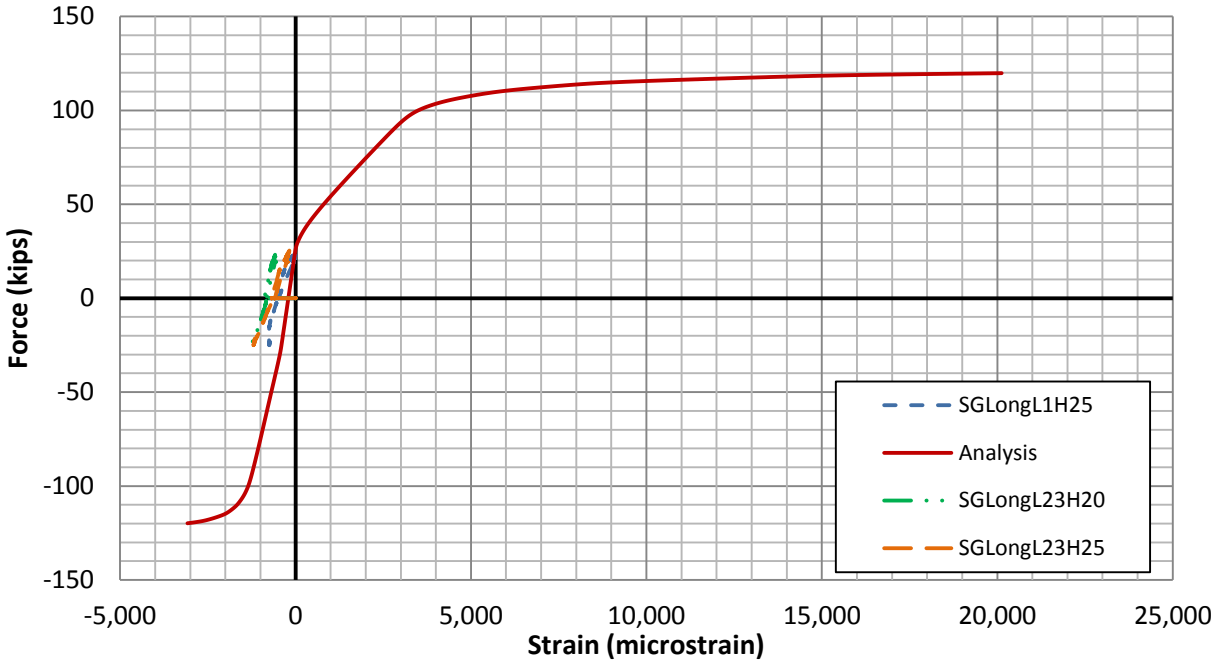

Figure 5-111: Specimen H1.25S3-C Longitudinal Strain near Longitudinal Bar One vs. Applied Load

As shown in the figures, the OpenSees analysis matches up fairly closely with the measured response from the strain gauges on the longitudinal reinforcement. Even for the hollow specimens for which early failure occurred, the analysis matches up well with the initial stiffness for most of these specimens. Similarly to the longitudinal strains for the hollow columns, the longitudinal strains in compression for these specimens can sometimes be fairly high. To verify these strains and provide a further comparison between the analytical and experimental results, the strains measured by the LEDs attached to the concrete are examined in the next section.

5.2.2.2.5 Concrete strain

The concrete strains near the extreme tension and compression fibers of the sections were found using the LED grid in the constant moment region. The location of the presented LEDs was fairly close to the extreme tension and compression fibers of the sections, so the

longitudinal reinforcement strains from the extreme tension and compression reinforcement found in the OpenSees analysis have been plotted for comparison. The tension and compression strains are presented in the same plot as well as the analytical strains. The measured strains are labeled either “Strain57,” representing the strain measured between LEDs 5 and 7, or “Strain1820,” representing the strain measured between LEDs 18 and 20. The measured LED strains have been processed to remove noise and outliers.

The layout of the LEDs used during testing is shown in Figure 5-112 for reference. The measured LED strains presented in this section were measured in the constant moment region. The strain gauge sets from which the strains were measured are highlighted in the figure.

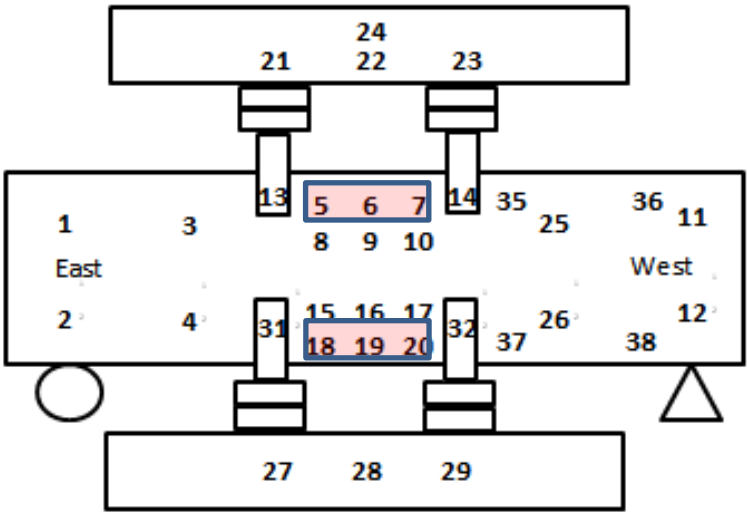

Figure 5-112: LED Layout with Highlighted Strain Locations

The measured and analytical strains are plotted against the applied lateral load for several of the specimens in Figure 5-113 through Figure 5-115. The plots show good agreement between the measured and analytical strains for most specimens. Additionally, the compressive strains measured by the LEDs are not as large as was shown by the strain gauges and agree

better with the visual results of the test specimens. The test specimens did not show signs of high compressive strains, since there was not a large amount of crushed concrete near the extreme compression region. The predicted failure mode for all of the specimens was longitudinal steel rupture. However, the hollow specimens failed early due to local and shear effects, and thus the analytical results for these specimens predict larger loads at the ultimate failure. Despite this difference, the initial slope of the measured and analytical strains agrees well for most specimens, up until the point where the test specimens experienced early failure. The general comparison between experimental and analytical results is fairly similar for all specimens of the same wall thickness, and therefore, only one of the cyclically loaded specimens for each wall thickness has been shown for brevity.

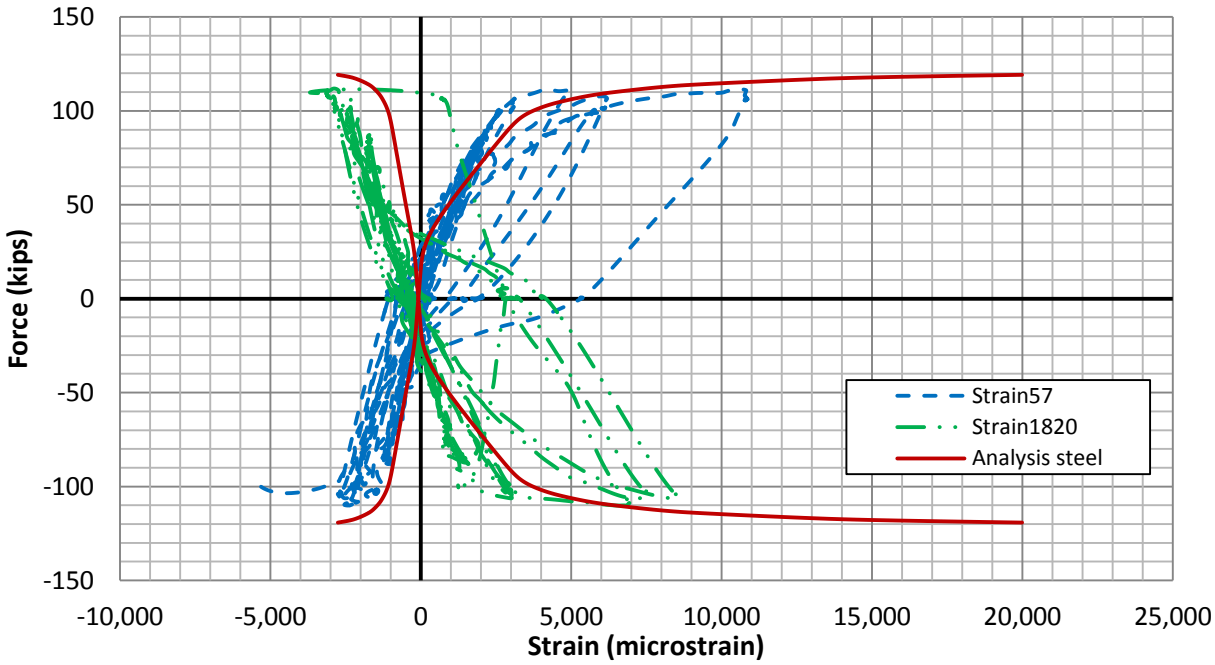

Figure 5-113: Attached LED Concrete Strain Measured During Testing and Analytical Steel Strain vs. Applied Lateral Load for Specimen SS2-C

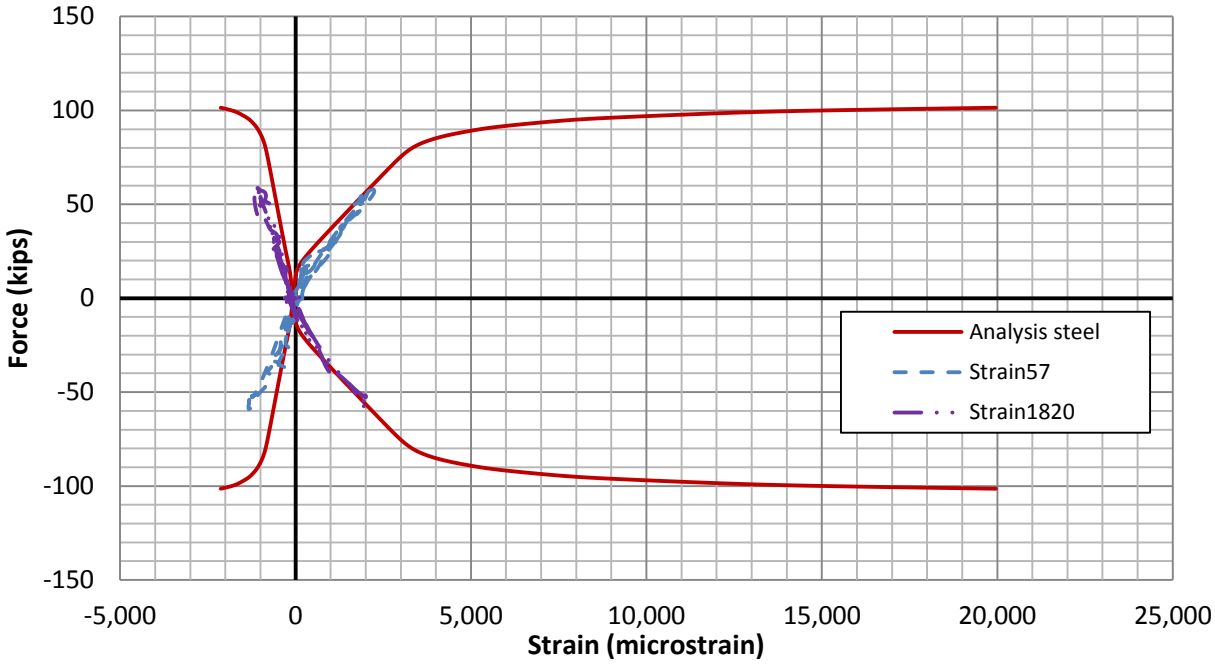

Figure 5-114: Attached LED Concrete Strain Measured During Testing and Analytical Steel Strain vs. Applied Lateral Load for Specimen H2S2-C

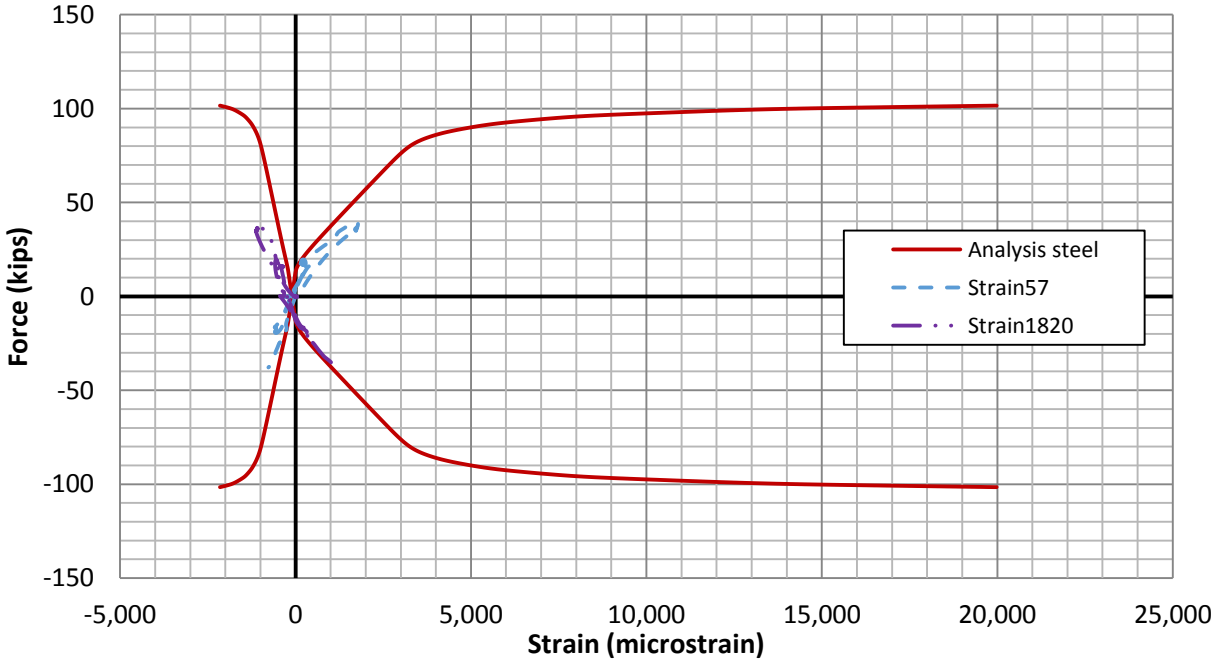

Figure 5-115: Attached LED Concrete Strain Measured During Testing and Analytical Steel Strain vs. Applied Lateral Load for Specimen H1.25S2-C

5.2.2.2.6 Square hoop strain

The strains in the transverse reinforcement were also measured within each wall for the square sections within the constant moment region. The measured strains can provide a good indication of how much demand is being applied to the transverse reinforcement. By examining the transverse strains for all of the specimens, it was found that the transverse reinforcement was subjected to low demand, with strains typically not reaching above 2,000 microstrain. This indicates that the transverse reinforcement was adequate to prevent fracture of the transverse reinforcement and restrain radial displacement.

Figure 5-116 through Figure 5-118 show the strain measured in the transverse reinforcement during the testing of test unit SS2-C. Three plots are shown for the specimen, with each plot showing strain gauges near the extreme fiber tension or compression face or on the side of the specimen. Theoretically, the transverse reinforcement would reach higher tensile strains when the section near the reinforcement is subjected to compression, since the transverse reinforcement must restrain the dilation of the concrete. Slight evidence of this pattern can be seen in Figure 5-116, where the transverse reinforcement strains become slightly higher when loading in the negative direction is applied, which would put compression on the section near longitudinal bar number one. However, the pattern is not very strong, and the demand of the transverse reinforcement is very low. The plots for specimen SS2-C are shown as an example of the other specimens. The remainder of the specimens either had somewhat similar patterns or no pattern, with transverse steel strains not typically reaching higher than those shown for specimen SS2-C.

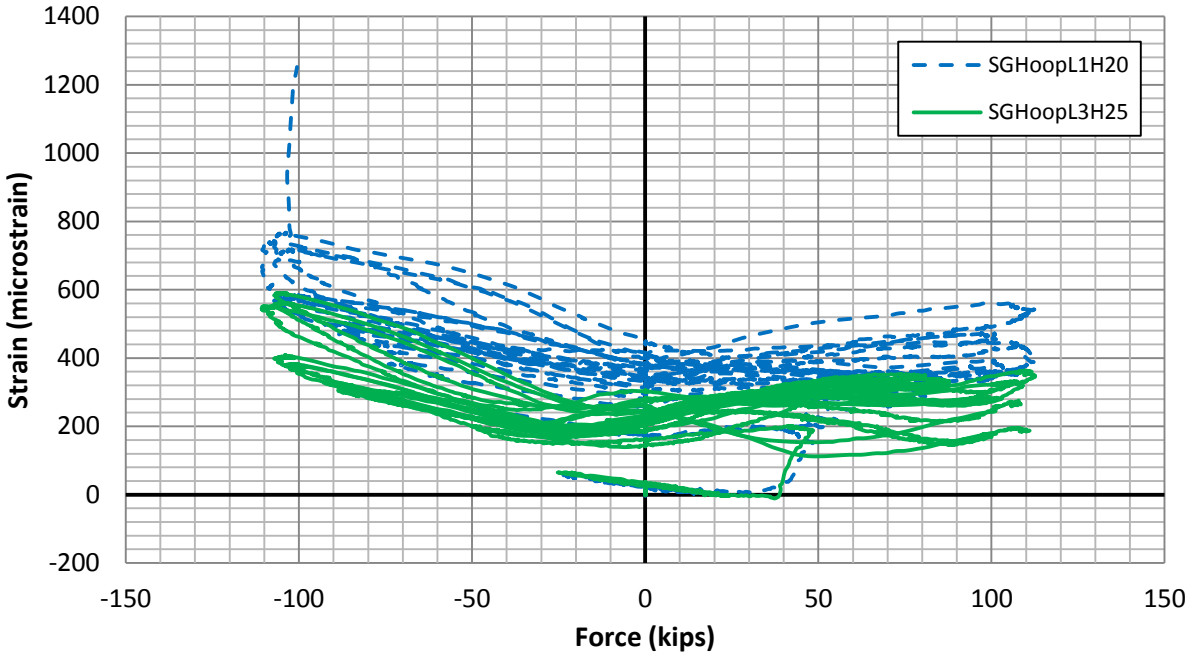

Figure 5-116: Specimen SS2-C Hoop Strain near Longitudinal Bar 1 vs. Applied Load

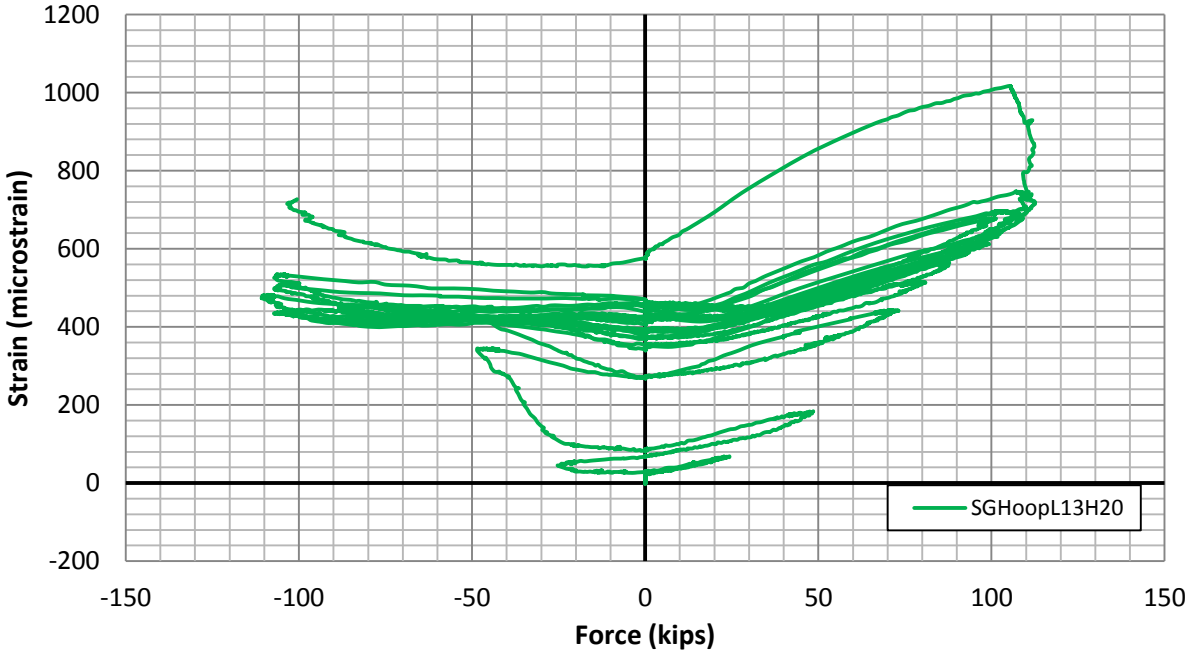

Figure 5-117: Specimen SS2-C Hoop Strain near Longitudinal Bar 12 vs. Applied Load

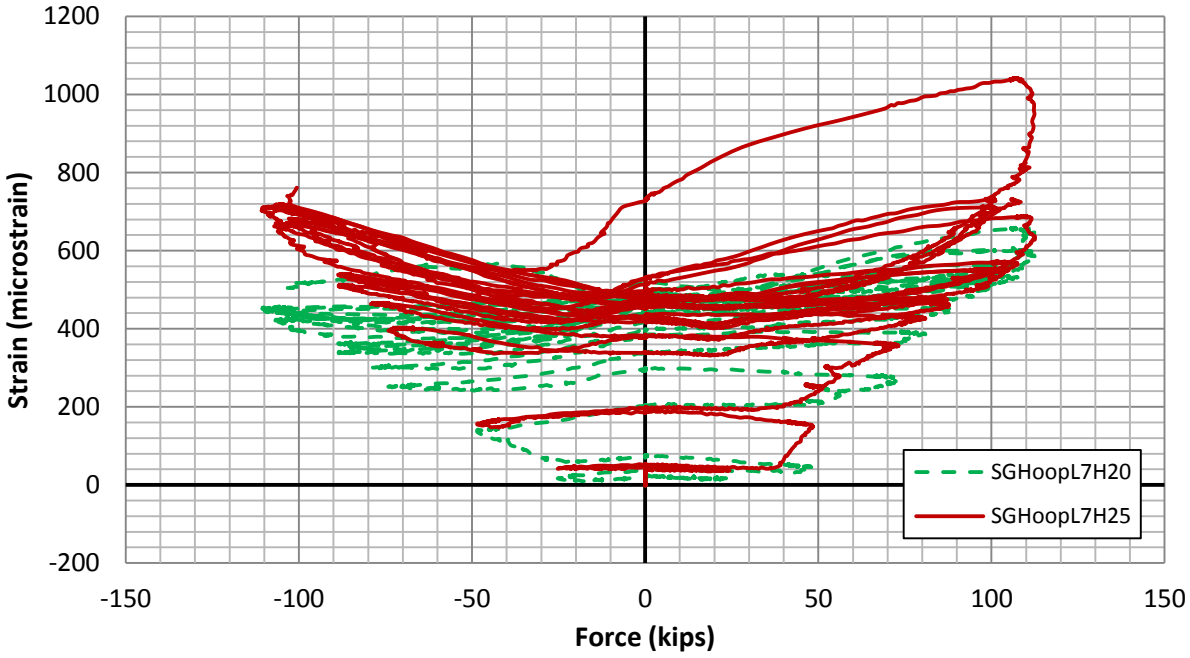

Figure 5-118: Specimen SS2-C Hoop Strain at Side of Section vs. Applied Load

5.3 Analytical Accuracy

The experimental results and comparison to analytical results presented in Section 5.2 have shown that the analytical model is capable of representing the flexural response of hollow columns fairly accurately. However, to be sure that the test results and the analytical method agree, it is useful to show more detailed comparisons. This section provides comparisons of the strain profiles and the strain versus displacement of the materials for specimen H2C1-M. This specimen was selected because it was hollow and loaded monotonically, which would allow for a more direct comparison to the analyses and are also performed monotonically. Specimen H2C1-M was found to show good response and did not experience early or local failure.

Figure 5-119 shows the measured and analytical strain values plotted against the displacements, with the shear component of the displacement subtracted. As shown, the OpenSees analysis agrees very well with the concrete tension strain measured by the LEDs (labeled Strain57). The longitudinal steel strains measured on the most extreme tension bar are also plotted and agree well with the analysis. These strains were only plotted to around

5,000 microstrain because after that, they began to increase in strain rapidly, which might be due to damaged gauges. In the compression region, the measured concrete compressive strains (labeled Strain1820 in the plot) were higher than those predicted by the OpenSees analysis, which may be due to local effects.

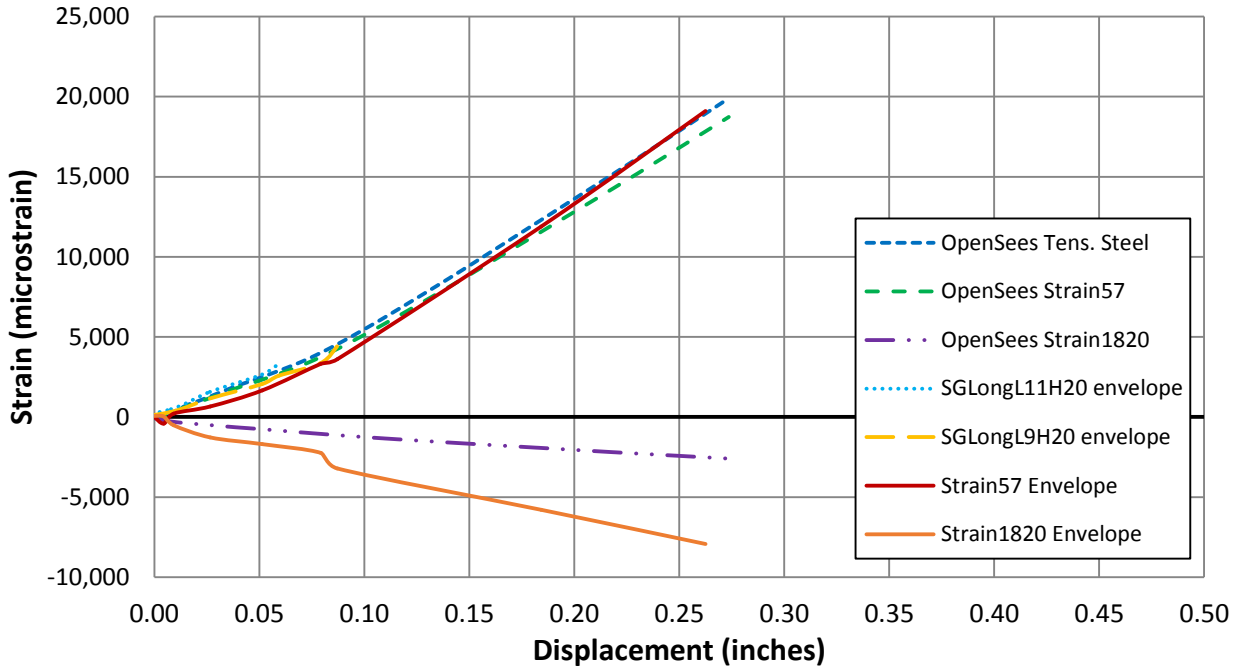

Figure 5-119: Measured and Analytical Strain vs. Displacement for Specimen H2C1-M

Additionally, several strain profiles are shown in Figure 5-120 through Figure 5-122, taken at different points in the testing. The points were chosen based on the measured tension strains of longitudinal reinforcement, and the analysis strain profiles were chosen based on tension steel strain corresponding to the measured point. In Figure 5-120 it can be seen that several points were plotted for the experimental results and OpenSees analysis at first yield. For the test results, the points are the measured tension steel strain and the four LED strains along the section in the moment region. The points on the analysis profiles correspond to tension steel strain, strain in concrete at the location of the most extreme tension LED set, strain at the inside compression face, and concrete compression strain at the point of the most extreme

compression LEDs. The strain at the inside compression face as given by the analysis is at a similar depth to a set of LEDs, which were used to measure strains. As shown, the profile is fairly similar, with some small differences, especially at the compression face.

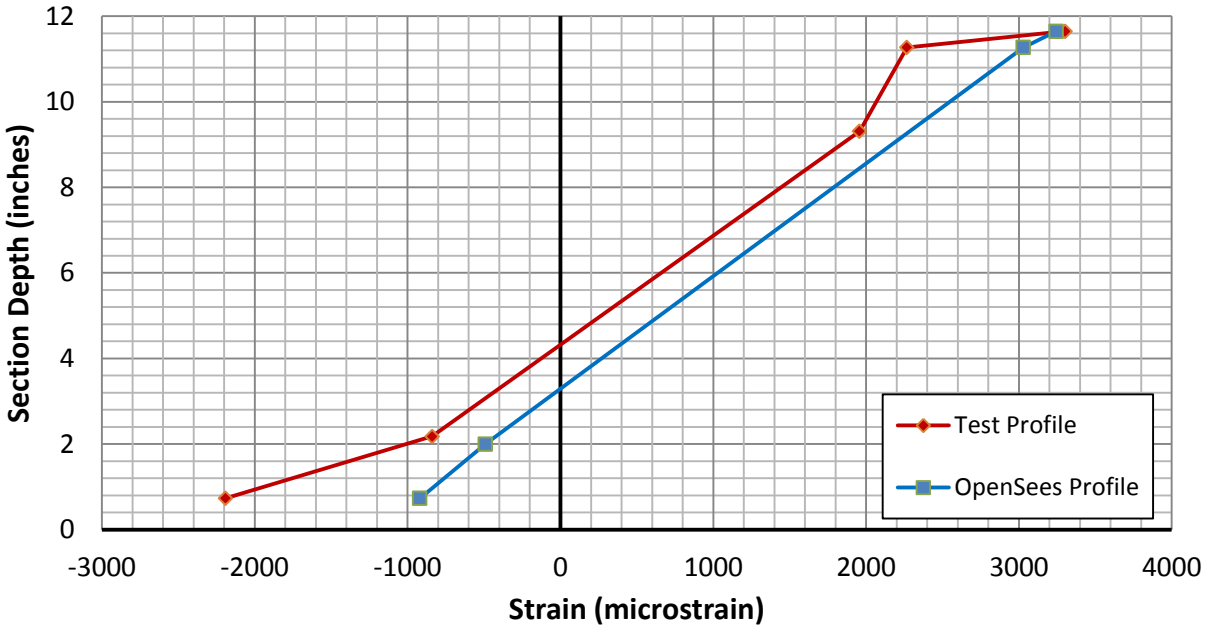

Figure 5-120: Specimen H2C1-M Strain Profile at First Yield (Measured Steel Strain 3300 Microstrain)

Another strain profile is shown in Figure 5-121. This strain profile was chosen because it was near to the last point in which the second LED row on the compression side was visible. The presence of this second LED row provides an additional data point, which gives a better idea of the strain profile, and this plot provides a good idea of the strain profile at higher extreme fiber strains. At this point, the specimen was well into the nonlinear range, as the tension strain was approximately 15,000 microstrain. The test profile is made up of the four LED strains measured along the section. The tension steel strain is not shown due to the early increase in measured tension steel strains, which might be due to the gauges being damaged. The analysis profiles are made up of the same points, as described for the last plot. The most extreme compression

strain measured by the LEDs is somewhat higher than the analyses, which might be due to some local effects due to the low amount of cover concrete. This may also explain why the strain versus displacement plot in Figure 5-119 has higher measured compression strains than the analysis suggests it should have. The rest of the strain profile is fairly close to the analytical prediction.

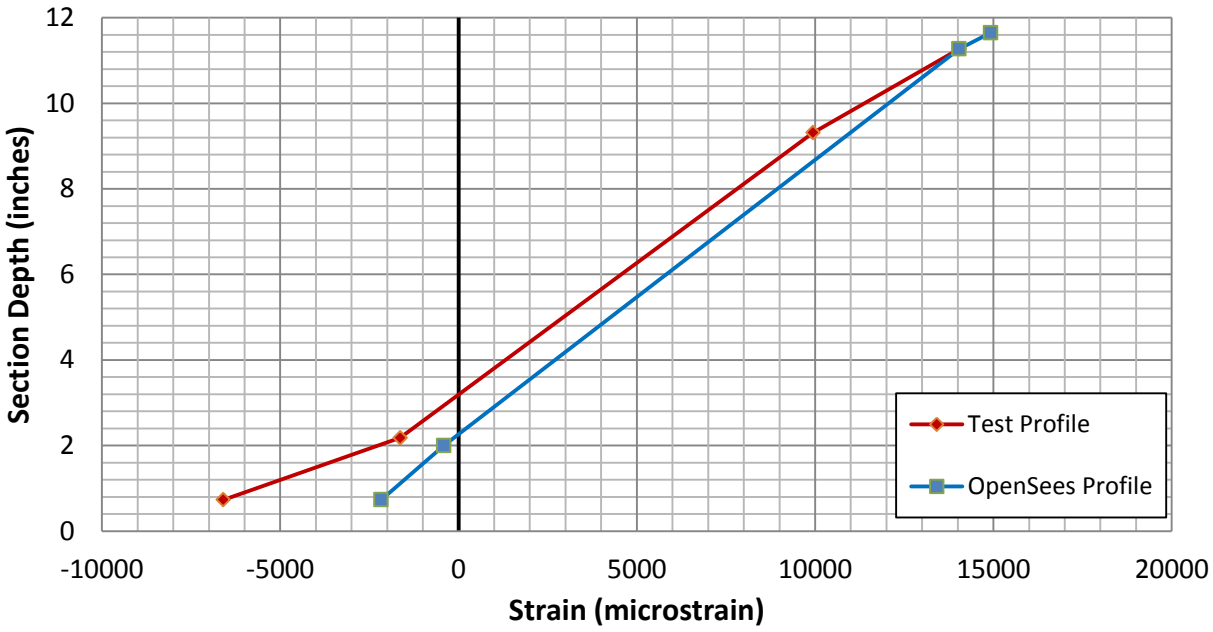

Figure 5-121: Specimen H2C1-M Strain Profile Between Yield and Ultimate

Additionally, the strain profile near the ultimate point is shown in Figure 5-122. This point was chosen at extreme tension steel strain of approximately 20,000 microstrain, and the analysis profile was chosen based on this strain as well. In this case, the test profile is based on only three sets of LEDs, as the second row of LEDs on the compression side was not visible. Due to this, the test strain profile does not appear to match up with the analysis profiles as well, but this may be skewed due to higher measured compression strains at the extreme LED set, like those shown in Figure 5-121.

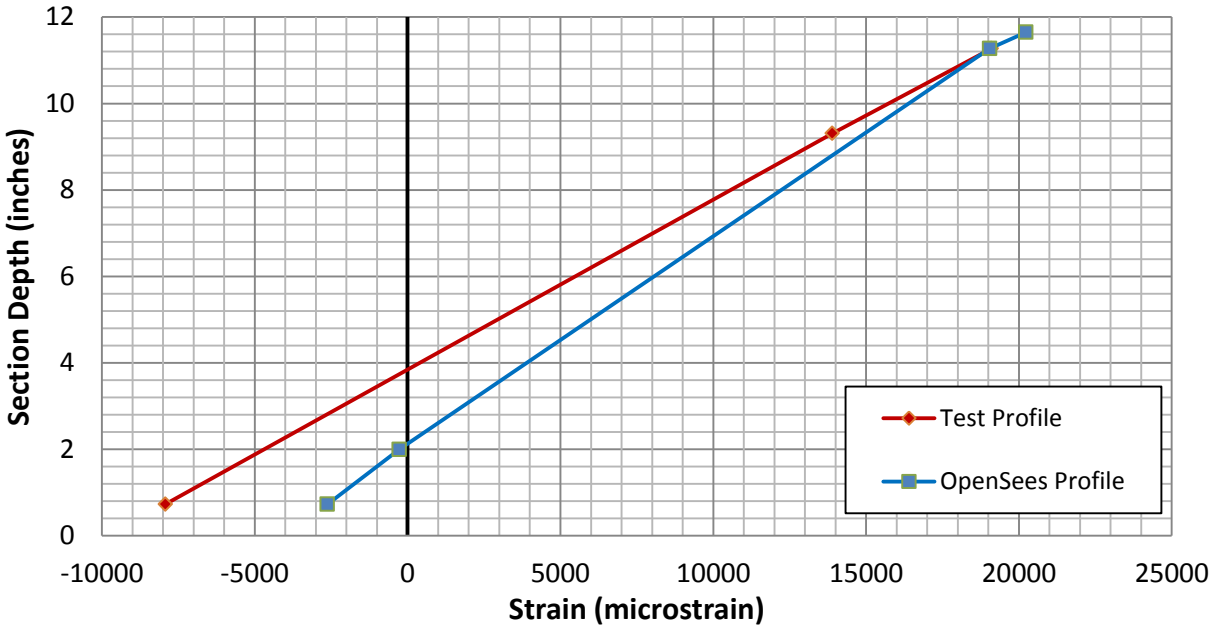

Figure 5-122: Specimen H2C1-M Strain Profile at Ultimate (Tension Strain 20,000 Microstrain)

The plots presented in this section indicate that the analysis methods are capable of modeling the flexural response of this specimen, including fairly accurate strain values and strain profiles. Combined with the remainder of the plots which compare the other specimens to the analytical results, it indicates that the analysis methods can provide an accurate response for both solid and hollow columns.

5.4 Ideal Specimens

The longitudinal reinforcing steel used in the test had an extremely low ductility as well as significantly high yield stress, as discussed in Section 4.3. The ultimate strain of longitudinal steel commonly used in bridges is typically around 0.08, while the longitudinal reinforcement used in this testing had an ultimate strain of only 0.02. Additionally, the longitudinal reinforcing steel had a yield stress of 95 ksi, significantly greater than typical longitudinal reinforcing steel which usually has a yield stress of approximately 60 ksi. These factors, especially the low ultimate strain, have caused the experimental test results to have a reduced ductility.

In order to better understand how hollow columns may behave in actual bridges, an additional analysis of some of the test specimens has been performed. This additional analysis has been performed using material properties that are more typical of actual bridge columns, including longitudinal reinforcement with higher ductility. The extension of the analysis has been justified based on the comparison to the actual tests presented in Sections 5.2 and 5.3 as well as the comparisons to past research. As shown in the comparison to the experimental results, the hollow circular columns with a two-inch wall thickness experienced flexural failure and agreed well with the analytical model. The experimental results of the solid circular columns also compared well with the analytical model. The geometry of these specimens has been used for the analysis with realistic material properties, since the analysis of these specimens has shown good agreement with the experimental results.

The longitudinal and transverse reinforcement used in the extension of the analytical results has a yield strength of 60 ksi, with ultimate strain of 0.08, and ultimate strength of 90 ksi. The concrete strength chosen is 4.5 ksi, which is a more common concrete strength. The dimensions and reinforcing steel amounts used for this analysis are the same as for the solid circular test specimens and the two-inch thick test specimens. Although the specimens showed good comparison to the OpenSees analysis, the confined concrete model was unable to be verified since the longitudinal reinforcement ruptured so early. However, the confined concrete model has been compared to tests by Hoshikuma and Priestley (2000) and has been found to be fairly conservative, as shown in Section 3.4.2.1. Additionally, in Section 5.3 it was shown that the strain values and strain profiles from the analysis were comparable to the test results for the hollow specimen as well.

The solid and hollow specimens with realistic material properties were subjected to two different axial loads for the extended analysis. The force vs. displacement responses of the analyses are shown in Figure 5-123 through Figure 5-126. The plots show the response as well as several possible failure points, with tension steel failure considered at a tension steel strain of 0.08 and inside face failure at a concrete compressive strain at the inside face of 0.005. The ultimate concrete compressive strain and the ultimate concrete compressive strain increased

by 50 percent have also been shown in the figures. As discussed in previous sections, the ultimate compressive strain prediction has been shown to be very conservative for hollow columns. It is also important to note that the OpenSees model does not account for material failure. Despite the force-displacement response in the plots continuing on without a loss in load capacity after inside face or tension steel failure, in reality, the column would lose significant capacity. Despite this, the plots have been continued to show when other failure modes may occur.

As shown in the figures, the hollow two-inch thick specimen loaded with 22.6 kips axial load is expected to fail by inside concrete face crushing, with a small reduction in ductility when compared to the solid specimen under 22.6 kips of axial load. The solid specimen is predicted to fail due to longitudinal steel failure, since the ultimate concrete compression strain prediction is often conservative by 50 percent and is therefore not considered to be the failure point. The hollow two-inch thick specimen under 45.2 kips axial load is expected to fail due to inside concrete face crushing but at a much smaller ductility compared to the solid section under 45.2 kips of axial load. The solid section is also expected to fail due to longitudinal tension failure due to the conservatism of the estimate of ultimate concrete strain. As shown, a fairly ductile response would be achieved by the hollow column under 22.6 kips of axial load, while the hollow column under 45.2 kips of axial load has a more brittle response due to the larger axial load causing the neutral axis to develop further into the void.

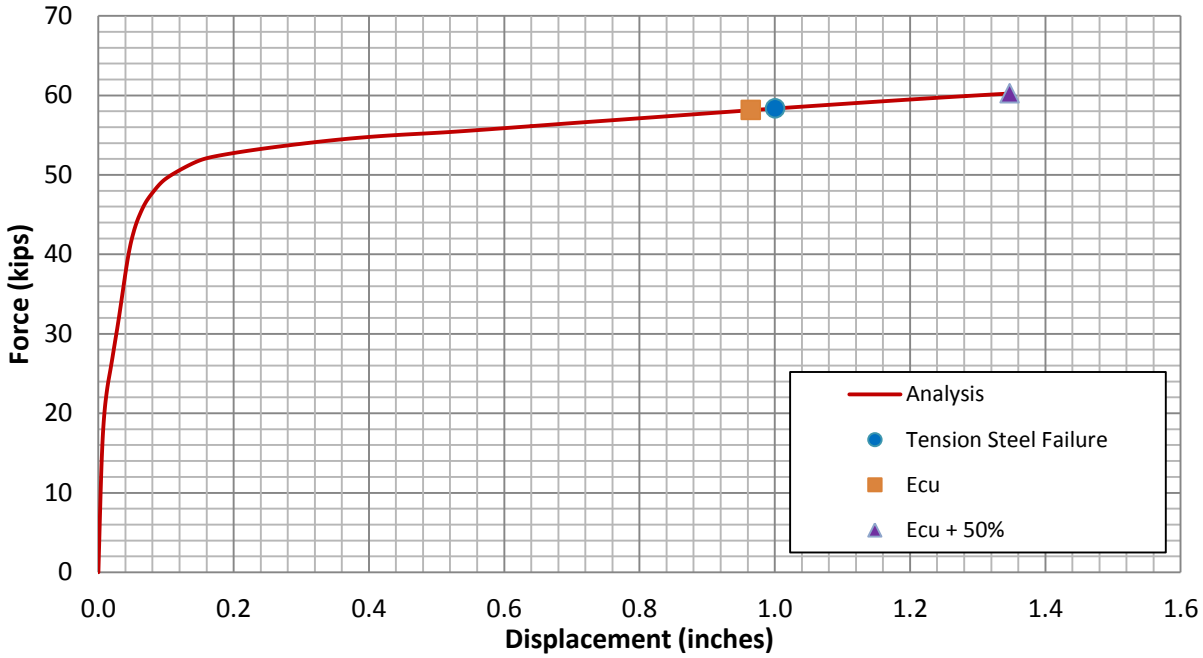

Figure 5-123: Analytical Force-Displacement Response of Ideal Solid Specimen under 22.6 kips Axial Load

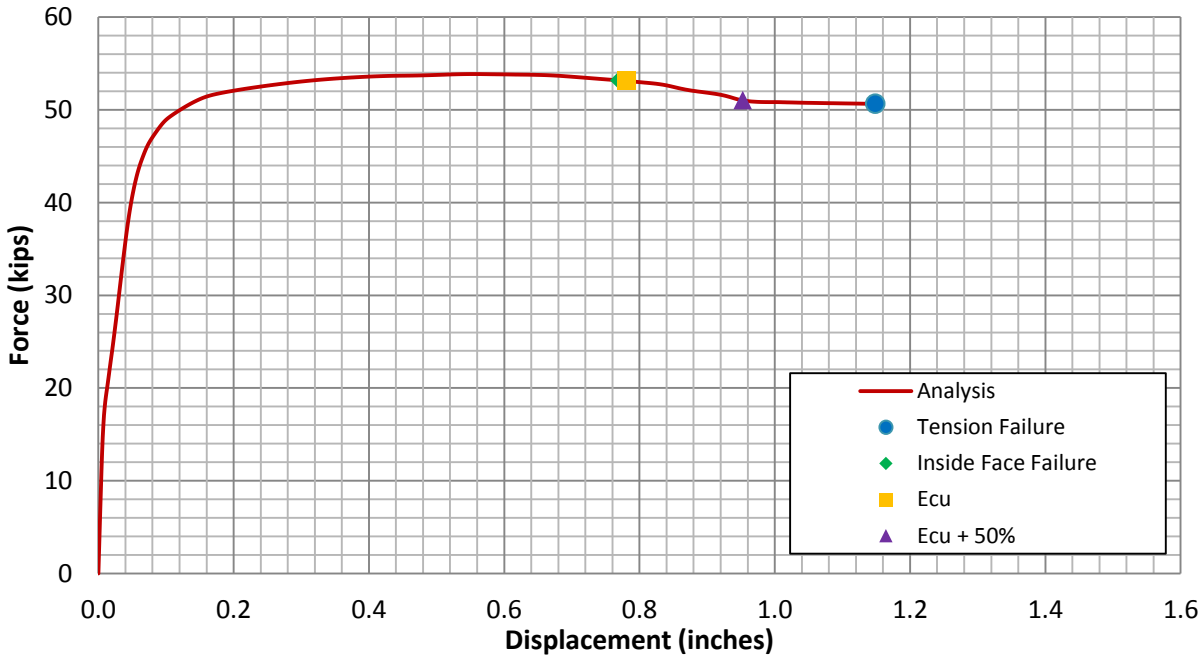

Figure 5-124: Analytical Force-Displacement Response of Ideal Hollow 2" Thick Specimen under 22.6 kips Axial Load

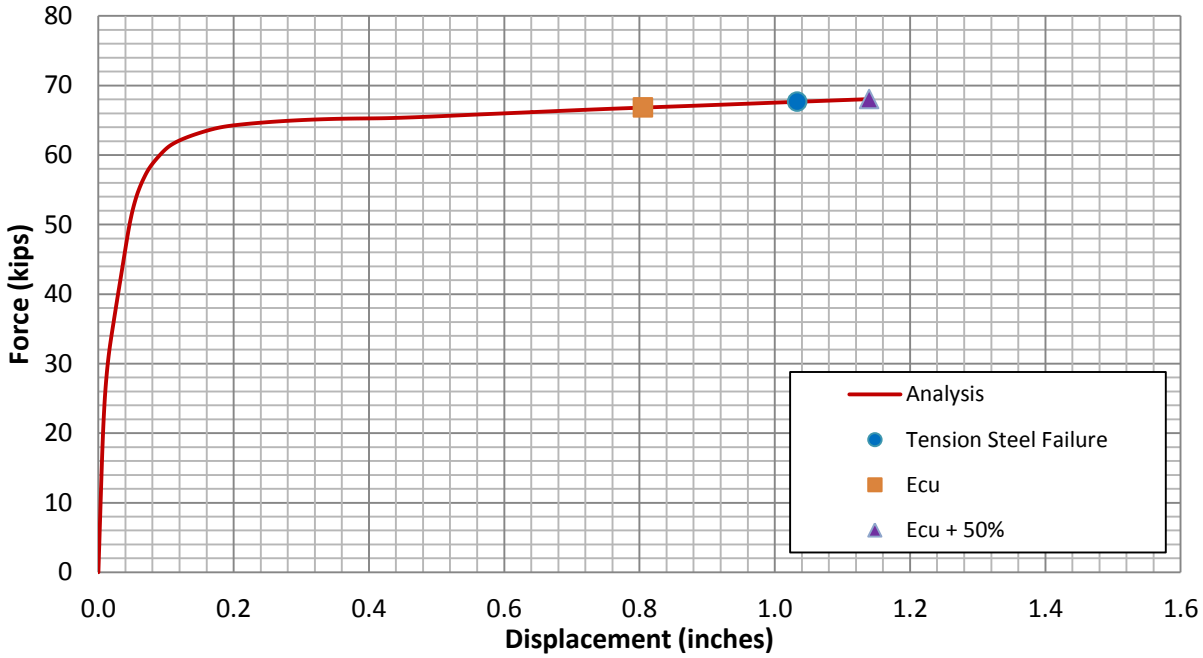

Figure 5-125: Analytical Force-Displacement Response of Ideal Solid Specimen under 45.2 kips Axial Load

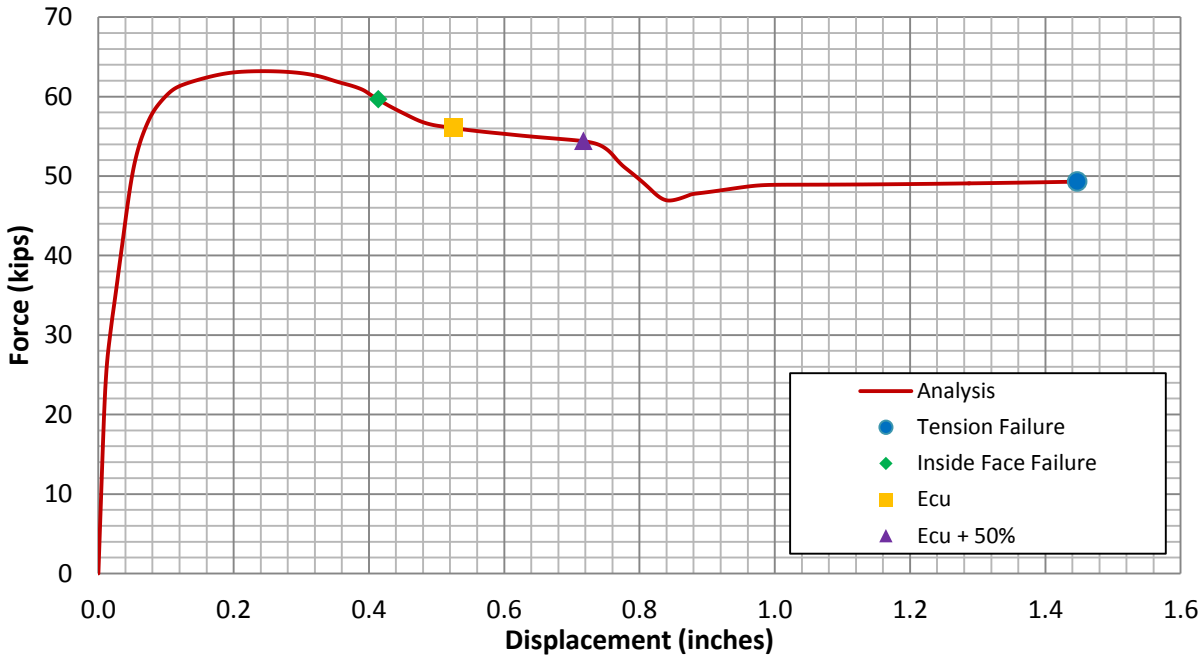

Figure 5-126: Analytical Force-Displacement Response of Ideal Hollow 2" Thick Specimen under 45.2 kips Axial Load

5.5 Alternative Analysis Method

The proposed analytical method for hollow concrete columns has been shown to provide a fairly accurate estimate of the response of hollow columns through comparison to the experimental results of previous researchers and the experimental results of this research. However, it has been shown that the analytical method can often be conservative by underestimating the ultimate displacement of the column. While a conservative analysis method is useful, it is also worthwhile to explore the analysis further and attempt to determine ways the analysis could be improved.

Recent investigation by Liang et al. (2015) of the finite element analysis has provided a better idea of the stresses that develop in the wall of hollow columns. This investigation has suggested that it may be overly conservative to consider the inside face concrete wall as unconfined. The adjustment factor, k_h, proposed by Liang et al. (2015) was based on the reduction in radial stress which was found to occur in hollow columns in the finite element analysis. The recent investigation has found that it may not be necessary to consider the concrete portion near the void as unconfined concrete, since this adjustment factor seems to reflect the average radial stress state throughout the wall thickness.

An additional modification to the analysis method, discussed previously in Section 3.4.1.1, has been proposed by Liang et al. (2015). Currently the influence of circumferential stress has been ignored due to the lack of information about how much circumferential stress actually develops in the walls of hollow columns with one layer of transverse reinforcement subjected to flexure. As previously discussed, the circumferential stress has been conservatively assumed to be equal to the modified radial stress. The recent finite element investigation has suggested that this may be overly conservative and that the influence of the higher circumferential stress that develops in hollow columns should be taken into account. The method recommended by Liang et al. (2015) to take into account the circumferential stress uses a weighted average, with a weight of 0.9 applied to the radial stress and a weight of 0.1 applied to the circumferential stress. The calculation of the circumferential stress would be similar to the method used for

radial stress, where the stress is calculated for a solid section and a modification factor is applied to it.

As previously discussed, for a solid section, the transverse stresses in orthogonal directions are approximately equal to one another. The modified method applies a factor of D/(2t), derived from the theoretical investigation presented in Section 3.3, to the transverse stress calculated for the solid section to determine the circumferential stress in the hollow section. The weighted average is then used to calculate the average lateral stress in the wall of the hollow section. The original analysis method proposed in this report is summarized below, where $f_{rhollow}$is the adjusted radial stress for a hollow column. The variable f_l is the lateral stress calculated for a solid column.

Circular columns: $k_h = \frac{t}{D} + 0.45$ Rectangular Columns: $k_h = 0.28$

$$f_{rhollow} = k_h f_l$$

Equation 5-1 and Equation 5-2 summarize the modification to the analysis method to include some of the effect of circumferential stress. This modification takes into account a portion of the theoretical circumferential stress, $f_{crhollow}$, in the calculation of $f_{lhollow}$. The effective lateral stress for a hollow column, $f'_{lhollow}$, is then calculated as previously described using the confinement effectiveness factor k_e, proposed by Mander et al. (1988). The confinement effectiveness factor is typically taken as 0.95 for circular columns and 0.75 for square or rectangular columns.

$$f_{crhollow} = \frac{D}{2t} f_l \quad \text{(Equation 5-1)}$$

$$f_{lhollow} = 0.9 f_{rhollow} + 0.1 f_{crhollow} \quad \text{(Equation 5-2)}$$

$$f'_{lhollow} = k_e f_{lhollow} \quad \text{(Equation 5-3)}$$

Using the method described above reduces the conservative nature of the originally described method by taking the entire wall thickness within the transverse reinforcement as confined concrete, which accounts for some of the confinement effect seen by the concrete near the inside face. The calculation of the confined concrete properties is also less conservative due to the incorporation of some of the effect of circumferential stress, which is theoretically much higher for a hollow column. The modified approach is likely still fairly conservative, since it uses a weighted average to apply the circumferential stress, with more weight applied to the radial stress in a ratio of nine to one.

This modified method has been compared to the experimental results of the testing by Hoshikuma and Priestley (2000), as well as the original analytical method, which was compared to these results in Section 3.4.2.1. The original analytical method analyzed the section with the inside concrete near the void as unconfined and without accounting for higher circumferential stress, as described in Section 3.4.1.1.1. The modified method uses the entire concrete wall within the transverse reinforcement as confined concrete, with the adjustment factor, k_h, used to calculate the radial stress from the stress calculated for a solid column as well as incorporating the circumferential stress using a weighted average as described above. The results of this comparison can be seen in Figure 5-127. As shown in the figure, the modified analysis provides a slightly less conservative estimate of the ultimate displacement when compared to the original analysis. As previously discussed, the ultimate concrete compressive strain estimates are very conservative for hollow sections, and inside compression face crushing has been considered as the ultimate failure mode for this analysis, which matches the results of the experimental analysis. The modified analysis provides a response slightly closer to the experimental response but is still fairly conservative.

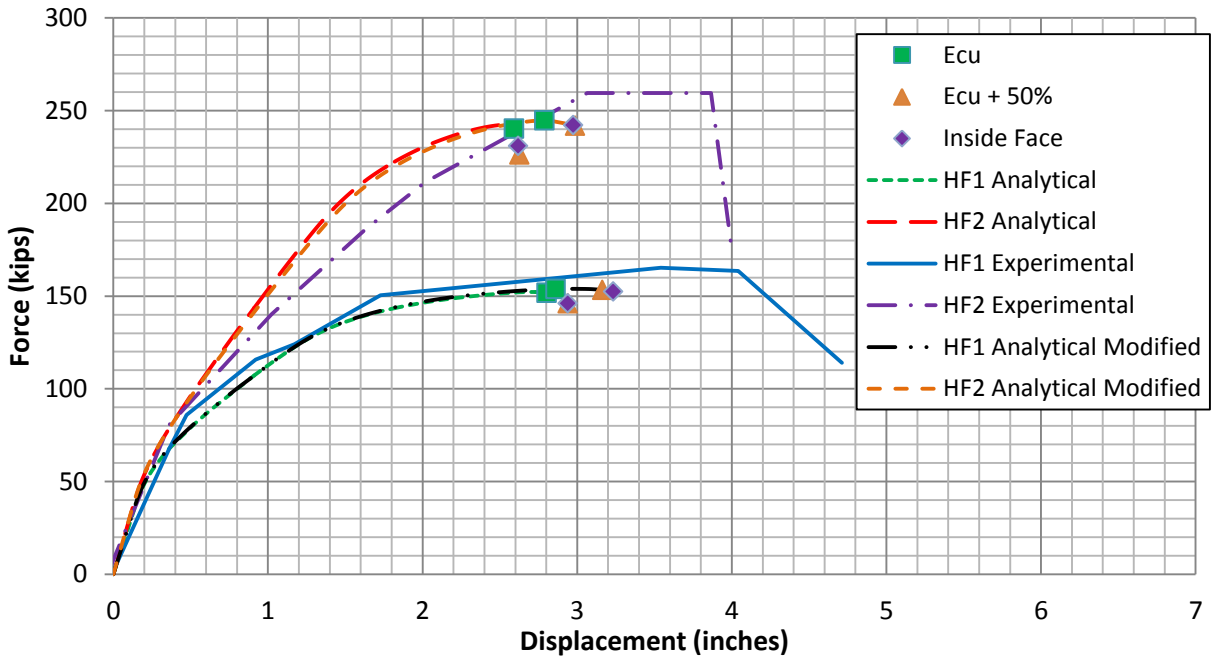

Figure 5-127: Comparison between Original and Modified Analysis and Experimental results of Specimens HF1 and HF2 Tested by Hoshikuma and Priestley (2000)

The effect of using the modified analysis depends on the section geometry and location of the neutral axis, since the analysis results will depend on the compressive strain applied to the concrete wall. To provide an example of the effect of the modified analysis for a different section, the analysis has been compared for the ideal specimens, which were analyzed and discussed in Section 5.4. The results of the comparison for the ideal specimen under 22.6 kips of axial load and 45.2 kips of axial load can be seen in Figure 5-128 and Figure 5-129, respectively.

As shown in the figures, the modified analysis seems to have a larger effect than what was found for the analysis of the experimental specimens from the research by Hoshikuma and Priestley (2000). Additionally, the effect of the modified analysis is more apparent for the ideal specimen subjected to 45.2 kips of axial load, since the original analysis indicates a much earlier failure. The modified analysis does still show that the ideal specimen subjected to 45.2 kips of axial load experiences early failure due to the crushing of the inside compression face, while the

ideal specimen subjected to 22.6 kips of axial load was predicted by the modified analysis to fail due to rupture of the tensile reinforcement.

It is important to note that although the analytical response has been continued past the initial predicted failure mode, the response beyond the inside compressive face failure prediction or tensile rupture prediction may be meaningless. The OpenSees analysis used in this research does not account for material failure, and in reality, there would be a sudden loss of strength after the initial failure. As previously discussed, the confined concrete compressive failure has not been considered as a failure mode due to the conservative nature of the estimate but has been included for illustrative purposes. Despite the fact that the response after the initial failure may not have meaning, it has been included to show what the response might look like if the initial estimate were conservative and also to show how close the specimen was to reaching the other mode of failure.

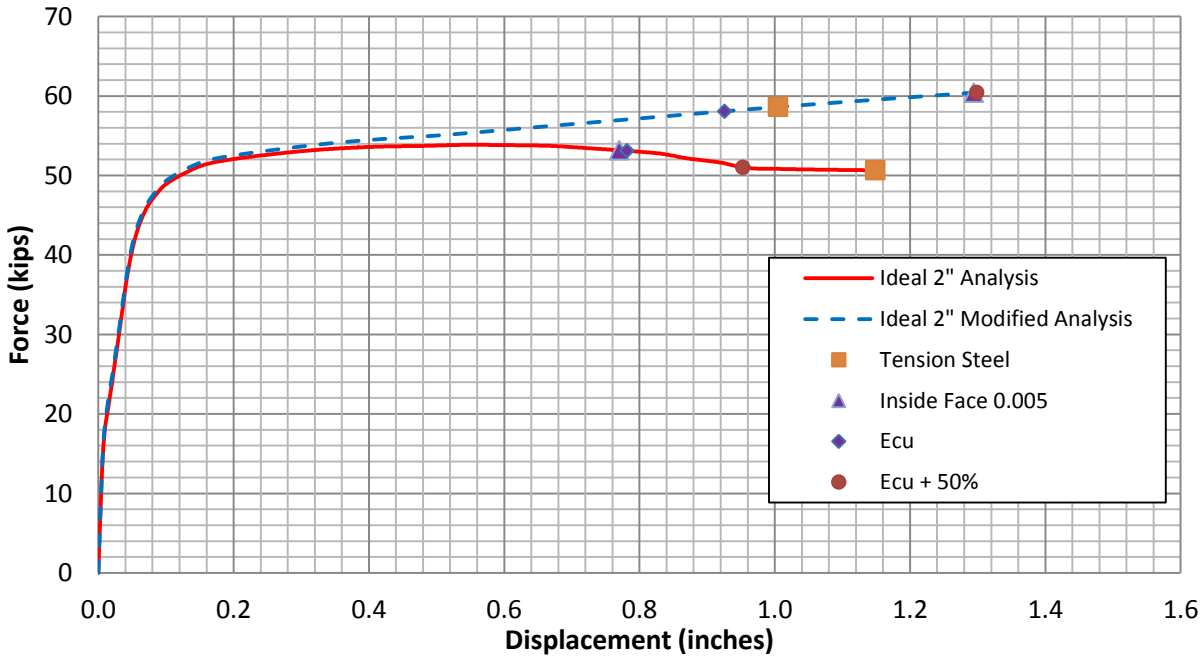

Figure 5-128: Comparison between Original and Modified Analysis for Ideal Two-Inch Thick Specimen under 22.6 kips Axial Load

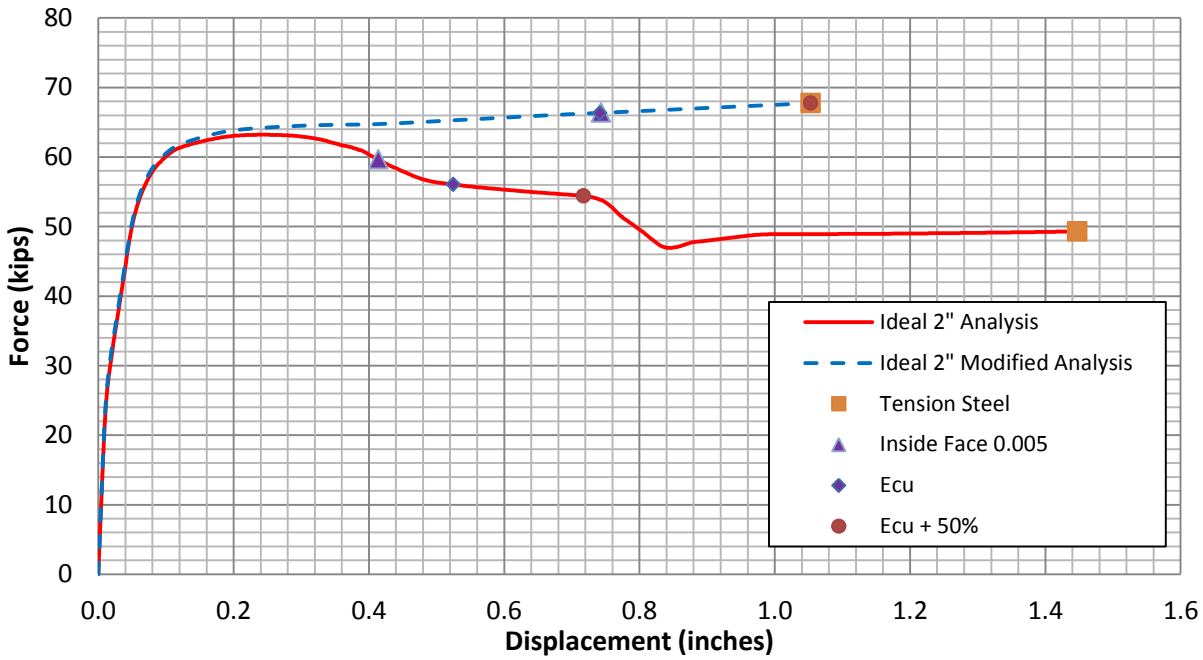

Figure 5-129: Comparison between Original and Modified Analysis for Ideal Two-Inch Thick Specimen under 45.2 kips Axial Load

The comparison of the modified and original response has shown that the method used for analysis can have some effect on the predicted response, with the amount of effect dependent upon the geometry of the section and the applied loading. Each method has shown to provide a conservative response when compared to the testing by Hoshikuma and Priestley (2000). However, it was shown that the analysis did not significantly change when the modified analysis method was used for that comparison. The comparison to the ideal specimens under different axial loads has shown that the effect of using the modified analysis can have significant effect in certain cases. It is difficult to determine which method is more appropriate due to the lack of previous experimental research and the early failure of the specimens in this research. With the lack of experimental verification, it may be appropriate to use the original analysis procedure for design, since it provides a more conservative estimate of the response and ultimate failure. Further investigation and experimental work may be able to show that the modified method is more accurate, which would produce a more economical design method. More in depth

discussion of the applicability and accuracy of the modified method is discussed by Liang et al. (2015).

CHAPTER 6. CONCLUSIONS AND RECOMMENDATIONS

6.1 Conclusions

6.1.1 Experimental study

The experimental study has demonstrated that hollow specimens with good concrete quality and sufficient wall thicknesses can produce a response which is comparable to that of solid sections. The tests have shown that the specimens were capable of withstanding quasi-static simulated earthquake loading, which is a good indicator of performance under real earthquake events. The two-inch thick circular hollow specimens produced comparable responses to the solid circular specimens and have demonstrated that providing one layer of reinforcing steel can be adequate as long as the neutral axis is in a favorable location. The neutral axis should be near to the wall so that the concrete compression strains at the inside wall are limited to avoid brittle failure. Providing a hollow column with only one layer of transverse reinforcement can produce good savings in cost due to the reduction of materials, such as concrete and reinforcing steel, as well as reducing the construction and labor costs and reducing the mass on supporting structures. Providing only one layer of transverse reinforcement where possible allows for better constructability and more room for concrete fill, as opposed to the typical hollow column design, which has an additional layer of inner reinforcement. Other findings of the experimental program are summarized below.

1. The two-inch thick circular specimens failed due to flexure and did not experience compressive damage on the inside face concrete. The specimen experienced flexural failure due to tensile steel rupture at a low ductility, but the lack of damage at the inside face suggests that the analytical does not overestimate the displacement at which the inside face fails.
2. The two-inch thick circular specimens experienced a similar capacity and ultimate displacement as the solid specimens. This further verifies that hollow columns with sufficient wall thickness and neutral axis location can experience similar capacity and response when compared to solid columns with the same outside diameter and reinforcement.

3. Shear displacement of hollow columns seems to be more significant than that of similar solid columns, and a trend has been shown with higher shear displacement for smaller wall thicknesses.
4. Local failure of hollow specimens was identified as an issue, which may be due to local forces applied to a small wall thickness, as well as the contribution of patches used to address poor concrete quality.

6.1.2 Analytical study

An OpenSees fiber-based analysis was used to model the response of the solid and hollow specimens. This type of analysis is comparable to the typical analytical methods used by engineers in the design of concrete bridge columns. Based on the collaborative finite element analysis (Liang et al., 2015), an adjustment to Mander's model was implemented in the OpenSees analysis to more accurately reflect the stress state in hollow columns. The adjustment accounts for the reduced radial stress, which has been found to occur in hollow concrete columns, with zero radial stress at the inside face. The analysis was shown to be fairly accurate when compared to previous research as well as to the tests performed in this report, when the effects of shear are not included. Based on these factors, the analysis was extended using more realistic material properties. It was demonstrated that good ductility can be achieved in hollow concrete columns with one layer of transverse reinforcement, although concrete crushing at the inside face can be a limiting factor and should be considered in the design. The neutral axis location is critical to ensuring that inside concrete face crushing does not occur too early, and by designing the neutral axis to occur near the inside concrete face, this limits the compression strains in order to avoid early crushing.

The other compression limit state in hollow concrete columns is crushing of confined concrete near the transverse reinforcement. Mander's model was adjusted based on the finite element analysis (Liang et al., 2015) and the test results. Several key findings were realized from this adjustment as well as from the results of experimentation by previous researchers.

1. Concrete near the transverse reinforcement in hollow columns experiences a lower radial stress than do solid concrete columns with similar reinforcement at similar axial strains. This is likely due to the increased deformability of hollow columns, with the radial deformation requiring less confining pressure to contain, and with the ability of the concrete to move toward the void.
2. Concrete near the transverse reinforcement in hollow columns experiences a smaller strength increase, due to confinement, than a similar solid column. The smaller radial confining stress likely contributes to this smaller increase in strength, as does the existence of the void.
3. Transverse reinforcement failure appears to be less of a concern for hollow columns than for solid columns, due to the increased deformability of the hollow columns. The radial displacement of a hollow column is easier to contain than that of a solid column, resulting in lower transverse reinforcement stresses. Previous research has demonstrated this low confinement demand, although further study is needed in order to quantify this behavior and provide a more accurate ultimate strain for confined concrete based on transverse reinforcement failure.

Recent investigation by Liang et al. (2015) has suggested that the analytical method discussed in this research may be overly conservative by assuming that the concrete near the inside face is unconfined, and by neglecting the higher circumferential stress that develops in hollow columns. A modified analysis approach was suggested by Liang et al. (2015), which uses a weighted average to take into account some of the effect of the higher circumferential stress in hollow columns, and also suggests that the entire wall thickness within the transverse reinforcement be modeled as confined concrete. This method has been investigated in Section 5.5, and has been shown to provide a more accurate response when compared to previous testing by Hoshikuma and Priestley (2000). This brief investigation has shown that the modified analysis method may be more realistic, thus providing a more economical response. However, due to the lack of available experimental research of hollow concrete columns with one layer of transverse reinforcement it is currently difficult to conclusively determine the accuracy of the modified analysis method. The research presented by Liang et al. (2015) may provide further

evidence that the modified method is more accurate and does not overestimate the ultimate displacement of hollow columns. However, at this time the original analysis method presented in Section 3.4.1.1 is recommended to be used since it is more conservative.

6.2 Design Recommendations

6.2.1 Applicability of Mander's model to hollow sections

Based on the comparison to previous test results, it has been shown that Mander's model can be applied to hollow columns with one layer of transverse reinforcement, as long as an adjustment to Mander's model is used along with adjusted modeling recommendations. The proposed adjustment is simple and easy to apply and has been shown to be fairly conservative for circular columns when compared to experimentation by previous researchers. The proposed adjustment factor for circular columns is:

$$k_h = \frac{t}{D} + 0.45$$

And for square columns the adjustment factor is:

$$k_h = 0.28$$

These adjustment factors were proposed as a part of hollow column finite element research performed in collaboration with this project (Liang et al., 2015), which found reduced radial stress near the transverse reinforcement for hollow columns. For circular columns, this reduction seemed to depend on the wall thickness ratio, and for square columns, the reduction seemed relatively constant. The adjustment factor for circular columns has been shown to be conservative, while the proposed adjustment for square columns has not been verified and requires further testing. An example which illustrates the use of the adjustment factor is provided in Section 6.3.

6.2.2 Design parameters

A more uniform definition of commonly used column design parameters has been suggested for hollow columns in order to facilitate a better comparison to solid columns. Parameters such as reinforcement ratios and axial load ratios are recommended to be reported using the gross section, as if the section was solid. This allows the engineer to compare the capabilities of solid and hollow columns more efficiently. This can be a source of confusion and error, so it is important to clearly state how the ratios were developed, regardless of whether the gross section or net section is used. Gross section ratios can provide easier comparisons to solid columns in order to determine whether a hollow or solid column may be preferable in certain design situations, while net section ratios (using only the area of present concrete for hollow columns) can be useful for determining how much of the concrete capacity is utilized by the axial load.

6.2.3 Recommended hollow column design procedure with one layer of transverse reinforcement

Review of the design practices for hollow columns found that there are very few guidelines in existence and even fewer recommendations for design procedure. The test results presented in this paper and in previous literature have suggested that solid and hollow columns with one layer of transverse reinforcement can have comparable capacity and ductility, as long as the hollow column is designed to ensure that the neutral axis is located near the inside wall to prevent large compression strains in the inside wall concrete. Based on recommendations by Hoshikuma and Priestley (2000), these inside face concrete strains should be limited to 0.005 for theoretical analysis, but they recommend a safe design limit of 0.0035.

The neutral axis location is thus very critical, and some iteration may be necessary in the design process in order to achieve a design with a safe neutral axis location and low inside face concrete compression strain. Inside face failure may still be the limiting factor in some cases, but with adequate neutral axis location, it can be made to occur at sufficient ductility. Due to the similarities between solid columns and hollow columns with the same details and well-

designed neutral axis location, it has been found that the initial preliminary design and analysis can be performed as if the specimen were solid. A solid section can be initially assumed, and the required diameter and amount of transverse reinforcement can be estimated in the usual fashion. Then, the neutral axis location of this preliminary solid column design can be calculated at the nominal moment capacity, which provides a good initial estimate of the neutral axis depth of the hollow column. Setting this neutral axis depth as the preliminary wall thickness then provides a good starting point for the hollow column design, which typically produces low concrete strains at the inside face concrete until a fairly ductile response is achieved. Then, further analysis and iteration of this section can be performed using the recommended adjustment to Mander's model. The wall thickness can then be increased or decreased as necessary. This relatively simple initial estimate of the required wall thickness can be a good indicator of whether a hollow column will be preferable to a solid column. If the required wall thickness is too large, it may be preferable to use a solid column. Alternatively, the wall thickness could be decreased further, and a second layer of transverse reinforcement near the inside face could be provided for increased ductility, with cross-ties connecting it to the outside layer of transverse reinforcement.

Other factors can be adjusted to enable a safe hollow column design, such as axial load ratio and longitudinal reinforcement amount. High axial load and high amount of longitudinal reinforcement cause the neutral axis to move more toward the center of the section, which can cause high axial strains at the inside wall of hollow columns. If the initial design indicates that inside concrete crushing may occur and the desired ductility may not be achieved, or that the required wall thickness may be too high, the amount of axial load or longitudinal reinforcement could be reduced, if possible, which could reduce the required thickness of the wall.

6.3 Design Example

A demonstration of the suggested adjustment factor and methodology for hollow columns design is described in this section. An example of a simple bridge column design is presented, which illustrates the process of selecting the void dimension in a hollow column as well as

adjusting Mander's model for the hollow column. The example makes some simplifying assumptions and shows the basic process suggested by this research without discussing detailing and other considerations such as shear design, which are outside the scope of this report.

The material properties were chosen to represent standard material properties used in typical columns.

Concrete:

Compressive strength of column at 28 days: $f'_c = 4.5\ ksi$

Reinforcing steel:

Yield strength $f_y = 66\ ksi$

Ultimate strength $f_u = 90\ ksi$

Ultimate strain $\varepsilon_u = 0.08\ in/in$

Typical transverse and longitudinal reinforcement yield strengths of 66 ksi are used, with ultimate strength of 90 ksi. Ultimate steel reinforcement strain of 0.08 is assumed. A clear cover of two inches to the transverse reinforcement is typically required by codes and is used in this example.

The example presents the design of a single column with dimensions intended to be fairly typical of those used in actual bridge columns in earthquake prone regions such as California. The column height is 20 feet and the initial column demands have been chosen as 650 kips of axial load and 220 kips of base shear. Based on this axial load, a diameter of 5 feet has been chosen to provide an axial load ratio of approximately 5 percent. The column has been initially designed identically to that of a solid column. The first step of the design process is to estimate the required amount of longitudinal reinforcement. This is typically done by utilizing provided

column interaction charts to estimate the amount of longitudinal reinforcement necessary to achieve the required moment demand.

$$M_r = (Base\ shear) \cdot (Column\ height) = (220) \cdot (20 \cdot 12) = 52{,}800\ k \cdot in.$$

Using this required moment demand, an initial longitudinal reinforcement ratio of 0.0085 was chosen. The required area of longitudinal reinforcement was then calculated.

$$A_{l\ required} = 0.0085 \cdot \frac{\pi}{4} \cdot 60^2 = 24.03\ in.^2$$

To meet this required demand, 32 number 8 bars were chosen, which produces an actual area of longitudinal reinforcement of 25.3 in^2 and an actual ρ_l of 0.0089. After determining the initial longitudinal reinforcement amount, the transverse reinforcement ratio can be calculated. The following equation proposed by Priestley et al. (1996) was used to define the required amount of transverse reinforcement to achieve a ductile design.

$$\rho_s \geq 0.16 \frac{f_c'}{f_y}\left(0.5 + \frac{1.25P}{f_c' A_g}\right) + 0.13(\rho_l - 0.01)$$

$$= 0.16\left(\frac{4.5}{66}\right)\left(0.5 + \frac{1.25(650)}{4.5\left(\frac{\pi}{4} \cdot 60^2\right)}\right) + 0.13(0.0089 - 0.01) = 0.006$$

An initial transverse reinforcement spacing of 3.5 inches was then chosen, and the required diameter of transverse reinforcement was calculated as follows. Since the transverse reinforcement size is initially unknown a D' of 56 inches is assumed, corresponding to the column diameter with the concrete clear cover subtracted.

$$\rho_s = \frac{4A_s}{D's} \rightarrow A_s = \frac{\rho_s D's}{4} \rightarrow A_s = \frac{0.006(56)(3.5)}{4} = 0.294\ in.^2$$

$$d_{transverse} = \sqrt{\frac{4}{\pi}(0.294)} = 0.61\ inches$$

Based on this required diameter of transverse reinforcement, a spiral composed of a number 5 bar spaced at 3.5 inches was chosen.

$$\rho_s = \frac{4(0.31)}{(54.6)(3.5)} = 0.0065$$

The actual transverse reinforcement ratio is 0.0065, which is greater than the requirement of 0.006. The next step of the design process is to perform a moment curvature analysis in order to ensure that the required moment capacity can be achieved and that adequate ductility can be provided. Mander's model is used with the calculated transverse reinforcement ratio in the usual manner in order to provide the confined concrete properties. The analysis was performed using OpenSees, and a nominal moment capacity of 55,056 k-in was found, which is greater than the required moment of 52,800 k-in, but which does not exceed the required moment by too much. Therefore this preliminary design is acceptable. If the required moment capacity was not met or if it was exceeded by too much, the amount of longitudinal reinforcement would be adjusted as well as the amount of transverse reinforcement if necessary. The analysis would be performed again until a satisfactory amount of longitudinal and transverse reinforcement was found. For this example, 32 number 8 longitudinal bars with a transverse reinforcement spiral composed of a number 5 bar spaced at 3.5 inches is satisfactory.

Once the analysis has shown that a design meets required capacity, the analysis results can then be used to estimate the depth of the neutral axis at the nominal moment. For this example, the neutral axis depth, when the section reached nominal moment capacity, was approximately 11.7 inches. This neutral axis depth provides a good initial estimate of a wall thickness that can provide a fairly ductile response. A wall thickness of 13 inches was then chosen, which is fairly close to the neutral axis depth and which provides a $\frac{t}{D}$ ratio of 0.22. The next step is to calculate the confined concrete properties for this specimen using the adjustments proposed for hollow columns. Two layers of concrete were used, as previously described, with the half of the wall near the inside face modeled as unconfined concrete and the half near the transverse reinforcement modeled as confined concrete with the adjustment to Mander's model. The lateral reinforcement pressure was estimated as if the column was solid, and then the adjustment factor k_h for hollow columns was applied.

$$\rho_s = 0.0065 \qquad k_e = 0.95$$

$$f_l = \frac{1}{2}\rho_s f_{yh} = \frac{1}{2}(0.0065)(66) = 0.21\ ksi$$

For solid circular columns, a confinement effectiveness coefficient of 0.95 is typically assumed and would then be applied to this calculated lateral stress. The remainder of Mander's model would be performed as usual, including the calculation of the confined concrete peak strength and strain at peak strength. This procedure was performed for the initial analysis of this column as if it were solid as described above. However for hollow columns, it was shown in this report that less lateral stress is required to confine the hollow columns, so an adjustment factor was proposed. The adjustment factor, k_h, is applied as shown, in addition to k_e, which is still applied since it accounts for the arching effect between longitudinal and transverse reinforcement.

$$k_h = \frac{t}{D} + 0.45 = \frac{13}{60} + 0.45 = 0.67$$

$$f_l' = k_e k_h f_l = 0.95 \times 0.67 \times (0.21) = 0.13\ ksi$$

The confined concrete strength and peak strain is then calculated using the equations proposed by Mander. This assumes that the calculated lateral pressure is the same in both directions in the plane, which is likely a conservative assumption, since it has been demonstrated that circumferential stresses can be much higher in hollow columns.

$$f_{cc}' = f_c'\left(-1.254 + 2.254\sqrt{1 + \frac{7.94 f_l'}{f_c'}} - 2\frac{f_l'}{f_c'}\right)$$

$$= 4.5\left(-1.254 + 2.254\sqrt{1 + \frac{7.94(0.13)}{4.5}} - 2\frac{(0.13)}{(4.5)}\right) = 5.34\ ksi$$

$$\epsilon_{cc} = \epsilon_c\left[1 + 5\left(\frac{f_{cc}'}{f_c'} - 1\right)\right] = 0.002\left[1 + 5\left(\frac{5.34}{4.5} - 1\right)\right] = 0.0039$$

The resulting confined concrete strength is 5.34 ksi, and the strain at peak strength is 0.0039. For comparison, the confined concrete strength and peak strain for this column when calculated as solid was 5.74 ksi and 0.0048, respectively. Using the calculated design properties, a pushover analysis of the hollow column was then performed. Based on this analysis, the displacement ductility was determined to be 3.8. The controlling factor was the inside concrete face crushing, which was assumed to occur at a strain of 0.0035 and was recommended as a conservative design limit by Hoshikuma and Priestley (2000). For comparison, a pushover analysis of the same column as if it was solid was performed. The results of both analyses have been plotted in Figure 6-1, with several markers representing predicted failure points. The points labeled “Ecu” and “Ecu + 50%” represent the ultimate compression strain predicted by Priestley et al. (1996) and the ultimate compression strain with an additional 50 percent, respectively. The additional 50 percent point is added since it is known that the prediction of ultimate compression strain in the confined concrete can be significantly conservative. The tension failure is considered at strain in tensile steel of 0.08. The displacement ductility of the solid section is 5.4 if the ultimate point is considered at tension steel failure or 5.3 if the ultimate point is considered at the ultimate concrete compression strain plus 50 percent. When compared to the estimated displacement ductility of the hollow column of 3.8, it can be seen that the hollow column does experience a reduction in ductility due to the inside face crushing.

As shown in Figure 6-1, the columns have a similar response until close to the point where the hollow column inside face strain reaches 0.0035. The loss of capacity is due to the downward slope of the confined concrete at this point. This in turn causes the hollow column to rely more on the inside face concrete for strength and causes higher strains at the inside face, leading to inside concrete face crushing. For further comparison, an analysis of the same hollow column, except with a wall thickness of seven inches, has also been included in Figure 6-1. A wall thickness of seven inches corresponds to a wall thickness ratio of 0.12, and the k_h adjustment factor for this specimen would be 0.57. This wall thickness is much less than the neutral axis depth, and as a result, a brittle response is found. The ductility of the seven-inch thick specimen, when inside face failure is considered at a strain of 0.0035, was found to be 1.8.

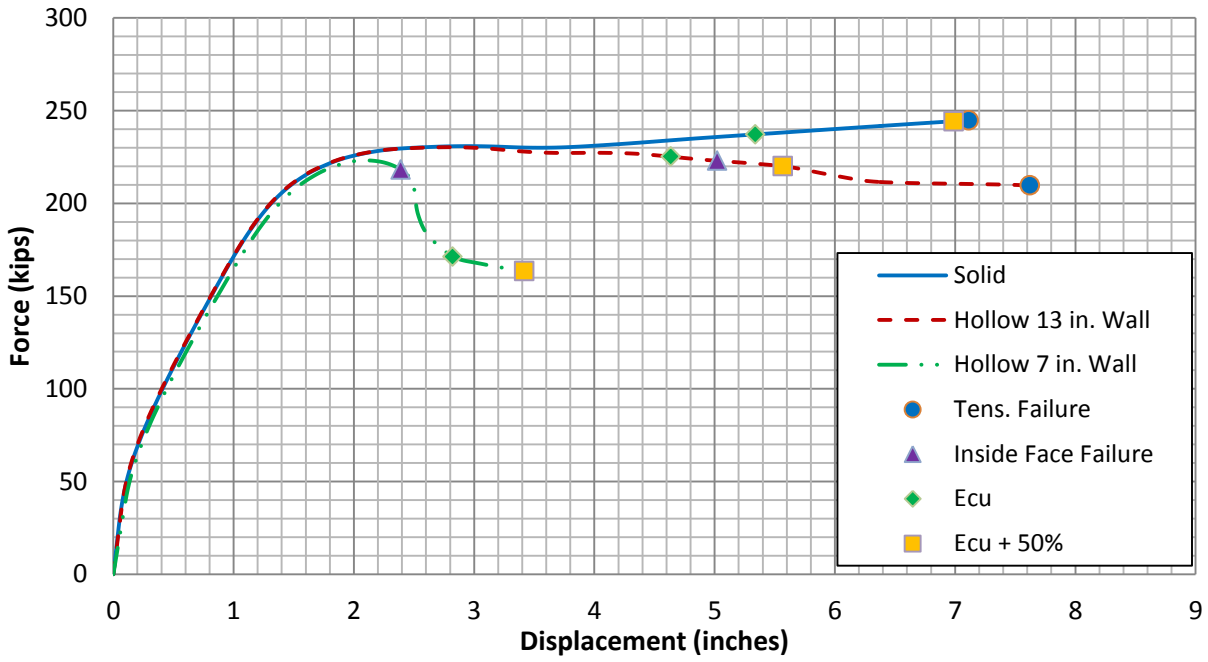

Figure 6-1: Pushover Analysis of Example Column as Hollow and Solid

This example illustrates that certain columns with limited axial load demand and lower amounts of longitudinal reinforcement can experience relatively ductile behavior, which may be satisfactory in many cases. The wall thickness ratio of 0.22, used in the example column, would correspond to a drop in mass and concrete material of 32 percent. Depending on the column demands and dimensions, even larger drops in material could be achieved while still providing adequate ductility. It is important to note that the limiting inside face strain of 0.0035 was recommended by Hoshikuma and Priestley (2000) as a conservative design method and that actual ductility could be larger. For the 13-inch thick wall example, if inside face failure is considered as 0.005, this would correspond with a ductility of 4.1.

As described in the example, it is fairly simple to estimate the required wall thickness of the hollow column, which can help the designer to decide between using a solid or hollow column. If the design check shows that the wall thickness would be too large to have any advantages, two layers of transverse reinforcement could instead be provided to further reduce the wall thickness and help avoid inside concrete face failure.

6.4 Future Research

The research performed has been able to provide recommendations for the design of hollow concrete columns with one layer of transverse reinforcement. Using the proposed analytical modeling method with an adjustment to Mander's model has been found to provide a fairly conservative estimate of the ultimate failure point for hollow circular columns. However, the proposed adjustment for square columns has been based solely off results of a companion finite element analysis (Liang et al., 2015) due to a lack of previous research and due to the early failure of square hollow specimens in this study. Although the finite element analysis has been shown to be comparable to actual test results, it is still recommended that further large-scale experimentation and research of square hollow columns with one layer of transverse reinforcement be performed.

Another area where future research is recommended is in the investigation of crushing of confined concrete near the transverse reinforcement in hollow columns. Transverse reinforcement failure is typically the limit for confined concrete crushing in solid columns, but no instances of transverse reinforcement failure have been reported in tests of hollow columns with one layer of transverse reinforcement. The increased deformability of hollow columns seems to make their radial displacement easier to contain, which could possibly allow a reduction in the amount of transverse reinforcement used for hollow columns. It would be beneficial to perform experimentation of hollow columns with one layer of transverse reinforcement and a reduced transverse reinforcement ratio. These tests should be designed in order to achieve transverse reinforcement failure to better quantify the concrete compression strain at which this failure mode occurs, as well as how much transverse reinforcement is necessary for hollow concrete columns.

Further research into the shear capacity and deformability of hollow columns is also recommended. The experimental program presented in this report demonstrated higher shear deformability of hollow columns, and the exact reason for this increase is not well known. It would be useful to be able to predict the shear deformation of hollow columns and to compare this deformation to similar solid columns.

CHAPTER 7. REFERENCES

AASHTO Guide Specifications for LRFD Seismic Bridge Design (2nd Edition) with 2012 and 2014 Interim Revisions. (2011; 2012; 2014). American Association of State Highway and Transportation Officials.

Beyer, K., Dazio, A., & Priestley, N. (2011). Shear deformations of slender reinforced concrete walls under seismic loading. *ACI Structural Journal*, 167-177.

Caltrans Seismic Design Criteria Version 1.7. (2013, April). California Department of Transportation.

Calvi, G. M., Pavese, A., Rasulo, A., & Bolognini, D. (2005). Experimental and Numerical Studies on the Seismic Response of R.C. Hollow Bridge Piers. *Bulletin of Earthquake Engineering*, 267-297.

Chang, G., & Mander, J. (1994). *Seismic energy based fatigue damage analysis of bridge columns: part 1 - evaluation of seismic capacity.* NCEER.

Filippou, F., Popov, E., & Bertero, V. (1983). *Effects of bond deterioration on hysteric behavior of reinforced concrete joints.* EERC.

Hoshikuma, J.-I., & Priestley, M. (2000). *Flexural behavior of circular hollow columns with a single layer of reinforcement under seismic loading.* Structural Systems Research Project, University of California, San Diego, Department of Structural Engineering.

Liang, X., Beck, R., & Sritharan, S. (2015). *Understanding the confined concrete behavior on the response of hollow bridge columns.* Ames: Iowa State University, Department of Civil, Construction and Environmental Engineering.

Lignola, G. P., Prota, A., Manfredi, G., & Cozenza, E. (2008). Unified theory for confinement of RC solid and hollow circular columns. *Composites: Part B, 39*, 1151-1160.

Mander, J., Priestley, M., & Park, R. (1988). Observed stress-strain behavior of confined concrete. *Journal of Structural Engineering*, 1827-1849.

Mander, J., Priestley, M., & Park, R. (1988). Theoretical stress-strain model for confined concrete. *Journal of Structural Engineering*, 1804-1826.

McKenna, F., Fenves, G., Scott, M., & Jeremic, B. (2000). Open System for Earthquake Engineering Simulation (OpenSees). Univeristy of California, Berkeley, CA: Pacific Earthquake Engineering Research Center.

Mohd Yassin, M. (1994). *Nonlinear Analysis of Prestressed Concrete Structures under Monotonic and Cycling Loads.* Berkeley: PhD dissertation, University of California.

Priestley, M., Seible, F., & Calvi, G. (1996). *Seismic Design and Retrofit of Bridges.* John Wiley & Sons, Inc.

Ranzo, G., & Priestley, M. (2001). *Seismic performance of circular hollow columns subjected to high shear.* Structural Systems Research Project, University of California, San Diego, Department of Structural Engineering.

Sritharan, S. (1998). *Analysis of Concrete Bridge Joints Subjected to Seismic Actions.* San Diego: Doctoral Dissertation, University of California.

Waugh, J. (2007). Nonlinear analysis of T-shaped concrete wall subjected to multi-directional displacements. *PhD Thesis*. Iowa State University.

Yeh, Y., Mo, Y., & Yang, C. (2001). Seismic performance of hollow circular bridge piers. *ACI Structural Journal, 98*(6).

Yeh, Y.-K., Mo, Y., & Yang, C. (2002). Full-scale tests on rectangular hollow bridge piers. *Materials and Structures*, 117-125.

Zahn, F., Park, R., & Priestley, M. (1990). Flexural strength and ductility of circular hollow reinforced concrete columns without confinement on inside face. *ACI Structural Journal*, 156-166.

Zahn, F., Park, R., & Priestley, M. (1990, March-April). Flexural Strength and Ductility of Circular Hollow Reinforced Concrete Columns without Confinement on Inside Face. *ACI Structural Journal, 87*(2), 156-166.

Zhao, J., & Sritharan, S. (2007). Modeling of strain penetration effects in fiber-based analysis of reinforced concrete structures. *ACI Structural Journal*, 133-141.